

2015

FT-IR and Interfacial Matrix Stabilization Spectroscopy Studies of CO and O₂ adsorption over Nanostructured TiO₂ and AuTiO₂

Nina Jarrah
Lehigh University

Follow this and additional works at: <http://preserve.lehigh.edu/etd>

 Part of the [Chemistry Commons](#)

Recommended Citation

Jarrah, Nina, "FT-IR and Interfacial Matrix Stabilization Spectroscopy Studies of CO and O₂ adsorption over Nanostructured TiO₂ and AuTiO₂" (2015). *Theses and Dissertations*. 2648.
<http://preserve.lehigh.edu/etd/2648>

This Dissertation is brought to you for free and open access by Lehigh Preserve. It has been accepted for inclusion in Theses and Dissertations by an authorized administrator of Lehigh Preserve. For more information, please contact preserve@lehigh.edu.

FT-IR and Interfacial Matrix Stabilization Spectroscopy Studies of CO and O₂
Adsorption over Nanostructured TiO₂ and Au/TiO₂

by

Nina Katherine Jarrah

A Dissertation

Presented to the Graduate and Research Committee

of Lehigh University

in Candidacy for the Degree of

Doctor of Philosophy

in

Chemistry

Lehigh University

January 2015

© 2014 Copyright
Nina Katherine Jarrah

Approved and recommended for acceptance as a dissertation in partial fulfillment of the requirements for the degree of Doctor of Philosophy

Nina Katherine Jarrah

FT-IR and Interfacial Matrix Stabilization Spectroscopy Studies of CO and O₂ Adsorption over Nanostructured TiO₂ and Au/TiO₂

Defense Date

Dr. David T. Moore
Dissertation Director

Approved Date

Committee Members:

Dr. Gregory S. Ferguson

Dr. James E. Roberts

Dr. Mark A. Snyder

ACKNOWLEDGMENTS

The completion of this work could not have been possible without the support and mentoring of the strong network of people which I have been so blessed with over the years. To start, I would like to thank my research advisor, Dr. David Moore. I am truly grateful for his guidance and advice. It has molded my professional development as a scientist, and as a person. In particular, I am thankful for the many rich scientific discussions, and for all that I have learned in his lab while working towards my degree. Thank you for always being understanding, and for all your help with research throughout the years. I would also like to thank the members of my committee, Professor Gregory Ferguson, Professor James Roberts, and Professor Mark Snyder, for their insightful conversations and helpful suggestions over the years, as well as all their assistance while editing and completing this dissertation.

I also want to express my thanks to my parents, my husband's parents, and my friends, including those I have met during my time at Lehigh. I always knew I could count on you to be there, even though I was almost always busy with school. I am so thankful for your love, support, and limitless understanding, and for being there when I needed a break (and making sure that I took one!).

Most importantly, I would like to thank my husband, Justin Jarrah, for everything he has done for me over the past 5 and a half years. The ways in which he has supported me during this process are simply too long to list. From all the dinners brought to campus late at night while I was essentially living in the lab, to the encouragement to continue, I am forever in debt. Thank you so much for always being there.

TABLE OF CONTENTS

Copyright	ii
Certificate of Approval	iii
Acknowledgements	iv
List of Figures	x
List of Tables	xxii
Abstract	1
Chapter 1: CO oxidation nanocatalysis and spectroscopic mechanism studies	3
1.1 Over-arching research goals	3
1.2 Introduction to catalysis	5
1.3 Supported nanoparticulate gold catalysts for CO oxidation.....	8
1.4 Characterization of surface-bound species: FT-IR Detection	10
1.4.1 Vibrational Spectroscopy Theory.....	11
1.4.2 FT-IR detection of molecular vibration.....	13
1.4.3 Detection of molecules on TiO ₂ and Au/TiO ₂ surfaces.....	14
1.4.4 Coverage effects on vibrational spectra of surface-bound molecules	18
1.5 Previous spectroscopic studies of CO binding at TiO ₂ and Au/TiO ₂ surfaces.....	20
1.6 Cryogenic spectroscopy studies under vacuum.....	23
1.6.1 Mapping the potential energy surface: temperature studies.....	25
1.6.2 Using cryogenic matrices to observe pre- and post-reactive complexes.....	27
1.7 Dissertation Overview	29
1.8 References	31
Chapter 2: Experimental methods and instrumentation	34
2.1 Introduction	34
2.2 Sample preparation and characterization.....	35
2.2.1 Powder TiO ₂ film preparation	35
2.2.2 Nanostructured Au/TiO ₂ film preparation.....	38
2.2.3 TEM characterization	39

2.3 Instrumental Apparatus	39
2.3.1 Gas-delivery system	39
2.3.2 Custom vacuum chamber	42
2.3.3 Fixed-bed flow reactor	47
2.4 Gas adsorption experiments	48
2.4.1 Direct adsorption experiments.....	48
2.4.2 Steady-state pressure experiments.....	49
2.4.3 IMSS Experiments.....	50
2.5 Collection of reference FT-IR spectra.....	51
2.6 References	54
Chapter 3: Elucidating the binding of CO to TiO₂ using cryogenic FT-IR	
spectroscopy: surface diffusion and desorption between 40 and 150 K.....	55
3.1 Abstract.....	55
3.2 Introduction	56
3.3 Experimental methods.....	57
3.4 Results	58
3.4.1 Pre-treatment of TiO ₂	58
3.4.2 Thermal desorption spectroscopy.....	60
3.5 Discussion.....	65
3.6 Conclusion.....	69
3.7 Acknowledgements	70
3.8 Appendix	70
3.9 References	85
Chapter 4: The effect of thermal pre-treatment, dosing rate, and exposure on CO	
adsorption over TiO₂ determined from cryogenic FT-IR spectroscopy:	
population of sites of weaker Lewis acidity.....	86
4.1 Abstract.....	86
4.2 Introduction	87
4.3 Experimental methods.....	89
4.4 Results	90

4.4.1	Pre-treatment of support: temperature effects	90
4.4.2	CO adsorption under vacuum conditions over thermally treated support: effect of exposure and dosing rate	96
4.5	Discussion.....	107
4.5.1	Effects of thermal pretreatment	107
4.5.2	Effects of deposition conditions	108
4.6	Conclusion.....	111
4.7	Appendix	113
4.8	References	117
Chapter 5: FT-IR studies of sample pre-treatment temperature on CO		
adsorption at 40 K over nanostructured Au/TiO₂ generated via thermal de-		
wetting of gold film..... 118		
5.1	Abstract.....	118
5.2	Introduction	119
5.3	Experimental methods.....	120
5.4	Results	122
5.4.1	Thermal processing of Au/TiO ₂ prior to CO deposition	122
5.4.2	CO adsorption over Au/TiO ₂ and TiO ₂ at 40 K	126
5.4.3	Isotopic study of CO/Au band.....	133
5.4.4	TEM imaging of AuNPs formed via thermal de-wetting of Au film.....	134
5.4.5	Thermal behavior of CO/Au band: effect of support processing	134
5.5	Discussion.....	139
5.5.1	Sample preparation: Thermal de-wetting of gold film.....	139
5.5.2	FT-IR Spectroscopy: CO binding on Au/TiO ₂ and TiO ₂ at 40 K.....	140
5.5.3	Effect of processing TiO ₂ prior to Au film deposition on CO/Au signal.....	142
5.6	Conclusion.....	145
5.7	Appendix	146
5.8	References	153
Chapter 6: Exploration of the CO adsorption over Au/TiO₂ and TiO₂ at steady-		
state pressure from 10 to 150 K..... 154		

6.1 Abstract.....	154
6.2 Introduction	155
6.3 Experimental methods.....	157
6.4 Results	158
6.4.1 CO adsorption at steady-state pressure.....	158
6.4.2 Regeneration of bands under steady-state pressure.....	160
6.5 Discussion.....	164
6.6 Conclusion.....	169
6.7 Appendix	170
6.8 References	172
Chapter 7: Adsorption of both CO and O₂ over TiO₂ and Au/TiO₂ under vacuum at 40 K.....	173
7.1 Abstract.....	173
7.2 Introduction	173
7.3 Experimental methods.....	175
7.4 Results	176
7.4.1 Adsorption studies over TiO ₂ with both CO and O ₂	176
7.4.2 Adsorption studies over Au/TiO ₂ and TiO ₂ with CO and O ₂	180
7.5 Discussion.....	184
7.6 Conclusion.....	186
7.7 Appendix	187
7.8 References	188
Chapter 8: Interfacial Matrix Stabilization Spectroscopy (IMSS) studies of CO and O₂ interactions over nanoparticulate TiO₂ and Au/TiO₂: FT-IR investigation of matrix-controlled transport of reactant molecules to surfaces and complex stabilization at matrix/surface interfaces	189
8.1 Abstract.....	189
8.2 Introduction	190
8.3 Experimental methods.....	194
8.4 Results	196

8.4.1	Matrix-controlled transport of CO to catalyst	196
8.4.2	Stabilization of weakly bound species	202
8.4.3	Stabilization of transient species formed during annealing.....	204
8.5	Discussion.....	208
8.5.1	Matrix-controlled transport of CO to catalyst	208
8.5.2	Stabilization of weakly bound species	209
8.5.3	Isolation of transient species formed during annealing.....	210
8.6	Conclusion.....	212
8.7	References	213
Chapter 9: Conclusions and future continuation of this work.....		214
9.1	Conclusions	214
9.2	Future work	216
9.2.1	Isotope studies to demonstrate catalytic conversion of CO to CO ₂	216
9.2.2	Experimental design modifications	217
9.2.3	Expansion of sample characterization methods	220
9.3	Experimental plan for moving forward with this research	221
9.4	References	223
Curriculum Vitae.....		224

LIST OF FIGURES

Figure 1.1	Schematic illustration of proposed Bond-Thompson model showing CO oxidation mechanism over Au supported on TiO ₂ . Figure adapted from Ref 1.	4
Figure 1.2	Schematic diagram of changes to a reaction path in presence of a catalyst.	7
Figure 1.3	Diagram illustrating electric field of infrared light interacting with adsorbed molecule dipole moment.	15
Figure 1.4	Carbon monoxide molecular orbital diagram illustrating HOMO and LUMO.	16
Figure 1.5	Schematic illustration of IMSS technique for O ₂ in argon matrix coated over CO-covered Au/TiO ₂ surface after A) matrix deposition (isolation of CO and O ₂ reactants) and B) matrix annealing (transport of O ₂ and stabilization at CO-covered catalytic interface).	29
Figure 2.1	Image of aluminum mask used for coating CaF ₂ windows with TiO ₂ powder during spraying procedure: a) mask base, b) mask cover, and c) assembled mask.	37
Figure 2.2	Schematic block diagram of gas storage, mix preparation, and delivery system for reagent gases used in adsorption experiments.	42
Figure 2.3	Block diagram of experimental apparatus used for direct adsorption experiments, including cryostat and custom vacuum chamber.	45
Figure 2.4	Schematic block diagram of fixed-bed flow reactor for use in assessment of catalytic activity of nanostructured sample material. Initial design created by a previous undergraduate working in Moore group, Nickolas Greybush, later modified by NKJ.	48
Figure 2.5	FT-IR difference spectra demonstrating temperature dependence of surface carbonate bands on TiO ₂ prior to deposition of reagent gas. To emphasize the increased intensity of bands at colder temperatures, the pre-deposition spectra collected at 4 K was referenced to pre-deposition spectra collected at 120 K (red), 90 K (green), 60 K (blue), and 40 K (purple).	52

Figure 2.6	FT-IR difference spectrum demonstrating the temperature dependence of bands caused by absorbance of impurities in the CaF ₂ window. To clearly emphasize the increased intensity of bands at colder temperatures, the pre-deposition spectrum collected at 4 K was referenced to the pre-deposition spectrum collected at 120 K.	53
Figure 2.7	Schematic diagram of experiment profile indicating temperature over time during a typical adsorption experiment. Reference scans were collected at each temperature indicated on the graph during the cool-down from the heating step, prior to deposition (labelled “Dep”).	54
Figure 3.1	FT-IR spectra collected at 40 K of TiO ₂ before (black) and after (red) thermally processing sample at 582 K showing. a) C-H stretch and b) O-H stretch region	59
Figure 3.2	FT-IR spectra collected at 40 K of CO of TiO ₂ following CO deposition at 40 K (0.5% in Ar at 11 sccm for 10 min) before (black) and after (red) thermally processing sample at 582 K showing a) C-H stretch and b) O-H stretch region	60
Figure 3.3	FT-IR spectra collected in 10-K increments from 40 to 150 K of TiO ₂ following CO deposition at 40 K (0.5% in He at 11 sccm for 10 min) after thermally processing sample at 625 K showing A) entire CO-stretch region and B) expanded view of band(s) near 2180 cm ⁻¹	62
Figure 3.4	Lorentz fit values demonstrating temperature dependence of bands “d” (closed symbols) and “e” (open symbols) during TDS steps of CO on TiO ₂ from 40 to 150 K. The dashed line indicates the summed areas of the two components, showing population transfer to these sites as temperature increases to 120 K.....	63
Figure 3.5	Total area sum of A) chemisorbed (open square) and physisorbed (filled square) bands plotted with total area sum of “fitting” (open circle) bands and B) all empirically fit bands during TDS steps of CO on TiO ₂ from 40 to 150 K.	64
Figure 3.6	Scheme of potential energy surface showing potential wells corresponding to distinct binding sites of varied enthalpy, labeled “a” – “e”, with values indicating barrier heights calculated from Redhead analysis of TPS results (Table 1). The barrier separating minimas corresponding to “b” and “c” sites could not be determined from the data. The solid line indicates sites in chemisorption wells, the dotted line indicates sites in the physisorption well, and the bold dashed line indicates the desorption threshold.	69

Figure 3.7	Lorentzian fitting analysis of FT-IR spectra taken at 40 K of CO adsorbed over TiO ₂ . Spectrum fit by 7 bands with 3 varying parameters.....	72
Figure 3.8	Lorentzian fitting analysis of FT-IR spectra taken at 50 K of CO adsorbed over TiO ₂ . Spectrum fit by 8 bands with 3 varying parameters.....	72
Figure 3.9	Lorentzian fitting analysis of FT-IR spectra taken at 60 K of CO adsorbed over TiO ₂ . Spectrum fit by 9 bands with 3 varying parameters.....	72
Figure 3.10	Lorentzian fitting analysis of FT-IR spectra taken at 70 K of CO adsorbed over TiO ₂ . Spectrum fit by 8 bands with 3 varying parameters.....	72
Figure 3.11	Lorentzian fitting analysis of FT-IR spectra taken at 80 K of CO adsorbed over TiO ₂ . Spectrum fit by 7 bands with 3 varying parameters.....	73
Figure 3.12	Lorentzian fitting analysis of FT-IR spectra taken at 90 K of CO adsorbed over TiO ₂ . Spectrum fit by 6 bands with 3 varying parameters.....	73
Figure 3.13	Lorentzian fitting analysis of FT-IR spectra taken at 100 K of CO adsorbed over TiO ₂ . Spectrum fit by 6 bands with 3 varying parameters.....	73
Figure 3.14	Lorentzian fitting analysis of FT-IR spectra taken at 110 K of CO adsorbed over TiO ₂ . Spectrum fit by 6 bands with 3 varying parameters.....	73
Figure 3.15	Lorentzian fitting analysis of FT-IR spectra taken at 120 K of CO adsorbed over TiO ₂ . Spectrum fit by 4 bands with 3 varying parameters.....	74
Figure 3.16	Lorentzian fitting analysis of FT-IR spectra taken at 130 K of CO adsorbed over TiO ₂ . Spectrum fit by 2 bands with 3 varying parameters.....	74
Figure 3.17	Lorentzian fitting analysis of FT-IR spectra taken at 140 K of CO adsorbed over TiO ₂ . Spectrum fit by 2 bands with 3 varying parameters.....	74

Figure 3.18 Lorentzian fitting analysis of FT-IR spectra taken at 150 K of CO adsorbed over TiO ₂ . Spectrum fit by 2 bands with 3 varying parameters.....	74
Figure 3.19 Lorentzian fit values demonstrating temperature dependence of band “a” during TDS steps of CO desorption on TiO ₂ from 40 to 150 K.	75
Figure 3.20 Lorentzian fit values demonstrating temperature dependence of 2150 cm ⁻¹ band during TDS steps of CO desorption on TiO ₂ from 40 to 150 K.	76
Figure 3.21 Lorentzian fit values demonstrating temperature dependence of 2127 cm ⁻¹ band during TDS steps of CO desorption on TiO ₂ from 40 to 150 K.	77
Figure 3.22 Lorentzian fit values demonstrating temperature dependence of band “b” during TDS steps of CO desorption on TiO ₂ from 40 to 150 K.	78
Figure 3.23 Lorentzian fit values demonstrating temperature dependence of band “c” during TDS steps of CO desorption on TiO ₂ from 40 to 150 K.	79
Figure 3.24 Lorentzian fit values demonstrating temperature dependence of 2133 cm ⁻¹ “fitting” band during TDS steps of CO desorption on TiO ₂ from 40 to 150 K.	80
Figure 3.25 Lorentzian fit values demonstrating temperature dependence of 2168 cm ⁻¹ “fitting” band during TDS steps of CO desorption on TiO ₂ from 40 to 150 K.	81
Figure 3.26 Lorentzian fit values demonstrating temperature dependence of 2178 cm ⁻¹ “fitting” band during TDS steps of CO desorption on TiO ₂ from 40 to 150 K.	82
Figure 3.27 Lorentzian fit values demonstrating temperature dependence of 2183 cm ⁻¹ “fitting” band during TDS steps of CO desorption on TiO ₂ from 40 to 150 K.	83
Figure 4.1 FT-IR spectra collected at 4 K of TiO ₂ surface of sample “T” prior to thermal processing (purple) and after heating <i>in vacuo</i> at set-point of 400 K (blue), 500 K (green), 600 K (orange), and 700 K (red) showing the a) carbonate region and b) C-H stretching region. Both panels displayed at same vertical scale and labelled temperature values indicate the temperature measured at Pt sensor.	91

Figure 4.2	FT-IR difference spectra collected at 4 K of TiO ₂ sample “T” emphasizing changes before and after heating <i>in vacuo</i> at set-point of 400 K (blue), 500 K (green), 600 K (orange), and 700 K (red). Labelled temperature values indicate temperatures measured at Pt sensor.....	93
Figure 4.3	FT-IR spectra collected at 4 K of blank CaF ₂ window a) before (black) and after (red) heating sample at 626 K (750 K set-point) and b) difference spectrum calculated from panel a. Spectra collected by RDK, figure prepared and data analyzed by NKJ.	95
Figure 4.4	FT-IR spectra collected at 4 K of CaF ₂ window coated with TiO ₂ powder a) before (black) and after (red) heating sample at 604 K (750 K set-point) and b) difference spectrum calculated from panel a. Spectra collected by RDK, figure prepared and data analyzed by NKJ.....	95
Figure 4.5	FT-IR difference spectra at 40 K following CO deposition (36 ML CO at 0.6 ML / min) on TiO ₂ sample “T” before heating (purple) and after heating at a temperature set-point of 400 K (blue), 500 K (green), 600 K (orange), and 700 K (red). Labelled temperature values indicate temperatures measured at Pt sensor.....	96
Figure 4.6	FT-IR spectra taken during surface warming steps following CO deposition (36 ML CO at 0.6 ML / min) on sample “T” A) before heating and after heating at a temperature of B) 372 K, C) 432 K, D) 490 K, and E) 578 K, indicating the temperature measured at the platinum sensor. Spectra collected at 40 to 150 K, as indicated in legend.. All panels follow same legend and are displayed at the same vertical scale.....	99
Figure 4.7	FT-IR spectra collected at 40 K during first 3 min of CO deposition (900 ML CO at 300 ML/min) over TiO ₂ sample “X” after thermally processing sample at 625 K (750 K set-point). Data shown collected during experiments discussed in Chapter 3, in which binding sites labelled “a” – “d” are explained in detail. Spectrum collected at a resolution of 0.5 cm ⁻¹ . Spectrum collected by RDK, figure prepared and data analyzed by NKJ.	101
Figure 4.8	FT-IR spectra collected at 40 K during a 15 minute CO deposition (60 ML /min at 40 K) over TiO ₂ sample “Y” that had been heated at 591 K (750 K set-point).....	102

Figure 4.9	FT-IR spectra collected at 40 K throughout 4.67 h CO deposition (60 ML at 0.6 ML/min followed by 10800 ML at 60 ML/min deposited at 40 K) over TiO ₂ sample “W” that had been preheated at 413 K (500 K set-point). Spectra shown include A) deposition of both reagent mixes and B) expanded view of the window with only deposition of CO at the low rate. Red, dashed spectrum indicates switch to the higher deposition rate in panel A.	103
Figure 4.10	FT-IR spectra collected at 40 K throughout the 3 h deposition of CO (10800 ML at 60 ML/min deposited at 40 K) on TiO ₂ sample “W” that had been preheated at 413 K (500 K set-point). Series of spectra show deposition over time during successive 10 min intervals following the first 20 min of deposition.	105
Figure 4.11	Incremental changes in intensity integrated over the spectral region from 2100 – 2200 cm ⁻¹ for each difference FT-IR spectrum collected at 40 K throughout 3 h deposition of CO (10800 ML at 60 ML/min deposited at 40 K) on TiO ₂ sample “W” that had been preheated at 413 K (500 K set-point). Series of integrated intensities demonstrate changes in deposition over time during successive 10 min intervals. Linear fit of data fit to equation $y = -0.00353x + 0.1537$ with $R^2 = 0.713$	106
Figure 4.12	FT-IR spectra in the Ti-O stretching region collected at 40 K throughout 4.67 h CO deposition (60 ML at 0.6 ML/min followed by 10800 ML at 60 ML/min deposited at 40 K) on TiO ₂ sample “W” that had been preheated at 413 K (500 K set-point). The red dashed line indicates the switch to the faster deposition rate	107
Figure 4.13	FT-IR spectra collected at 4 K of a CaF ₂ window coated with TiO ₂ powder before (black) and after (red) heating : a) Sample “T” heated at 578 K and b) heavily coated TiO ₂ sample prepared by RDK heated at 626 K. Spectra in panel b collected by RDK; figure prepared and data analyzed by NKJ	113
Figure 4.14	FT-IR difference spectra at 40 K following CO deposition (36 ML CO at 0.6 ML / min) on TiO ₂ sample “T” before heating (purple) and after heating at a temperature set-point of 400 K (blue), 500 K (green), 600 K (orange), and 700 K (red). Labelled temperature values indicate temperatures measured at Pt sensor.....	114
Figure 4.15	FT-IR spectra collected during deposition of CO (4.2 ML/min) on TiO ₂ which was preheated at 597 K. Spectra collected by RDK; figure prepared and data analyzed by NKJ.....	115

Figure 4.16	FT-IR spectra collected at 40 K throughout 4.67 h CO deposition (60 ML at 0.6 ML/min followed by 10800 ML at 60 ML/min deposited at 40 K) over TiO ₂ sample “W” preheating at 413 K (500 K set-point) showing a) carbonate region and b) C-H stretch region. The red dashed line indicates the switch from 0.6 ML/min to 60 ML/min.....	116
Figure 5.1	FT-IR spectra collected at 4 K of sample Au-UP prior to thermal processing (purple) and after heating <i>in vacuo</i> at set-point of 400 K (blue), 500 K (green), 600 K (orange), and 700 K (red) showing a) carbonate region and b) C-H stretching region. Both panels show same vertical scale and are labelled temperature with the temperature measured at the Pt sensor.....	124
Figure 5.2	FT-IR difference spectra collected at 4 K of Au/TiO ₂ emphasizing changes before and after heating <i>in vacuo</i> at set-point of 400 K (blue), 500 K (green), 600 K (orange), and 700 K (red) for samples a) Au-UP, b) Au-LP, and c) Au-HP. All panels show same vertical scale and are labelled temperature with the temperature measured at the Pt sensor.....	125
Figure 5.3	FT-IR spectra taken at 40 K following CO deposition at 40 K (36 ML CO at 0.6 ML/min) before heating (purple) and after heating at a set-point of 400 K (blue), 500 K (green), 600 K (orange), and 700 K (red) of samples a) T b) Au-UP and c) Au-LP. All panels show same vertical scale and are labelled temperature with the temperature measured at the Pt sensor.	126
Figure 5.4	FT-IR spectra collected during the first 5 – 10 min of CO deposition at 40 K (0.1% in He at 1sccm) before heating (purple) and after heating sample at a set-point of 400 K (blue), 500 K (green), 600 K (orange), and 700 K (red) for samples a) T b) Au-UP c) Au-LP and d) Au-HP. All panels show same vertical scale, and labelled temperature was measured at the Pt sensor.....	129
Figure 5.5	FT-IR spectra collected following CO adsorption at 40 K (36 ML CO at 0.6 ML/min) on sample Au-UP (blue spectrum; processed at 566 K), Au-LP (red spectrum; processed at 585 K), and Au-HP (green spectrum; processed at 593 K).	131
Figure 5.6	FT-IR spectra tracking deposition of CO over Au/TiO ₂ (sample Au-HP) at 40 K over time (36 ML CO at 0.6 ML/min) after heating sample at 453 K (500 K set-point).	132

Figure 5.7	FT-IR spectra of ^{12}CO (black) and ^{13}CO (blue) adsorbed on Au/TiO ₂ (sample Au-UP40) at 40 K following CO deposition at 40 K (36 ML at 0.6 ML/min) after processing samples at 409 – 414 K for 1h. Band at 2090 cm ⁻¹ is shifted to 2037 cm ⁻¹ when depositing isotopically labelled reagent gas, indicating CO/Au spectral feature corresponds to vibration of CO oscillator adsorbed to Au site. Spectra collected at 0.5 cm ⁻¹ resolution.....	133
Figure 5.8	TEM images shown at 250,000x of Au/TiO ₂ material a.) before thermal processing and after thermal processing at b.) 420 – 448 K and c.) 566 – 585 K.	134
Figure 5.9	FT-IR spectra taken following CO deposition (0.1% in He at 1scm for 60 min at 40 K) on AuNPs formed over TiO ₂ support processed to various degrees, samples Au-UP (blue), Au-LP (red), and Au-HP (green). The AuNPs were prepared at a de-wetting temperature of 420 K (Au-UP), 448 K (Au-LP), and 453 K (Au-HP). Spectra collected at a) 40 K and after warming CO-covered surface up to b) 120 K and c) 150 K.	136
Figure 5.10	Absolute area sums of FT-IR spectra taken during surface warming steps following CO deposition (0.1% in He at 1scm for 60 min at 40 K) on AuNPs formed over TiO ₂ support processed to various degrees, samples a) Au-UP, b) Au-LP, and c) Au-HP. The AuNPs were prepared at a de-wetting temperature of 420 K (Au-UP), 448 K (Au-LP), and 453 K (Au-HP). The error bars in area appear smaller than data points on the figure....	138
Figure 5.11	FT-IR spectra taken during surface warming steps following CO deposition (0.1% in He at 1scm for 60 min at 40 K) on AuNPs formed over TiO ₂ support processed to various degrees, samples a) Au-UP, b) Au-LP, and c) Au-HP. The AuNPs were prepared at a de-wetting temperature of 420 K (Au-UP), 448 K (Au-LP), and 453 K (Au-HP). Spectra collected at deposition temperature of 40 K and at each temperature shown while warming CO-covered surface up to 150 K. All panels display same vertical scale.	146
Figure 5.12	Lorentzian fitting analysis of FT-IR spectrum taken of sample Au-UP at 40 K. (Fit by 6 bands; 3 varying parameters).....	147
Figure 5.13	Lorentzian fitting analysis of FT-IR spectrum taken of sample Au-UP at 60 K. (Fit by 6 bands; 3 varying parameters).....	147
Figure 5.14	Lorentzian fitting analysis of FT-IR spectrum taken of sample Au-UP at 90 K. (Fit by 5 bands; 3 varying parameters).....	147

Figure 5.15	Lorentzian fitting analysis of FT-IR spectrum taken of sample Au-UP at 120 K. (Fit by 5 bands; 3 varying parameters).....	147
Figure 5.16	Lorentzian fitting analysis of FT-IR spectrum taken of sample Au-UP at 150 K. (Fit by 1 band; 3 varying parameters)	147
Figure 5.17	Lorentzian fitting analysis of FT-IR spectrum taken of sample Au-LP at 40 K. (Fit by 6 bands; 3 varying parameters)..	149
Figure 5.18	Lorentzian fitting analysis of FT-IR spectrum taken of sample Au-LP at 60 K. (Fit by 6 bands; 3 varying parameters)	149
Figure 5.19	Lorentzian fitting analysis of FT-IR spectrum taken of sample Au-LP at 90 K. (Fit by 6 bands; 3 varying parameters).	149
Figure 5.20	Lorentzian fitting analysis of FT-IR spectrum taken of sample Au-LP at 120 K. (Fit by 5 bands; 3 varying parameters)	149
Figure 5.21	Lorentzian fitting analysis of FT-IR spectrum taken of sample Au-LP at 150 K. (Fit by 2 bands; 3 varying parameters).	149
Figure 5.22	Lorentzian fitting analysis of FT-IR spectrum taken of sample Au-HP at 40 K. (Fit by 6 bands; 3 varying parameters).....	151
Figure 5.23	Lorentzian fitting analysis of FT-IR spectrum taken of sample Au-HP at 60 K. (Fit by 6 bands; 3 varying parameters).....	151
Figure 5.24	Lorentzian fitting analysis of FT-IR spectrum taken of sample Au-HP at 90 K. (Fit by 5 bands; 3 varying parameters).....	151
Figure 5.25	Lorentzian fitting analysis of FT-IR spectrum taken of sample Au-HP at 120 K. (Fit by 5 bands; 3 varying parameters).....	151
Figure 5.27	Lorentzian fitting analysis of FT-IR spectrum taken of sample Au-HP at 150 K. (Fit by 3 bands; 3 varying parameters).....	151
Figure 6.1	FT-IR spectra of CO adsorbed on TiO ₂ a) under 1 Torr CO steady-state pressure conditions at 105 – 150 K and b) after evacuation to 10 ⁻⁸ Torr at 90 – 150 K.	159
Figure 6.2	FT-IR spectra of CO adsorbed on Au/TiO ₂ a) under 1 Torr CO steady-state pressure conditions at 105 – 150 K and b) after evacuation to 10 ⁻⁸ Torr at 90 – 150 K.....	160

Figure 6.3	FT-IR spectra demonstrating effect of repeated sample use. Spectra collected at 40 K of CO adsorbed over Au/TiO ₂ on day 1 (blue spectrum), day 4 (red spectrum), and day 6 (black spectrum) following CO deposition under vacuum (10 ⁻⁵ Torr). Spectra were collected at a) 40 K and b) 120 K after warming up CO-covered surface.....	162
Figure 6.4	FT-IR spectra of CO adsorbed on Au/TiO ₂ collected at 120 K on Day 6 (black spectrum; after 40 K CO exposure at 10 ⁻⁵ Torr, prior to exposure to steady-state CO pressure) and Day 13 (blue spectrum; following evacuation after exposure to CO at 1 Torr steady-state pressure at 105 – 150 K).....	163
Figure 6.5	FT-IR difference spectra collected at 4 K after preheating Au/TiO ₂ . All spectra are referenced to spectrum collected at 4 K following thermal processing on day 1 to emphasize progressive changes to surface occurring over repeated experiments.....	170
Figure 6.6	FT-IR difference spectra collected at 40 K after CO deposition over Au/TiO ₂ on day 1 (black spectrum), day 4 (blue spectrum), and day 5 (red spectrum) showing a) CO stretching region changes and b) OH stretching region changes. All spectra are referenced to spectrum collected on the same experiment day at 40 K, prior to CO deposition.	171
Figure 6.7	FT-IR difference spectra collected under vacuum (10 ⁻⁸ Torr) at 90 K after exposure of Au/TiO ₂ to CO on day 1 (black spectrum; deposition at 40 K at 10 ⁻⁵ Torr), day 4 (blue spectrum; deposition at 40 K at 10 ⁻⁵ Torr), and day 13 (red spectrum; steady-state exposure of 1 Torr CO at 105 K). All spectra referenced to spectrum collected at 90 K on the same experiment day, prior to CO exposure.....	171
Figure 7.1	FT-IR difference spectra collected following layered deposition of CO (black spectrum; 720 ML CO at 12 ML/min) / O ₂ (blue spectrum; 36 ML ¹⁸ O ₂ at 0.6 ML/min) / CO (red spectrum; 720 ML CO at 12 ML/min) showing a) carbonate region and b) CO region.....	177
Figure 7.2	FT-IR difference spectra of incremental changes during adsorption over TiO ₂ of the first layer of deposition (720 ML CO at 12 ML/min), showing a) carbonate region and b) CO region	179
Figure 7.3	FT-IR difference spectra of incremental changes during adsorption over TiO ₂ of a) the second layer of deposition (36 ML ¹⁸ O ₂ at 0.6 ML/min) and b) the third layer of deposition (720 ML CO at 12 ML/min)..	180

Figure 7.4	FT-IR difference spectra collected at 40 K of Au/TiO ₂ (red spectrum) and TiO ₂ (black spectrum) following a) CO deposition (36 ML CO at 0.6 ML/min at 40 K) and subsequent b) O ₂ deposition (36 ML O ₂ at 0.6 ML/min at 40 K). Spectra in panel b are referenced to spectra collected following CO deposition to emphasize O ₂ -dependent changes to CO vibrational bands.	181
Figure 7.5	FT-IR difference spectra during surface warming steps of CO adsorbed over TiO ₂ at 40 K (blue spectrum), 60 K (green spectrum), 90 K (red spectrum), and 120 K (black spectrum)	183
Figure 7.6	FT-IR difference spectra during surface warming steps of CO adsorbed over Au/TiO ₂ at 40 K (blue spectrum), 60 K (green spectrum), 90 K (red spectrum), and 120 K (black spectrum), showing a) the full CO region and b) expanded view of the CO/Au region	184
Figure 7.7	FT-IR difference spectra of TiO ₂ following adsorption of ¹⁸ O ₂ (orange) and ¹⁶ O ₂ (blue) after exposure of 36 ML (0.6 ML/min).	188
Figure 7.8	FT-IR difference spectra of TiO ₂ following adsorption of ¹⁶ O ₂ (36 ML at 0.6 ML/min).....	188
Figure 8.1	Schematic illustration of matrix isolation of CO above TiO ₂ surface A) with and B) without the presence of un-doped argon under-layer protecting support sites.....	192
Figure 8.2	Schematic illustration of IMSS technique for O ₂ in Argon matrix deposited over CO-covered Au/TiO ₂ surface after A) deposition (isolation of CO and O ₂ reactants) and B) annealing (transport of O ₂ and stabilization at CO-covered catalytic interface)	194
Figure 8.3	Experimental profile illustrating temperature progression throughout duration of experiment during gas deposition and annealing steps.....	195
Figure 8.4	FT-IR difference spectra collected at 4 K during IMSS experiment with argon under-layer (Ar at 1 sccm for 20 min // 0.5% CO in Ar at 1 sccm for 1 h // Kr at 2 sccm for 30 min; black spectrum) and without argon under-layer (0.5% CO in Ar at 1 sccm for 1 h // Kr at 2 sccm for 30 min; red spectrum) after a) 20 K matrix deposition, b) annealing matrix at 32 K for 30 min, and c) annealing matrix at 37 K for 30 min. All panels and insets display the same vertical scale.	199

Figure 8.5	FT-IR difference spectra collected at 4 K during IMSS experiment after 20 K matrix deposition with argon under-layer (Ar at 1 sccm for 20 min // 0.5% CO in Ar at 1 sccm for 1 h // Kr at 2 sccm for 30 min; black spectrum) and annealing matrix at 37 K for 30 min (blue spectrum).	200
Figure 8.6	FT-IR collected at 4 K during IMSS experiment a) matrix deposition with argon under-layer (Ar at 1 sccm for 20 min // 0.5% CO in Ar at 1 sccm for 1 h // Kr at 2 sccm for 30 min) at 4 K (shown in red) and 20 K (shown in black), b) after annealing matrix at 32 K for 30 min, and c) after annealing matrix at 37 K for 30 min. All panels and insets display the same vertical scale.	202
Figure 8.7	FT-IR difference spectra collected at 4 K following deposition (0.1% CO in He at 1 sccm for 1 h at 40 K // Ar at 1 sccm for 1 h // Kr at 2 sccm for 30 min; black spectrum) and annealing at 32 K for 30 min (blue spectrum).....	203
Figure 8.8	FT-IR spectra tracking CO bands after deposition (black), annealing to 32 K (blue) for argon matrices containing O ₂ deposited over CO-saturated a) Au/TiO ₂ and b) TiO ₂	204
Figure 8.9	FT-IR spectra tracking CO bands after deposition (black), annealing to 32 K (blue), and annealing to warmer temperatures (red) for argon matrices without O ₂ deposited over CO-saturated a) Au/TiO ₂ and b) TiO ₂	206
Figure 8.10	FT-IR spectra of Au/TiO ₂ after deposition (0.1% CO in He at 1 sccm for 1 h at 40 K // 1% O ₂ in Ar at 1 sccm for 1 h at 20 K // Kr at 1 sccm for 20 min at 20 K; black spectrum), annealing to 32 K for 30 min (blue spectrum), and annealing at 37 K for 30 min (red spectrum) using a) ¹² CO and b) ¹³ CO. These spectra indicate the isotopic shift in band position of the 2112 cm ⁻¹ feature to 2065 cm ⁻¹ with substitution of ¹³ CO for the ¹² CO in reagent gas. Both panels displayed at same vertical scale.....	207
Figure 9.1	Top view of FT-IR spectrometer, illustrating modifications to incorporate the use of a copper integrating sphere as a sample substrate to be installed on the sample stage of the cryostat	219

LIST OF TABLES

Table 1.1	Assignments of bands due to carbonate and carboxylate species bound to TiO ₂ and Au/TiO ₂ surfaces.....	23
Table 3.1	Calculated binding energies based on desorption temperature using Redhead analysis.....	67
Table 3.2	Lorentzian fit values showing temperature dependence of chemisorbed bands	84
Table 3.3	Lorentzian fit values showing temperature dependence of “fitting” bands	84
Table 3.4	Lorentzian fit values showing temperature dependence of physisorbed / hydrogen-bonded bands	84
Table 4.1	Dosing rates and CO exposure for all samples and experiments presented in this chapter.....	90
Table 5.1	Description of samples prepared for this work	120
Table 5.2	Lorentzian fit values showing temperature dependence of physisorbed CO band during surface warming of sample Au-UP from 40 to 150 K.....	148
Table 5.3	Lorentzian fit values showing temperature dependence of TiO ₂ support CO bands during surface warming of sample Au-UP from 40 to 150 K.....	148
Table 5.4	Lorentzian fit values showing temperature dependence of CO/Au band during surface warming of sample Au-UP from 40 to 150 K.....	148
Table 5.5	Lorentzian fit values showing temperature dependence of physisorbed CO band during surface warming of sample Au-LP from 40 to 150 K.....	150
Table 5.6	Lorentzian fit values showing temperature dependence of TiO ₂ support CO bands during surface warming of sample Au-LP from 40 to 150 K	150
Table 5.7	Lorentzian fit values showing temperature dependence of CO/Au band during surface warming of sample Au-LP from 40 to 150 K	150
Table 5.8	Lorentzian fit values showing temperature dependence of physisorbed CO band during surface warming of sample Au-HP from 40 to 150 K.....	152

Table 5.9	Lorentzian fit values showing temperature dependence of TiO ₂ support CO bands during surface warming of sample Au-HP from 40 to 150 K....	152
Table 5.10	Lorentzian fit values showing temperature dependence of CO/Au band during surface warming of sample Au-HP from 40 to 150 K.....	152
Table 8.1	Isotopic shift of CO bands with substitution of ¹³ CO in IMSS experiments	211

ABSTRACT

This dissertation focuses on the development of Interfacial Matrix Stabilization Spectroscopy (IMSS) for study of the mechanism of catalytic oxidation of CO over gold nanoparticles (AuNPs) supported on titanium dioxide (TiO₂). In this unique application of matrix isolation, reactant molecules isolated in a cryogenic matrix are deposited over a thin-film of catalyst at 4 K to 20 K, in which subsequent annealing up to 40 K promotes diffusion to the catalytic interface and formation of reactive complexes. Energy-dissipating conditions trap species, and the evolution of vibrational bands during annealing is tracked with Fourier Transform Infrared (FT-IR) Spectroscopy to obtain structural information of reactive intermediates. In particular, this work demonstrates the value of IMSS as a spectroscopic tool to identify short-lived, hard to detect species.

Films of Au/TiO₂ powder were prepared *via* thermal de-wetting of Au film over TiO₂ NPs *in vacuo* at 500 K. Direct adsorption studies at 40 K under high vacuum conditions (10⁻⁸ to 10⁻⁵ Torr) of CO deposited in helium over Au/TiO₂ and TiO₂, in the absence of the cryogenic matrix, reveal CO vibrational bands in the range of 2090 cm⁻¹ – 2106 cm⁻¹ attributed to binding at Au sites, dependent on de-wetting conditions, as well as pressure/temperature conditions for CO binding. Comparison of these results to binding under equilibrium pressure (1 Torr CO) allows for differentiation between weakly-bound species present in dynamic equilibrium with the gas phase, and those existing in stable potential wells. These studies in the absence of the cryogenic matrix serve as foundational work towards understanding the adsorption of species without added stabilization of the matrix.

The ability of IMSS to control the delivery of reactant molecules to the catalyst interface is first demonstrated through deposition of CO isolated in an argon matrix with a krypton over-layer, followed by incremental annealing steps between 25 K and 40 K. Results reveal a band at 2180 cm^{-1} only after annealing to sufficiently high temperatures, in which this band indicates CO chemisorption at the support. Additional experiments demonstrate that, following pre-saturation of CO binding sites during a direct adsorption step, O_2 deposition in an argon matrix over-layer reveals a new band at 2112 cm^{-1} upon annealing. This band is most pronounced for samples containing gold and with O_2 present in the matrix, demonstrating the isolation of transient complexes at the surface previously unobserved for CO and O_2 direct adsorption experiments in the absence of the matrix.

Chapter 1

CO oxidation nanocatalysis and spectroscopic mechanism studies

1.1 Over-arching research goals

The work presented in this dissertation is part of a large effort of the catalysis community towards elucidating mechanisms of catalyzed reactions at surfaces, in particular that for catalyzed CO oxidation over gold nanoparticles supported on titanium dioxide (Au/TiO₂).¹ Gas-phase reactions at nanostructured surfaces such as Au/TiO₂ are governed by crystal structure, particle size, and coordination of surface species, all of which can influence the structures of reactive intermediates formed at the surface.² Experimental study of the CO oxidation reaction mechanism focuses on the determination of these structures, especially those which correspond to transient reactive intermediates formed along the reaction coordinate. Structures of these transient species are mechanism-specific, making their experimental characterization crucial to unraveling subtle differences in distinct mechanistic pathways which ultimately reach the same product state. The transient nature of these species inherently makes observation and characterization a difficult task. The efforts of the Moore group are devoted to overcoming this experimental barrier so that that the catalytic mechanism may be elucidated through the stabilization, observation, and characterization of these transient species.

Several reaction mechanisms have already been proposed for the conversion of CO to CO₂ over nanostructured Au/TiO₂ surfaces, including that described by the Bond-

Thompson model.¹ This reaction pathway is illustrated in *Figure 1.1*, in which it is proposed that CO first binds to neutral gold sites on the AuNP, followed by creation of an anion vacancy on the oxide surface adjacent to the AuNP as a hydroxide ion (OH^-) moves to an oxidized gold site at the gold/oxide interface. Reaction occurs when the chemisorbed CO migrates to this site and reacts with the hydroxide ion to form a carboxylic acid group. Subsequent oxygen binding at the anion vacancy site creates the superoxide species, O_2^- , which serves to oxidize the carboxylic group to form the CO_2 product, and regenerate the Ti-OH site.

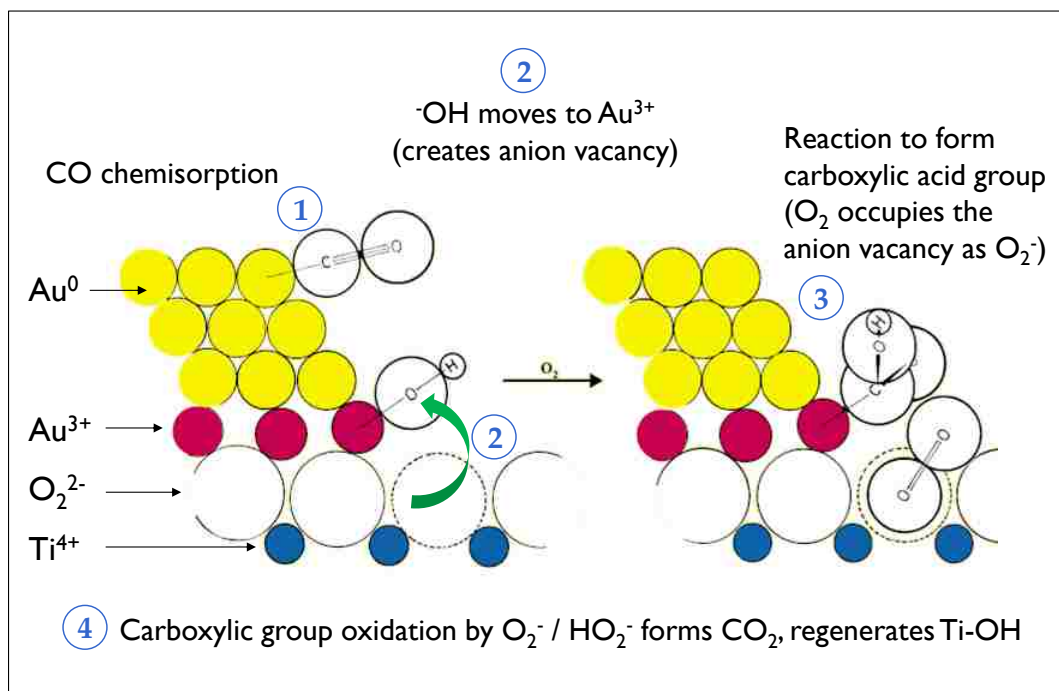


Figure 1.1 Schematic illustration of proposed Bond-Thompson model showing CO oxidation mechanism over Au supported on TiO_2 . Figure adapted from Ref 1.

This reaction model is particularly relevant as it accounts for the experimental results demonstrating the importance of both cationic and neutral gold species, and proposes the involvement of short-lived intermediates not yet confirmed given the

currently available experimental tools.^{1,2} A more complete mechanistic understanding requires additional experimental evidence to characterize transient intermediates formed along the catalyzed reaction coordinate and identify the oxidation state(s) of the involved species, a task well-suited for the energy-dissipating environment of frozen noble-gas matrices combined with cryogenic, FT-IR spectroscopy, the focus of the work described here.

Establishment of a new cryogenic, infrared instrumental probe for CO oxidation over Au/TiO₂ first requires an understanding of the Au/TiO₂ surface, as well as binding of reactant molecules at this surface. The work presented here summarizes the development of this understanding, which largely includes the methods for experimental signal interpretation. These findings serve as the foundation for research on the binding of transient species at the surfaces, and pave the way for characterization of species formed at catalytic active sites.

1.2 Introduction to catalysis

The ability to control the rate of chemical reactions using catalysts has transformed the chemical production industry, enabling economical large scale production of materials relying on key reactions, including the Haber process for ammonia production, the water-gas shift reaction for hydrogen production, and the oxidation of sulfur dioxide to form sulfuric acid, to name a few.³ In general, catalyst systems can be described as either homogeneous (single phase) or heterogeneous (multiphase), with the majority of industrial catalysts being the latter.³ The work

described here focuses on the study of heterogeneous catalysts, in particular those in which the reactants are gas phase species, and the catalyst is solid phase and nanoparticulate. Catalysts are defined as materials which, when added to a chemical reaction, both increase the rate of product formation and are regenerated after the reaction in their initial state, ready for use in repeated reaction cycles. Catalysts increase the rate of chemical reactions by decreasing the activation energy required to initiate the conversion of reactants into products, while the reactant and product energies remain the same. The energy levels of reactants, products, and the barriers separating them are described by the reaction Potential Energy Surface (PES),⁴ and catalysts change this surface in several ways. In addition to reduction of the reaction barrier, a foundational hypothesis for this research is that catalysts also serve to create small potential wells before (pre-reactive minima) and after (post-reactive minima) the reaction barrier. These minima correspond to pre- and post-reactive complexes that form between the catalyst and the reactants and products, respectively, at lower energy than each species. This modified energy surface is illustrated in *Figure 1.2*, showing the reaction pathway and how it is modified in the presence of the catalyst.

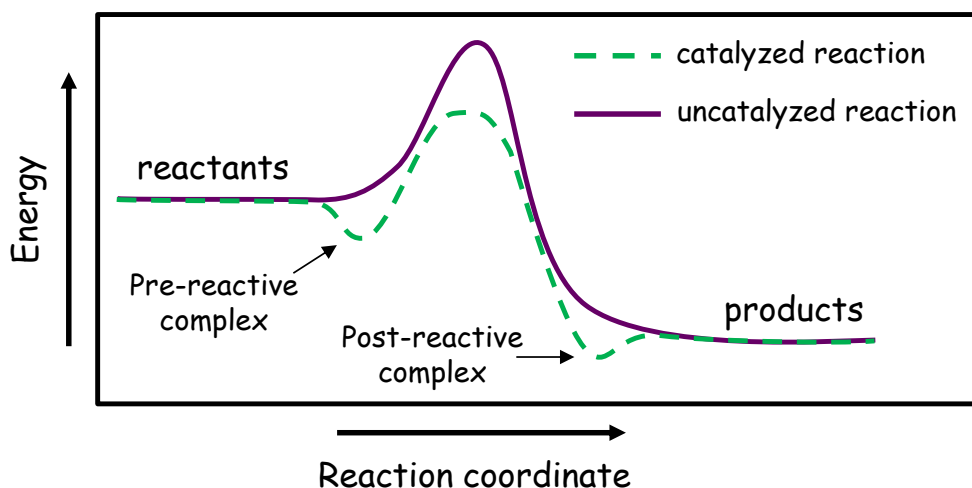


Figure 1.2. Schematic diagram of changes to a reaction path in presence of a catalyst.

The structures of pre- and post-reactive complexes will provide valuable information about how the catalyst participates in the chemical reaction. Mechanistic studies strive to understand the structures of complexes found in the pre- and post-reactive minima in order to describe the chemical species, morphology, and binding conditions involved at the catalytic active site, the chemical location on the catalyst where the rate-determining step in the reaction occurs.¹ Structural characterization of active species and, ultimately, complete mechanistic understanding is desirable to improve catalyst performance, efficiency, and design efforts to maximize the number density of active bindings sites over catalysts, especially important for processes which require the use of precious metals such as gold, silver, and platinum without generating excess wasted material.

1.3 Supported nanoparticulate gold catalysts for CO oxidation

The functionality of nanostructured catalysts stems from physical attributes of the solid structure that give rise to enhanced chemical reactivity at the nanoscale compared to that of the bulk, namely: high surface area, lattice distortions arising from surface stress and support contact, and morphology effects which create varied surface sites such as steps, edges, defects, and terraces.² Chemisorption of reactants occurs only when a significant proportion of the metal surface sites are of low coordination, and the number of these sites are increased as particle size is decreased from the bulk.⁵ Due to the strong correlation between particle size and catalytic activity, nanocatalyst material is typically supported, meaning it is dispersed onto a support substrate of porous nature, as that offers a practical way to contain a large amount of fine particles which could otherwise not be introduced into the reactor.³ Dispersion of catalyst NPs over the support material also results in strong particle-support interactions which can strongly influence activity, an effect shown to be particularly significant for supported Au catalysts.⁶

Increased reactivity at the nanoscale is particularly prominent for gold nanoparticles (AuNPs), which transition from the most inert of all metals in the bulk regime, to exhibiting high chemical activity at the nanoscale.^{2,5} While several reactions show promising potential applications for AuNP catalysts, including the water-gas shift (WGS) reaction, oxidation of carbon monoxide, selective epoxidation of propene, and hydrogen peroxide formation, CO oxidation is by far the most studied.² The catalytic activity of finely dispersed gold nanoparticles (AuNPs) supported over metal-oxides for low temperature CO oxidation, at 203 K, was first demonstrated by Haruta in 1987.⁷ The

full catalytic cycle including all reactive intermediates, however, has not yet been experimentally confirmed. Catalyzed oxidation at room temperature is significant for environmental applications in H₂ purification for the protection of Proton Exchange Membrane (PEM) fuel-cell catalysts^{2,8} and CO emission reduction⁹⁻¹¹ technologies, stimulating extensive computational and experimental research aimed at identifying active binding sites to improve catalyst development. In the case of PEM fuel-cell catalyst protection, the WGS reaction is currently employed to remove CO impurities down to a few ppm, however platinum catalysts require more complete removal to ensure longevity.² The activity of supported Au catalysts for CO oxidation make them a viable solution for CO removal at low concentrations if placed upstream to the Pt catalyst.^{2,8}

Investigations into the source of the high activity for Au have demonstrated that, while unsupported Au powder is active for CO oxidation, the highest activity is observed for supported AuNPs.¹² Analysis of kinetic and adsorption data suggests that both the decreased size of AuNPs afforded through dispersion over the support, as well as a strong interaction between the support and the AuNP at the Au/oxide interface are responsible for the observed enhancement of activity in the supported catalyst.¹² Regarding particle size, the increased number of sites of low coordination number at small particle sizes has been proposed by Norskov¹³ to explain the high activity, which maximizes in the size range of 2 – 5nm for supported AuNPs.^{2,5,14,15}

The large influence of support choice on observed catalytic activity further indicates its active role in the reaction. Active supports for CO oxidation are reducible, containing chemically available oxygen at the surface, and exhibit a strong metal-support

interaction (SMSI).^{2,6,16} A commonly used, active support for catalyst material preparation is titanium dioxide (TiO_2)^{14,17}, a reducible metal-oxide¹ that can sustain oxygen vacancy sites thought to facilitate O_2 dissociation and formation of chemically available oxygen at the surface.¹⁸ Dissociation of O_2 is a step necessary for CO_2 formation from gas phase O_2 under models following a Langmuir-Hinshelwood mechanism, such as the well-known Bond-Thompson model which involves separate adsorption of CO and O_2 on the catalyst followed by diffusion to the active site where reaction occurs to form CO_2 .^{1,19} In addition, the TiO_2 surface can sustain hydroxyl species, carboxylates, and water at the surface,^{20,21} all previously proposed to contribute to the mechanistic pathway.²² The presence of water vapor has been suggested to aid in the decomposition of stable carbonate species, which also are stable on the surface and form during the reaction.^{2,23,24} Hydroxyl coverage and carboxylate intermediates on the support, as well as the presence of an oxidized gold layer at the metal-support interface, play a significant role in the mechanism as proposed by Bond-Thompson.¹

1.4 Characterization of surface-bound species: FT-IR Detection

To study the CO oxidation mechanism using infrared spectroscopy, the binding of reactants at the surface and the nature of these binding sites must first be understood and characterized. Nanostructured Au/ TiO_2 contains a distribution of reactant binding sites owing to variations in surface morphology, surface-bound species, metal-support contact, and Au NP size described previously.²⁵ These variations in surface chemistry create a distribution of binding sites where these reactant species, including H_2O , CO, and O_2 , can

bind reversibly, in which the binding molecule adsorbs and desorbs unchanged from its initial state, as well as irreversibly, resulting in formation of complex compounds or decomposition into simpler adatoms at the surface.²¹ These species can be characterized by using vibrational spectroscopy to detect the vibrational signature of molecules at the surface, and this characterization of reactant binding, primarily CO, is the central goal of the work presented in this dissertation. This section provides the necessary background information required to interpret FT-IR spectra of these reactant species at the surface of Au/TiO₂ nanostructured catalysts.

1.4.1 Vibrational Spectroscopy Theory

The principal theory behind vibrational spectroscopy utilizes the model of bound atoms in molecules described as weights on a spring, typically called the harmonic oscillator model, in which the bond is represented by the spring and molecular vibrations are the spring motion. Bond stiffness is accounted for by the spring constant, k , where the restoring force necessary to return the bond to its equilibrium position (x_0) is given by equation 1.1.²⁶ Increasing bond stiffness, or k , increases the required force.

$$(1.1) \quad F = -k(x - x_0)$$

In the classical description of molecular vibration, displacement of the spring from the equilibrium position stores potential energy. During the vibration, potential energy is alternately converted to kinetic energy as the spring oscillates, existing completely in kinetic form when the bond returns to equilibrium position.

The potential energy function, $U(x)$, describes the stored potential energy and is derived by integrating the force, as shown by equation 1.2.²⁶

$$(1.2) \quad U(x) = - \int_{x_0}^x F(x)dx = \frac{1}{2}kx^2$$

True molecular vibration differs from spring motion in that it is governed by quantum mechanics. In the quantum mechanical description, the potential energy becomes quantized, and the value of the spring constant determines the energy level spacing and the curvature of this function. Using the harmonic oscillator approximation, quantum mechanical calculations include this potential energy function in the molecular Hamiltonian required to compute the vibrational energy level spacing using the Schrödinger equation.²⁶ The calculated energy spacing, given by equation 1.3, is the specific experimental variable probed during infrared experiments. For real molecules,

$$(1.3) \quad \Delta E = \hbar\nu$$

however, the potential surface is anharmonic and energy spacing is not equal. Vibrational spectroscopy measures the energy stored when a single photon of infrared light is absorbed by the molecule and promotes vibrational excitation from the vibrational ground state to the first excited state, an event known as the fundamental vibrational transition. At the temperatures probed in these cryogenic experiments, below 90 K, it is expected that all molecular transitions arise from the ground state and that the fundamental transition is exclusively measured.

The relationship between vibrational frequency (ν), reduced mass of the molecule (μ), and spring constant is given by equation 1.4, demonstrating the effect of mass

$$(1.4) \quad \nu = \frac{1}{2\pi} \sqrt{\frac{k}{\mu}}$$

exchange in the vibrational frequency. In the simplest case of a diatomic molecule, increasing the mass of one atom through isotope exchange only increases the molecular reduced mass with no effect on the spring constant, and in turn lowers the observed vibrational frequency of the fundamental transition. Vibrational spectroscopy utilizes these relationships, often employing isotopic labeling, to interpret the observed peaks in the spectra.

1.4.2 FT-IR detection of molecular vibration

In a transmission spectroscopy experiment measuring infrared absorption, incident light from the infrared source (I_0) passes through the sample, and species in the beam path exhibiting vibrational transitions that satisfy the selection rules for vibrational excitation absorb specific frequencies of the light, while the remaining frequencies in the infrared beam (I) pass through the sample and reach the detector. Absorbance is defined as the negative logarithm of the ratio of final to initial to beam intensity (transmittance), and is predicted by Beer's law as having a linear dependence on sample path length (l), concentration or number density of oscillators (N), and attenuation cross section (σ), as shown in equation 1.5.²⁷

$$(1.5) \quad A = \sigma l N$$

The work here utilizes a specific type of detection to probe molecular vibrational frequencies, Fourier Transform Infrared Spectroscopy (FT-IR). Analysis with FT-IR provides the ability to simultaneously measure all frequencies, known as the multiplex advantage, by spatially overlapping all frequencies in the infrared region (400 – 4000

cm⁻¹) and Fourier transforming the signal to provide the transmission spectrum.²⁷ This technique affords faster acquisition, increased resolution, and higher signal to noise ratio than dispersive techniques,²⁷ making it suitable to distinguish between the different species that exhibit similar spectral signatures at low signals on surfaces of Au/TiO₂ catalysts.

1.4.3 Detection of molecules on TiO₂ and Au/TiO₂ surfaces

Adsorption of gas-phase species can change the electronic structure of the molecule due to electron acceptance/donation at the surface, altering the spectral signature of the molecule.²¹ Detection requires that the molecule have a nonzero transition dipole moment along the axis of oscillation of the electric field of the incoming infrared light.²⁶ For some species, such as O₂, modes that are infrared inactive in the gas phase become active upon adsorption due to breaking of molecular symmetry upon binding to the surface, and enable detection at the surface. Oxygen can acquire a negative charge upon surface adsorption to Ti³⁺ centers on the TiO₂ surface, with a vibrational signature of 1180 cm⁻¹ for superoxide form.²¹ The activation and detection of vibrational frequencies of surface-adsorbed species is illustrated for the similar case of the CO molecule adsorbed over TiO₂ in *Figure 1.3*, showing the interaction between the electric field of the infrared light and bound CO at the oxide surface.

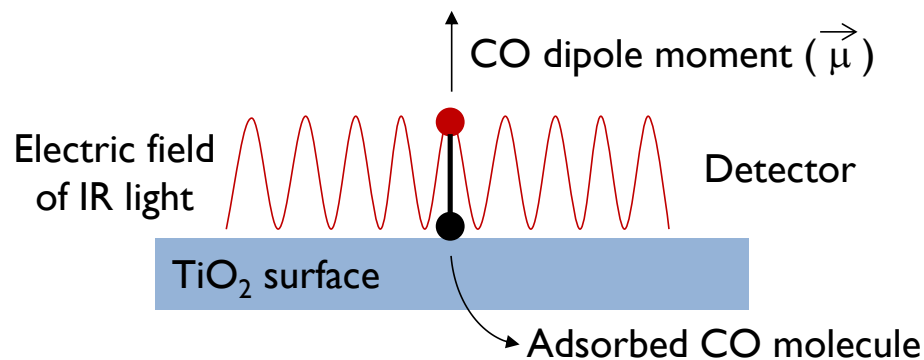


Figure 1.3. Diagram illustrating electric field of infrared light interacting with adsorbed molecule dipole moment.

Reversible binding of CO, the main focus of the studies presented here, allows for probing of the different types of surface sites on the oxide support and gold NP surface. Chemically unique CO binding sites on Au/TiO₂ and TiO₂ surfaces are detected by adsorption-induced shifts from the reference CO vibrational frequency, observed in the gas phase at 2143 cm⁻¹.^{28,29} The shift arises from a change in the CO bond order occurring when CO adsorbs to a metal, in which binding occurs carbon-end-on through a synergistic interaction between sigma donation to the metal and electron acceptance from the metal into the pi anti-bonding orbital of the CO.^{28,29} This back-bonding is easily understood by considering the molecular orbital diagram of CO, provided in *Figure 1.4*, which illustrates the antibonding LUMO for CO into which electrons are accepted upon bonding to the surface. While these interactions typically cause a red-shift, in particular for neutral species or late transition metals such as Au where there is increased pi back-bonding character, carbonyls formed with cationic species such as Ti⁴⁺ appear blue-shifted in the spectra, mainly due to electrostatic polarization of the CO bond in the field of the cation.²⁸ The HOMO is also slightly antibonding, so sigma donation may also

contribute slightly to blue-shifting the frequency, however polarization of the CO bond is believed to be the main contributor of this effect. The range of CO bands formed from reversible adsorption in this system is $2000 - 2200 \text{ cm}^{-1}$.²¹

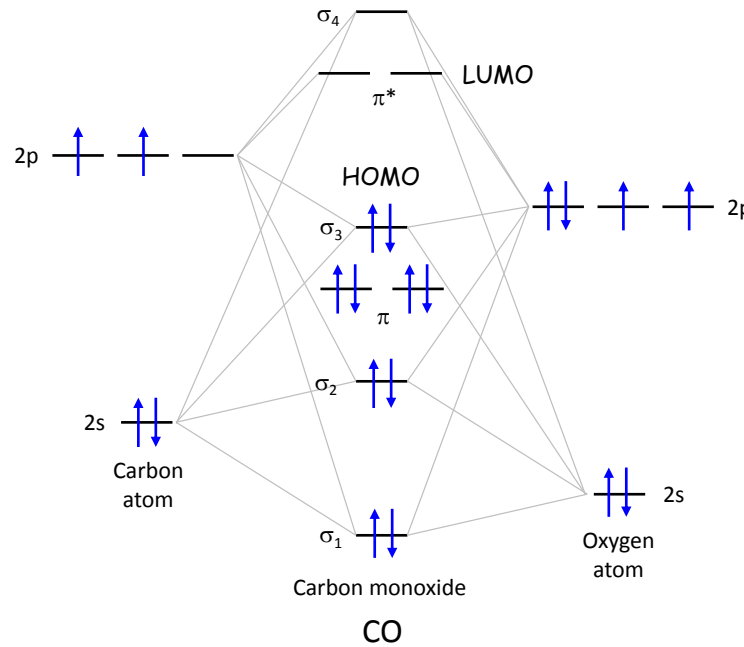


Figure 1.4. Carbon monoxide molecular orbital diagram illustrating HOMO and LUMO

When CO binds irreversibly to the metal oxide and reacts with surface hydroxyl groups, oxygen, and coordinatively unsaturated surface cations, carbonate and carboxylate species form on the surface which result in complicated, overlapping vibrational bands in the spectral region of $1000 - 1700 \text{ cm}^{-1}$.²¹ Carboxylate and formate surface groups have two active modes in the IR caused by a symmetric stretch and antisymmetric stretch of the O-C-O bond. The C-H stretch of the formate is also noted in the spectra, in the region of $2800 - 3000 \text{ cm}^{-1}$. These species are proposed side products from the CO oxidation reaction, and as previously mentioned, several groups have shown

that they break down in the presence of water.^{2,23,24} Activity studies have demonstrated enhanced activity of Au/TiO₂ catalysts with the presence of atmospheric water under reaction conditions,³⁰ and breakdown of these species may explain this trend. Carbonate groups can also form over the surface, and can exist with a varied degree of coordination to surface oxygen.²¹ The free carbonate ion has two modes in the region of 1000 – 1700 cm⁻¹ resulting from the symmetric and antisymmetric stretch, and the symmetric mode becomes active when ions are associated or physisorbed with the surface.²¹ When coordinated to surface oxygen, the antisymmetric stretch splits into two bands which are separated by about 100 cm⁻¹ for the monodentate species and 300 cm⁻¹ for the bidentate species.²¹ These species are more stable than carboxylate and bicarbonate groups, and have been proposed by Overbury and others^{23,24,31} to be potential catalyst poisons, formed by reaction of the CO₂ product at the surface.

In addition to carbon and oxygen species, the surface of titanium dioxide also contains hydroxyl groups arising from the breakdown of water on the surface when exposed to atmosphere.^{20,21} These hydroxyl species can be associated and linked by hydrogen bonds, or isolated. By detecting the frequency of the OH stretching vibration, we can identify the nature of these groups on the surface. Isolated Ti-OH groups appear as sharp features in the spectra, and are located at 3600-3800 cm⁻¹, whereas associated Ti-OH groups or undissociated water appear as red-shifted, broad features in the region of 3200-3600 cm⁻¹.^{21,32}

1.4.4 Coverage effects on vibrational spectra of surface-bound molecules

As described in the previous section, the vibrational frequency of a single adsorbed molecule on the surface undergoes a shift from the natural frequency observed in the gas phase molecule. When many molecules adsorb to the surface in close proximity, additional shifts occur in the vibrational frequency due to dipole-dipole coupling effects, the coupling that occurs between nearby oscillators as coverage is increased.³³ These effects have been predominantly studied on single crystal metal surfaces,³⁴⁻³⁶ where oscillators can exist in large groups on extended planar surfaces; however, researchers have also shown these effects to be significant in the spectra of adsorbates bound over nanocrystalline samples such as Au/TiO₂.^{33,37} Nanocrystalline surfaces are multifaceted, where coupling of many adsorbates over large areas is not as prominent as over single crystal surfaces, however it is important to understand these effects exist when interpreting some of the spectra presented in this dissertation, so a brief explanation is provided here.

Coupling shifts can be broken down into two separate components, static and dynamic dipole-dipole interactions. Static interactions, also known as chemical shifts, arise from changes to the bonding electrons of the adsorbate as a result of like molecules adsorbed in close proximity to the site. When many adsorbates are bonded in close proximity, the electrons involved in bonding at the surface can be influenced, resulting in changes to the spatial distribution and energy levels. In the case of CO, high coverage can alter the amount of electrons available for pi-backbonding at the surface. Additional sources of chemical shifts include orbital overlap of oscillators and changes to the work

function of the surface as coverage increases.^{33,34} The effect of chemically-induced shifts on adsorbed CO has been shown to be primarily a red-shift in the observed frequency, as compared to the singly adsorbed molecule.^{35,36} This chemical shift is expected to be less significant for wide band-gap semiconductor materials such as TiO₂ relative to metal crystals. For CO bound to cationic centers on the TiO₂ surface, the electrons involved in bonding are expected to be more localized due to the reduced communication of electrons between surface sites through the metal oxide. In metal crystals, electron movement is expected to be more facile and delocalization occurs more readily, contributing more to this effect.

Dynamic dipole-dipole coupling is mechanistically different from static coupling, and stems from the coupled vibrational motion of grouped oscillators. These interactions arise from coupling between oscillators of equal or similar vibrational frequency (within 10% of the single oscillator frequency), with the strongest effects for oscillators located within a distance of 2 nm.³³ In the simplest model in which all oscillators vibrate at the same frequency, these coupled oscillations produce two different modes of vibration, one in which all the oscillations are in-phase, and one where all oscillations are out-of-phase. The in-phase mode causes a blue-shift of the vibration, whereas the out-of-phase mode redshifts the collective frequency to a lower wavenumber than the single oscillator. This splitting of the modes is very similar to the traditional model of splitting described for degenerate energy levels in perturbation theory of quantum mechanics. For oscillators with modes of equivalent energy, only the high frequency, in-phase mode is observed. In the limit that only two oscillators are present, this mode appears with twice the intensity

of the single oscillator. The low frequency, out-of-phase mode is infrared inactive, as the total change in dipole moment is cancelled by the opposing motion of the oscillators. However, in the case for similar, but not exact oscillators, both the high and low frequency modes are active and the splitting of the modes is reduced as the energies are not quite degenerate. For this case, intensity is transferred to the higher frequency mode, and the low frequency mode is only weakly active.³³ The overall effect of dynamic coupling is most often a blue-shift in the observed frequency at higher coverages, although this effect is often overcompensated by the dominating red-shift occurring as a result of chemical shifts described above.³⁴ While these considerations are important in the characterization of adsorbates on surfaces using infrared spectroscopy, the nanocrystalline surfaces of the Au/TiO₂ and TiO₂ surfaces studied in this work are rough, and the effect of dynamic coupling should be diminished in comparison to smooth surfaces such as single crystal planes. This is based on the trend that maximum coupling of the oscillators requires similar orientation in close proximity,³³ and these large domains are less likely over rough surfaces.

1.5 Previous spectroscopic studies of CO binding at TiO₂ and Au/TiO₂ surfaces

The surface of Au/TiO₂ available for CO interaction is strongly determined by the sample preparation method, pre-treatment of the surface prior to CO exposure, and experimental conditions at which CO binding is measured. There is a long history of using infrared spectroscopy to probe the interactions of CO at the surface of nanoparticulate TiO₂,^{32,38-44} as well as over the surface of nanostructured

Au/TiO₂.^{17,19,25,45-51} Spectroscopic assignments for CO adsorption over the titanium dioxide support sites are generally agreed upon,^{32,38-44} however controversy remains in the frequency assignment of CO adsorption at gold sites of specific oxidation states (Au⁰, Au⁺, and Au³⁺) and surface morphologies (step, face, or interface sites)^{47,51} due to the aforementioned contributions to binding-site chemistry.

Techniques for catalyst preparation and subsequent pretreatment of the sample prior to CO exposure can affect the surface chemistry of binding sites due to changes in metal-support contact and the size of supported nanoparticles obtained from the synthesis, as well as create differences in the oxidation state of surface sites.^{1,52} The population of chemically unique CO binding sites over the nanostructured surface has also been shown to be dependent on the crystalline phase (anatase vs. rutile) of the TiO₂ particles.^{53,54} Preparation of Au/TiO₂ materials for FT-IR studies is commonly accomplished by impregnation (IMP), deposition-precipitation (DP) or co-ppt (CP) methods which rely on precursor materials for the metal and/or the support.¹⁴ Subsequent heating in air at 473 – 673 K (calcination) drives nucleation of the gold species into metallic NPs, a step also concomitant with an increase catalytic activity.⁵⁵ However, calcination conditions can cause sintering and loss of AuNP structure at reported temperatures as low as 473 K.⁵⁶ The mobility of the Au at the surface is non-negligible in this temperature range owing to the reduced melting point of nanometer-sized Au where quantum size effects begin to dominate.¹⁴ Heating samples prior to CO exposure is also employed to remove surface-bound species and free sites for CO binding.^{45,48} The Boccuzzi^{37,47} and Hadjivanov⁴⁸ groups have focused on the effects of surface heating

prior to CO exposure on binding-site populations; however this process remains poorly understood.

Studies of sample pretreatment effects on binding also include effects of oxidation state changes following exposure to O₂ or H₂ at various temperatures.^{48,50,51,56,57} Exposure to reductant,^{17,58} oxidant,⁵⁰ water,^{22,59} or heat under vacuum⁴⁸ have given rise to markedly different results in the observed profile of binding sites over the support as well as the AuNPs. Although calcination is expected to produce metallic gold species,¹ Hadjivanov proposed that the Au oxidation state of as-synthesized Au/TiO₂ *via* the DP method is cationic (Au³⁺) in nature and is easily reduced to monovalent Au⁺ under mild, ambient conditions or exposure to CO.⁴⁸ In general, adsorbing to more highly oxidized surfaces results in a larger blue-shift from the frequency of gas-phase CO, since the Lewis acidity of the binding sites is higher.²⁹ A range of assignments are reported for cationic^{48,56} bands (CO-Au⁺) from 2151-2174 cm⁻¹, and neutral^{19,45,47-50,55,60} bands (CO-Au⁰) from 2098 – 2130 cm⁻¹. Behavior of these bands during evacuation of the CO vapor after adsorption and when warming the surface after adsorption indicates that surface coverage effects of both adsorbed CO and hydration also can influence band position.^{32,37,48} In general, however, the literature indicates that most researchers observe an intense band at 2100 to 2110 cm⁻¹, which is assigned to CO on metallic gold (Au⁰). These effects of sample preparation are crucial to consider in the study of CO adsorption on supported gold catalysts due to the importance of oxidation state considerations and metal/support contact, and are especially relevant to the study of the active site as proposed by Bond-Thompson.¹

In addition to reversibly-bound CO studies, assignments for carbonate and carboxylate species formed from irreversible binding of CO to the surface and as intermediate oxidation products have also been proposed by researchers,^{19,21,23,31} in an attempt to characterize all species present on the surface of the catalyst during the oxidation reaction. Specific bands have been assigned by several groups, and an overview of the ranges of these assignments are provided in Table 1.^{19,21,23,31} In general,

Table 1.1. Assignments of bands due to carbonate and carboxylate species bound to TiO₂ and Au/TiO₂ surfaces

species	band assignment (cm ⁻¹)	
	carboxylate / formate	$\nu_s(\text{OCO}^-)$ 1350 - 1420
carbonates	$\nu_s(\text{CO}_3^{2-})$	$\nu_{as}(\text{CO}_3^{2-})$
non-coordinated carbonate	1020 - 1090 (IR inactive)	1415 no splitting
monodentate carbonate	1040 - 1080	1300 - 1370 1430 - 1530
bidentate carbonate	1020 - 1030	1250 - 1291 1527 - 1590
bridged carbonate	980 - 1020	1135 - 1180 1700 - 1570

species formed from the irreversible reaction of CO with the surface appear to be mechanistically relevant, and as a result, spectral changes in this region that occur when studying CO and O₂ binding at the surface are important to track for a more complete understanding of the surface interactions that occur during CO oxidation.

1.6 Cryogenic spectroscopy studies under vacuum

In previous investigations, CO binding over bare TiO₂ nanocrystals has been primarily measured under conditions of static CO pressure and at temperatures between room temperature,^{32,40,41,61} down to 77 K.^{43,44} A similar temperature range has been sampled in past studies of CO binding at the surface of Au/TiO₂ samples, also under

static equilibrium pressure.^{19,45,48,50-52,56,59,62-64} Under equilibrium pressure conditions, weakly-bound surface species can be in equilibrium with the gas phase so that empty binding sites are continuously replenished and are observed experimentally, in addition to more stably-bound species.^{18,65-67}

Cryogenic, spectroscopy studies *in vacuo* offer a simpler picture of binding at nanostructured surfaces, in which surface-bound CO is in contact with a dynamic gas phase. Weakly bound species that have a non-negligible probability of being found in the gas phase will be quickly pumped away before surface re-adsorption can occur, and thus will not be observed experimentally. Gas adsorption under vacuum conditions is temperature dependent, and the desorption threshold defines the temperature at which there is sufficient thermal energy to promote the dissociation of surface-bound species. Under these conditions, only binding sites that are well below the desorption threshold at a given temperature are observed.⁶⁸ This suggests that reducing the CO vapor pressure during CO binding should provide additional clarification of absorption bands, and indicate which species are thermodynamically stable in absence of the CO bath. In addition, the ability to probe CO binding at temperatures as low as 40 K serves to remove as much thermal energy from the surface as possible without condensing all CO into a frozen matrix, which occurs below 40 K.

Preliminary studies for this work were conducted under direct adsorption conditions, with reactant species deposited on the surface using helium as a carrier gas in absence of the cryogenic matrix. These studies provide the picture of binding for species observable without added stabilization of an inert matrix, conditions which are described

in detail below in Section 1.6.2. Direct adsorption studies of CO and O₂ at 40 K under high vacuum conditions (10⁻⁸ to 10⁻⁵ Torr) on the surfaces of the bare TiO₂ support are studied in parallel to deposition on the supported Au catalyst so that binding sites on the AuNPs can be characterized and identified separately from sites on the support. Comparison of these results to binding under equilibrium pressure (1 Torr CO) at 90 K enables differentiation between weakly-bound species observed only in the presence of a static CO gas phase and those that exist in stable potential wells and are observed under vacuum conditions. This section describes the theory behind adsorption studies of CO initially bound at 40 K and warmed incrementally while monitoring the thermal evolution of spectral bands. In addition, it discusses the basis and proof-of-concept for matrix-isolated reactant studies over the surface of the nanostructured catalyst.

1.6.1 Mapping the potential energy surface: temperature studies

The population of binding sites observed after deposition at 40 K provides a picture of the low energy PES of CO sites present on TiO₂ and Au/TiO₂ under vacuum conditions. The relative stability of these binding sites can be understood by observing the trends in the binding-site population while warming the surface from 40 to 150 K, which promotes population transfer over thermally accessible barriers and desorption from sites of lower stability. The PES of binding can be described by a series of potential wells of varied depths that correspond to chemically unique sites of varied adsorption enthalpy, ΔH_a . As thermal energy is provided to the system during warming steps, population is removed from shallow wells and transferred to binding sites of greater

stability, described by deeper potential wells. Tracking the thermal evolution of spectral bands following deposition as the surface is warmed allows for a careful study of the PES. Heating of the sample causes molecules in less stable sites to mobilize or desorb, so that temperature dependent changes in the spectra can be interpreted similarly to temperature programmed desorption (TPD) results. Traditional TPD studies involve heating a reactant-covered surface to promote desorption, followed by detection of products in the gas phase using a mass spectrometer.⁶⁷ Redhead⁶⁸ has developed a model for interpretation of data acquired in this way, where the binding energy of surface-bound molecules can be calculated based on the temperature of desorption into a vacuum, provided additional parameters such as temperature ramp rate and rate constant (predicted from reaction order) are known. This model assumes no equilibrium between the gas-phase and surface-bound species, and a negligible probability for re-adsorption.⁶⁵ Similarly, in the adsorption experiments presented here, reactant species were deposited on the sample and subsequent heating of the surface was used to drive the desorption of species into vacuum from chemically unique binding sites. An additional assumption required for the use of this model to calculate binding energies in this way is that dissociation from the surface is barrierless. This analysis is based on a kinetic model (in which species at the surface are desorbed into vacuum without reaching equilibrium with the gas phase) and predicts only the activation energy, not the binding energy specifically.

While the gas-phase products are not monitored in these experiments, the population at each chemically unique binding site is monitored *via* the vibrational

signature of the reactant in particular binding sites. Analysis of shifts in band intensity and position with increasing surface temperature can provide an estimation of the relative binding energies, which follow a linear dependence on desorption temperatures according to the Redhead formula, provided in equation 1.6.⁶⁸ Assuming first-order desorption of

$$(1.6) \quad \frac{E}{R*T_D} = \ln\left(\frac{v_1*T_D}{\beta}\right) - 3.64$$

CO and a typical value of 10^{13} for the rate constant v_1 , binding energies should have a linear dependence on desorption temperature and fall roughly in the range from 10.8 to 42.1 kJ/mol for desorption temperatures ranging 40 K to 150 K and a heating rate, β , of 5 K/min. Application of this Redhead analysis to spectra collected after deposition and during surface warming steps reveals details about the binding energies of the binding-site population and elucidates quantitative features of the potential energy surface for CO binding, such as barrier heights and well depths. This model is used to interpret spectra presented throughout this dissertation.

1.6.2 Using cryogenic matrices to observe pre- and post-reactive complexes

In addition to monitoring binding at the surface under vacuum conditions, the interactions of CO and O₂ at the surface of Au/TiO₂ and pure TiO₂ samples were also studied in the presence of a cryogenic argon matrix deposited over a thin-film of catalyst in a newly developed spectroscopic technique by the Moore group, coined Interfacial Matrix Stabilization Spectroscopy (IMSS). This unique application of matrix isolation employs energy-dissipating matrices, creating conditions which “trap” weakly-bound species at the catalyst interface, and the evolution of vibrational bands during matrix

warming steps (annealing) is tracked with FT-IR to obtain structural information of reactive intermediates.

The general theory behind matrix isolation is that properties of reactive species can be measured while isolating the species and preventing decomposition or reaction, a process most advantageous for transient, short-lived species.⁶⁹⁻⁷⁴ Our catalytic mechanism studies aim to identify the pre- and post-reactive complexes along the reaction coordinate, expected to be transient in nature and making matrix isolation an ideal technique for the study of CO oxidation over supported AuNPs.⁷⁵ The reactant molecules, including CO and O₂, are deposited as a mix with the matrix gas which then freeze upon contact with the cooled catalyst sample, creating a layer of isolated reactants above the catalyst. Annealing steps promote transport of these species down to the catalyst interface as the matrix is warmed and the species become mobile. Subsequent cooling of the matrix back to freezing temperatures allows for spectroscopic observation of the species formed from the interaction of reactant molecules at the catalyst interface which are stabilized by the matrix.

Matrix experiments can be modified in several ways to capture species formation at the catalyst surface, including initial saturation of one reactant at the surface in absence of the matrix, followed by isolation of the second in a frozen matrix above the catalyst. Annealing promotes transport of the second reactant down towards the surface where formation of pre- or post- reactive complexes can occur. This effectively separates the two reactant molecules, and allows for temperature-controlled formation of complexes. An example of this type of IMSS experiment is illustrated in *Figure 1.5*, in which O₂ is

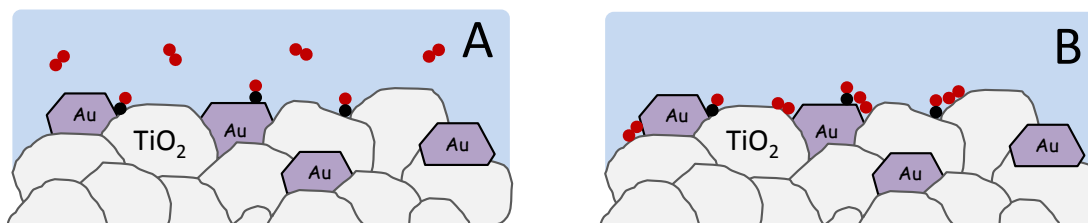


Figure 1.5. Schematic illustration of IMSS technique for O_2 in argon matrix coated over CO-covered Au/ TiO_2 surface after A) matrix deposition (isolation of CO and O_2 reactants) and B) matrix annealing (transport of O_2 and stabilization at CO-covered catalytic interface).

isolated in an argon matrix and deposited as a layer over the CO-saturated Au/ TiO_2 (Fig. 1.5A). The O_2 remains separated from the CO and catalyst surface until interaction is promoted *via* annealing steps, as illustrated in *Figure 1.5B*. The work presented in this dissertation develops the ideas needed to interpret IMSS spectra for the characterization of species formed between CO and O_2 at the Au/ TiO_2 surface.

1.7 Dissertation Overview

The structure of this dissertation begins with a description of the instrumentation used to acquire FT-IR spectra in Chapter 2, which also includes a description of all experimental methods. Studies began by assessing CO binding over the bare TiO_2 support material used in the absence of a cryogenic matrix and are presented in Chapter 3. Included in this chapter is the method development for obtaining a profile of the PES, acquired from fitting temperature-dependent spectra. Here CO binding over the oxide was studied under vacuum conditions (10^{-3} to 10^{-8} Torr) at temperatures ranging from 40 K to 150 K. An expanded study of CO binding over the TiO_2 under vacuum is described in Chapter 4, where the effects of sample processing and experimental parameters on the

observed binding site profile are explored in detail. The dependence of site population on CO exposure and dosing rate is explored. In Chapter 5, the knowledge gained from CO adsorption studies over TiO₂ is used to understand CO adsorption over Au/TiO₂ surfaces. This chapter mainly focuses on the development of a sample preparation method, as well as the identification and characterization of the spectral signature for CO binding to AuNP sites. For these studies, CO adsorption was characterized over Au/TiO₂ under vacuum conditions (10^{-5} to 10^{-8} Torr) at temperatures between 40 and 150 K.

Following characterization of CO binding over both TiO₂ and Au/TiO₂ under vacuum conditions, CO adsorption over both surfaces under steady state conditions was explored in the temperature range of 90 to 150 K. These studies, the focus of Chapter 6, were conducted to provide insight the effect of equilibrium pressures on the binding site profile and help to indicate the relative stability of adsorbed CO bound under the vacuum conditions explored in the first several chapters. Once the adsorption of CO over the surfaces of both TiO₂ and Au/TiO₂ were explored, the research was extended to include studies involving adsorption of both CO and O₂ under vacuum conditions. These investigations were conducted in preparation for adsorption studies in the presence of a cryogenic matrix, and a summary of the findings from these experiments is presented in Chapter 7. In Chapter 8, proof-of-concept for the IMSS technique is developed and presented. This includes verification of matrix-controlled transport of CO to the catalyst/matrix interface, stabilization of weakly-bound species at the interface, and stabilization of transient species formed at the matrix/catalyst interface.

Finally, Chapter 9 provides a summary of the most significant conclusions and describes the future directions for the continuation of this project. This chapter includes isotopic studies, the addition of experimental design modifications, and application of additional, complimentary sample characterization techniques. In closure, an experimental plan is given for moving forward with these ideas.

1.8 References

- 1 Bond, G. C.; Thompson, D. T., *Gold Bull.* **33**, 41-50 (2000).
- 2 Heiz, U.; Landman, U., Eds.; *Nanocatalysis*; Avouris, P., Bhushan, B., Bimberg, D., von Klitzing, K., Sakaki, H. and Wiesendanger, R., Eds.; Nanoscience and Nanotechnology; (Springer-Verlag: Berlin, 2007).
- 3 Anderson, J. A.; Fernández Garcia, M.; *Supported Metals in Catalysis*; Catalytic Science Series (Hackensack, NJ: London, 2005) Vol. 5.
- 4 Laidler, K. J.; King, M. C., *J. Phys. Chem.* **87**, 2657-64 (1983).
- 5 Bond, G. C.; Thompson, D. T., *Catal. Rev.* **41**, 319-388 (1999).
- 6 Goodman, D. W., *Catal. Lett.* **99**, 1-4 (2005).
- 7 Haruta, M.; Kobayashi, T.; Sano, H.; Yamada, N., *Chem. Lett.* **16**, 405-408 (1987).
- 8 Jacobs, G.; Patterson, P. M.; Williams, L.; Chenu, E.; Sparks, D.; Thomas, G.; Davis, B. H., *Appl. Catal., A* **262**, 177-187 (2004).
- 9 Twigg, M. V., *Catal. Today* **117**, 407-418 (2006).
- 10 Twigg, M. V., *Appl. Catal., B* **70**, 2-15 (2007).
- 11 Twigg, M. V., *Catal. Today* **163**, 33-41 (2011).
- 12 Iizuka, Y.; Tode, T.; Takao, T.; Yatsu, K.; Takeuchi, T.; Tsubota, S.; Haruta, M., *J. Catal.* **187**, 50-58 (1999).
- 13 Lopez, N.; Janssens, T. V. W.; Clausen, B. S.; Xu, Y.; Mavrikakis, M.; Bligaard, T.; Nørskov, J. K., *J. Catal.* **223**, 232-235 (2004).
- 14 Haruta, M., *Cattech* **6**, 102-115 (2002).
- 15 Widmann, D.; Behm, R. J., *Acc. Chem. Res.* **47**, 740-749 (2014).
- 16 Haruta, M.; Tsubota, S.; Kobayashi, T.; Kageyama, H.; Genet, M. J.; Delmon, B., *J. Catal.* **144**, 175-192 (1993).
- 17 Schumacher, B.; Denkwitz, Y.; Plzak, V.; Kinne, M.; Behm, R. J., *J. Catal.* **224**, 449-462 (2004).
- 18 Schubert, M. M.; Hackenberg, S.; Veen, A. C. v.; Muhler, M.; Plzak, V.; Behm, R. J., *J. Catal.* **197**, 113-122 (2001).
- 19 Bollinger, M. A.; Vannice, M. A., *Appl. Catal., B* **8**, 417-443 (1996).

- 20 Wendt, S.; Matthiesen, J.; Schaub, R.; Vestergaard, E. K.; Laegsgaard, E.; Besenbacher, F.; Hammer, B., *Phys. Rev. Lett.* **96**, 0661071-0661074 (2006).
- 21 Davydov, A. A.; Rochester, C. H. *Infrared Spectroscopy of Adsorbed Species on the Surface of Transition Metal Oxides* (Wiley: Chichester; New York; Brisbane; Toronto; Singapore, 1990).
- 22 Gao, F.; Wood, T. E.; Goodman, D. W., *Catal. Lett.* **134**, 9-12 (2010).
- 23 Clark, J. C.; Dai, S.; Overbury, S. H., *Catal. Today* **126**, 135-142 (2007).
- 24 Tanaka, K.; White, J. M., *J. Phys. Chem.* **86**, 4708-4714 (1982).
- 25 Meyer, R.; Lemire, C.; Shaikhutdinov, S. K.; Freund, H. J., *Gold Bull.* **37**, 72-124 (2004).
- 26 Atkins, P. W.; Friedman, R. S. *Molecular Quantum Mechanics*; (OUP, Oxford: 2011).
- 27 Johnston, S. F., *Fourier Transform Infrared: A Constantly Evolving Technology*; (Ellis Horwood: New York; London, 1991).
- 28 Khriachtchev, L. *Physics and Chemistry at Low Temperatures*; (Pan Stanford: 2011).
- 29 Blyholder, G. Molecular Orbital View of Chemisorbed Carbon Monoxide. *J. Phys. Chem.* **68**, 2772-2777 (1964).
- 30 Date, M.; Okumura, M.; Tsubota, S.; Haruta, M., *Angew. Chem. Int. Ed.* **43**, 2129-2132 (2004).
- 31 Denkwitz, Y.; Zhao, Z.; Hörmann, U.; Kaiser, U.; Plzak, V.; Behm, R. J., *J. Catal.*, **251**, 363-373 (2007).
- 32 Morterra, C., *J. Chem. Soc., Faraday Trans.* **84**, 1617-1637 (1988).
- 33 Hollins, P., *Adsorpt. Sci. Technol.* **2**, 177-93 (1985).
- 34 Dumas, P.; Tobin, R. G.; Richards, P. L., *Surf. Sci.* **171**, 579-99 (1986).
- 35 Ueba, H., *J. Electron Spectrosc. Relat. Phenom.* **44**, 37-46 (1987).
- 36 France, J.; Hollins, P., *J. Electron Spectrosc. Relat. Phenom.* **64-65**, 251-258 (1993).
- 37 Boccuzzi, F.; Chiorino, A.; Manzoli, M., *Surf. Sci.* **502**, 513-518 (2002).
- 38 Deiana, C.; Fois, E.; Coluccia, S.; Martra, G., *J. Phys. Chem. C* **114**, 21531-21538 (2010).
- 39 Cerrato, G.; Marchese, L.; Morterra, C., *Appl. Surf. Sci.* **70-71**, 200-205 (1993).
- 40 Hadjiivanov, K.; Lamotte, J.; Lavalley, J., *Langmuir* **13**, 3374-3381 (1997).
- 41 Yates, D. J. C., *J. Phys. Chem.* **65**, 746-753 (1961).
- 42 Hadjiivanov, K. I.; Klissurski, D. G., *Chem. Soc. Rev.* **25**, 61-69 (1996).
- 43 Zaki, M. I.; Knozinger, H., *Mater. Chem. Phys.* **17**, 201-215 (1987).
- 44 Martra, G., *Appl. Catal., A* **200**, 275-285 (2000).
- 45 Green, I. X.; Tang, W.; Neurock, M.; Yates, J. T., Jr., *Science* **333**, 736-739 (2011).
- 46 Boccuzzi, F.; Chiorino, A.; Tsubota, S.; Haruta, M., *J. Phys. Chem.* **100**, 3625-3631 (1996).
- 47 Boccuzzi, F.; Chiorino, A.; Manzoli, M.; Lu, P.; Akita, T.; Ichikawa, S.; Haruta, M., *J. Catal.* **202**, 256-267 (2001).
- 48 Venkov, T.; Fajerweg, K.; Delannoy, L.; Klimev, H.; Hadjiivanov, K.; Louis, C. *Appl. Catal., A* **301**, 106-114 (2006).

- 49 Liu, H.; Kozlov, A. I.; Kozlova, A. P.; Shido, T.; Asakura, K.; Iwasawa, Y., *J. Catal.* **185**, 252-264 (1999).
- 50 Dekkers, M.; Lippits, M.; Nieuwenhuys, B., *Catal. Lett.* **56**, 195-197 (1998).
- 51 Manzoli, M.; Chiorino, A.; Boccuzzi, F., *Surf. Sci.* **532**, 377-382 (2003).
- 52 Kung, M. C.; Davis, R. J.; Kung, H. H. *J. Phys. Chem. C* **111**, 11767-11775 (2007).
- 53 Yan, W. F.; Chen, B.; Mahurin, S. M.; Schwartz, V.; Mullins, D. R.; Lupini, A. R.; Pennycook, S. J.; Dai, S.; Overbury, S. H., *J. Phys. Chem. B* **109**, 10676-10685 (2005).
- 54 Beck, A.; Magesh, G.; Kuppan, B.; Schay, Z.; Geszti, O.; Benko, T.; Viswanath, R. P.; Selvam, P.; Viswanathan, B.; Guzzi, L., *Catal. Today* **164**, 325-331 (2011).
- 55 Schumacher, B.; Plzak, V.; Kinne, M.; Behm, R. J., *Catal. Lett.* **89**, 109-114 (2003).
- 56 Green, I. X.; Tang, W.; McEntee, M.; Neurock, M.; Yates, J. T., Jr., *J. Am. Chem. Soc.* **134**, 12717-12723 (2012).
- 57 Klimev, H.; Fajerweg, K.; Chakarova, K.; Delannoy, L.; Louis, C.; Hadjiivanov, K., *J. Mater. Sci.* **42**, 3299-3306 (2007).
- 58 Piccolo, L.; Daly, H.; Valcarcel, A.; Meunier, F. C., *Appl. Catal., B.* **86**, 190-195 (2009).
- 59 Boccuzzi, F.; Chiorino, A., *J. Phys. Chem. B* **104**, 5414-5416 (2000).
- 60 Grunwaldt, J. D.; Maciejewski, M.; Becker, O. S.; Fabrizioli, P.; Baiker, A., *J. Catal.* **186**, 458-469 (1999).
- 61 Garrone, E.; Bolis, V.; Fubini, B.; Morterra, C., *Langmuir* **5**, 892-899 (1989).
- 62 Boccuzzi, F.; Chiorino, A.; Manzoli, M.; Lu, P.; Akita, T.; Ichikawa, S.; Haruta, M., *J. Catal.* **202**, 256-267 (2001).
- 63 Grunwaldt, J.; Baiker, A. *J. Phys. Chem. B* **103**, 1002-1012 (1999.)
- 64 Henao, J. D.; Caputo, T.; Yang, J. H.; Kung, M. C.; Kung, H. H., *J. Phys. Chem. B* **110**, 8689-8700 (2006).
- 65 Masel, R. I. *Principles of Adsorption and Reaction on Solid Surfaces* (Wiley: New York, 1996).
- 66 Haruta, M., *Catal. Today* **36**, 153-166 (1997).
- 67 Gottfried, J. M.; Schmidt, K. J.; Schroeder, S. L. M.; Christmann, K., *Surf. Sci.* **536**, 206-224 (2003).
- 68 Redhead, P. A., *Vacuum* **12**, 203-211 (1962).
- 69 Ludwig, R. M.; Moore, D. T., *J. Chem. Phys.* **139**, 244202-244209 (2013).
- 70 Whittle, E.; Dows, D. A.; Pimentel, G. C., *J. Chem. Phys.* **22**, 1943 (1954).
- 71 Becker, E. D.; Pimentel, G. C., *J. Chem. Phys.* **25**, 224 (1956).
- 72 Jacox, M. E., *Chem. Soc. Rev.* **31**, 108-115 (2002).
- 73 Andrews, L., *Annu. Rev. Phys. Chem.* **22**, 109-132 (1971).
- 74 Ault, B., *Rev. Chem. Intermed.* **9**, 233-269 (1988).
- 75 Dunkin, I. R. *Matrix Isolation Techniques: A Practical Approach*; (Oxford University Press: Oxford; New York, 1998).

Chapter 2

Experimental methods and instrumentation

2.1 Introduction

This chapter describes the experimental methods and instrumentation used for preparation of samples and acquisition of data presented in this dissertation. A significant amount of work was devoted to development of sample preparation methods to create appropriate nanostructured material suitable for gas adsorption experiments under vacuum. The first section provides a complete description of these techniques, which begin with the preparation of support powder films. Samples that contain supported AuNPs were created from these prepared support samples *via* thermal de-wetting of an Au film over the support. In order to assess the effectiveness of the thermal de-wetting method, analysis with Transmission Electron Microscopy (TEM) was completed to verify the existence of AuNPs over the TiO₂ support. Specifics of instrumental settings and sample preparation for this analysis are provided here.

Following the description of sample preparation and characterization methods, a section is devoted to the instrumental apparatus designed to spectroscopically monitor gas adsorption on TiO₂ and Au/TiO₂ samples using FT-IR. Reagent gases used in these studies were prepared from stock gases that were mixed and delivered through a gas-delivery system, which feeds into a custom vacuum chamber. These studies required the design of a custom vacuum chamber containing a closed-cycle cryostat that is integrated with an FT-IR spectrometer. The full details of the gas-delivery system and

instrumentation included in the vacuum chamber are described in this section. In addition, a description of an auxiliary fixed-bed reactor that can be integrated into the spectrometer is also provided here. This apparatus is suitable for FT-IR analysis of CO conversion to CO₂ to assess the catalytic activity of the powder samples.

The work presented in this dissertation includes gas adsorption studies that were conducted under a variety of experimental conditions, including adsorption *in vacuo*, under steady-state pressure, and in the presence of a cryogenic matrix. A great deal of effort was put into experimental design to develop techniques to explore gas adsorption under these conditions, and these often required significant changes in the experimental procedure. The details of these procedures for analysis of gas adsorption under all three of these conditions can be found in Section 2.4.

The final section was included to provide the reader with some detail about the data processing and interpretation following the completion of an experiment. Measurement of powder samples coated on CaF₂ substrate using FT-IR presented complications to the data analysis, including low signal and vibrational bands due to CaF₂ impurities which appeared near the CO stretching region of the spectrum.

2.2 Sample preparation and characterization

2.2.1 Powder TiO₂ film preparation

The TiO₂ support samples used for exploration of CO adsorption studies presented in this dissertation were prepared by coating powder films over an IR-transparent substrate, using a method adapted from Yates.¹ The TiO₂ powder was coated

onto 1" diameter (2 mm width) salt windows (CaF₂, Koch Crystal Finishing) by flash evaporation of solvent from a suspension of TiO₂ NPs (Titanium (IV) Oxide, Aeroxide, P25; Acros Organics) in an acetone:water mixture (0.025 g/mL). The as-purchased P25 NPs have a BET surface area of 80 m²/g and comprised a ratio of 70:30 anatase:rutile structured crystal faces. The ratio of acetone:water mixture was varied between 10:1 and 1:10 depending on the particular experiment, and the specific ratio is indicated as appropriate. The suspension was then converted to a fine mist using an atomizer (Aldrich® chromatography sprayer) and sprayed onto windows that were placed in a heated custom aluminum mask (70 °C for 10:1 acetone:water; 110 °C for 1:10 acetone:water) to remove solvent.

The purpose of the aluminum mask was to coat the inner area of the window surface, and leave a 2-3 mm space of bare window around the perimeter of the coated side which was free of titanium dioxide powder. This enabled better thermal conductivity once the sample was installed in the cryostat sample holder, described in Section 2.3.1, as this portion of the window maintained direct contact with the annealed silver ring (Fig. 2.3). Aluminum masks consisted of two components, a base and a cover. The base contained cylindrical cutout(s) with a 1" diameter clearance at a depth of 2 mm to contain the window(s) during the spraying process. The cover fit over the base, and provided the protection of the window perimeter from contact with the powder during coating. An image of a representative mask capable of preparing 4 samples simultaneously is provided in *Figure 2.1*.

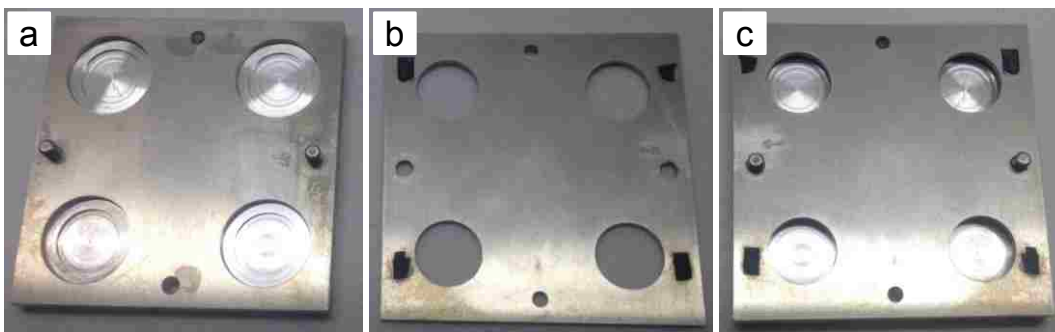


Figure 2.1. Image of aluminum mask used for coating CaF_2 windows with TiO_2 powder during spraying procedure: a) mask base, b) mask cover, and c) assembled mask.

The aluminum mask was heated by placing it on a hot plate. Obtaining the mass of TiO_2 coated on the windows was difficult due to changes in water coverage with temperature, as well as the small amount of TiO_2 powder that was coated during sample prep. Masses typically ranged from 0.0015 – 0.003 g. The amount of material coated on the CaF_2 windows was assessed by taring the windows prior to film deposition while the windows were hot, and measuring their mass after coating the window. Massing the windows while hot was important as water was given off by the windows during heating, which influences the measured mass. Additionally, cooling the windows with the TiO_2 film causes water adsorption at the surface, which is increased by the presence of the oxide coating given the high surface area of the NPs. Sample preparation was completed in-vacuo (10^{-8} Torr) *via* thermal processing at 400 – 700 K. This process allowed for the powder films, which were created under exposure to atmosphere, to be prepared for experimental use under high vacuum conditions in an effort to remove atmospheric contaminants. Thermal processing preceded direct adsorption experiments, which are described in detail in Section 2.3. While the set-point of the temperature was targeted at

the range mentioned above, imperfect thermal conductivity prevented the sample from reaching that temperature. Actual temperatures measured at the sample are indicated in relevant spectra.

2.2.2 Nanostructured Au/TiO₂ film preparation

For adsorption experiments on TiO₂ support samples containing AuNPs, nanostructured Au/TiO₂ films were created *via* thermal de-wetting (Chapter 5). For these samples, support films (prepared using the method described in Section 2.2.1) were coated with a 5 – 40 nm thick film of Au using an argon-plasma sputtering source (Polaron E5100). Masks, similar to those pictured in *Figure 2.1*, were used during the sputtering process as well to avoid coating the outside edge of the CaF₂ with sample. For some samples, a glass slide or rectangular piece of aluminum was placed over half of the opening of the mask cover to allow only half of the support material to be coated with AuNPs. Following deposition, the films were exposed to atmosphere during transfer of the samples from the sputtering source to the cryostat sample holder. The time between these two stages was typically on the order of several hours. Some samples were stored in a desiccator for several days or longer, in which cases these samples were stored to reduce exposure to atmospheric water vapor. For some experiments, the Au film was coated over the TiO₂ support material, which had been previously thermally processed and used in adsorption experiments. In these cases, details are provided as appropriate. Preparation of AuNPs from the Au film was completed *in-vacuo* (10⁻⁸ Torr) *via* thermal

de-wetting of the Au film at 400 – 700 K, prior to CO deposition. The actual temperatures measured at the sample are indicated in relevant spectra.

2.2.3 TEM characterization

Transmission Electron Micrographs were collected at various stages of the sample preparation of both TiO₂ and Au/TiO₂ samples to verify formation of AuNPs over the. Samples for TEM analysis were prepared by scraping the powder films from the CaF₂ window using a glass microscope slide. The powder was ground with the edge of a glass slide until fine and uniform in size, with no large pieces remaining. The powder was then coated onto a copper TEM grid using a holey carbon film mesh (SPI Supplies, 3630C-CF; Holey Carbon Coated Grids on 300 mesh copper, 3mm).

Sample analysis was conducted on a JEOL 1200EX electron microscope using an acceleration voltage of 120 KV. The microscope was equipped with a charge-coupled device (CCD) camera, and images were collected at a magnification of 120,000 – 300,000x. For comparison of images of varied magnification, images were scaled to 250,000x magnification using PowerPoint software by matching the scale bar size and maintaining original height and width aspect ratio of scaled images.

2.3 Instrumental Apparatus

2.3.1 Gas-delivery system

Prior to gas adsorption experiments, mixtures of reagent gas were prepared from stock gases. These reagents were stored, prepared, and delivered from mixing bottles that

are part of a gas rack system developed and customized for these experiments (*Figure 2.2*). Gas mixtures for each experiment were prepared at least 12 hours in advance to allow for complete mixing of the gases. Mix concentrations were determined by pressure dosing into an aluminum mixing bottle (aluminum is required to avoid contamination from $\text{Ni}(\text{CO})_4$ that would be formed during CO storage in stainless steel²). The low-pressure gauge shown in *Figure 2.2* is a piezo transducer pressure gauge (Kurt J Lesker; series 902 piezo transducer, M/N K9021113) capable of measuring pressures of 1 – 1000 Torr and is used to measure the amount of stock gas dosed into the evacuated mixing bottle. An additional low-pressure gauge was also connected to the system (not shown) which measured pressures of 1 – 1000 milliTorr (Kurt J Lesker; KJL-6000 pirani gauge) and was connected to a digital readout (KJL610TC, thermocouple display) to display the gas rack pressure when the gas rack was in the standard resting state, under vacuum. This gauge provided a measurement for how well the gas rack was maintaining vacuum, and indicated if any leaks were present. The gas rack is typically maintained at a pressure of <10 milliTorr using a roughing pump that ran continuously (Edwards XDS10 Scroll pump). The high pressure gauge is a Bourdon gauge (Swagelok, EN-837-1), capable of measuring up to 4 atmospheres (3040 Torr), and was used to monitor the pressure of the buffer gas while diluting the stock gas to its final concentration. Once reagent gas mixtures were prepared, they were delivered into the vacuum chamber through a mass flow controller (MFC, MKS 1179A01311CR1BV) capable of maintaining a constant flow of gas in the range of 1 – 10 sccm (standard cubic centimeters per minute) by use of a digital display controller (MKS 247D).

All gas lines up to the MFC were made from 1/4" stainless steel tubing (Allentown Valve and Fitting), aside from lines that connected the gas cylinders to the gas mixing and delivery rack, which were made of 1/4" copper tubing (Allentown Valve and Fitting). Downstream of the MFC, a reducing union converted the 1/4" diameter tubing to 1/8" diameter tubing. This arrangement allowed additional mechanical flexibility in the line to permit insertion of a cold trap. The cold trap was prepared by winding the 1/8" tubing into a coil which could be placed inside a Dewar flask filled with coolant. The purpose of this cooling bath was to trap impurities present in the gas mixtures, including CO₂, H₂O, and Ni(CO)₄, to prevent contamination of the sample surface during deposition. For all work presented, the Dewar flask was filled with a slurry of liquid N₂ and ethanol, which reaches a temperature of 157 K and is cold enough to trap the aforementioned species.³ The line exiting the cold trap was then further reduced to capillary tubing, and these deposition tubes were fed into the vacuum chamber. Additional details on the deposition lines and their integration into the vacuum system used for adsorption experiments are discussed below in Section 2.3.2.

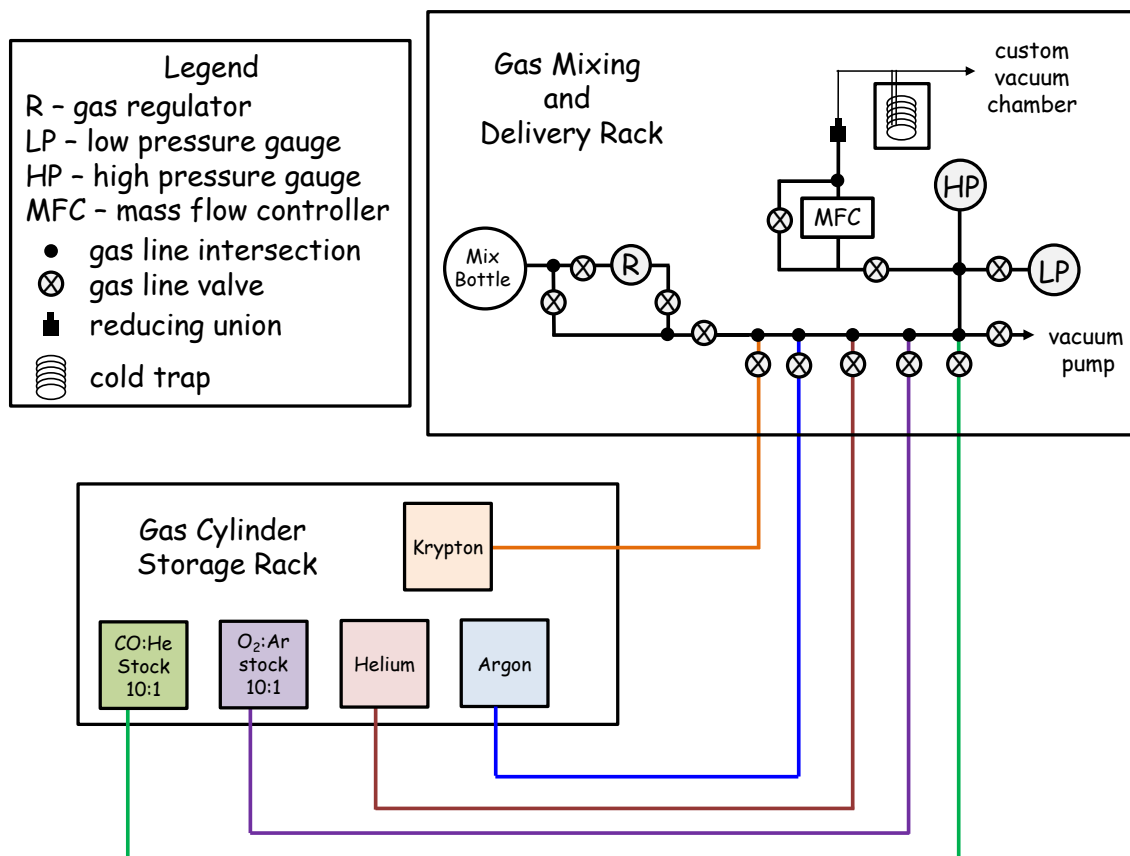


Figure 2.2. Schematic block diagram of gas storage, mix preparation, and delivery system for reagent gases used in adsorption experiments.

2.3.2 Custom vacuum chamber

Gas-adsorption experiments were performed inside a custom vacuum chamber, which is connected to the gas-delivery system. The vacuum chamber was maintained at a base pressure of 10^{-6} Torr with a turbo pump (BOC Edwards EXT 70H 24V) that was backed by a scroll pump (Edwards XDS10). The foreline connects the backing pump to the turbo pump, and is monitored with a high-pressure thermocouple gauge (Edwards ATC-E) connected to an 8-pin port (KJL-6000), capable of measuring pressures from $1 - 10^{-3}$ Torr. The fore-line pressure was maintained at 10^{-3} Torr by the scroll pump. The

pressure on the low-pressure side of the turbo pump was measured by an inverted magnetron pressure gauge (Edwards AIM-X-NW25) capable of measuring pressures from $10^{-2} - 10^{-9}$ Torr, and this gauge indicates the pressure inside the vacuum chamber. The system of vacuum pumps and pressure gauges was operated using a digital controller (Edwards D397-21-000) situated on a movable cart.

The main feature of the vacuum chamber is a commercially available two-stage, closed-cycle cryostat (Advanced Research Systems (ARS) DE-210SF), which is capable of cooling samples down to temperatures as low as 4 K. The operating principle behind the closed-cycle cryostat is a Gifford-McMahon (GM) refrigeration cycle, in which high-pressure helium (10 atm) is expanded isothermally and absorbs heat from the system. The refrigeration takes place in the expander, typically referred to as the cold-head, which is fitted with ports attached to high-pressure helium lines. These gas lines permit the flow of helium to and from a helium compressor (ARS-10HW Compressor), which is cooled using a water heat exchanger. A detailed schematic diagram of the cryostat instrumentation is provided in *Figure 2.3*.

Sample-coated windows were mounted inside a nickel-plated copper sample mount at the sample stage of the cryostat inside the vacuum chamber maintained at 10^{-6} Torr. An annealed silver ring was positioned inside the sample mount between each side of the CaF_2 window and copper mount to ensure proper thermal contact between the CaF_2 and the nickel, which was mechanically secured together using four screws (size 2-56). The sample mount was separated from the second stage of the cryostat by a high temperature interface, which contained a sapphire crystal to prevent damage to the cryostat when heating the sample at high temperatures (Fig. 2.3). The use of sapphire for

this application is advantageous as it exhibits a thermal conductor-insulator transition which enables high thermal conductivity at low temperatures, and excellent insulation at high temperatures.⁴ This feature is important for efficient cooling the sample to 4 K, and protection of the cryostat cold head and various stages during thermal processing of the sample above room temperature, such that the temperature of the second stage does not exceed 30 K during high temperature heating up to 800 K. To ensure cooling down to temperatures as low as 4 K, a nickel-plated copper radiation shield was attached to the first stage of the refrigerator which protected the entire second stage and sample mount from radiation which permeates into the system through heat transfer between gas molecule collisions with room temperature surfaces, even at the low operating pressure of 10^{-8} Torr.

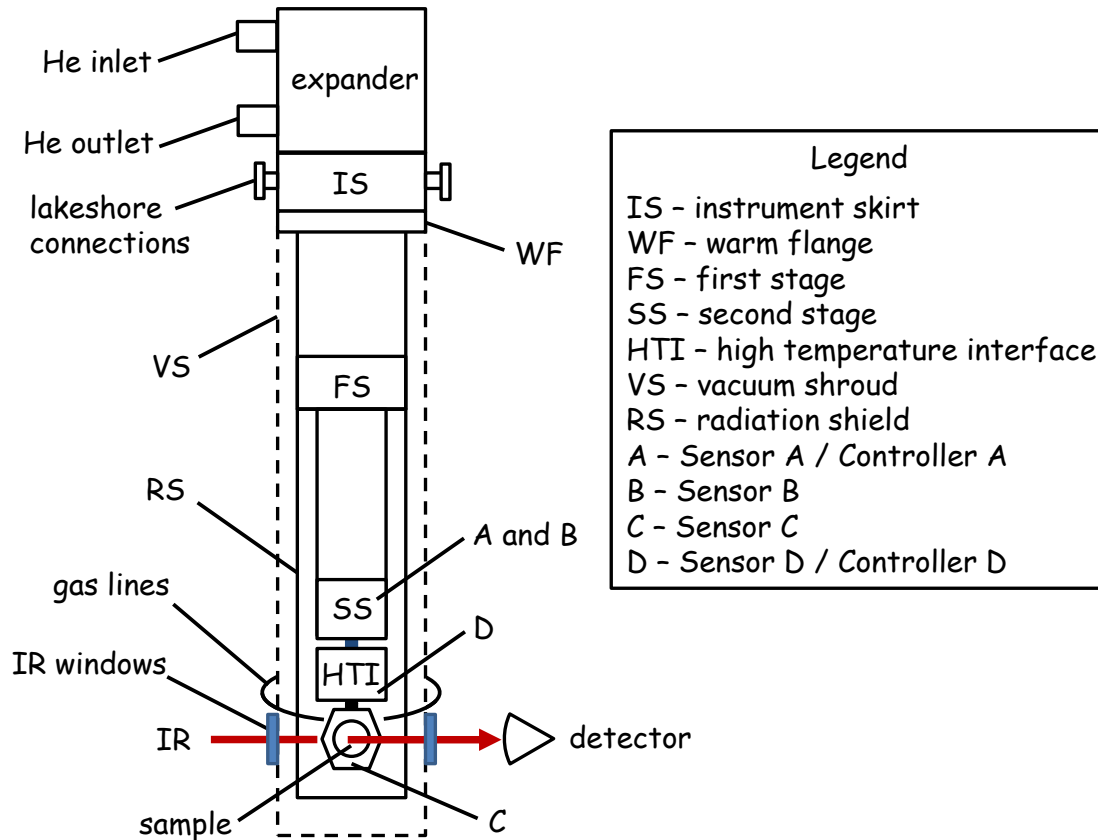


Figure 2.3. Block diagram of experimental apparatus used for direct adsorption experiments, including cryostat and custom vacuum chamber

A digital temperature controller (Lakeshore 336) enabled thermal control of the sample from 4 to 800 K. The controller was equipped with four temperature sensor inputs (labeled sensor A, B, C, and D), two of which were integrated with heaters connected to proportional-integral-derivative (PID) control loops and permit temperature adjustment in addition to measurement. The temperature sensors were fed into the vacuum system through electrical feed-through ports located on the instrument skirt (Fig. 2.3). Sensor A is a 25-V silicon diode situated on the first stage of the cryostat and was wired to one of the two control loops. The diode is wrapped under a band heater wrapped around the first stage, which was controlled by the control loop with the capability to

ramp the temperature up or down at a programmable rate (typically set to 5 – 10 K/min for the adsorption experiments discussed in this work). The operating temperature range of the silicon diode is 1.4 K to 500 K. Although the maximum operating temperature is 500 K, this is significantly above the operating temperature of the cold-head to which it is attached, which should not exceed 350 K. Sensor B, also a 2-V silicon diode, was a free length sensor that was typically is kept tucked away near the cold head due to the restriction of the operating temperature. It has the capability of being extended and attached to the sample mount if high temperature (>500 K) thermal processing is avoided. This feature is advantageous as it can read the temperature at the sample down to 4 K. Sensor C is a platinum sensor positioned near the sample on the sample mount, and can read the sample mount temperature in the range of 14 to 873 K. The fourth sensor, sensor D, is a type-E thermocouple with a maximum power of 50 W and controlled the high-temperature interface used to bake out the sample during thermal processing steps. The sensor was positioned on the sample side of the sapphire break, and was capable of measuring and controlling the temperature up to 850 K.

To enable the use of a standard spectrometer for FT-IR analysis, the spectrometer sample compartment was removed to accommodate samples held under vacuum. For these experiments, the vacuum chamber was positioned in the beam path of the spectrometer, and IR-transparent KBr windows on either side of the vacuum shroud were installed to permit the passage of IR light and allow for sample analysis. To substitute for the standard sample compartment lid on the spectrometer which maintains a nitrogen environment around the optics within the spectrometer, the space between the beam port and the KBr windows on the vacuum shroud were fitted with custom-built purge collars

to prevent contact with atmospheric gases. The entire cryostat was positioned on a translational stage, which allowed both vertical and horizontal translation of the sample window in the beam position. This feature was necessary for experiments in which different samples were coated on either half of the CaF₂ window. The cryostat could be moved in the beam path to permit analysis of either sample. All spectra were collected with a Nicolet 6700 FT-IR spectrometer employing a MCTA detector (0.5 – 2 cm⁻¹ resolution; averaged over 200 – 1000 scans). Data collection was completed using Omnic Software, version 8.3. A system for background spectra collection was developed to assist in data processing and interpretation, and the details for these procedures are described in Section 2.5.

2.3.3 *Fixed-bed flow reactor*

A fixed-bed flow reactor was designed to assess the catalytic activity of samples used in gas adsorption experiments. Reactants CO and O₂ were flowed over a powder sample supported on glass wool packed into a 1/4" quartz sample tube, and the output gas was monitored for CO₂ content using FT-IR. The sample tube was fit with Teflon ferrules that protected it from breakage while tightening the nuts to secure the tube into the reactor. The gas-rack delivery system contained a gas line that ran from the mass flow controller (MFC) to a fixed-bed reactor, enabling the flow of prepared gas mixtures into the reactor. The reactor is illustrated in the schematic diagram in *Figure 2.4*. The MFC maintained a constant flow of gas over the sample during the experiment; however, pressure was maintained in the reactor through use of a back pressure regulator (BPR) which isolated the reactor from the vacuum pump. The setting of the BPR determined

how much pressure was kept in the system, while the overflow was permitted to flow through and into the vacuum pump (diaphragm pump, Vacuubrand, MD4).

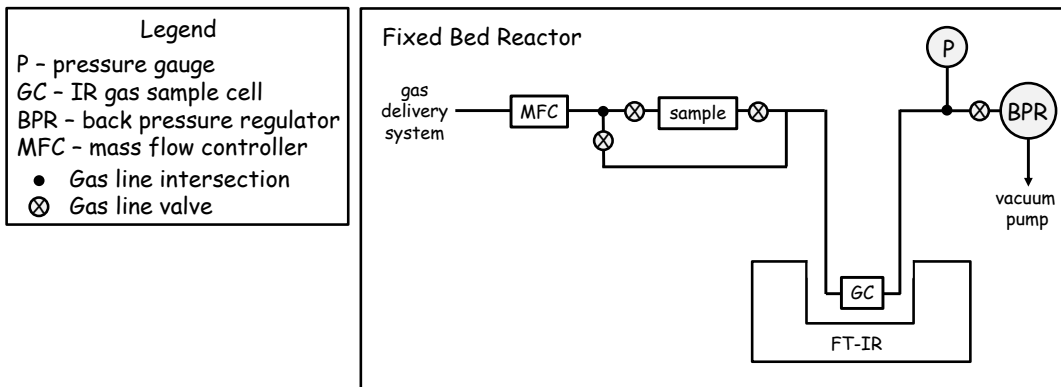


Figure 2.4. Schematic block diagram of fixed-bed flow reactor for use in assessment of catalytic activity of nanostructured sample material. Initial design created by a previous undergraduate working in Moore group, Nickolas Greybush, later modified by NKJ.

2.4 Gas adsorption experiments

2.4.1 Direct adsorption experiments

Following sample installation, direct adsorption experiments were performed on TiO_2 and Au/TiO_2 samples to acquire spectroscopic data for CO and O_2 . Samples were first cooled to 4 K at a pressure reduced to 10^{-8} Torr by cryo-pumping. Pre-treatment prior to reagent-gas exposure, as indicated, was accomplished *via* thermal processing under vacuum at a temperature of 400 K – 750 K for 1 h, followed by cooling the sample back down to 4 K (10 K/min). Actual temperatures measured at the sample window using the platinum sensor are indicated in corresponding figures. Following cooling to 4 K, samples were warmed to the deposition temperature (noted in figure captions as appropriate) and a spectrum was collected to gather data about the surface prior to gas

exposure. For direct adsorption experiments, the deposition temperature was dependent on the reagent carrier gas, with species in argon were deposited at 40 K or warmer to prevent matrix formation. Helium deposition does not risk matrix formation and consequently did not have similar temperature restrictions. Gas deposition was then initiated, and reagent gas was deposited onto the surface (total exposure and dosing rates indicated where appropriate) with continuous spectroscopic monitoring of the surface throughout the process. Following deposition, a post-deposition spectrum was collected. For some experiments, the gas-covered surface was warmed (5 K/min) to promote surface diffusion and thermal desorption of surface-bound species, which was also tracked with FT-IR. Development of this technique is the subject of Chapter 3.

2.4.2 Steady-state pressure experiments

Investigation of gas adsorption over TiO_2 and Au/TiO_2 samples under conditions of steady-state pressure was also performed using the same vacuum system described above (Fig. 2.3). Slight modification of the apparatus was made to allow the system to maintain a pressure of 10 Torr under flow conditions. The turbo-molecular pump was turned off, and a valve in the fore-line was closed to prevent gas flow into the standard set of vacuum pumps used for the system. A gas line was then attached to the vacuum chamber at a valve position (not shown in figure) that could be opened to allow the flow of gas into a diaphragm pump through a back-pressure regulator (see Section 2.3.3 for details on pump and operation of the BPR). The regulator was set to 10 Torr and reagent gas was constantly flowed into the system through the MFC, which was set to 10 sccm. To begin the experiment, helium buffer gas without dopant was flowed into the chamber

to allow for the BPR to be set to the desired pressure, after which the reagent gas mixed was flowed into the chamber. This procedure created a system in which the sample was under steady-state pressure of a flowing reagent gas mixture.

2.4.3 IMSS experiments

Similarly to the direct adsorption experiments described in the previous section, matrix experiments were performed on TiO_2 or Au/TiO_2 samples that were heated in vacuum at the start of the experiment, prior to exposure to reagent gas. Following this step, the samples were cooled for matrix formation in the range of 4 to 20 K for argon studies, and then reagent species in argon carrier gas were deposited over the TiO_2 or Au/TiO_2 surface (concentration, flow rate, and deposition temperature specified where appropriate). Following deposition of the argon-reagent mix matrix, krypton was deposited to form a protective over-layer and allow for surface warming to higher temperature because krypton has a higher melting point.⁵ For some matrix experiments, reagent gas was first deposited on the surface in helium with no matrix present, and the saturated surface was cooled down for deposition of a matrix over-layer. These variations in matrix experiments are described in Chapter 8. Following matrix deposition, annealing steps that involve incremental warming and cooling of the matrix were completed at a temperature ramp rate of 5 K/min. Following deposition of matrices at temperatures above 4 K, as well as annealing steps, samples were cooled back to 4 K to collect spectra after each step so that changes due to matrix annealing could be isolated from thermal changes in the spectra.

2.5 Collection of reference FT-IR spectra

During gas adsorption experiments, reference FT-IR spectra were collected to emphasize deposition-dependent components to the signal and to remove CaF_2 impurity peaks (“window peaks”). These reference spectra have been subtracted from the presented spectra. A detailed overview of methods for reference spectra collection and reasoning is provided here.

A common practice in CO adsorption experiments is to collect the spectrum of the sample prior to gas exposure, and present adsorption data as a series of difference spectra that are all referenced to the pre-deposition spectrum in order to emphasize CO-dependent features in the data.⁶ This technique is used in the presented work. For this particular system, an important consideration of these reference spectra is temperature because some features, such as carbonate and water bands, are temperature dependent. Correct interpretation requires the collection of reference spectra at a matched temperature so that the subtraction truly reflects only the CO-dependent changes in band position and intensity, and not temperature-induced changes. An example of this temperature dependence is evident in the calculated difference spectra of bare TiO_2 collected at various temperatures while cooling from 120 K to 4 K. Difference spectra were calculated by manual subtraction of the spectra. These spectra, provided in *Figure 2.5*, reveal that in the carbonate region, many of the features have a maximum intensity at 4 K relative to higher temperatures. Here, positive peaks in the spectrum indicate that a greater intensity of the bands was present at 4 K, and it’s clear that the largest increase is

observed over the temperature interval of 4 K to 120 K. The CO region does not contain bands prior to deposition, however, so subtraction of temperatures that are not exactly alike is sometimes used as it does not change the interpretation of the data.

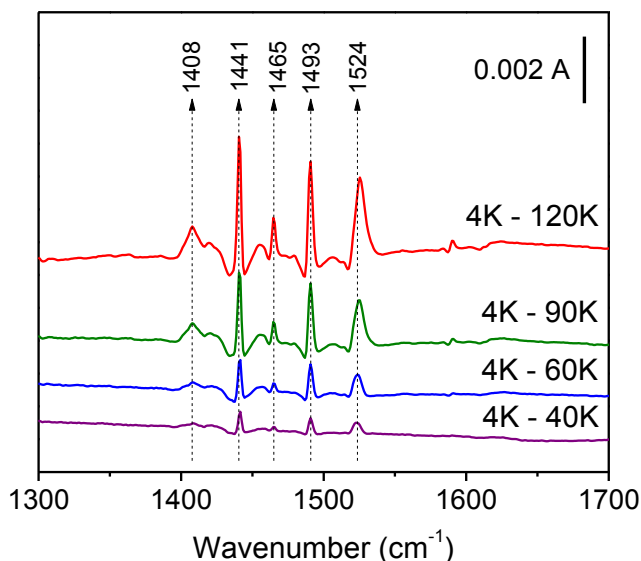


Figure 2.5. FT-IR difference spectra demonstrating temperature dependence of surface carbonate bands on TiO_2 prior to deposition of reagent gas. To emphasize the increased intensity of bands at colder temperatures, the pre-deposition spectra collected at 4 K was referenced to pre-deposition spectra collected at 120 K (red), 90 K (green), 60 K (blue), and 40 K (purple).

As mentioned previously, another reason for collecting reference spectrum is that many CaF_2 sample windows obtained from the manufacturer contain impurities that caused absorption near the CO region, complicating data interpretation and presentation. Sharp vibrational bands appear at 2030.7, 2094.8, 2104.0, and 2190.8 cm^{-1} at 4 K, and were verified as impurity peaks during control experiments in which the spectrum of the window in the absence of sample was measured at cold temperatures. These bands were also found to be temperature dependent, exhibiting the most intense signal at the lowest

measured temperature of 4 K. The temperature dependence of these bands is clear from the difference of spectra collected at 120 K and 4 K (c.f. Fig. 2.6). The subtraction of the 120 K spectrum from the 4 K spectrum produces positive peaks, with some evidence in shifting at the base of the peak where slight depletion is observed due to the shift. A way to correct for the presence of these bands is to collect a reference spectrum of the window at each temperature probed during the experiment and subtract the bands in a subsequent step. This approach complements the method used to emphasize CO-dependent spectral features that are not influenced by temperature.

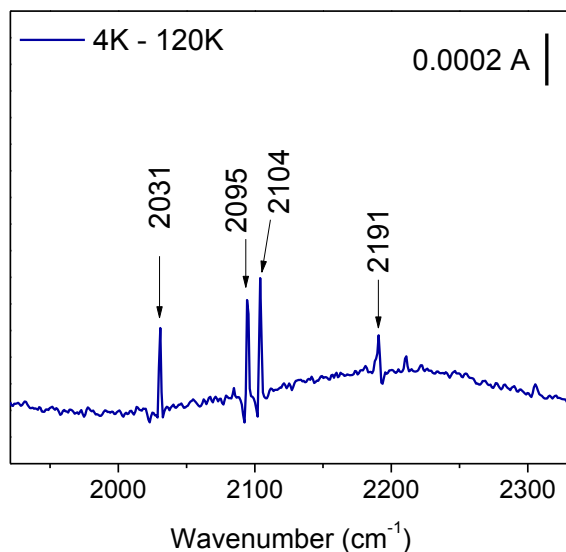


Figure 2.6. FT-IR difference spectrum demonstrating the temperature dependence of bands caused by absorbance of impurities in the CaF₂ window. To clearly emphasize the increased intensity of bands at colder temperatures, the pre-deposition spectrum collected at 4 K was referenced to the pre-deposition spectrum collected at 120 K.

The process for collecting reference spectra at multiple temperatures is illustrated by the experiment profile in *Figure 2.7*, in which the temperature of the sample is plotted

as a function of time. This profile represents a typically direct adsorption experiment (see Section 2.4.1 for experimental details) in which the sample was cooled from room temperature to 4 K, thermally processed at a temperature above room temperature, re-cooled to 4 K, warmed to 40 K to deposit gas, and finally warmed in incremental temperature steps to collect spectra at temperatures in the range of 40 to 150 K.

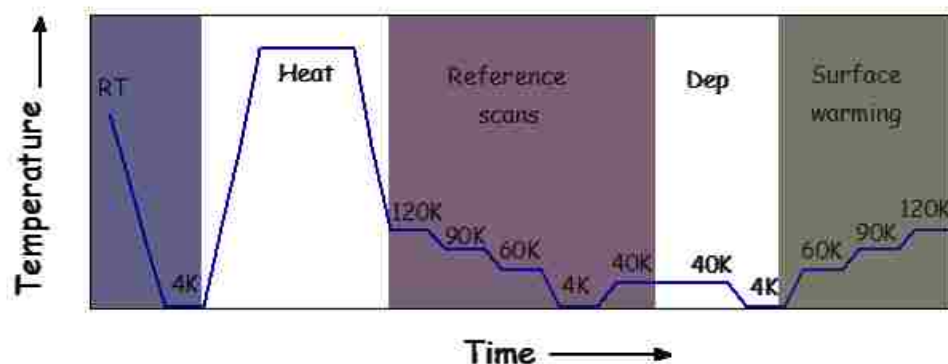


Figure 2.7. Schematic diagram of experiment profile indicating temperature over time during a typical adsorption experiment. Reference scans were collected at each temperature indicated on the graph during the cool-down from the heating step, prior to deposition (labelled “Dep”).

2.6 References

- 1 Yates, J. T.; Duncan, T. M.; Worley, S. D.; Vaughan, R. W., *J. Chem. Phys.* **70**, 1219-1224 (1979).
- 2 Ludlum, K. H.; Eischens, R. P., *Surface Sci.* **40**, 397-8 (1973).
- 3 Rondeau, R. E., *J. Chem. Eng. Data* **11**, 124-124 (1966).
- 4 Ventura, G.; Perfetti, M., *Thermal Properties of Solids at Room and Cryogenic Temperatures*; (Springer, 2014).
- 5 Johnston, R. L. *Atomic and Molecular Clusters*; (Taylor & Francis: 2002).
- 6 Dekkers, M.; Lippits, M.; Nieuwenhuys, B., *Catal. Lett.*, **56**, 195-197 (1998).

Chapter 3

Elucidating the binding of CO to TiO₂ using cryogenic FT-IR spectroscopy: surface diffusion and desorption between 40 and 150 K

This chapter includes material that has been reproduced in part from the following publication: Jarrah, N. K.; Klimas, R. D.; Moore, D. T., Elucidating the binding of CO to TiO₂ using cryogenic FT-IR spectroscopy: surface diffusion and desorption between 40 – 150 K. *J. Phys. Chem. C*, submitted 7/10/14.

Note: The data used to develop the ideas in this chapter, including sample preparation and data acquisition, were collected by a previous Master's student in the Moore group, RDK. The data have been re-analyzed by NKJ, who is responsible for all peak fitting, subsequent data interpretation, and creation of figures of the work presented here.

3.1 Abstract

Adsorption of CO on TiO₂ was investigated under high vacuum ($<10^{-5}$ Torr) using FT-IR spectroscopy. A film of TiO₂ nanoparticles (Degussa P25) was first heated in vacuum to remove surface contaminants, and then cooled to 40 K and saturated with CO. Bands corresponding to physisorbed CO and CO chemisorbed in 5-coordinate Ti⁴⁺ surface sites were observed, as well as in “reduced” sites perturbed by the presence of oxygen vacancies. The sample was then heated step-wise with spectra recorded in 10 K increments up to 150 K. Thermal evolution of the spectral bands revealed population transfer *via* surface diffusion from shallower to deeper wells up to 120 K, at which all the population was in the most strongly bound site. Blue-shifting and intensity loss due to desorption was observed at higher temperatures. Redhead analysis was used to estimate barriers between minima based on temperature thresholds for disappearance of associated bands.

3.2 Introduction

Before initiating studies on CO adsorption over Au/TiO₂ catalysts, we had to first understand binding of the adsorbate over the bare TiO₂ support. As described in Chapter 1, currently available assignments were acquired under conditions of static CO pressure and at temperatures ranging from room temperature¹⁻⁴ down to 77 K.^{5,6} Under these conditions, the population of chemically unique sites sampled spectroscopically reflect a combination of stably-bound adsorbates that occupy sites below the desorption threshold, as well as weakly-bound surface species that are bound only when in equilibrium with the gas phase. To better understand CO binding to both Au and the support in the cryogenic, FT-IR studies *in vacuo* presented here, CO adsorption over powder TiO₂ in absence of AuNPs was studied at 40 K under pressures of 10⁻⁶ to 10⁻⁸ Torr. The importance of heat treatment to the support prior to CO exposure on the observed binding site population was assessed.

Following deposition of CO on the support at 40 K, the surface was warmed in steps between 40 and 150 K in order to promote mobilization or desorption of molecules in less stable sites. Infrared spectra were collected to monitor progress of this site-specific desorption process, such that the temperature dependent changes in the spectra can be interpreted similarly to temperature programmed desorption (TPD) results. This chapter develops the analysis of spectra collected after deposition and during surface warming steps to reveal details about the relative stability of the binding site population over TiO₂ and Au/TiO₂ nanocatalysts. Application of the Redhead⁷ equation was used to compute binding energies and provide insight to the potential energy surface of CO

binding over nanostructured TiO₂, and ultimately for binding over Au/TiO₂, is presented and developed.

3.3 Experimental methods

A description of the instrument setup for gas adsorption experiments, sample preparation, and experiment parameters is provided in Chapter 2. Details specific to the experiments discussed in this chapter are provided here, briefly. Samples were prepared from a slurry in 10:1 acetone:water. All spectra were collected at a resolution of 0.5 cm⁻¹ and averaged over 200 scans. A peak-fitting method was developed for analysis of temperature-dependent changes in the population of surface-bound CO observed in spectra of TiO₂ and Au/TiO₂ samples, and is described in the Appendix, Section 3.8. Peak fitting results are included in Tables 3.2 – 3.4, and the temperature trends in the peak positions, areas, and line-widths are represented graphically in *Figures 3.19 – 3.27*. Error bars in the total area plots were calculated by taking the root mean square of the noise in the region of the spectrum that does not contain signal (1900 – 2000 cm⁻¹), and taking the square root of the peak area scaled by the noise level (resulting in the square root of signal to noise as the error).

3.4 Results

3.4.1 Pre-treatment of TiO₂

Our initial attempts to observe spectra of CO adsorbed on TiO₂ nanocrystals failed to reproduce any of the bands from the literature, showing only physisorbed CO

instead. These results led us to hypothesize that there was an over-layer of contamination on the surface that was not pumped away, even after several days at room temperature in the vacuum chamber. We therefore modified our cryostat to include a heating stage (see Experimental methods), so that the sample could be heated *in vacuo*, as this treatment has been shown previously to remove surface bound contaminants.^{8,9} The FT-IR spectra tracking changes in surface species in the C-H and O-H stretching region after heating the sample to 582 K *in vacuo* for 1 h are shown in *Figure 3.1a and 3.1b*, respectively. Before heating there are several strong C-H stretching bands, which are almost completely removed by the heating step. The O-H region also exhibits several strong bands, including a sharp feature at 3638 cm⁻¹ corresponding to isolated hydroxyl species on the oxide surface,^{10,11} and these are similarly diminished after thermal treatment.

The clear implication is that the heating removed an over-layer of organic contaminants from the surface, and the effects on CO adsorption behavior can clearly be seen in the spectra shown in *Figure 3.2a*, which were recorded following deposition of 0.5 % CO in Ar for 10 min at 40 K, before and after the sample was heated. Before heating, only weak, fairly broad bands were observed in the CO region, with features corresponding to physisorbed CO, CO hydrogen bonded to surface OH groups, and a small amount of CO chemisorbed to TiO₂ at 2138, 2150 and 2180 cm⁻¹, respectively.^{1,3,4,12} After heating, the spectrum changed dramatically, becoming more consistent with what has been reported previously for CO adsorbing on anatase TiO₂ nanocrystals.³ The band for H-bonded CO had disappeared, and the main CO-TiO₂ band at 2180 cm⁻¹ band is sharp and intense. The broad band at 2138 cm⁻¹ is more intense,

confirming the presence of physisorbed CO, and two weak bands at 2165 and 2174 cm^{-1} are also evident. The latter two bands have been previously assigned to CO binding in “less oxidized” sites on the TiO_2 surface.^{3,9} Figure 3.2b shows the OH stretching region for these two spectra taken before and after heating, again illustrating that surface OH-species are much less prevalent following heating. The rate of growth of the spectral bands during the deposition time had gone essentially to zero, indicating that surface binding sites were effectively saturated.

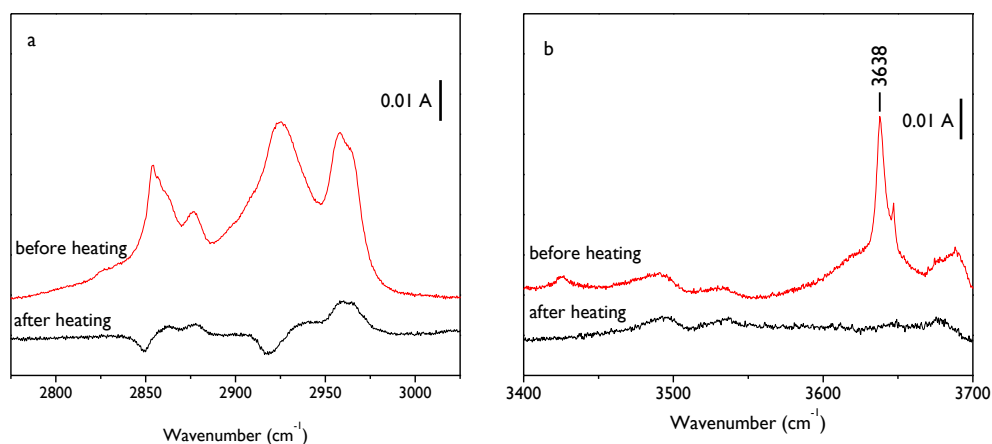


Figure 3.1. FT-IR spectra collected at 40 K of TiO_2 before (black) and after (red) thermally processing sample at 582 K showing a) C-H stretch and b) O-H stretch region.

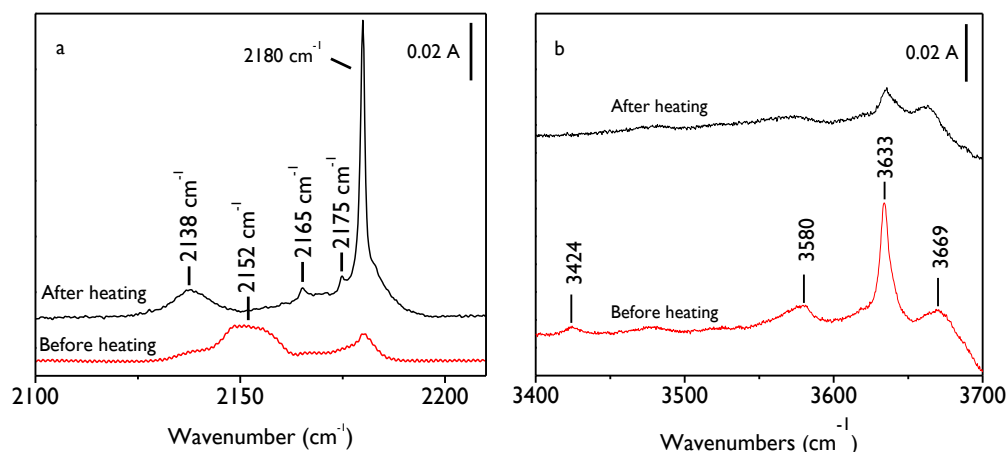


Figure 3.2. FT-IR spectra collected at 40 K of CO of TiO₂ following CO deposition at 40 K (0.5% in Ar at 11 sccm for 10 min) before (black) and after (red) thermally processing sample at 582 K showing a) C-H stretch and b) O-H stretch region.

3.4.2 Thermal desorption spectroscopy

Infrared spectra tracking the evolution of CO bands during the stepwise warming of TiO₂ from 40 – 150 K, after preheating at 625 K and subsequent CO deposition, are provided in *Figure 3.3*. For each temperature step, the sample was first allowed to equilibrate until the temperature stabilized, and then multiple spectra were taken to ensure that the relative band intensities were not changing while the sample was held at constant temperature.

The first major spectral change observed was the loss of the physisorbed CO band at 2138 cm⁻¹ (band “a”), which was strongly reduced at 50 K, and almost entirely gone at 60 K. The peaks at 2165 and 2174 cm⁻¹ (bands “b” & “c”, respectively) were the next to disappear, which occurred between 80 and 90 K. The main peak at 2180 cm⁻¹ persisted all the way up to 150 K, though it broadened and blue-shifted significantly at the higher temperatures. Careful inspection of the band (Fig 3.3B) reveals that it actually consists of

two features. There is a lower-frequency component (band “d”) that is present from the time of deposition at 40 K, and shows a slight red-shift with increasing temperature. A second, higher-frequency component (band “e”) began to grow in at 90 K and increased in intensity up to 120 K, at which point band “d” was gone from the spectrum. Peak fitting analysis was employed to quantify these trends, and the results for bands “d” and “e” are plotted in *Figure 3.4* (a full data set is provided in Tables 3.2 – 3.4 and *Figures 3.19 – 3.27* of the appendix). The peak areas suggest that there is shift in the CO population reflecting these bands between 90 K and 120 K, and then at higher temperatures there was a rapid loss of intensity, presumably due to desorption.

As explained in the experimental section, the peaks used to fit the spectrum were split into two groups: the primary group of sharper peaks corresponding to CO in distinct chemisorption (and physisorption) sites (bands “a” – “e”), as well as a secondary set of broader “fitting” peaks. The summed areas of these different groups of peaks, as well as the total summed area of all peaks, are shown as a function of temperature in *Figures 3.5A* and *3.5B*, respectively. It is interesting to note that while the physisorbed band “a” decreases sharply between 40 and 60 K, both the chemisorbed and fitting peaks increase in area over this same range, suggesting that some of the physisorbed CO may be converted to chemisorbed species. Between 70 and 90 K, the areas of both sets of peaks stay approximately constant, but above 90 K, the collective intensity of the fitting bands starts to diminish while that of the chemisorbed bands shows a slight increase up to 120 K, above which all bands decrease. The physical significance of these trends is explored in more detail in the discussion section; here we just note that the smooth monotonic

decrease in the overall intensity of all CO bands (c.f. Fig. 3.5B) suggests that the oscillator strengths associated with the various bands are similar and essentially constant with temperature, so that the observed changes in intensity are correlated with changes in population in the various surface binding sites.

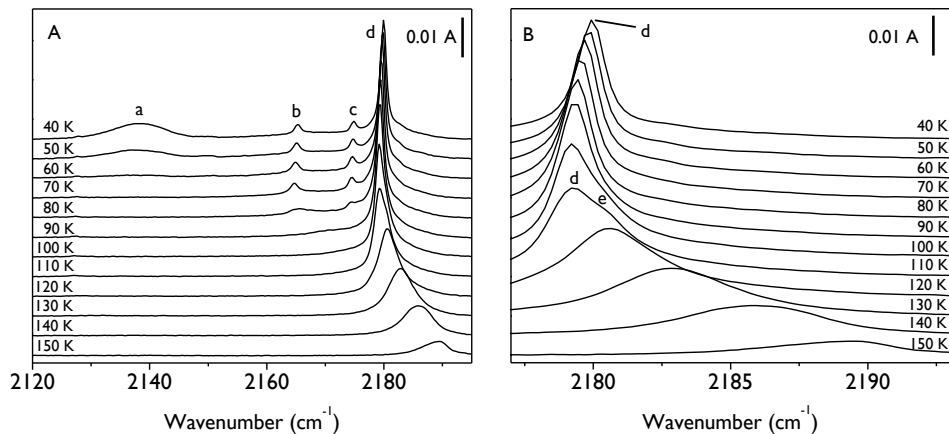


Figure 3.3. FT-IR spectra collected in 10-K increments from 40 to 150 K of TiO₂ following CO deposition at 40 K (0.5% in He at 11 sccm for 10 min) after thermally processing sample at 625 K showing A) entire CO-stretch region and B) expanded view of band(s) near 2180 cm⁻¹.

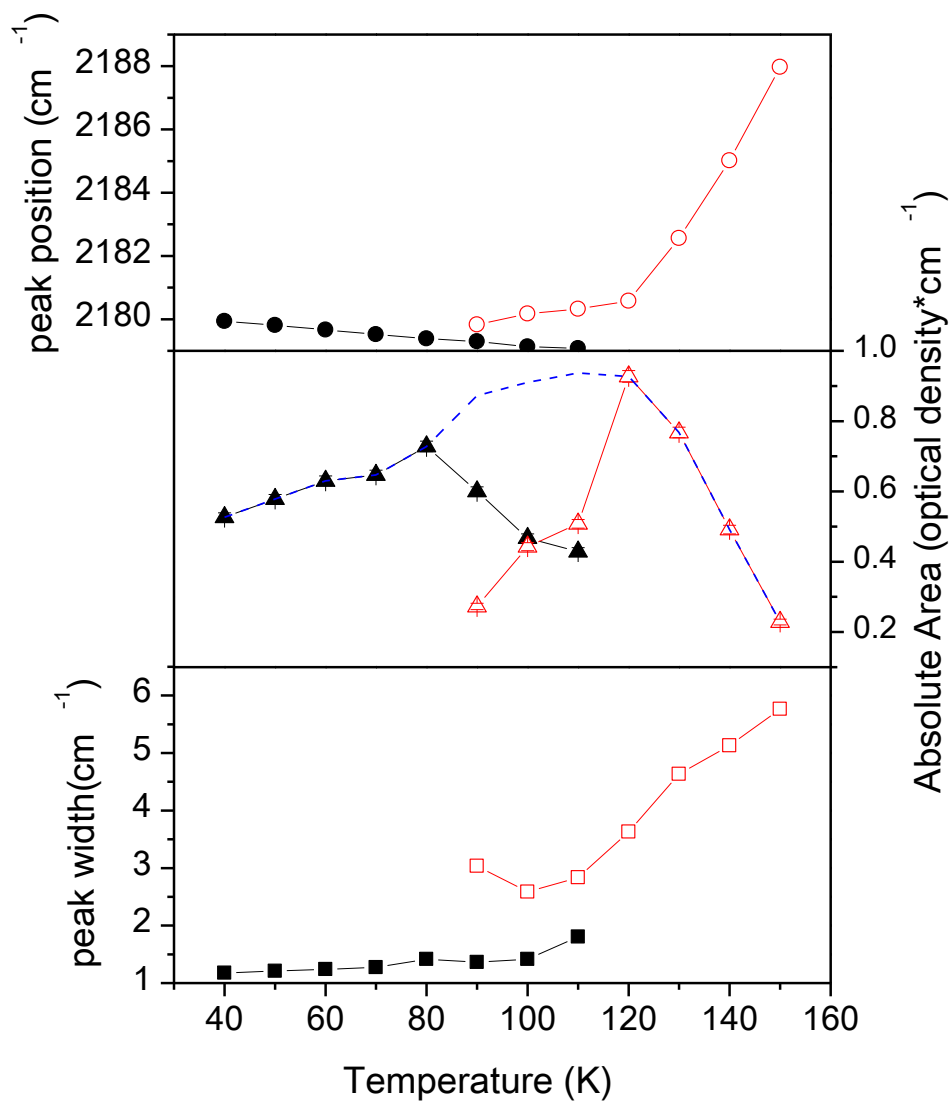


Figure 3.4. Lorentz fit values demonstrating temperature dependence of bands “d” (closed symbols) and “e” (open symbols) during TDS steps of CO on TiO₂ from 40 to 150 K. The dashed line indicates the summed areas of the two components, showing population transfer to these sites as temperature increases to 120 K.

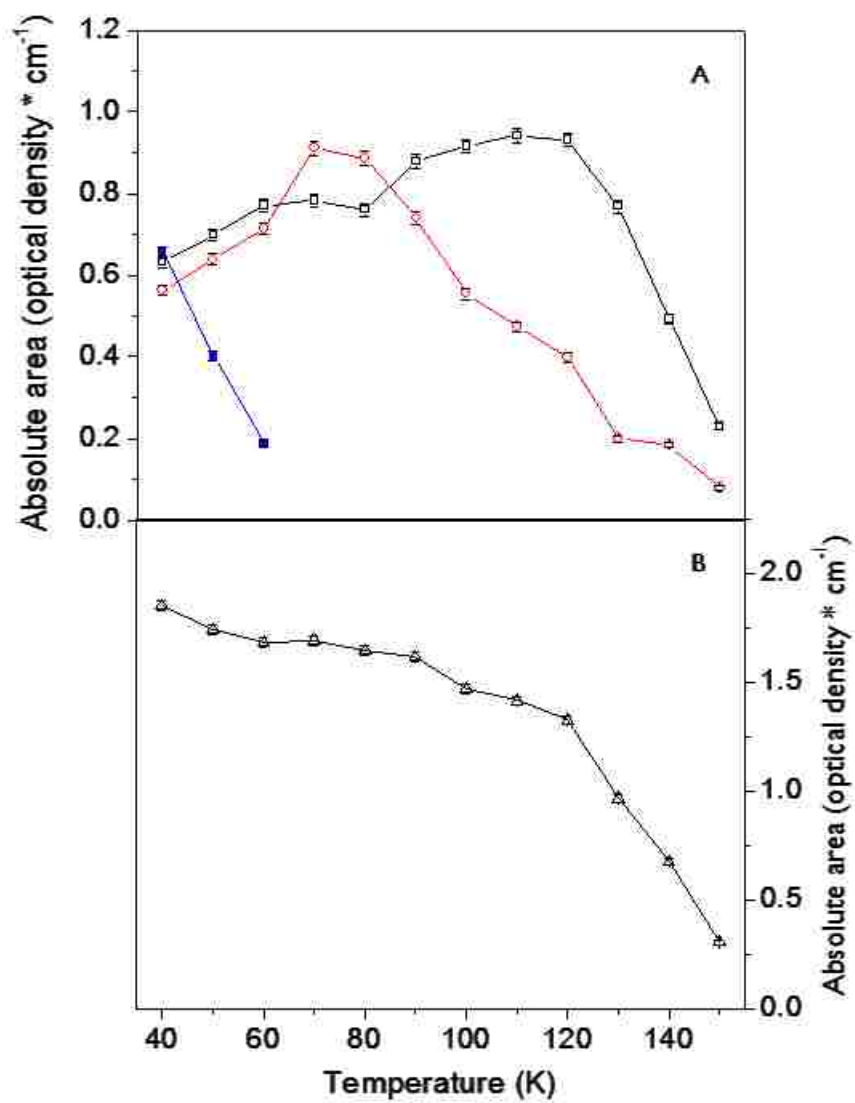


Figure 3.5. Total area sum of A) chemisorbed (open square) and physisorbed (filled square) bands plotted with total area sum of “fitting” (open circle) bands and B) all empirically fit bands during TDS steps of CO on TiO₂ from 40 to 150 K.

3.5 Discussion

The spectral bands observed in these studies for CO on TiO₂ powder films (after heat-treating to clean the surface) are consistent with what has been reported previously for CO adsorbing on oxidized TiO₂ nanocrystals.^{1,3-6,13-15} The strong band “d” at 2180 cm⁻¹ agrees well with the literature value for CO adsorbing to five-coordinate Ti₄⁺ (Ti_{5c}) sites at the surface of anatase TiO₂.^{1,3,4,12} The strong blue-shift from the gas phase CO stretching value of 2143 cm⁻¹ arises due to bond polarization from the interaction with local electric field of the cationic center.¹⁶ The weaker bands, “b” and “c”, observed at 2165 and 2174 cm⁻¹, are consistent with CO adsorbing to sites with lower Lewis acidity⁹, since the local electric field will be less intense due to the higher electron density. In our sample, these bands may arise from the presence of oxygen vacancies on the surface created during the initial heating step. It has been shown that heating *in vacuo* results in mild reduction of TiO₂ surfaces;¹⁷ furthermore, the removal of the organic contaminants from these samples may have proceeded through oxidation steps, whereby the TiO₂ surface became partially reduced. The presence of reduced sites might also explain the splitting of the 2180 cm⁻¹ band as the temperature was raised. While there does not appear to be a precedent for this in the literature on nanocrystalline TiO₂ samples, a recent study of CO adsorption on reduced single-crystal TiO₂ (110) showed two bands in this region.¹⁸ At high coverage, the two bands overlapped near 2179 cm⁻¹, but as the coverage was reduced, the more intense portion of the band split off and became increasingly blue-shifted.¹⁸ The authors attribute the splitting to CO bound to distinct surface sites; one which is nearby an oxygen vacancy site, and another which is distant to

vacancy sites. It is proposed that the coverage dependence on the behavior of this second band indicates it is chemically unaltered by the presence of vacancies on the surface. This distinction between sites associated with oxygen vacancies could explain our observations as well, since the higher frequency component (band “e”) split off at high temperature and exhibited a progressive blue-shift as the intensity of the band diminished due to desorption, which necessarily means that the surface coverage was also being lowered. There was no evidence of strong binding to the most-reduced sites, as was observed by Yates and co-workers following annealing of rutile TiO₂ (110) surfaces at 900 K.¹⁹

The temperature dependence of the various binding bands can be used to understand the corresponding binding sites on the potential energy surface. As mentioned in the introduction, as these experiments were conducted in vacuum, any surface-bound species that would be in dynamic equilibrium with the gas phase under static pressure conditions would quickly be pumped away. Thus as the sample was heated, CO molecules bound in shallower wells on the surface could either desorb, or diffuse along the surface to bind in deeper minima, with the branching ratios between these processes determined by the relative barrier heights. Thus the thermal desorption spectroscopy (TDS) studies performed are akin to temperature programmed desorption (TPD), however the analogy is not perfect because the spectroscopic detection is performed stepwise at various waiting temperatures, rather than continuously as with TPD. The reverse reaction for both processes, desorption and diffusion to more strongly bound sites, has essentially zero-probability, so Redhead analysis⁷ was used to estimate

the minimum barrier heights associated with each unique site from the loss of the spectral features corresponding to each surface-bound species. The highest temperature at which a given band was observed is taken as the critical temperature for desorption/diffusion in the analysis, which yielded the barrier estimates given in Table 1 for bands “a” – “e”, using the temperature ramp rate of 5 K/min and a typical assumed value of 10^{13} s^{-1} for the frequency parameter ν . Clearly, these are at best threshold values, but they are useful for assessing the relative energetics of the surface-bound species.

Table 3.1. Calculated binding energies based on desorption temperature using Redhead analysis

$\nu(\text{CO}) \text{ (cm}^{-1}\text{)}$	desorption temperature range (K)	binding energy range (kJ/mol)
2138	55 - 65	15.0 - 17.8
2165	75 - 85	20.6 - 23.5
2175	75 - 85	20.6 - 23.5
2179	105 - 115	29.2 - 32.1
2189	145 - 155	40.7 - 43.6

Only the last band lost (band “e”) at the highest temperature of 150 K can clearly be correlated to desorption (as opposed to surface diffusion). The value of 42.1 kJ/mol is in good agreement with measurements of the adsorption enthalpy of CO on single crystal TiO_2 , 41.4 kJ/mol,¹⁹ which provides support for the validity of this TDS analysis. For the rest of the bands, the temperature trends in the peak areas suggest that surface diffusion is the primary mode of intensity loss. Initially, when band “a” is lost between 40 – 60 K, there is a uniform increase of all the other spectral features, which is consistent with the migration of non-specific physisorbed CO molecules into more favorable binding sites.

Bands “b” and “c” are lost between 70 – 90 K, but it is hard to tell where their intensity goes, because the overall intensity of the chemisorbed and fitting peaks are fairly constant over this range. From 90 – 120 K however, the total intensity in the chemisorbed bands actually increases slightly, at the expense of the fitting-band intensity. This trend suggests that the physical interpretation of the fitting bands is that they are due to heterogeneous broadening of the primary bands “b” – “e”, and thus correspond to CO molecules bound in surface sites that are less stable and more prone to surface diffusion at lower temperatures.

These observations allow us to hypothesize the overall structure for the potential energy surface of CO binding to TiO₂ shown in *Figure 3.6*. The physisorbed CO in the well corresponding to site “a” is non-specifically adsorbed and can diffuse over low barriers to be trapped in any of the other minima; hence it is represented by the dotted curve intersecting the other barriers. The “reduced” sites “b” and “c” are the shallowest chemisorbed sites, and are separated from the deeper sites “d” and “e” by a forward barrier of ~22.1 kJ/mol. Site “e” is the deepest well, defining the desorption threshold energy of ~42.1 kJ/mol, and site “d” is coupled to site “e” over a forward barrier of ~30.6 kJ/mol. Note that because we only know the barrier heights for the rearrangement steps, there is some ambiguity regarding the relative positions of the minima in *Figure 3.6*; here the wells are arbitrarily chosen so that minima adjacent to larger barriers also lie deeper below the desorption limit. Furthermore, population transfer is **not** restricted to occur between adjacent minima on this surface. This figure represents the least complex PES that is semi-quantitatively consistent with all of the observed spectral trends.

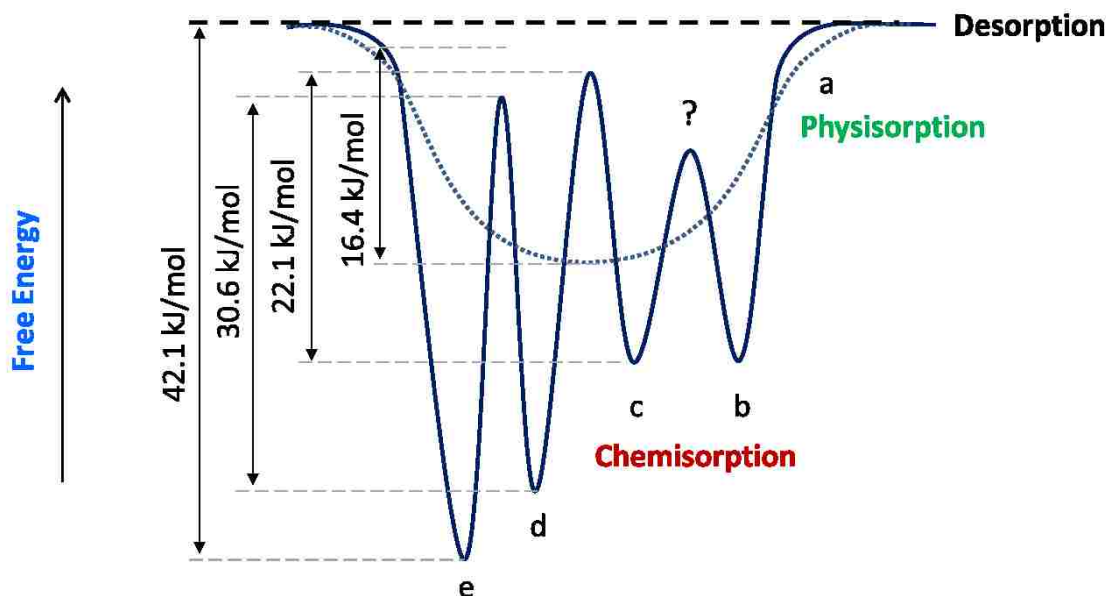


Figure 3.6. Scheme of potential energy surface showing potential wells corresponding to distinct binding sites of varied enthalpy, labeled “a” – “e”, with values indicating barrier heights calculated from Redhead analysis of TPS results (Table 1). The barrier separating minimas corresponding to “b” and “c” sites could not be determined from the data. The solid line indicates sites in chemisorption wells, the dotted line indicates sites in the physisorption well, and the bold dashed line indicates the desorption threshold.

3.6 Conclusion

Our results demonstrate the ability of cryogenic, infrared spectroscopy combined with thermally controlled desorption to probe the complicated potential energy surface for CO deposited on nanostructured titania, and to quantify the relative stabilities of chemically distinct binding sites on the surface. Distinct spectral bands were observed corresponding to physisorbed CO (most weakly bound), CO bound in “reduced” sites perturbed by oxygen vacancies presumably created during heat-cleaning of the TiO₂ (intermediate binding strength), and CO bound in “oxidized” 5-coordinate Ti⁴⁺ sites

(most strongly bound); the positions of these bands agree well with previous assignments from the literature.^{1,3,4,12,18} Warming the sample caused systematic changes in the absorbance spectrum, with population transfer from less stable to more stable sites *via* surface diffusion being the dominant mode up to ~120 K, and desorption dominating at higher temperatures. Estimates of barrier heights separating minima on the PES were obtained using Redhead analysis based on the critical temperatures at which the corresponding bands disappeared from the spectrum. At the highest temperatures, only the deepest sites were populated, and the critical temperature for desorption corresponded to an adsorption enthalpy of ~42 kJ/mol, which agrees well with literature values for CO bound on fully oxidized TiO₂.¹⁹

3.7 Acknowledgements

This work was funded by the National Science Foundation CAREER award CHE-0955637, as well as start-up funding from Lehigh University.

3.8 Appendix

Peak fitting analysis for FT-IR spectra collected at each temperature from 40 to 150 K, in 10 K increments, showing evolution of CO bands during surface warming of TiO₂ during thermal warming steps is provided here. To fit peaks in the FT-IR spectra, the area above baseline over the spectral range of 2096 and 2217 cm⁻¹ was fitted to a sum of Lorentzian peaks using the Levenberg-Marquardt non-linear least-squares algorithm (Origin 8.0 software package). Lorentzian band-fitting produced similar results to those

obtained for a Gaussian fitting analysis, resulting only in a negligible difference in the values obtained for parameters of the “fitting” bands, described below. This method was appropriate, as it has also been used by previous researchers to fit CO bands on nanostructured Au/TiO₂ samples.²⁰

The resulting peaks were typically divided into two groups: a set of narrower peaks corresponding to the positions of the sharp features in the spectrum presumed to arise from CO in distinct physi- or chemisorbed environments, and a minimal set of broader “fitting” peaks that were required for good agreement with the experimental data, but which failed to show any clear trends with temperature. Possible interpretations for the physical significance of this latter class of peaks are discussed in the context of individual datasets in the discussion, Section 3.5. The complexity of the spectra decreased as the temperature increased from 40 to 150 K, so the number of peaks of both types was reduced accordingly to avoid over-fitting. For example, at 40 K, more peaks were used for the fits than at 120 K. For each temperature, spectra were fit to a sum of Lorentzian peaks, shown in *Figures 3.7 – 3.18*, and the number of fitting bands is indicated in the figure captions. The temperature trends in the peak positions, areas and line-widths are represented graphically in *Figures 3.19 – 3.27*. For ease of interpretation, these trends have been tabulated and provided in Tables 3.2 – 3.4, in which values for the chemisorbed bands are provided in Table 3.2, values for “fitting” bands are provided in Table 3.3, and values for the remaining physisorbed and hydrogen-bonded bands are provided in Table 3.4.

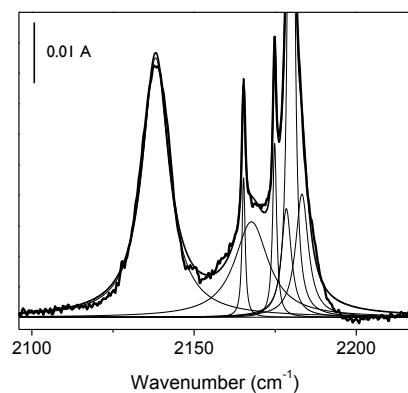


Figure 3.7. Lorentzian fitting analysis of FT-IR spectra taken at 40 K of CO adsorbed over TiO₂. Spectrum fit by 7 bands with 3 varying parameters.

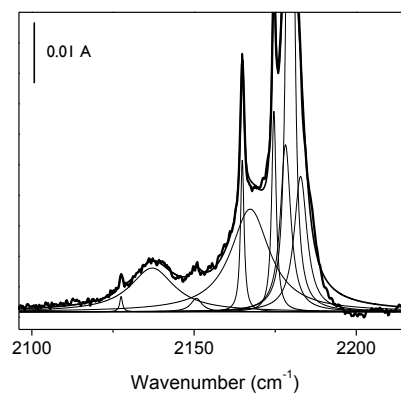


Figure 3.9. Lorentzian fitting analysis of FT-IR spectra taken at 60 K of CO adsorbed over TiO₂. Spectrum fit by 9 bands with 3 varying parameters.

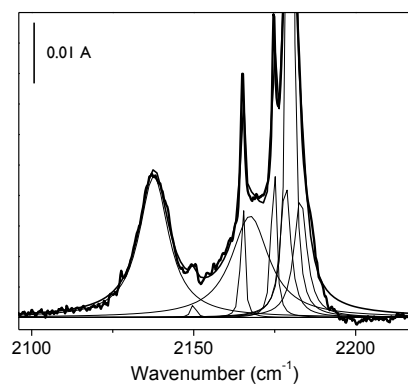


Figure 3.8. Lorentzian fitting analysis of FT-IR spectra taken at 50 K of CO adsorbed over TiO₂. Spectrum fit by 8 bands with 3 varying parameters.

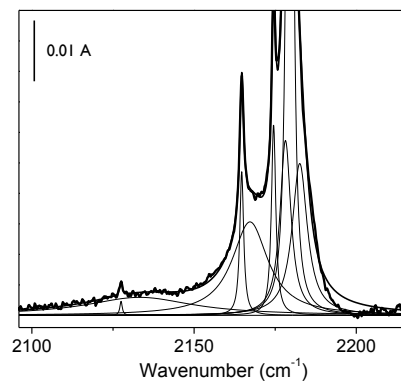


Figure 3.10. Lorentzian fitting analysis of FT-IR spectra taken at 70 K of CO adsorbed over TiO₂. Spectrum fit by 8 bands with 3 varying parameters.

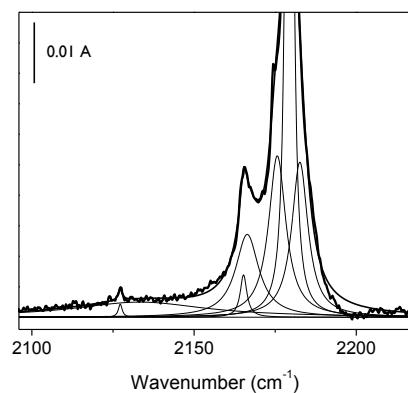


Figure 3.11. Lorentzian fitting analysis of FT-IR spectra taken at 80 K of CO adsorbed over TiO₂. Spectrum fit by 7 bands with 3 varying parameters.

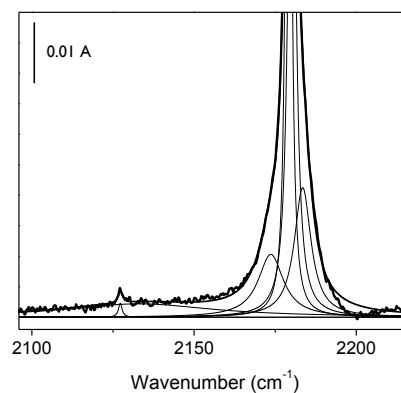


Figure 3.13. Lorentzian fitting analysis of FT-IR spectra taken at 100 K of CO adsorbed over TiO₂. Spectrum fit by 6 bands with 3 varying parameters.

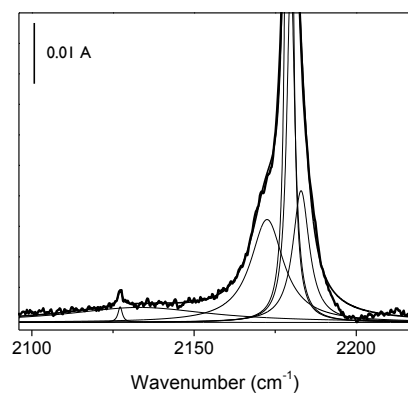


Figure 3.12. Lorentzian fitting analysis of FT-IR spectra taken at 90 K of CO adsorbed over TiO₂. Spectrum fit by 6 bands with 3 varying parameters.

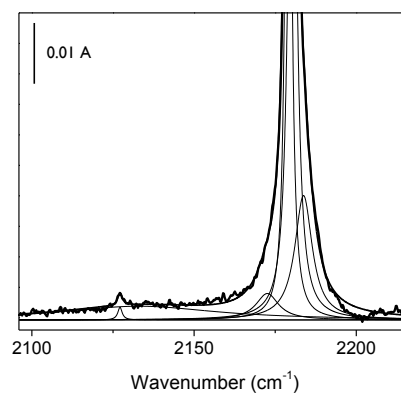


Figure 3.14. Lorentzian fitting analysis of FT-IR spectra taken at 110 K of CO adsorbed over TiO₂. Spectrum fit by 6 bands with 3 varying parameters.

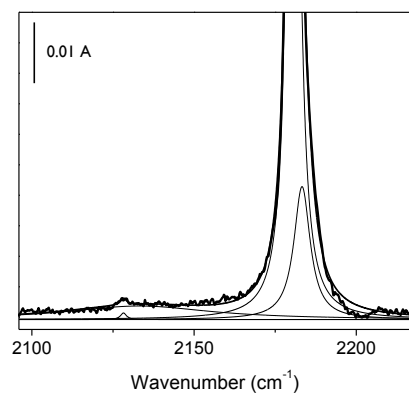


Figure 3.15. Lorentzian fitting analysis of FT-IR spectra taken at 120 K of CO adsorbed over TiO₂. Spectrum fit by 4 bands with 3 varying parameters.

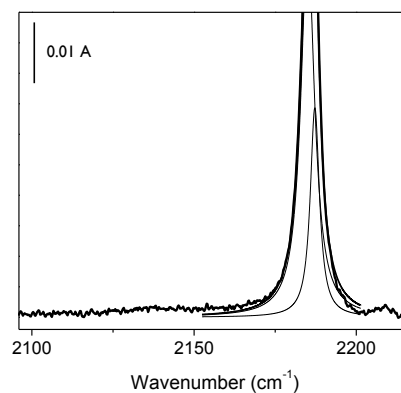


Figure 3.17. Lorentzian fitting analysis of FT-IR spectra taken at 140 K of CO adsorbed over TiO₂. Spectrum fit by 2 bands with 3 varying parameters.

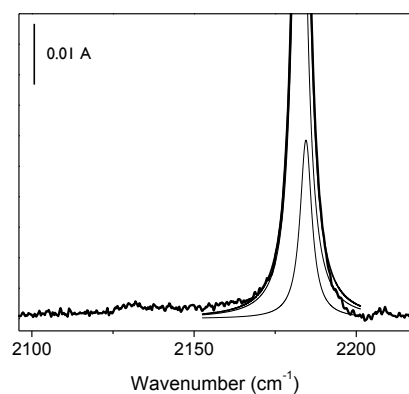


Figure 3.16. Lorentzian fitting analysis of FT-IR spectra taken at 130 K of CO adsorbed over TiO₂. Spectrum fit by 2 bands with 3 varying parameters.

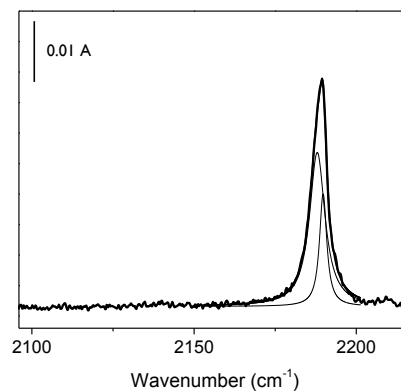
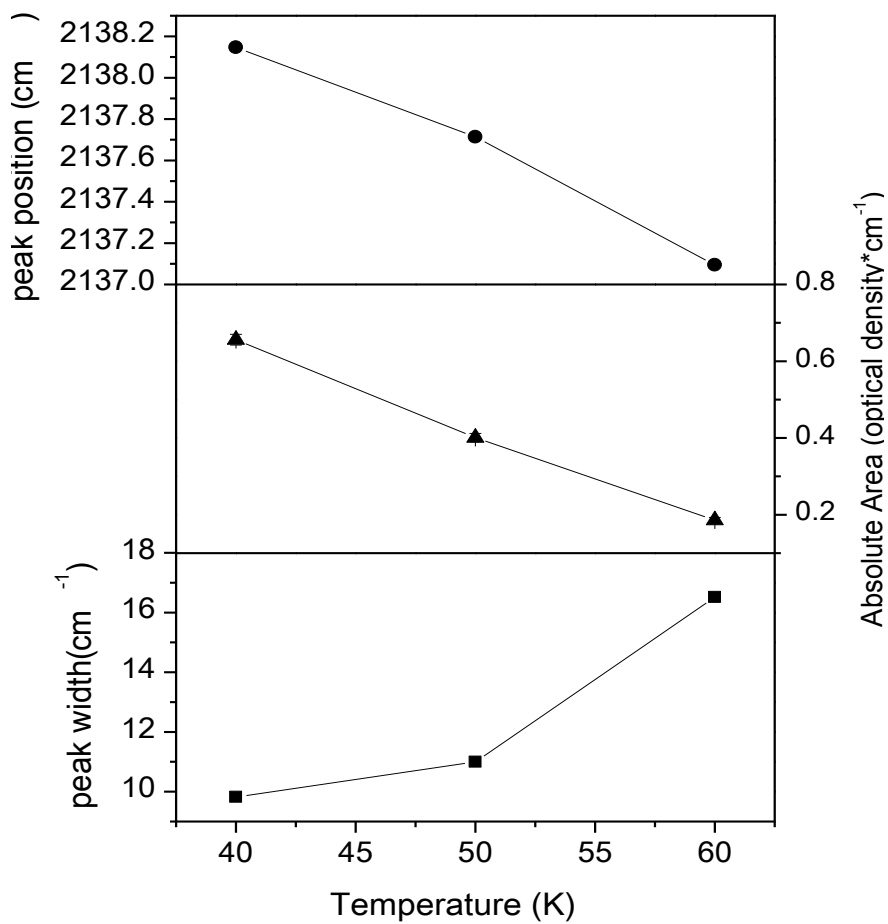
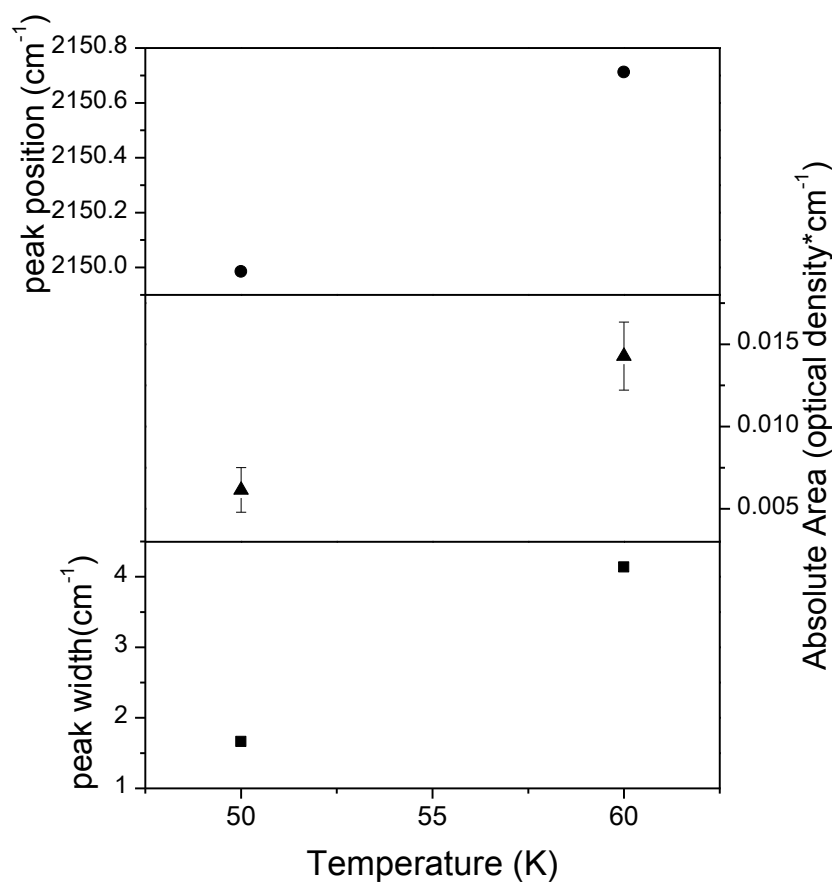


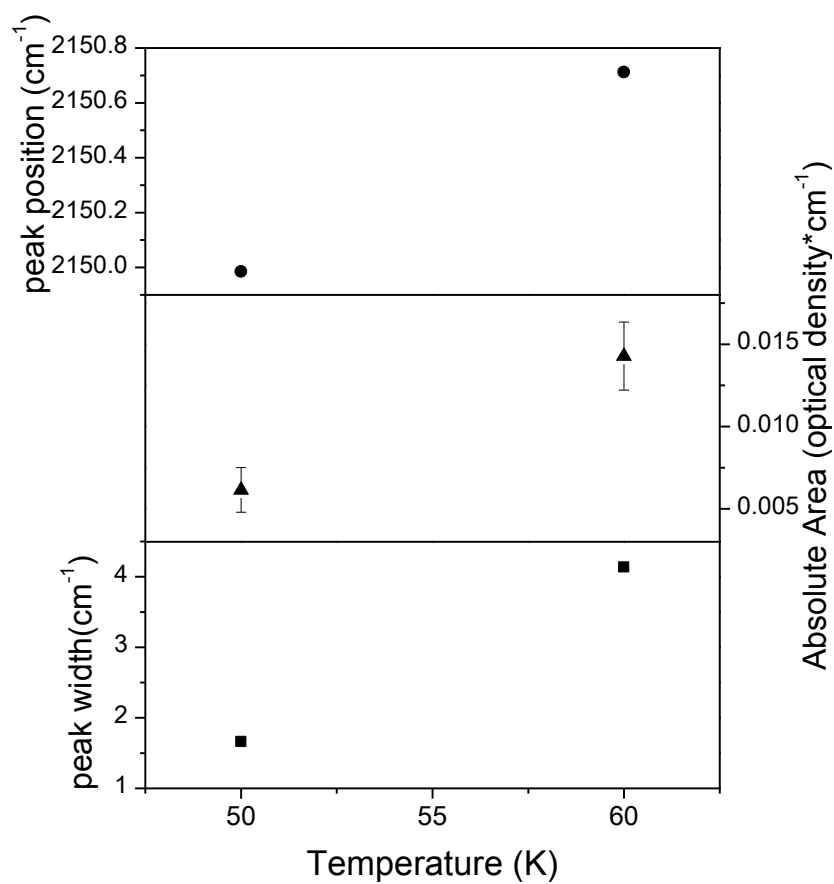
Figure 3.18. Lorentzian fitting analysis of FT-IR spectra taken at 150 K of CO adsorbed over TiO₂. Spectrum fit by 2 bands with 3 varying parameters.



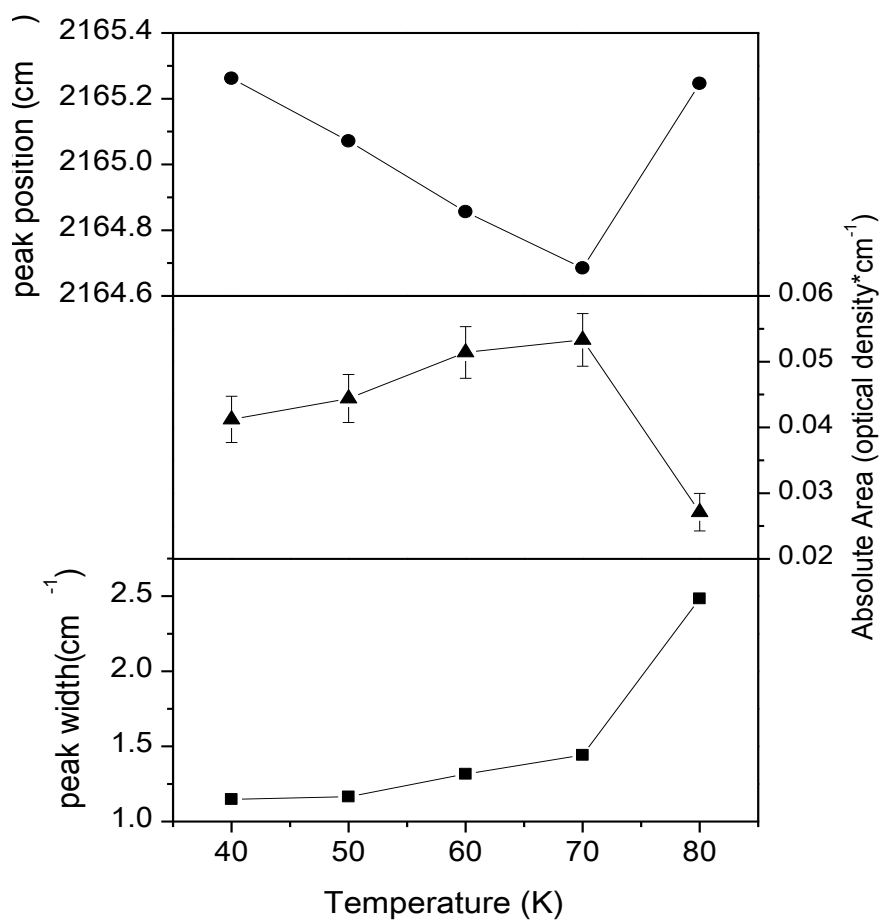
Figures 3.19. Lorentzian fit values demonstrating temperature dependence of band “a” during TDS steps of CO desorption on TiO₂ from 40 to 150 K.



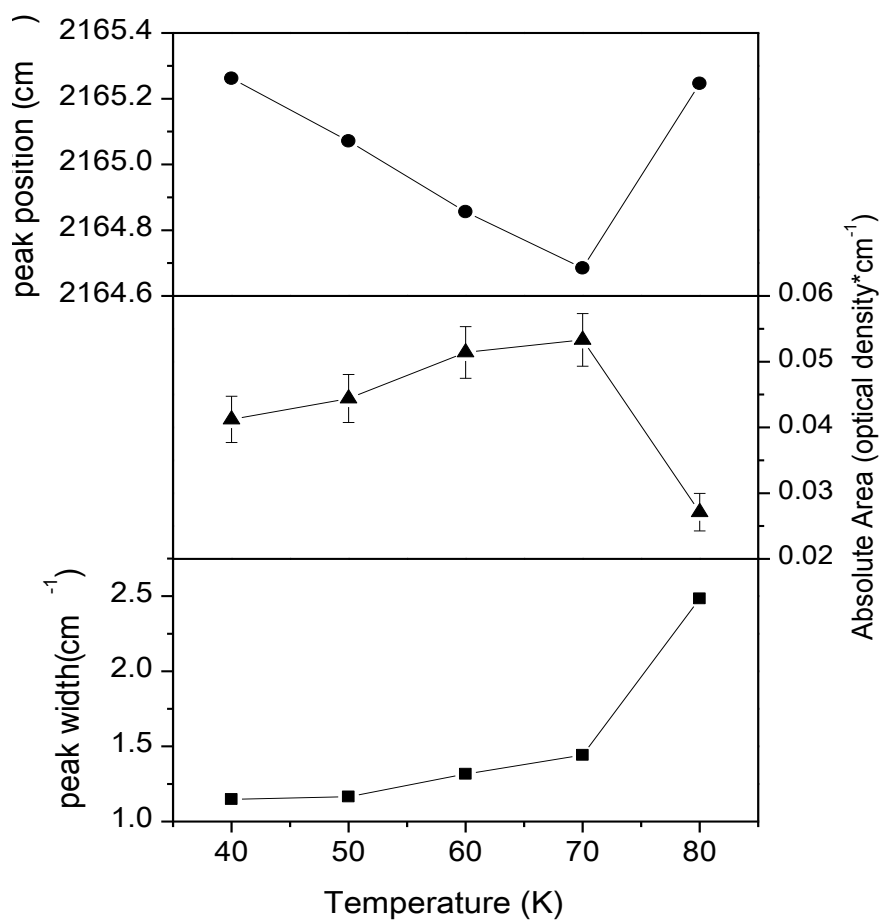
Figures 3.20. Lorentzian fit values demonstrating temperature dependence of 2150 cm⁻¹ band during TDS steps of CO desorption on TiO₂ from 40 to 150 K.



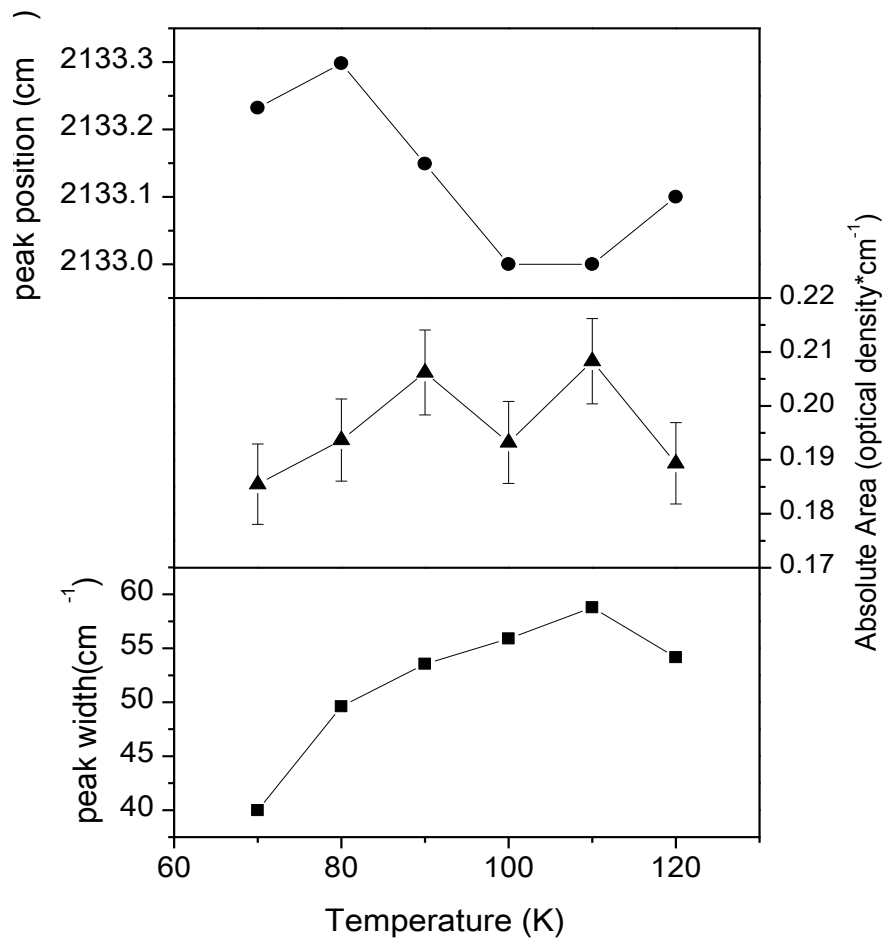
Figures 3.21. Lorentzian fit values demonstrating temperature dependence of 2127 cm⁻¹ band during TDS steps of CO desorption on TiO₂ from 40 to 150 K.



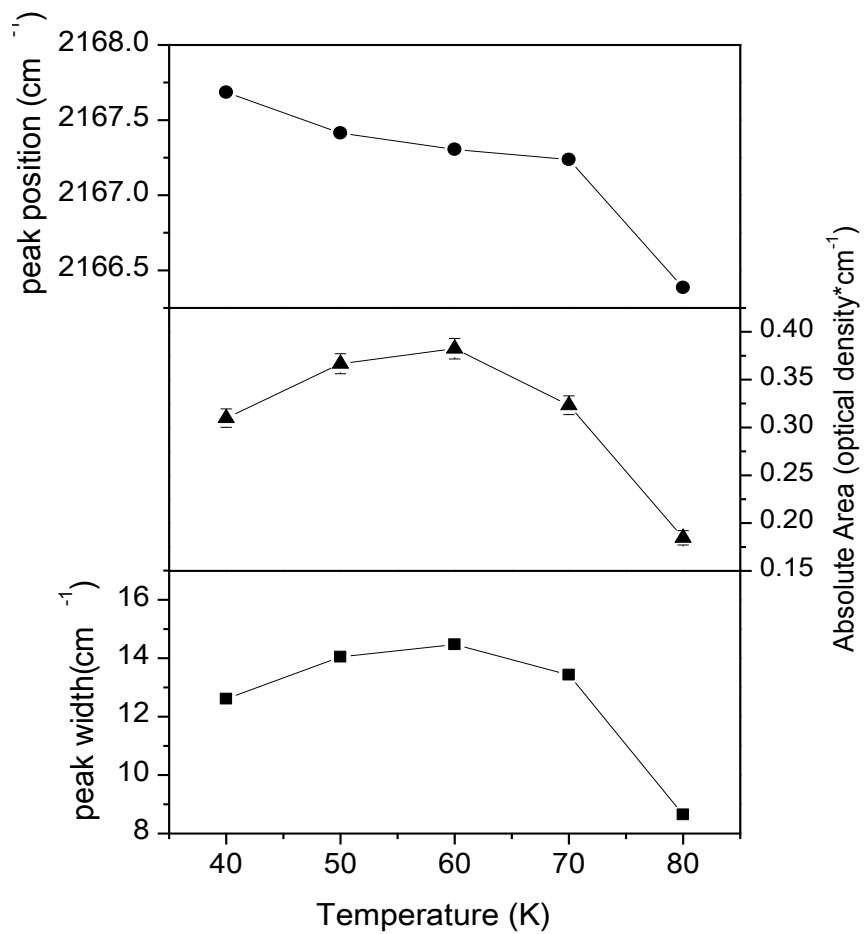
Figures 3.22. Lorentzian fit values demonstrating temperature dependence of band “b” during TDS steps of CO desorption on TiO₂ from 40 to 150 K.



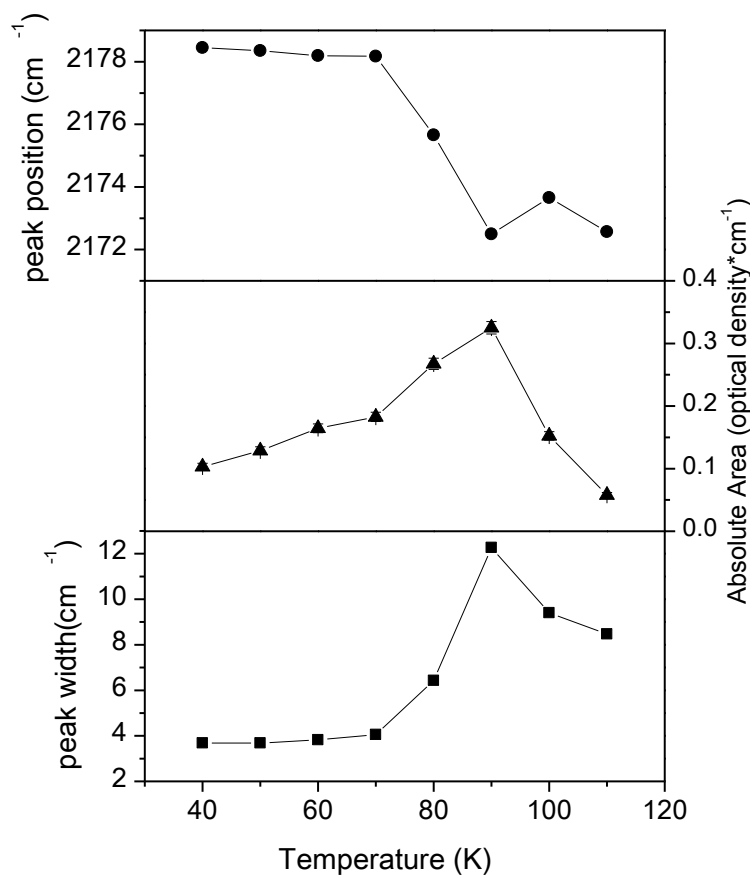
Figures 3.23. Lorentzian fit values demonstrating temperature dependence of band “c” during TDS steps of CO desorption on TiO₂ from 40 to 150 K.



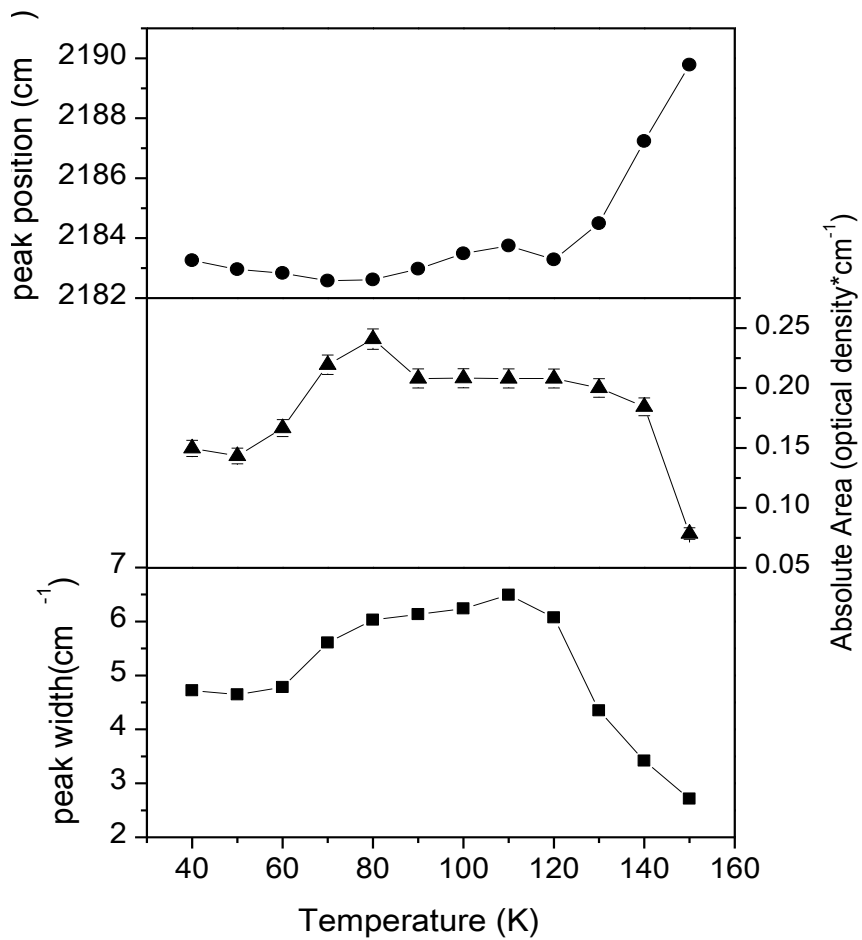
Figures 3.24. Lorentzian fit values demonstrating temperature dependence of 2133 cm^{-1} “fitting” band during TDS steps of CO desorption on TiO_2 from 40 to 150 K.



Figures 3.25. Lorentzian fit values demonstrating temperature dependence of 2168 cm⁻¹ “fitting” band during TDS steps of CO desorption on TiO₂ from 40 to 150 K.



Figures 3.26. Lorentzian fit values demonstrating temperature dependence of 2178 cm⁻¹ “fitting” band during TDS steps of CO desorption on TiO₂ from 40 to 150 K.



Figures 3.27. Lorentzian fit values demonstrating temperature dependence of 2183 cm^{-1} “fitting” band during TDS steps of CO desorption on TiO_2 from 40 to 150 K.

Table 3.2. Lorentzian fit values showing temperature dependence of chemisorbed bands

temp	band b			band c			band d			band e			2128 cm ⁻¹		
	peak center	width	area	peak center	width	area									
K	cm ⁻¹	cm ⁻¹	OD * cm ⁻¹	cm ⁻¹	cm ⁻¹	OD * cm ⁻¹	cm ⁻¹	cm ⁻¹	OD * cm ⁻¹	cm ⁻¹	cm ⁻¹	OD * cm ⁻¹	cm ⁻¹	cm ⁻¹	OD * cm ⁻¹
40	2165.26	1.15	0.041	2174.83	1.46	0.066	2179.94	1.18	0.527						
50	2165.07	1.17	0.044	2174.73	1.57	0.075	2179.81	1.21	0.578						
60	2164.86	1.32	0.051	2174.61	1.65	0.085	2179.66	1.24	0.630				2127.50	1.03	0.004
70	2164.68	1.44	0.053	2174.51	1.61	0.079	2179.52	1.27	0.647				2127.49	0.88	0.003
80	2165.25	2.48	0.027				2179.39	1.42	0.728				2127.24	1.42	0.005
90							2179.30	1.36	0.600	2179.83	3.03	0.273	2127.21	1.60	0.006
100							2179.13	1.41	0.468	2180.17	2.59	0.443	2127.25	1.33	0.005
110							2179.08	1.80	0.429	2180.33	2.84	0.508	2127.16	1.63	0.005
120										2180.58	3.63	0.927	2128.24	2.21	0.004
130										2182.56	4.63	0.768			
140										2185.01	5.13	0.492			
150										2187.97	5.77	0.229			

Table 3.3. Lorentzian fit values showing temperature dependence of “fitting” bands

temp	2133 cm ⁻¹ fitting band			2167 cm ⁻¹ fitting band			2178 cm ⁻¹ fitting band			2183 cm ⁻¹ fitting band		
	peak center	width	area									
K	cm ⁻¹	cm ⁻¹	OD * cm ⁻¹	cm ⁻¹	cm ⁻¹	OD * cm ⁻¹	cm ⁻¹	cm ⁻¹	OD * cm ⁻¹	cm ⁻¹	cm ⁻¹	OD * cm ⁻¹
40				2167.68	12.61	0.310	2178.45	3.68	0.103	2183.25	4.72	0.150
50				2167.41	14.04	0.367	2178.35	3.68	0.129	2182.96	4.65	0.143
60				2167.30	14.47	0.382	2178.19	3.82	0.164	2182.83	4.78	0.167
70	2133.23	39.98	0.185	2167.24	13.43	0.323	2178.17	4.05	0.183	2182.58	5.61	0.219
80	2133.30	49.60	0.194	2166.39	8.65	0.185	2175.66	6.43	0.267	2182.61	6.03	0.241
90	2133.15	53.55	0.206				2172.49	12.27	0.325	2182.98	6.13	0.208
100	2133.00	55.89	0.193				2173.66	9.40	0.152	2183.48	6.24	0.208
110	2133.00	58.78	0.208				2172.57	8.47	0.058	2183.74	6.49	0.208
120	2133.10	54.16	0.189							2183.28	6.07	0.208
130										2184.49	4.35	0.200
140										2187.23	3.42	0.184
150										2189.78	2.71	0.079

Table 3.4. Lorentzian fit values showing temperature dependence of physisorbed / hydrogen-bonded bands

temp	band a			2150 cm ⁻¹		
	peak center	width	area	peak center	width	area
K	cm ⁻¹	cm ⁻¹	OD * cm ⁻¹	cm ⁻¹	cm ⁻¹	OD * cm ⁻¹
40	2138.15	9.82	0.656			
50	2137.71	11.00	0.401	2149.98	1.66	0.006
60	2137.09	16.51	0.186	2150.71	4.14	0.014
70						
80						
90						
100						

3.9 References

- 1 Morterra, C., *J. Chem. Soc., Faraday Trans.* **84**, 1617-1637 (1988).
- 2 Garrone, E.; Bolis, V.; Fubini, B.; Morterra, C., *Langmuir* **5**, 892-899 (1989).
- 3 Hadjiivanov, K.; Lamotte, J.; Lavalley, J., *Langmuir* **13**, 3374-3381 (1997).
- 4 Yates, D. J. C., *J. Phys. Chem.* **65**, 746-753 (1961).
- 5 Martra, G., *Appl. Catal., A*, **200**, 275-285 (2000).
- 6 Zaki, M. I.; Knozinger, H., *Mater. Chem. Phys.* **17**, 201-215 (1987).
- 7 Redhead, P. A., *Vacuum* **12**, 203-211 (1962).
- 8 Green, I. X.; Tang, W.; Neurock, M.; Yates, J. T., Jr., *Science* **33**, 736-739 (2011).
- 9 Venkov, T.; Fajerweg, K.; Delannoy, L.; Klimev, H.; Hadjiivanov, K.; Louis, C., *Appl. Catal., A* **301**, 106-114 (2006).
- 10 Green, I. X.; Yates, J. T., Jr., *J. Phys. Chem. C* **114**, 11924-11930 (2010).
- 11 Takeuchi, M.; Bertinetti, L.; Martra, G.; Coluccia, S.; Anpo, M., *Appl. Catal., A* **307**, 13-20 (2006).
- 12 Bollinger, M. A.; Vannice, M. A., *Appl. Catal., B* **8**, 417-443 (1996).
- 13 Deiana, C.; Fois, E.; Coluccia, S.; Martra, G., *J. Phys. Chem. C* **114**, 21531-21538 (2010).
- 14 Cerrato, G.; Marchese, L.; Morterra, C., *Appl. Surf. Sci.*, **70-1**, 200-205 (1993).
- 15 Hadjiivanov, K. I.; Klissurski, D. G., *Chem. Soc. Rev.*, **25**, 61-69. (1996).
- 16 Khriachtchev, L. *Physics and Chemistry at Low Temperatures*; (Pan Stanford, 2011).
- 17 Davydov, A. A.; Rochester, C. H. *Infrared Spectroscopy of Adsorbed Species on the Surface of Transition Metal Oxides*; (Wiley: Chichester; New York; Brisbane; Toronto; Singapore, 1990).
- 18 Petrik, N. G.; Kimmel, G. A., *J. Phys. Chem. Lett.* **3**, 3425-3430 (2012).
- 19 Linsebigler, A.; Lu, G.; Yates, J. T., Jr., *J. Chem. Phys.* **103**, 9438-9443 (1995).
- 20 Manzoli, M.; Chiorino, A.; Boccuzzi, F., *Surf. Sci.* **532**, 377-382 (2003).

Chapter 4

The effect of thermal pretreatment, dosing rate, and exposure on CO adsorption over TiO₂ determined from cryogenic FT-IR spectroscopy: population of sites of weaker Lewis acidity

4.1 Abstract

The effect of deposition conditions, including the flow rate and concentration parameters, on the adsorption of CO over TiO₂ at 40 K was investigated using FT-IR spectroscopy. Thermal processing of TiO₂ nanoparticles (Degussa P25) under vacuum was explored in the range of 300 to 625 K to determine changes to surface species and effects on the CO binding population. Increased temperatures resulted in observation of increased chemisorption at 5-coordinate Ti⁴⁺ surface sites, appearing as a sharp band around 2180 cm⁻¹. Adsorption of CO at low dosing rate and low total exposure (36 ML at 0.6 ML/min) resulted in the lack of binding at sites of weaker Lewis acidity, signified by sharp features at the CO region at around 2165 cm⁻¹ and 2175 cm⁻¹, while these sites were observed during deposition of CO at increased dosing rates with comparable total exposure (21 ML at 4.2 ML/min) for samples treated above 597 K. Increasing surface temperature from 40 to 60 K promoted population transfer to these sites, however, for samples in which CO was deposited at the low dosing rate of 0.6 ML/min, when pre-heated above 490 K. A final study demonstrated that these sites of weaker Lewis acidity could be populated during deposition at 40 K for samples which were subjected to a milder heat treatment (413 K) if the CO dosing rate and total exposure was increased

(10,000 ML at 60 ML/min). These results suggest alteration of the initial binding site population by the CO during the deposition.

4.2 Introduction

As discussed in Chapter 1, the distribution of binding sites available for CO adsorption on the surface of nanostructured TiO₂ has been shown to be strongly dependent on surface pretreatment prior to CO exposure, as well as the adsorption parameters.¹⁻⁴ Studies presented in Chapter 3 on CO adsorption over the TiO₂ support material at 40 K demonstrated the requirement of pre-heating the sample *in-vacuo* prior to CO exposure in order to observe chemisorption of the CO at support sites. The effect of thermal pretreatment of the TiO₂ samples *in-vacuo* is thought to reduce the surface of the oxide through removal of oxygen from the oxide lattice surface.^{5,6} The surface structure of the TiO₂ can sustain oxygen vacancies,⁷ removal of surface oxygen results in oxygen defect sites through reduction of the titania cations in the surface. Exposure of the surface to CO also has been shown to have a reductive effect^{4,5}, whereby CO removes surface oxygen to produce CO₂.

To further explore the effects of surface heating on the support material used for the investigations presented in this dissertation, a systematic study was conducted to measure CO adsorption over TiO₂ that had been treated at several temperatures in the range of 372 to 578 K. This Chapter presents FT-IR spectra demonstrating the changes to the support material occurring during these heat treatments, as well as the spectra collected during subsequent CO deposition. These studies build on the concepts

developed in the previous chapter. The evolution of spectral bands upon warming the CO-covered surface following deposition from 40 to 150 K was used to observe population transfer between various binding sites on the surface. Qualitative trends in the bands upon warming were used to understand the effects of variations in sample pretreatment prior to CO exposure.

In addition to the more detailed studies on the effect of pretreatment temperatures on observed binding site population over the support, the effects of dosing rate and total CO exposure on the binding site profile were also investigated using FT-IR spectroscopy. Adsorption of CO at high dosing rates and high total exposure were compared to adsorption at low dosing rates and low total exposure in order to study changes to binding site chemistry that may occur during deposition. As described previously, CO exposure is also known to reduce the surface, a similar effect to thermal processing under vacuum.⁴⁻⁶ Since heating the sample is required to observe chemisorption at cationic centers on the oxide surface, including binding at sites of weaker Lewis acidity, the effect of increased CO exposure on the evolution of binding sites was measured for samples that had been treated using milder processing conditions. We expected that if thermal processing at elevated temperatures produces surface reduction necessary to observe chemisorption at cationic centers, similar results would be obtained during reduction through CO exposure for samples heated at milder temperatures.

4.3 Experimental methods

A description of the instrument setup, sample preparation, experiment parameters, and peak fitting analysis procedures is provided in Chapter 2. All spectra were collected at a resolution of 2 cm^{-1} and averaged over 500 – 1000 scans, unless otherwise noted. The main data discussed throughout this chapter involve adsorption experiments that were conducted on three separate TiO_2 samples. For clarity, samples were labelled “W”, “X”, and “T”. For one sample, labelled sample “W”, support powder was coated onto a W-mesh substrate (Unique wire weaving, CO; 100 by 100 Tungsten wire mesh Plain, 0.002” diameter) instead of CaF_2 . Both samples “W” and “T” were prepared by from a suspension of TiO_2 NPs in a 1:10 acetone:water solution, while sample “X” was prepared from a 10:1 acetone:water solution.

Samples were heated *in vacuo* to a temperature set-point ranging from 400 to 750 K prior to reagent gas deposition. The actual temperature measured at the sample by the Pt sensor (see Chapter 2, Section 2.3.2 and *Figure 2.3* for details) is indicated in the figure labels wherever relevant. Gas deposition time, concentration, and flow rate were varied across multiple adsorption experiments for this study. These parameters were controlled by adjusting the mole fraction of CO in helium carrier gas, and adjusting the flow rate during deposition. The actual exposure and dosing rates are provided in the captions of figures as relevant. As a guide, Table 4.1 provides the parameters of thermal processing temperature, exposure, and dosing rate varied for experiments involving all three samples. The values for monolayers/minute (ML/min) are known and based on the pressure in the vacuum chamber measured during deposition. Specifically, at a pressure

of 10^{-5} Torr, the collision rate is such that 10 ML/s of gas are deposited over the surface, which increases to 1000 ML/s at 10^{-3} Torr.⁸

Table 4.1. Dosing rates and CO exposure for all samples and experiments presented in this chapter

Sample ID	processing temperature	dosing rate	deposition time	exposure (θ)
	K	ML/min	min	ML CO
T	unheated	0.6	60	36
	372	0.6	60	36
	432	0.6	60	36
	490	0.6	60	36
	578	0.6	60	36
X	625	300	3	900
			7	2100
	597	4.2	2.5	10.5
			5	21
		7.5	31.5	
W	413	0.6	100	60
		60	180	10800

4.4 Results

4.4.1 Pretreatment of support: temperature effects

To study the effects of pretreatment temperature on binding site population, sample “T” was thermally processed during separate, sequential experiments by heating at 372 K, 432 K, 490 K, and 578 K under vacuum for 1 h prior to exposure to CO at 40 K. Infrared spectra of the support collected at 4 K after heating, as well as the spectrum of the unheated sample, are provided in *Figure 4.1*. The carbonate region and C-H stretching region are provided in *Figures 4.1a* and *4.1b*, respectively, to show the major changes which occurred during heating. These thermal pretreatments revealed a

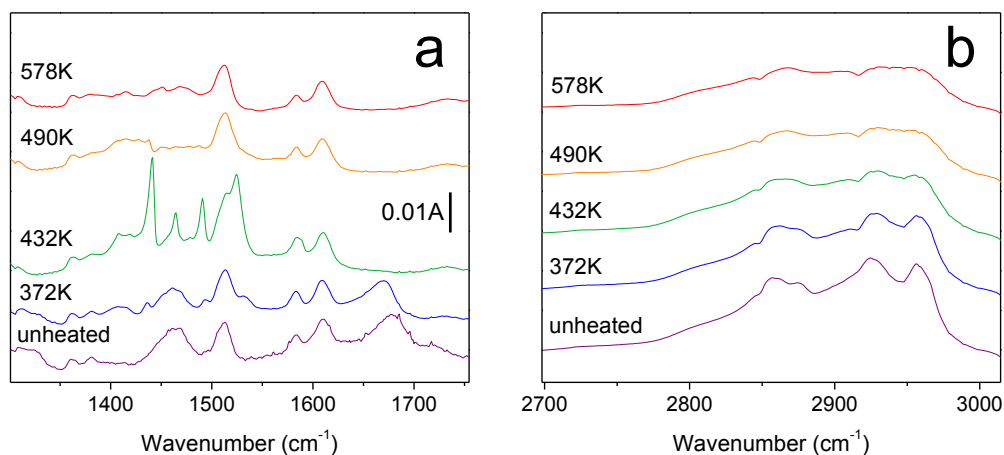


Figure 4.1. FT-IR spectra collected at 4 K of TiO₂ surface of sample “T” prior to thermal processing (purple) and after heating *in vacuo* at set-point of 400 K (blue), 500 K (green), 600 K (orange), and 700 K (red) showing the a) carbonate region and b) C-H stretching region. Both panels displayed at same vertical scale and labelled temperature values indicate the temperature measured at Pt sensor.

strong dependence of the surface species on the temperature of the pretreatment. The most striking features in the 1300 – 1700 cm⁻¹ region are the appearance of sharp vibrational bands after treatment at the intermediate temperature of 432 K, which are subsequently removed from the spectrum after heating to higher temperatures (Fig. 4.1a). As discussed in Chapter 1, these bands are associated with carbonate species on the surface of the oxide.^{5,9-11} The trend over all the temperatures is that the vibrational bands in this carbonate region are first increased at intermediate temperatures and then progressively decreased as the heating temperature is increased, with only a few bands remaining after heating at the highest temperature of 578 K. The C-H stretching region from 2800 – 3000 cm⁻¹ shows a smooth decrease in all bands as the temperature is increased from 372 to 578 K (Fig. 4.1b).

To emphasize the changes that occur during heating, difference spectra were also calculated from a subtraction of the spectra collected at 4 K before heating and after the heating step. These spectra, provided in *Figure 4.2*, confirm that the appearance of sharp bands in the region from 1400 – 1600 cm^{-1} after treatment at 432 K occurred during the heating step. Additionally, the difference spectrum showing changes occurring during heating at 490 K clearly shows the depletion of these bands at the higher treatment temperature. The most significant feature of these difference spectra, however, is the large increase of intensity between 800 and 900 cm^{-1} , the region where surface Ti-O stretching modes absorb.⁵ Heating to 372 K produces a small increase at approximately 840 cm^{-1} , and this feature becomes more intense and blue-shifted as the temperature of heat treatment is increased. These effects may reflect reduction of the surface and are explained in more detail in the discussion section.

The CaF_2 window also has a large absorbance just below 800 cm^{-1} , and some of these effects may be caused by thermal changes to the window. However, this is unlikely as the structure of the CaF_2 would be expected to remain the same at 4 K, the temperature at which both spectra were collected. More specifically, the reduction processes which occur over TiO_2 and involve the change in surface oxygen content would not be expected to occur with the salt structure of CaF_2 , and it is in the surface oxygen region (800 – 1100 cm^{-1}) that these changes are observed upon heating the sample. To verify that these

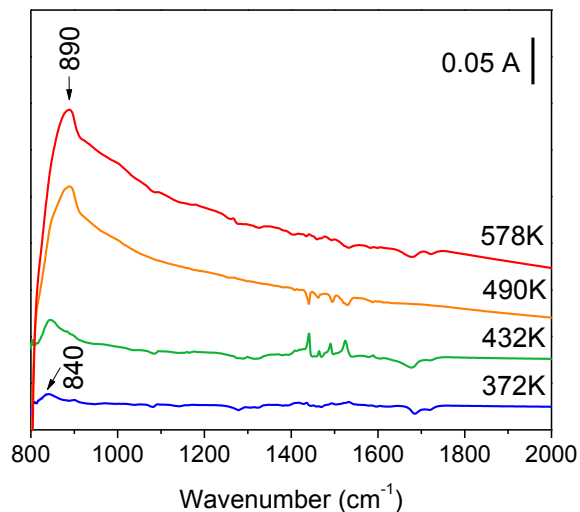


Figure 4.2. FT-IR difference spectra collected at 4 K of TiO₂ sample “T” emphasizing changes before and after heating *in vacuo* at set-point of 400 K (blue), 500 K (green), 600 K (orange), and 700 K (red). Labelled temperature values indicate temperatures measured at Pt sensor.

effects are indeed due to the TiO₂ sample, the spectrum of a blank CaF₂ window that did not contain TiO₂ was measured at 4 K before and after heating at 626 K. The spectra at 4 K before and after heating, provided in *Figure 4.3a*, are nearly overlapping. This overlap is reflected in the calculated difference spectra as well (Fig. 4.3b), which is clearly dissimilar from the difference spectra collected for samples containing TiO₂ which exhibit a progressive increase in the absorbance in the 800 – 1100 cm⁻¹ with increasing processing temperature. To demonstrate the reproducibility of this spectral trend, additional analogous spectra to those in *Figure 4.3* are provided in *Figure 4.4* for a CaF₂ window containing a different sample of TiO₂. Again, the presence of the sample causes the large changes in absorbance below 1100 cm⁻¹.

The similarity of the spectra in *Figure 4.4b* to the spectrum in *Figure 4.2* collected after heating at 578 K indicates that this change in band intensity is a reproducible

spectral feature that occurs during thermal processing of the TiO₂. One striking difference here, however, is increased intensity of the changes in the difference spectra for heating the TiO₂ sample in *Figure 4.4b* compared to heating the sample in *Figure 4.2*. The amount of TiO₂ on the CaF₂ window was much higher for the sample used to collect the data in *Figure 4.4* (prepared by RDK, actual amounts not available) than the amounts used to collect most of the data presented in this dissertation (samples prepared by NKJ). The thicker coating of sample on the window is also evident by comparison of the baseline of the raw spectra in *Figure 4.4a*, which has a baseline absorbance of 1 – 2 Absorbance units in the region around 1000 cm⁻¹, to the raw data used to generate the difference spectrum of the sample heated at 578 K in *Figure 4.2* (A comparison of spectra collected before and after the heating step for both samples is provided in *Figure 4.13* of the appendix). Increased baseline absorbance is due to scattering of the IR beam by the powder sample, which prevents beam transmission and absorbance at the surface. The blank window has the lowest baseline absorbance, as there is minimal scattering across the relatively flat CaF₂ surface (Fig. 4.3a).

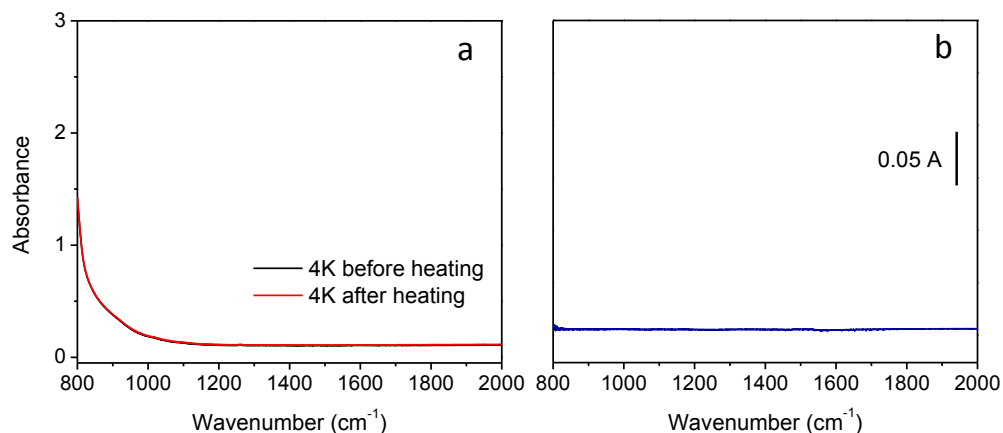


Figure 4.3. FT-IR spectra collected at 4 K of blank CaF_2 window a) before (black) and after (red) heating sample at 626 K (750 K set-point) and b) difference spectrum calculated from panel a. Spectra collected by RDK, figure prepared and data analyzed by NKJ.

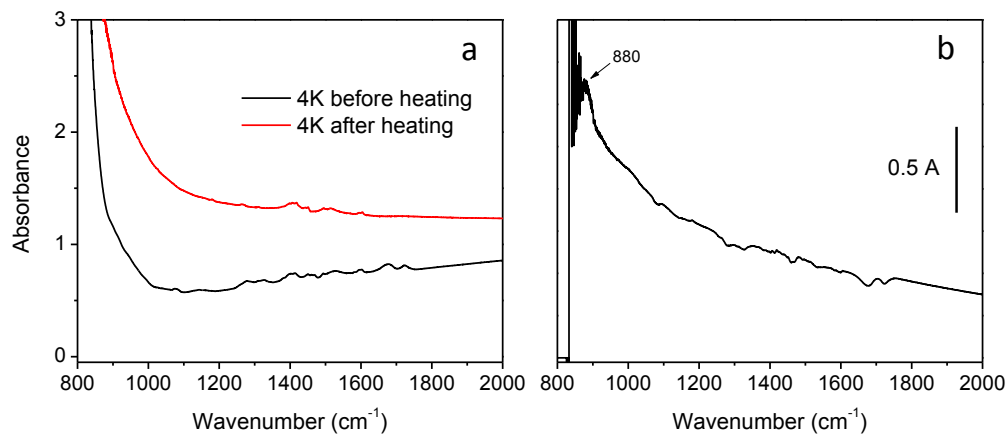


Figure 4.4. FT-IR spectra collected at 4 K of CaF_2 window coated with TiO_2 powder a) before (black) and after (red) heating sample at 604 K (750 K set-point) and b) difference spectrum calculated from panel a. Spectra collected by RDK, figure prepared and data analyzed by NKJ.

4.4.2 CO adsorption under vacuum conditions over thermally treated support: effect of exposure and dosing rate

Following thermal pretreatment under vacuum, the FT-IR spectra at 40 K was measured over sample “T” at an exposure of 36 ML CO at a dosing rate of 0.6 ML/min after thermal processing at temperatures in the range of 372 to 578 K (Figure 4.5) Each spectrum is referenced to the spectrum collected prior to CO deposition. The results of these adsorption experiments are compared to those obtained from CO absorption over the sample used to collect the data in Chapter 3. For comparison, the sample used to explore adsorption in Chapter 3 is labelled sample “X” here, and will be referred to in this way throughout the results and discussion sections.

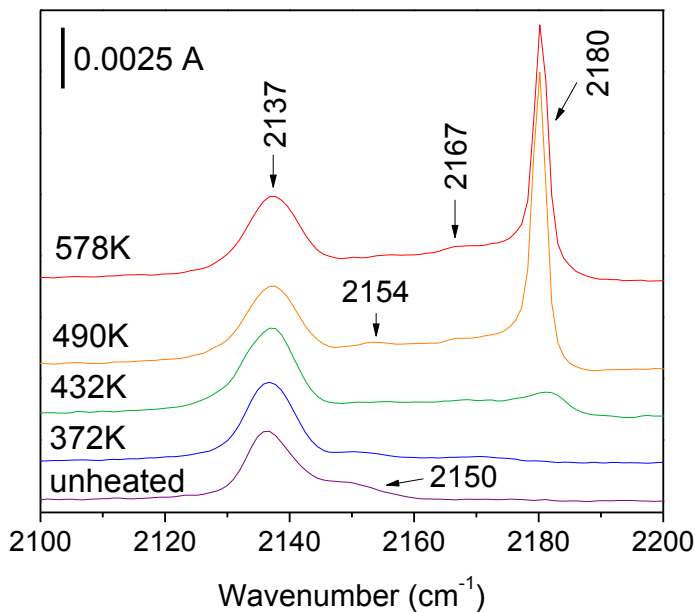


Figure 4.5. FT-IR difference spectra at 40 K following CO deposition (36 ML CO at 0.6 ML / min) on TiO₂ sample “T” before heating (purple) and after heating at a temperature set-point of 400 K (blue), 500 K (green), 600 K (orange), and 700 K (red). Labelled temperature values indicate temperatures measured at Pt sensor.

Vibrational bands in the spectra of CO adsorbed on nanoparticulate TiO₂ at 40 K revealed two distinct bands at 2137 cm⁻¹ and 2180 cm⁻¹, with continuous absorbance in between causing a spectral ‘filling in’ of additional bands. The band at 2137 cm⁻¹ was observed for both the unheated support material, as well as for TiO₂ samples after the full range of pretreatment temperatures. This band had negligible change in intensity dependent on preheat temperature, and is the vibrational signatures of CO occupying physisorption sites (Chapter 3). The intensity of the peak at 2180 cm⁻¹ depended greatly on the pretreatment temperature prior to CO exposure, and was only present after heating. This band appeared at low intensity, as a broad feature for samples heated at 372 and 432 K, and was sharp and narrow after heating to higher temperatures of 490 and 578 K. A broad, weak feature centered at 2167 – 2170 cm⁻¹ becomes more pronounced with increased pre-heating temperature. In contrast to samples prepared at higher dosing rates and increased total CO exposure (2100 ML at 300 ML/min), these experiments showed no distinct, sharp vibrational bands at 2165 cm⁻¹ and 2175 cm⁻¹ (sites “b” and “c”, see Chapter 3), even after heating at 578 K. As explained in the previous chapter, these sites correspond to sites of weaker Lewis acidity than the 2180 cm⁻¹ site. The broad feature centered at 2150 – 2154 cm⁻¹ is attributed to sites associated with hydrogen-bonded CO at hydroxylated groups over the oxide, and is most pronounced in the spectrum of the unheated sample, in accord with the analogous spectrum presented in *Figure 3.2a*. The region of the spectrum from 800 to 1300 cm⁻¹ was also monitored during deposition of CO over sample “T” following heating between 372 and 578 K. These results, provided in the appendix (*Figure 4.14*), reveal a decrease in absorbance over this region in the

difference spectra that is most prominent after thermal processing at 578 K. These changes mirror those observed during heating, which produced an increased absorbance in this region for Fig. 4.2; however, the total absorbance change was much greater in magnitude after heating the sample than following CO deposition.

Following the deposition of CO at 40 K, the sample was warmed from 40 to 150 K and simultaneously monitored spectroscopically. Spectra tracking the evolution of CO vibrational bands during this stepwise warming are provided in *Figure 4.6*. For the unheated sample and those heated at 372 K and 432 K, an inset containing an expanded view of the bands is provided to emphasize less intense bands in the spectra, shown in *Figures 4.6A, 4.6B, and 4.6C*, respectively.

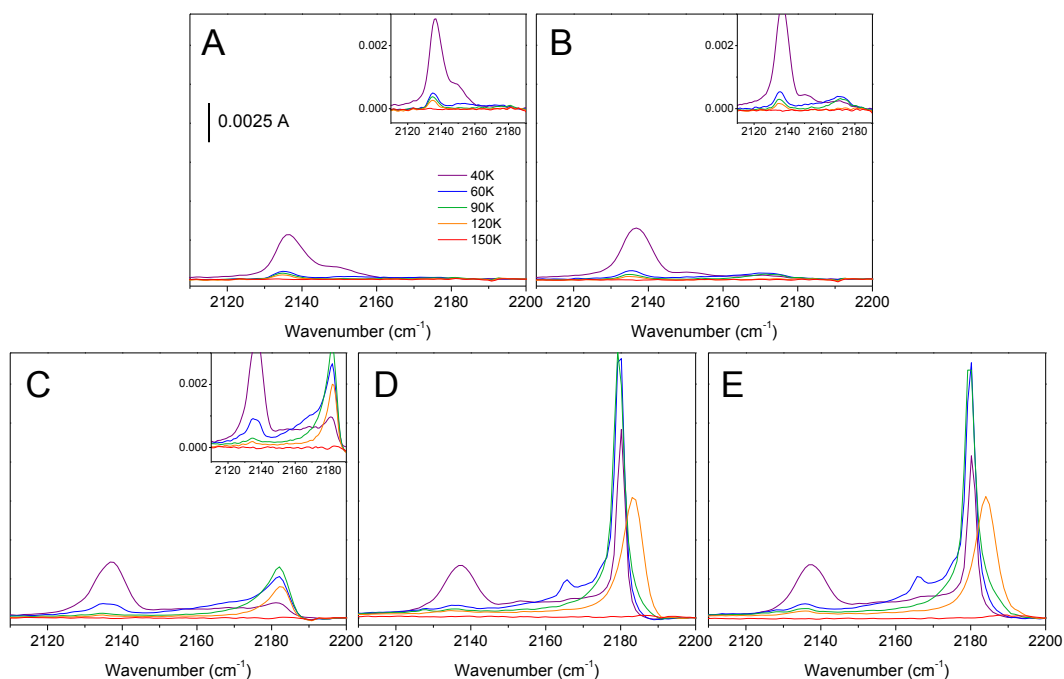


Figure 4.6. FT-IR spectra taken during surface warming steps following CO deposition (36 ML CO at 0.6 ML / min) on sample “T” A) before heating and after heating at a temperature of B) 372 K, C) 432 K, D) 490 K, and E) 578 K, indicating the temperature measured at the platinum sensor. Spectra collected at 40 to 150 K, as indicated in legend.. All panels follow same legend and are displayed at the same vertical scale.

Common to all five experiments, the first major spectral change observed is the loss of the physisorbed CO band at 2137 cm^{-1} upon warming the surface from 40 K to 60 K. For all cases except the sample that was not heated, this temperature change is also accompanied by an increased intensity in bands associated with chemisorption at the support. The observation of population transfer from the physisorbed site to chemisorbed support sites promoted by warming the surface from 40 to 60 K was presented in Chapter 3 for samples prepared at increased dosing rate and total CO exposure. A striking difference to the results presented here in comparison to those in Chapter 3, however, is the transfer of population to the chemisorption sites at 2165 and 2175 cm^{-1} over this same

temperature range for the sample “T” when preheated at 490 K and 578 K (Fig. 4.6D and 4.6E). In particular, the appearance of the band at 2165 cm^{-1} is distinct in the spectra collected at 60 K for these experiments in which deposition of CO was conducted at a much slower dosing rate (0.6 ML / min instead of 300 ML/min) and at lower total exposure (36 ML instead of 2100 ML).

During deposition, a spectrum was collected at the start to capture surface changes due to gas adsorption occurring within the first several min. To better understand the differences observed under these different deposition conditions (36 ML at 0.6 ML/min vs. 2100 ML at 300 ML/min), the spectra collected during the initial stages of deposition on sample “X” was compared to a fourth sample, labelled “Y”, both which were treated at a temperatures ranging from 591 to 625 K. The FT-IR spectrum collected during the first 3 min of deposition of CO at high dosing rate (900 ML at 300 ML/min deposited at 40 K) over sample “X” is provided in *Figure 4.7*, in which the sample had been heated at 625 K. Here, it is clear that the binding sites corresponding to vibrational bands at 2165 cm^{-1} and 2175 cm^{-1} (sites “b” and “c”) are populated very quickly during the deposition under these conditions. An additional experiment was also conducted with a low total exposure of CO adsorbed at an intermediate dosing rate (32 ML at 4.2 ML/min) over sample “X” after thermal processing at 597 K. Early spectra collected during the deposition, presented *Figure 4.15* in the Appendix section, also show binding at the “b” and “c” sites within the first 5 min of the CO adsorption.

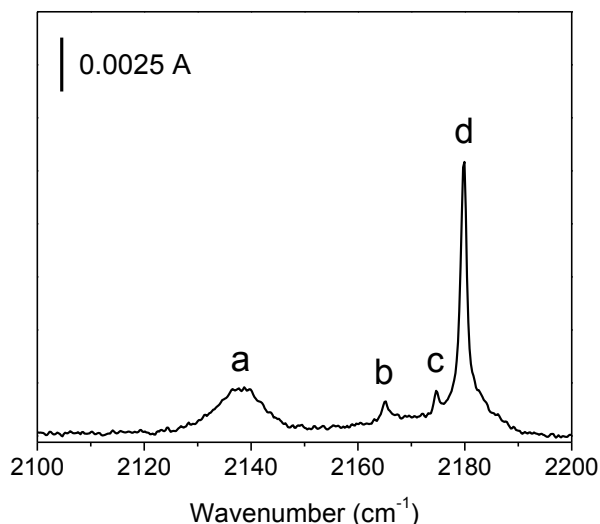


Figure 4.7. FT-IR spectra collected at 40 K during first 3 min of CO deposition (900 ML CO at 300 ML/min) over TiO₂ sample “X” after thermally processing sample at 625 K (750 K set-point). Data shown collected during experiments discussed in Chapter 3, in which binding sites labelled “a” – “d” are explained in detail. Spectrum collected at a resolution of 0.5 cm⁻¹. Spectrum collected by RDK, figure prepared and data analyzed by NKJ.

To test the effect of increased CO exposure while maintaining an intermediate dosing rate, adsorption was measured over TiO₂ sample “Y”, which had been heated at 591 K. For this study, deposition was monitored at 5, 10, and 15 min (60 ML/min deposited at 40 K), and FT-IR spectra (*Figure 4.8*) reveal that adsorption of CO at a total exposure of 300 ML resulted in population of the sites adsorbing at 2165 cm⁻¹ and 2175 cm⁻¹ during the first 5 min of deposition.

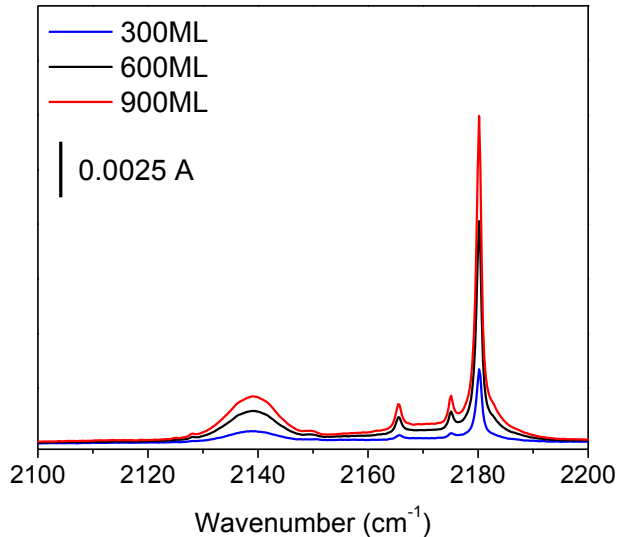


Figure 4.8. FT-IR spectra collected at 40 K during a 15 minute CO deposition (60 ML/min at 40 K) over TiO₂ sample “Y” that had been heated at 591 K (750 K set-point).

A final study was conducted using sample “W”, for which TiO₂ was coated over a W-mesh substrate. In this experiment, the sample was heated at 413 K. After this pretreatment step, a sequential deposition process was initiated in which CO adsorption was measured at low dosing rate and relatively low total exposure (CO exposure of 60 ML at 0.6 ML/min), followed by adsorption at an increased dosing rate and high total CO exposure (CO exposure of 10800 ML at 60 ML/min). After the sequence, totaling a 4.67 h deposition time, the sample had a combined total CO exposure of 10860 ML. Infrared spectra collected during the course of the deposition at both rates are provided in *Figure 4.9A*.

Analysis of these spectra indicates that as deposition time is increased, the complexity of the binding site population also increases. The dashed spectrum colored in red signifies the beginning of deposition at the higher rate, in which only broad bands

appear that are similar to those observed for the sample that had been heated to 432 K presented earlier in *Figure 4.6C*. The expanded view in *Figure 4.9B*, in which only the spectra collected during deposition at the low rate are shown, also reflects these same broad features. However, continued deposition at the higher rate throughout the 3 h time period results in appearance of sharp features in positions attributed to chemisorption at the support (at the “b”, “c”, and “d” sites identified in Chapter 3). The final spectrum collected has a strong resemblance to those in *Figure 4.8*, in which deposition was conducted over support material considered “clean” after thermal pretreatment at 591 K.

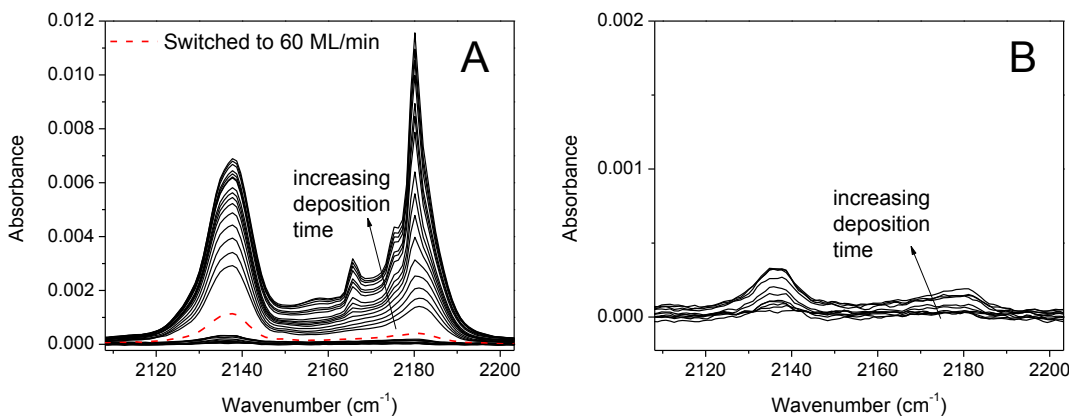


Figure 4.9. FT-IR spectra collected at 40 K throughout 4.67 h CO deposition (60 ML at 0.6 ML/min followed by 10800 ML at 60 ML/min deposited at 40 K) over TiO₂ sample “W” that had been preheated at 413 K (500 K set-point). Spectra shown include A) deposition of both reagent mixes and B) expanded view of the window with only deposition of CO at the low rate. Red, dashed spectrum indicates switch to the higher deposition rate in panel A.

A more detailed analysis of these spectral shows changes in the distribution of the CO intensity over time. Difference spectra for 10 min increments throughout the deposition at the higher dosing rate are provided in *Figure 4.10*, and show how the bands in the CO region evolve during deposition. This first spectrum is displayed at 4 times

greater intensity than the other spectra, and reveals that most of the intensity is initially in the 2137 cm^{-1} band, indicating non-specific CO physisorption. Over time, the dominant absorption band in the spectrum became the 2180 cm^{-1} band as intensity of the 2137 cm^{-1} decreases. These specific bands represent changes in population of distinct chemisorption wells, with the final difference spectrum containing very sharp features attributed to the “b”, “c”, and “d” sites previously described in Chapter 3. The total integrated intensity of CO vibrational bands in the region of $2100 - 2200\text{ cm}^{-1}$ is plotted in *Figure 4.11* for each 10 minute difference spectrum. As deposition time increased, the rate of intensity growth actually decreased.

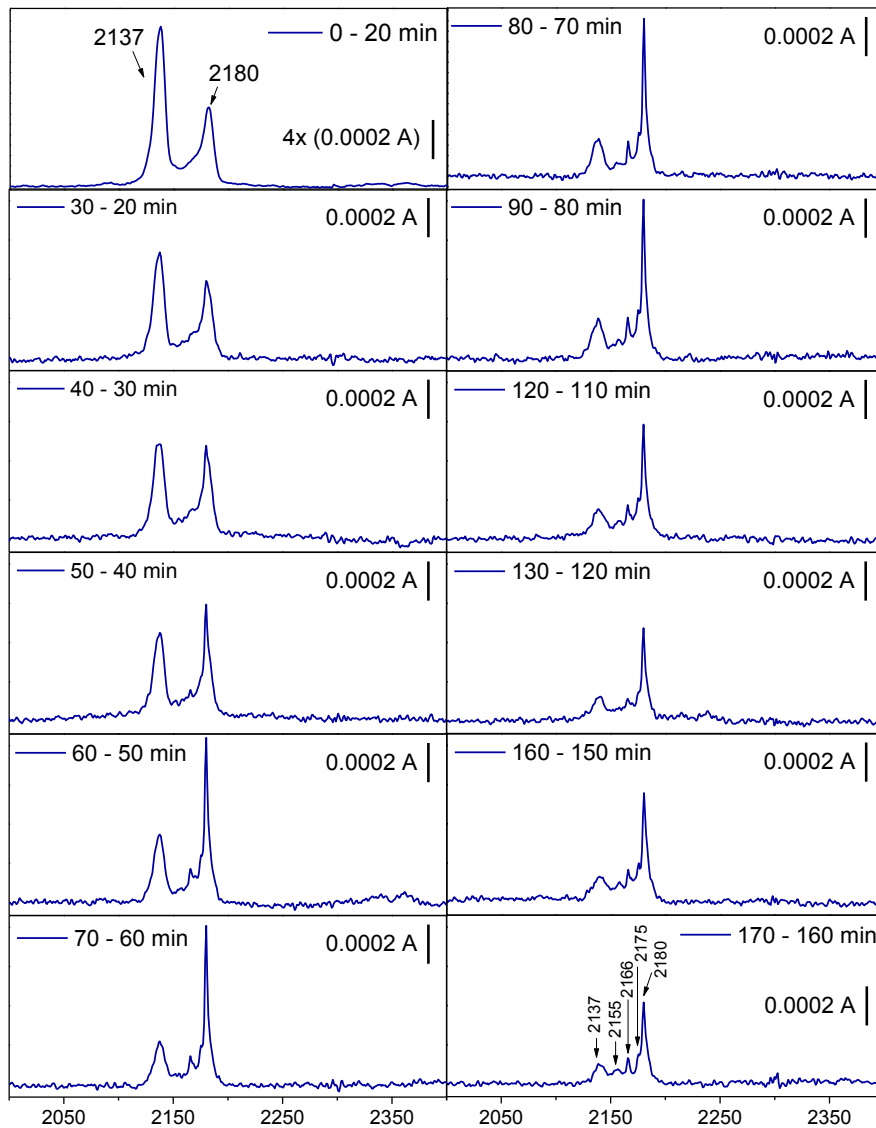


Figure 4.10. FT-IR spectra collected at 40 K throughout the 3 h deposition of CO (10800 ML at 60 ML/min deposited at 40 K) on TiO₂ sample “W” that had been preheated at 413 K (500 K set-point). Series of spectra show deposition over time during successive 10 min intervals following the first 20 min of deposition.

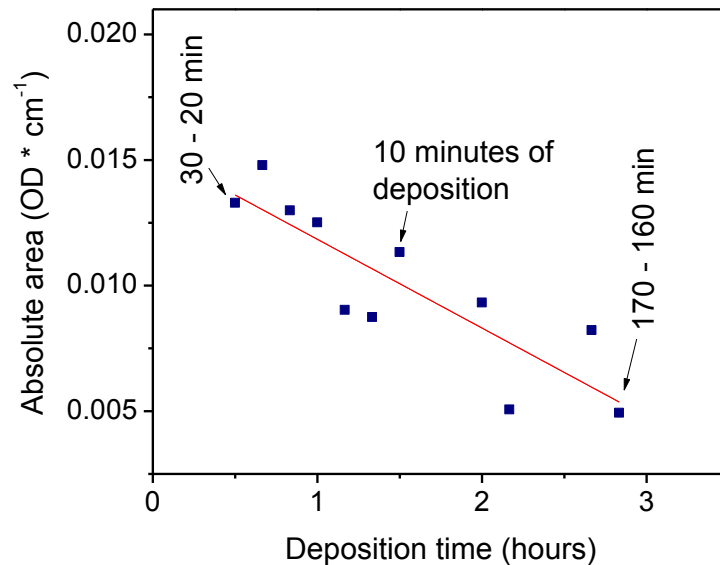


Figure 4.11. Incremental changes in intensity integrated over the spectral region from 2100 – 2200 cm^{-1} for each difference FT-IR spectrum collected at 40 K throughout 3 h deposition of CO (10800 ML at 60 ML/min deposited at 40 K) on TiO_2 sample “W” that had been preheated at 413 K (500 K set-point). Series of integrated intensities demonstrate changes in deposition over time during successive 10 min intervals. Linear fit of data fit to equation $y = -0.00353x + 0.1537$ with $R^2 = 0.713$.

While CO vibrational bands are of main interest in these studies, further understanding of the surface changes during the CO deposition process can be gained by looking at the changes observed in the Ti-O stretching region of 800 – 1100 cm^{-1} (Figure 4.12). Again, the switch to faster deposition rate is indicated by the red, dashed spectrum, and this is where the spectrum began to show dramatic changes. These changes are coincident with sharpening of the bands in the CO region which occur at about the same time during the deposition, as is evident from a comparison of Figures 4.9 and 4.12. Additional correlated changes in the spectra were noted in the carbonate and C-H stretching region of the spectrum, and are provided in Figure 4.16 in the appendix.

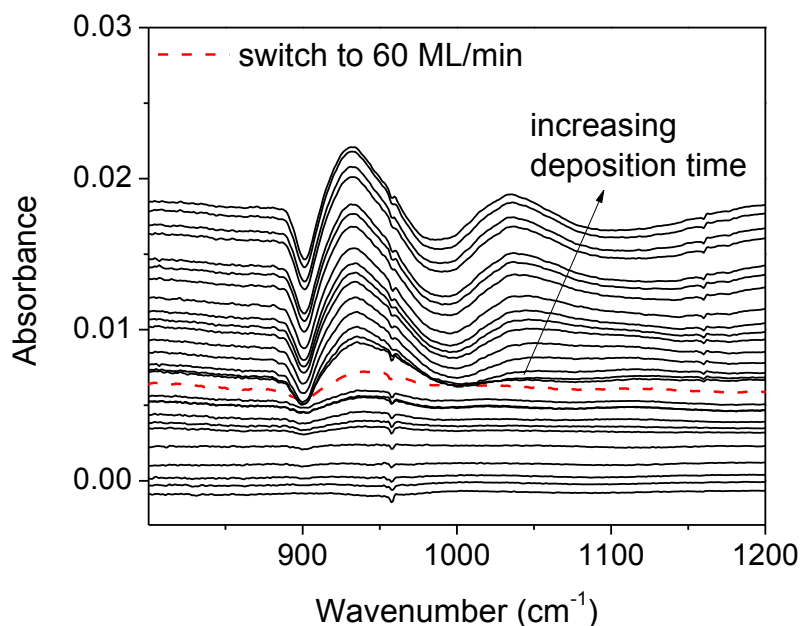


Figure 4.12. FT-IR spectra in the Ti-O stretching region collected at 40 K throughout 4.67 h CO deposition (60 ML at 0.6 ML/min followed by 10800 ML at 60 ML/min deposited at 40 K) on TiO₂ sample “W” that had been preheated at 413 K (500 K set-point). The red dashed line indicates the switch to the faster deposition rate.

4.5 Discussion

4.5.1 Effects of thermal pretreatment

The results of the spectroscopic studies of thermal treatment of the support prior to CO deposition revealed that the changes occurring to surface species during this cleaning step were strongly dependent on temperature. Most notably, difference spectra showing the changes before and after heating at each temperature reveal a progressive blue-shifting and intensity increase of bands in the region of 800 – 900 cm⁻¹. Vibrational bands in this region are typically attributed to the Ti-O stretches at the surface of the oxide, whereas bulk lattice vibrations occur at lower frequency⁵. Surface adsorbed oxygen appears to blue-shifted to this region, where the superoxide species O₂⁻ exhibits a

vibrational band at 1080 cm^{-1} , as described in Chapter 1. The spectra in *Figure 4.2* demonstrate that the heat treatment used during these experiments results in significant changes to the oxygen species over the surface, noted by the increased absorbance in the region of $800 - 1100\text{ cm}^{-1}$, which should be considered when interpreting changes to the CO region observed during the deposition process. Reduction occurring while heating the surface under vacuum should result in the creation of oxygen vacancy sites, though the complex nature of species at the surface likely results in incomplete reaction or secondary processes that complicate the spectrum. It is clear, however, that preheating at a higher temperature increases absorbance at increasingly blue-shifted frequencies, where superoxide complexes appear in the spectrum, and also decreases absorbance at lower frequency, where surface Ti-O bands appear.⁵

4.5.2 Effects of deposition conditions

The FT-IR spectra collected after CO adsorption at low dosing rate and low total exposure (36 ML CO at 0.6 ML / min) at 40 K over thermally treated TiO₂ sample “T” (Fig. 4.5) demonstrate that increasing the temperature of thermal treatment from 372 K to 490 K results in the increased intensity of the 2180 cm^{-1} vibrational band due to CO chemisorption at the support. Negligible difference was observed between spectra for adsorption in the CO region of the spectrum on the surface heated at 490 K and 578 K. Increased spectral intensity upon preheating to higher temperatures is attributed to thermal desorption of surface-adsorbed contaminants, a method previously shown in Chapter 3 and by other groups^{1,12} to free blocked sites and increase CO adsorption. The

absence of the 2180 cm^{-1} peak for substrates pretreated at lower processing temperatures supports the notion of blockage at this site is due to surface contaminants that are removed at higher temperatures (Fig. 4.1).

Most strikingly, however, no samples in this series of experiments showed binding at 40 K to the sites giving rise to peaks at 2165 and 2175 cm^{-1} (“b” and “c” sites, see Chapter 3) after deposition at 40 K. In the studies presented in Chapter 3, where CO was deposited at a higher dosing rate and higher total exposure (2100 ML at 300 ML/min) on samples preheated at 625 K, population of these binding sites occurred initially during deposition at 40 K, as evident from the early spectra collected during the deposition (Fig. 4.7). The population of binding sites observed over the support for these two very different deposition conditions suggests that increasing the number of collisions of CO with the surface during deposition results in a different binding-site populations. Variation of the dosing rate and exposure, however, indicated that the dosing rate is the dominant factor in determination of the binding site population. This is evident in the results in which the total exposure was further reduced to a value of 10.5 – 31.5 ML (at 2.5 – 7.5 min, Fig. 4.15), and the dosing rate was increased from 0.6 ML/min to 4.2 ML/min. While the overall exposure after the final deposition in both cases was comparable, binding at the weakly acidic sites “b” and “c” was not observed for the case where the dosing rate was reduced to 0.6 ML/min (Fig. 4.6E).

The correlation between dosing rate and binding site population suggests that some of the CO colliding with the surface does not contribute simply to chemisorption, but also changes the chemistry of binding sites at the surface. It may seem plausible that

the collisional energy is contributing to heating the surface, as the “b” and “c” sites on the oxide are populated at 60 K for the case where adsorption was measured under low dosing rate conditions. However, this would not be expected at such low temperatures given the constant cryo-cooling of the sample.

Another way to determine if the CO changes the binding-site chemistry during deposition is to vary the dosing rate and total exposure during adsorption over a sample which has not been fully processed during the thermal treatment under vacuum. The extended deposition of CO on TiO₂ sample “W”, which was not completely cleaned during thermal processing (heating to 413 K), resulted in a progression of bands in the CO region that changed in character during the deposition. Initial binding during adsorption at the low dosing rate (0.6 ML/min) resulted in the accumulation of intensity mainly at the physisorption site, with some low intensity broad features over the region of chemisorption bands (2160 – 2180 cm⁻¹) typical of samples thermally processed at this same mild temperature. Increasing the dosing rate to 60 ML/min resulted in the increase of intensity of all bands in this region, which continued during the extended deposition of 10800 ML. Most important, however, is that incremental steps during the deposition revealed that with increased time, CO began to increasingly chemisorb at the support. These results demonstrate that CO does in fact interact with the surface during the deposition process, and this interaction causes changes to the TiO₂ that activate chemisorption sites which were not previously available. Changes to the surface that occur during deposition of CO on the support are also evident in the region attributed to surface Ti-O vibrations and surface adsorbed oxygen. The series of spectra shown in

Figure 4.12 show the evolution of strong perturbations to bands in this region. The thin TiO₂ coating over the mesh wire used as a sample substrate for this experiment, as opposed to self-supported pellets used in studies by other authors,¹ significantly reduces the possibility of diffusion of CO to sites within the bulk material of the sample.

The results presented in this chapter are important to understanding the adsorption of CO over the surface of TiO₂ under these conditions, and especially studies conducted under static, equilibrium pressure conditions. As a great deal of characterization is required to understand the effects of sample pretreatment, which influence the binding-site profile, the effect of dosing rate and total exposure clearly cannot be ignored. The operating pressures of these experiments ought to result in even more drastic changes to the surface than those presented for the dosing rates used in these experiments, as these rates scale with pressure. Chapter 6 explores the effects of binding at conditions similar to equilibrium pressure, under steady-state flow, and results indicate changes to the Au binding sites for CO.

4.6 Conclusion

The systematic studies presented here on the thermal treatment of TiO₂ at various temperatures in the range of 372 to 578 K demonstrate that samples cleaned at higher temperatures resulted in an increase of chemisorption at support sites, whereas a negligible difference was detected for binding over samples cleaned at 490 to 378 K. Exploration of the effect of dosing rate and total CO exposure on adsorption of CO over surfaces thermally treated above 578 K revealed that the dosing rate controlled

observation of chemisorption at the support, resulting in sharp features at the CO region at around 2165 cm^{-1} and 2175 cm^{-1} , and increased intensity in the vibrational band at 2180 cm^{-1} . While deposition at low dosing rate and low total exposure (36 ML at 0.6 ML/min) did not populate the sites giving rise to bands at 2165 cm^{-1} and 2175 cm^{-1} during deposition at 40 K, transfer of population to these sites was observed during the post-deposition surface warming steps from 40 to 60 K for samples preheated above 490 K. In addition to the trends observed for various deposition parameters, we also found that CO adsorption at an increased dosing rate over samples preheated at a lower temperature (413 K) resulted in a profile of CO bands that approaches that of the sample preheated at higher temperatures (above 578 K). Extended deposition of CO was found to promote the chemisorption of CO at the surface and create site availability over time throughout the deposition.

4.7 Appendix

Preheating of TiO₂ sample “T” was compared to that of another TiO₂ sample coated in a much thicker layer of TiO₂ powder. Raw FT-IR spectra collected before and after heating were compared for both samples to demonstrate the effect of high sample amount on the baseline of the spectrum (Fig. 4.13). Preheating the sample coated by RDK resulted in a larger increase in absorbance in the spectral region of 800 – 1300 cm⁻¹. The initial baseline absorbance of this sample was also higher.

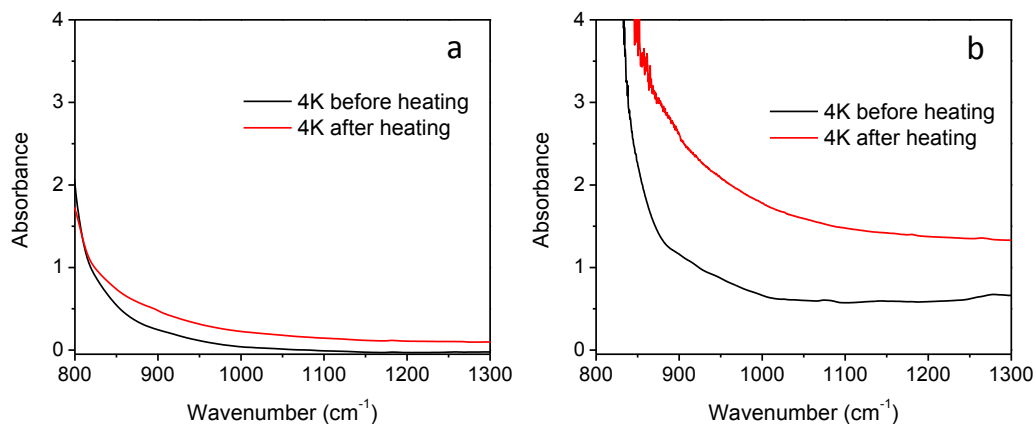


Figure 4.13. FT-IR spectra collected at 4 K of a CaF₂ window coated with TiO₂ powder before (black) and after (red) heating : a) Sample “T” heated at 578 K and b) heavily coated TiO₂ sample prepared by RDK heated at 626 K. Spectra in panel b collected by RDK; figure prepared and data analyzed by NKJ.

Adsorption of CO over sample “T” was measured after preheating at 372 to 578 K. The FT-IR difference spectra calculated between the spectra at 40 K before and after deposition are provided in *Figure 4.14*. The changes observed here in the Ti-O and surface oxygen region mirror opposite changes in the difference spectra calculated before and after the preheating step (Fig. 4.2).

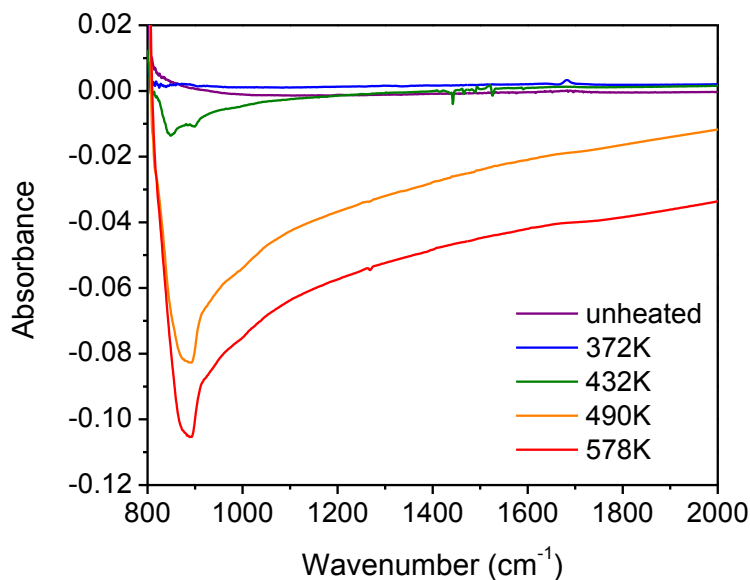


Figure 4.14. FT-IR difference spectra at 40 K following CO deposition (36 ML CO at 0.6 ML / min) on TiO₂ sample “T” before heating (purple) and after heating at a temperature set-point of 400 K (blue), 500 K (green), 600 K (orange), and 700 K (red). Labelled temperature values indicate temperatures measured at Pt sensor.

To evaluate the deposition of CO on TiO₂ under conditions of intermediate dosing rate and low total exposure, CO was deposited at 4.2 ML/min over TiO₂ sample “X” at 40 K. Infrared spectra collected at 2.5, 5, and 7.5 min during this deposition are provided in *Figure 4.15*.

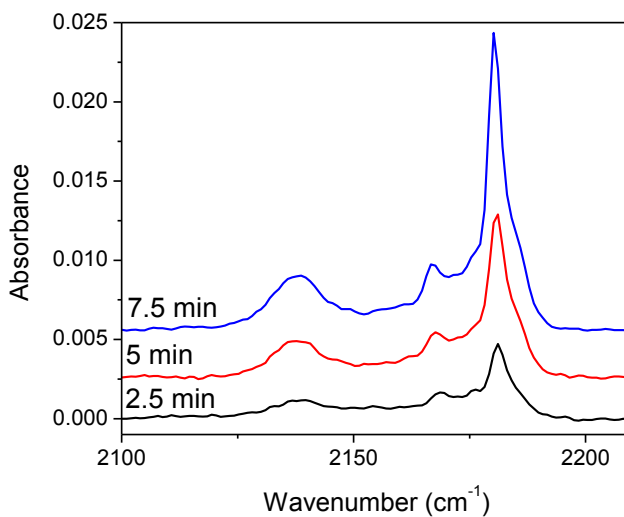


Figure 4.15. FT-IR spectra collected during deposition of CO (4.2 ML/min) on TiO₂ which was preheated at 597 K. Spectra collected by RDK; figure prepared and data analyzed by NKJ.

Infrared spectra collected during the extended deposition of CO on TiO₂ sample “W” are provided in *Figure 4.16*. The red, dashed spectrum indicates the time during the deposition when the dosing rate was increased from 0.6 ML/min to 60 ML/min.

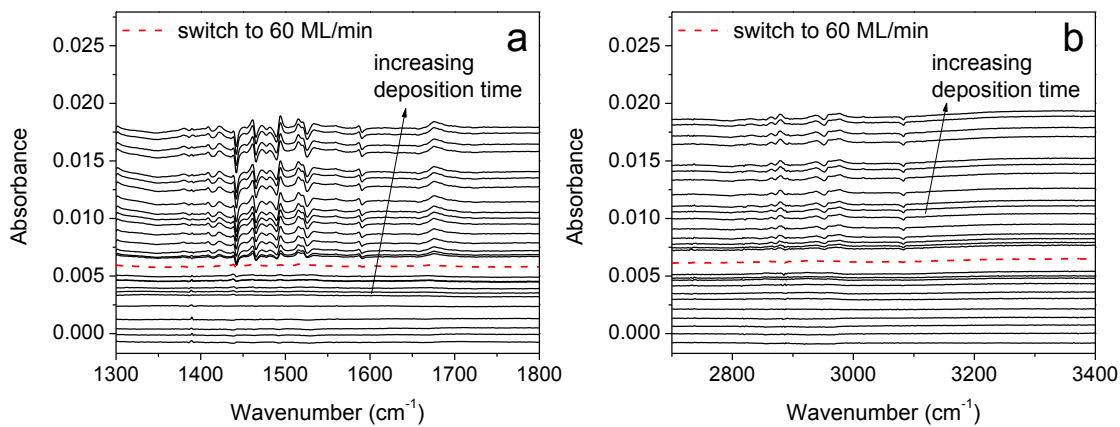


Figure 4.16. FT-IR spectra collected at 40 K throughout 4.67 h CO deposition (60 ML at 0.6 ML/min followed by 10800 ML at 60 ML/min deposited at 40 K) over TiO₂ sample “W” preheating at 413 K (500 K set-point) showing a) carbonate region and b) C-H stretch region. The red dashed line indicates the switch from 0.6 ML/min to 60 ML/min.

4.8 References

- 1 Venkov, T.; Fajerweg, K.; Delannoy, L.; Klimev, H.; Hadjiivanov, K.; Louis, C., *Appl. Catal., A* **301**, 106-114 (2006).
- 2 Boccuzzi, F.; Chiorino, A.; Manzoli, M., *Surf. Sci.* **502**, 513-518 (2002).
- 3 Boccuzzi, F.; Chiorino, A.; Manzoli, M.; Lu, P.; Akita, T.; Ichikawa, S.; Haruta, M., *J. Catal.* **202**, 256-267 (2001).
- 4 Morterra, C., *J. Chem. Soc., Faraday Trans.* **84**, 1617-1637 (1988).
- 5 Davydov, A. A.; Rochester, C. H. *Infrared Spectroscopy of Adsorbed Species on the Surface of Transition Metal Oxides* (Wiley: Chichester; New York; Brisbane; Toronto; Singapore, 1990).
- 6 Green, I. X.; Yates, J. T., Jr., *J. Phys. Chem. C* **114**, 11924-11930 (2010).
- 7 Schubert, M. M.; Hackenberg, S.; Veen, A. C. v.; Muhler, M.; Plzak, V.; Behm, R. J., *J. Catal.* **197**, 113-122 (2001).
- 8 Moore, J. H.; Davis, C. C.; Coplan, M. A. *Building Scientific Apparatus : A Practical Guide to Design and Construction*; (Westview Press: Cambridge, Mass.; Boulder, CO, 2002).
- 9 Clark, J. C.; Dai, S.; Overbury, S. H., *Catal. Today* **126**, 135-142 (2007).
- 10 Denkwitz, Y.; Zhao, Z.; Hörmann, U.; Kaiser, U.; Plzak, V.; Behm, R. J., *J. Catal.*, **251**, 363-373 (2007).
- 11 Bollinger, M. A.; Vannice, M. A., *Appl. Catal., B* **8**, 417-443 (1996).
- 12 Green, I. X.; Tang, W.; Neurock, M.; Yates, J. T., Jr., *Science* **333**, 736-739 (2011).

Chapter 5

FT-IR studies of sample pre-treatment temperature on CO adsorption at 40 K on nanostructured Au/TiO₂ generated via thermal de-wetting of gold film

5.1 Abstract

Low-temperature adsorption of CO on Au/TiO₂ and TiO₂ was studied at 40 K under high vacuum conditions ($<10^{-5}$ Torr) with FT-IR. Powder Au/TiO₂ films were prepared via thermal de-wetting of Au film over TiO₂ NPs *in vacuo*. The effects of sample pretreatment temperature on binding site population were studied at 373 to 585 K. A vibrational feature specific to CO binding at AuNP sites was observed at 2090 – 2096 cm⁻¹ for CO adsorption on Au/TiO₂ at 40 K following de-wetting of the sample. The intensity of the CO/Au band was found to be dependent on the temperature at which the sample was de-wet during thermal processing, with a maximum signal after de-wetting the Au film at 420 to 453 K. Blue-shifting and sharpening of the broad feature at 2090 cm⁻¹ occurred when the AuNPs were prepared over TiO₂ support material that had been previously heated under vacuum and exposed to CO prior to deposition of the Au film, for which the CO/Au vibrational band appeared at 2096 cm⁻¹. A series of FT-IR spectra are presented demonstrating the enhanced stability of adsorbed CO bound to AuNPs that were de-wet on support material that had previously been exposed to thermal treatment and CO adsorption.

5.2 Introduction

Following the preliminary studies aimed at understanding CO adsorption over TiO₂ support surfaces presented in Chapters 3 and 4, research on this project was expanded to begin developing techniques to explore gas adsorption over nanostructured Au/TiO₂. As described in Chapter 1, currently available spectroscopic assignments for CO binding on AuNPs supported on TiO₂ have been shown to be highly dependent on sample preparation method, pre-treatment prior to CO exposure, and experimental conditions¹⁻⁹ due to variations in surface morphology, surface-bound species, metal-support contact, and Au NP size dependent on these parameters.¹⁰ Preparation techniques can affect the surface chemistry of binding sites due to changes in metal-support contact and the size of supported nanoparticles obtained from the synthesis.^{1,2} Common preparation of Au/TiO₂ materials for FT-IR studies involves impregnation, deposition-precipitation or co-precipitation methods which rely on precursor materials for the metal and/or the support.¹¹ These details are discussed in more detail in Chapter 1.

This chapter describes a method for preparation of supported AuNPs and FT-IR spectroscopic studies on CO adsorption over these surfaces. Nanostructured Au/TiO₂ surfaces for this study were generated by spontaneous thermal de-wetting of a metallic Au film deposited on nanoparticulate TiO₂ by heating at 372 to 585 K *in vacuo* (10⁻⁸ Torr). Here we report FT-IR studies of temperature effects on Au film de-wetting, evident in the observed binding site population for CO adsorption on Au/TiO₂ samples at 40 K under high vacuum (10⁻⁵ – 10⁻⁸ Torr). Comparison is also made to binding on the TiO₂ support material, part of which was presented in the previous chapter, to better

understand changes to the support due to the presence of AuNPs. Surface-warming steps from 40 to 150 K were monitored by FT-IR to observe population transfer of CO between chemically unique binding sites on the AuNP and support. The thermal behavior of CO vibrational bands corresponding to adsorption at Au sites was studied in order to elucidate the relative stability of bound CO at these sites over samples prepared under different conditions.

5.3 Experimental methods

A description of the gas adsorption instrument setup, sample preparation, TEM imaging details, and experiment parameters are provided in Chapter 2. For this specific study, adsorption experiments were conducted on five separate samples of TiO₂ powder prepared from a slurry in 1:10 acetone:water. Different amounts of TiO₂ were coated on the CaF₂ for various samples, and these amounts are indicated in Table 5.1, shown below. The minimum amount used was ~0.0015g, labeled as the 1x coating. Samples were labeled for identification and easier communication as indicated in Table 5.1, and will be referred to by these labels throughout the text.

Table 5.1. Description of samples prepared for this work

sample	sample ID	approximate amount of TiO₂	support description
Bare TiO ₂	T	2x	
22.5 nm Au over TiO ₂	Au-UP	2x	never processed TiO ₂
22.5 nm Au over TiO ₂	Au-LP	1x	lightly processed TiO ₂
22.5 nm Au over TiO ₂	Au-HP	3x	heavily processed TiO ₂
40 nm Au over TiO ₂	Au-UP40	3x	never processed TiO ₂

Some of the data presented in this chapter for sample “T”, specifically the data shown in *Figure 5.1a*, have been previously shown in a different way in Chapter 4 (sample was also labelled “T” in Chapter 4 for consistency). The data are reproduced here in the context of the study of CO binding over AuNPs to emphasize Au-dependent features in the spectra. For experiments on supported gold NPs created via thermal dewetting, three support samples were coated with 22.5 nm and one with 40 nm of Au, as indicated in Table 5.1. Sample preparation was completed *in-vacuo* (10^{-8} Torr) via thermal processing at a temperature set-point of 400 – 700 K, as described in Chapter 2. Throughout the text, the set-point temperature is provided in the figure captions, and actual temperatures measured at the Pt sensor are indicated in the figure labels. Samples Au-LP and Au-HP are labelled as “processed TiO₂” in Table 5.1, indicating that the support coating was previously subjected to thermal treatment in vacuum and exposed to CO during direct adsorption experiments prior to coating with gold. The effect of processing under these conditions is thought to be reduction of the surface, as explained in Chapter 4. The “heavily processed TiO₂” sample (sample Au-HP) was held under vacuum for several months and cycled during multiple experiments, whereas sample Au-LP was only under vacuum for 2 weeks.

After thermal processing, samples were warmed to 40 K and reagent gas was deposited onto the surface (36 ML CO at 0.6 ML/min). During one experiment using sample Au-UP40, isotopically labelled CO was substituted in the deposition gas (36 ML ¹³CO at 0.6 ML/min). Following deposition at 40 K, the CO-covered surface was warmed from 40 to 150 K, and spectra were collected at 60 K, 90 K, 120 K, and 150 K

during warming steps to monitor the evolution of bands over samples Au-UP, Au-LP, and Au-HP. Lorentzian band-fitting of these spectra was conducted in a similar matter to the work previously described in section 3.3. For this analysis, however, bands were separated into three different groups: physisorbed CO, CO bound at support sites, and CO bound at Au sites. The fits for individual spectra collected during surface warming steps for all three samples are provided *Figures 5.12 – 5.26* in the Appendix, Section 5.7, with the tabulated data provided in Tables 5.2 – 5.10. The method for calculation of error bars applied to total-area sum plots was also described in Chapter 3. All FT-IR spectra collected during direct adsorption experiments were taken at a resolution of 2 cm^{-1} , unless otherwise noted, and averaged over 500 – 1000 scans. The post-deposition spectra reported here reflect subtraction of pre-deposition scans to emphasize CO-dependent features. Methods for reference spectra collection are described in Section 2.5.

5.4 Results

5.4.1 Thermal processing of Au/TiO₂ prior to CO deposition

For this study, samples T, Au-UP, and Au-LP were thermally processed during separate, sequential experiments by heating to 372 – 376 K, 420 – 448 K, 487 – 516 K, and 566 – 585 K under vacuum for 1 h prior to exposure to CO at 40 K. Changes in the carbonate and C-H stretching region ($1300 – 1700\text{ cm}^{-1}$ and $2800 – 3000\text{ cm}^{-1}$, respectively) observed after this pre-heating step for Au/TiO₂ samples were monitored using FT-IR. The spectra collected at 4 K after thermal processing sample Au-UP at temperatures ranging from 373 – 566 K are provided in *Figure 5.1*. Changes in surface-

bound species during heating steps prior to CO deposition are shown for both the carbonate and C-H stretching region in *Figures 5.1a* and *5.1b*, respectively.

In general, higher thermal processing temperatures depleted band intensity in these regions. The carbonate region, however, contained sharp bands appearing after processing at the intermediate temperature of 420 – 448 K, which subsequently diminished at higher temperatures. These observations are consistent with that for heating of the bare TiO₂ support at the same temperature range (Fig. 4.1). The similar behavior of these features for both Au/TiO₂ and TiO₂ samples suggests these species are associated with the support material. The C-H stretching region contains four main bands that decreased in intensity as the processing temperature was increased from 373 to 566 K (Fig. 5.1b). Similar to the carbonate bands, the temperature trends in the spectral features observed in the C-H stretching region over Au/TiO₂ are nearly identical to those observed for the bare support.

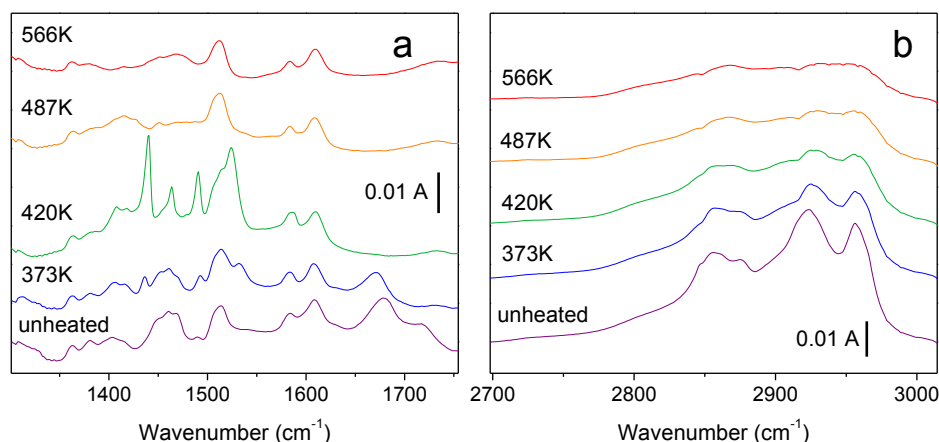


Figure 5.1. FT-IR spectra collected at 4 K of sample Au-UP prior to thermal processing (purple) and after heating *in vacuo* at set-point of 400 K (blue), 500 K (green), 600 K (orange), and 700 K (red) showing a) carbonate region and b) C-H stretching region. Both panels show same vertical scale and are labelled temperature with the temperature measured at the Pt sensor.

In addition to spectral changes in the carbonate and C-H stretching region, the effects of heating were also studied for the Ti-O and surface oxygen region. The difference spectra calculated for the 4 K spectrum before and after heating at each temperature in the range of 373 to 585 K for samples Au-UP and Au-LP are provided in *Figure 5.2a* and *5.2b*, respectively. The analogous spectra for sample “T” were presented in *Figure 4.2*. An additional sample, Au-HP, was also heated at 453 K for the adsorption studies that are discussed in Section 5.7.2. For ease of comparison of spectral changes to the Ti-O and surface oxygen region, a difference spectrum calculated before and after heating the sample is provided as well (Fig. 5.2c).

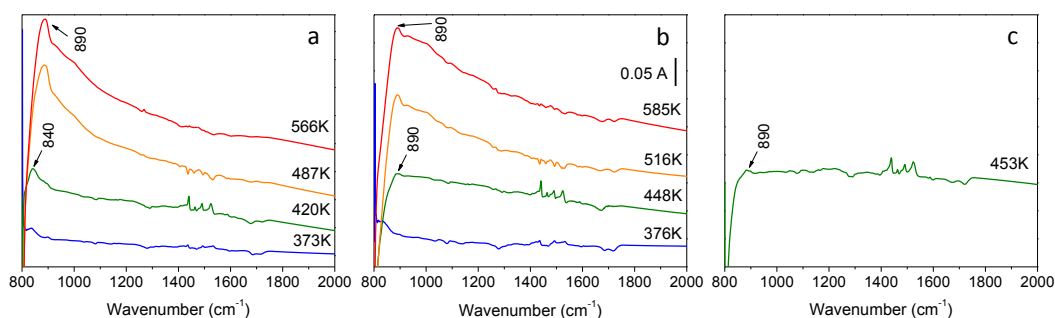


Figure 5.2. FT-IR difference spectra collected at 4 K of Au/TiO₂ emphasizing changes before and after heating *in vacuo* at set-point of 400 K (blue), 500 K (green), 600 K (orange), and 700 K (red) for samples a) Au-UP, b) Au-LP, and c) Au-HP. All panels show same vertical scale and are labelled temperature with the temperature measured at the Pt sensor.

The overall effect of heating samples that contain both TiO₂ and Au appears to be the same, producing an increased absorbance in the region of 800 – 1100 cm⁻¹. A comparison of the trends observed between samples Au-UP and Au-LP reveals that for the Au-UP, the Au/TiO₂ sample created without processing the TiO₂ support prior to Au film deposition, the strongest feature in the difference spectrum is an increasing band at approximately 840 cm⁻¹, and blue-shifts to 890 cm⁻¹ and increases in intensity with increasing temperature from 420 to 566 K. This result is nearly identical to that obtained for the bare TiO₂ support sample (Fig. 4.2). The feature showed slightly different thermal behavior in sample Au-LP, for which increased absorbance around 890 cm⁻¹ was observed for the lower thermal processing temperature of 448 K, and the remained at this position as the temperature was increased to 585 K. These spectra also show increased absorbance around 1000 cm⁻¹ that is not present in samples “T” and Au-UP (Fig. 4.2 and

5.2a). Heating sample Au-HP, the Au/TiO₂ sample also prepared over processed TiO₂, at 453 K produced similar results to those for sample Au-LP that was processed at 448 K.

5.4.2 CO adsorption on Au/TiO₂ and TiO₂ at 40 K

Following thermal processing of samples T, Au-UP, and Au-LP under vacuum, CO adsorption was measured at 40 K using FT-IR during a series of experiments in order to assess the effect of heating temperature on the binding site population, in a similar way to those experiments conducted using the bare support (Chapter 4). The FT-IR spectra tracking CO adsorption onto pure TiO₂ support before and after thermal treatment are provided in *Figure 5.3a*, and similar spectra for samples Au-UP and Au-LP are provided in *Figures 5.3b* and *5.3c*, respectively. Similar treatment of samples with and without Au over the support surface allowed for detection of Au-dependent features in the spectrum.

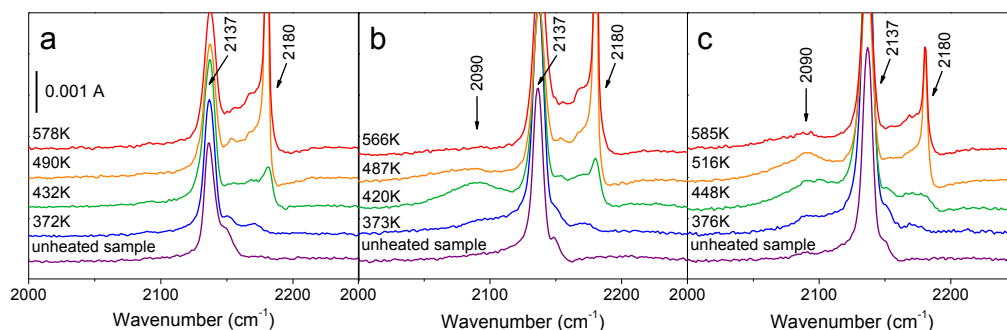


Figure 5.3. FT-IR spectra taken at 40 K following CO deposition at 40 K (36 ML CO at 0.6 ML/min) before heating (purple) and after heating at a set-point of 400 K (blue), 500 K (green), 600 K (orange), and 700 K (red) of samples a) T b) Au-UP and c) Au-LP. All panels show same vertical scale and are labelled temperature with the temperature measured at the Pt sensor.

Comparison of spectra collected after CO deposition at 40 K on both Au/TiO₂ samples and sample “T” revealed a new vibrational band at 2090 cm⁻¹, in addition to the features observed from interactions with the support alone. Systematic studies of the effect of pre-treatment temperature on CO bands demonstrated temperature-dependent trends reflected in this feature unique to samples containing Au. The broad feature had the greatest intensity after heating the sample at 420 – 448 K, with diminished intensity after treatment at 373 – 376 K, 487 – 516 K, and 566 – 585 K. The diminishing intensity of the 2090 cm⁻¹ band at higher pre-heating temperatures was most prominent for samples prepared from support material that had not been heated under vacuum prior to deposition of the Au film (Au-UP). Interestingly, sample Au-UP also had a lower ratio of Au:TiO₂ when compared to sample Au-LP, and thus inherently a greater surface area for de-wetting the Au film. This is because de-wetting the gold over more TiO₂ would mean there was additional surface for the AuNPs to disperse over. The origin of the vibrational intensity of this band as the CO-stretch was confirmed with isotopic studies, presented later in Section 5.4.3.

Vibrational bands in the spectra of both nanoparticulate TiO₂ and Au/TiO₂ samples revealed two distinct CO bands at 2137 cm⁻¹ and 2180 cm⁻¹, with continuous absorbance in the region between 2137 cm⁻¹ and 2180 cm⁻¹ causing a spectral ‘filling in’ of additional bands. The behavior of the bands in this region was qualitatively the same for samples containing AuNPs as for those of bare TiO₂ for which the deposition conditions were kept identical. The dependence of vibrational bands attributed to binding

at the support on thermal processing have been described previously in the studies on the bare TiO₂ support in Chapter 3, and in greater detail in Chapter 4.

In order to gain more understanding of the dependence of the CO/Au feature on the de-wetting temperature, as well as on the effect of heating the TiO₂ support prior to coating with Au, the progression of CO bands at early times during the deposition were compared for each sample. To facilitate this analysis, spectra were collected throughout the duration of the deposition to monitor the growth of these bands as a function of deposition time. *Figure 5.4* shows the initial spectra collected within the first 5–10 min of CO deposition over TiO₂ (sample “T”, *Figure 5.4a*) and Au/TiO₂ (samples Au-UP and Au-LP, *Figures 5.4b, and 5.4b*, respectively) following pre-heating at the full range of temperatures. In addition to these samples, the early spectrum collected during CO deposition over a third Au/TiO₂ sample (Au-HP) after pre-heating at 453 K is also shown, in *Figure 5.4d*.

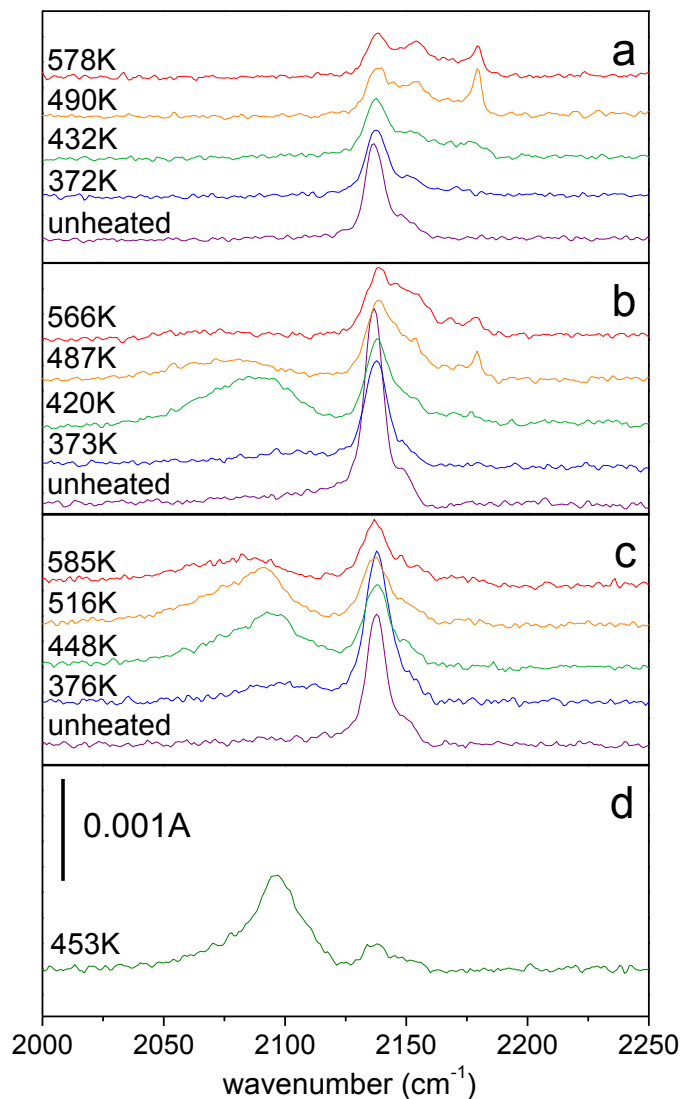


Figure 5.4. FT-IR spectra collected during the first 5 – 10 min of CO deposition at 40 K (0.1% in He at 1sccm) before heating (purple) and after heating sample at a set-point of 400 K (blue), 500 K (green), 600 K (orange), and 700 K (red) for samples a) T b) Au-UP c) Au-LP and d) Au-HP. All panels show same vertical scale, and labelled temperature was measured at the Pt sensor.

Inspection of these early time spectra reveals that the band specific to samples containing AuNPs is the first to appear and saturate in the spectra, before binding at the support sites begins. In the spectra for all three Au/TiO₂ samples, the most prominent

bands appear first at 2090 – 2096 cm^{-1} (CO/Au) and at 2137 cm^{-1} (CO physisorption). Also apparent from these spectra is that when the CO/Au signal is present to a greater intensity, the intensity of the 2180 cm^{-1} band is not evident at early times. This relationship is clearest when comparing spectra for Au-LP and Au-UP after heating at the highest temperatures of 487 – 516 K and 566 – 585 K, for which binding to the support is only observed for Au-UP, the sample which also has a low CO/Au signature in the spectra.

As an additional experiment to further understand the effect of increased thermal processing temperatures on the signal of CO bound at AuNPs on these samples, Au-HP was also heated at the increased temperature of 593 K. The FT-IR spectra collected after the full CO adsorption cycle (36 ML CO at 0.6 ML/min) at 40 K over all three Au/TiO₂ samples following heating at this upper temperature range (measured temperature of 566 – 593 K) are provided in *Figure 5.5*. Comparison of these spectra indicates that the lowest CO/Au signal is observed for adsorption over sample Au-UP, in comparison to the samples that were prepared over processed TiO₂ (Au-LP and Au-HP).

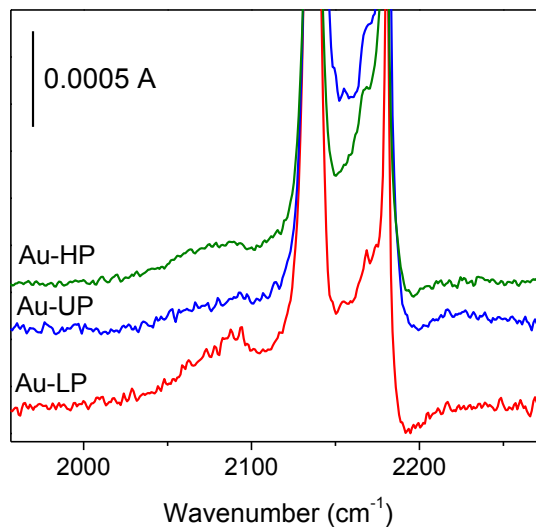


Figure 5.5. FT-IR spectra collected following CO adsorption at 40 K (36 ML CO at 0.6 ML/min) on sample Au-UP (blue spectrum; processed at 566 K), Au-LP (red spectrum; processed at 585 K), and Au-HP (green spectrum; processed at 593 K).

The progression of CO bands throughout the adsorption period was also analyzed to better understand the evolution of the population of support and Au sites during CO exposure. The entire deposition profile is provided for CO adsorption over sample Au-HP in *Figure 5.6*. From the collection of spectra, it is clear that almost all the intensity of the CO/Au feature develops during the first 5–10 min of CO exposure. The initial interaction of CO with Au sites prior to the support sites during the CO deposition is also evident in the carbonate region of the spectrum. Deposition of CO causes an overall depletion of carbonate bands (1400 – 1600 cm⁻¹) for samples pre-heated at 453 K, the temperature at which carbonate species were observed to form on the surface during the preheating. Also clear from these spectra is an increase in intensity in some of the carbonate region, suggesting some formation of species occurring during the deposition.

Tracking the difference spectra (all referenced to the spectrum collected at 40 K prior to CO exposure) over the entire duration of deposition reveals these changes to the carbonate region only occur after binding at the support begins, noted by the appearance of intensity around 2180 cm^{-1} , and once the Au sites have been saturated. This is additional evidence that these species are a property of the support, which corroborates with the conclusions from the FT-IR spectra analysis comparing surface changes between TiO_2 and Au/TiO_2 samples upon thermal processing (Fig. 4.1 and 5.1, respectively). Bands in the Ti-O region are also depleted in a similar manner; however only after CO bands attributed to the support are present (Fig. 5.6). Similar findings in the spectra were noted in Chapter 4, where CO binding at support chemisorption sites was concomitant with depletion of carbonate, C-H stretching, and Ti-O stretching vibrational bands.

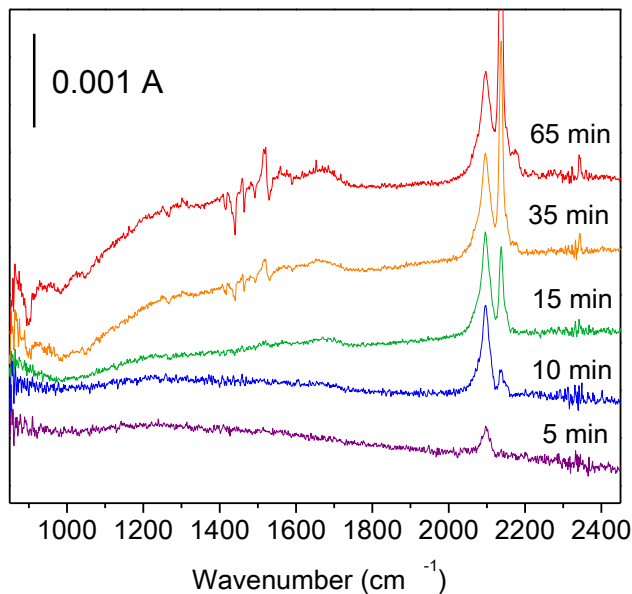


Figure 5.6. FT-IR spectra tracking deposition of CO over Au/TiO_2 (sample Au-HP) at 40 K over time (36 ML CO at 0.6 ML/min) after heating sample at 453 K (500 K set-point).

5.4.3 Isotopic study of CO/Au band

Isotope confirmation of CO stretching frequency contributions to FT-IR spectra were accomplished during two separate experiments, comparing deposition of ^{12}CO to ^{13}CO (36 ML at 0.6 ML/min) on sample Au-UP40 after preheating at 409 to 414 K. Deposition of isotopically labeled CO induced shifts in the vibrational frequency of all peaks observed in the CO region (2000 – 2200 cm^{-1}), shown in *Figure 5.7*. The observed red-shift in vibrational frequency of the CO/Au feature from 2090 cm^{-1} to 2037 cm^{-1} verifies that the source of the band is due to a single CO oscillator adsorbed to the AuNP. These frequency shifts are as predicted based on Equation 1.4.

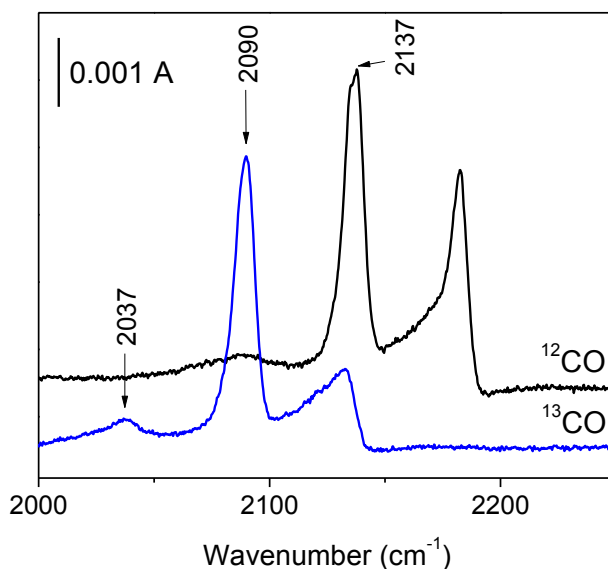


Figure 5.7. FT-IR spectra of ^{12}CO (black) and ^{13}CO (blue) adsorbed on Au/TiO₂ (sample Au-UP40) at 40 K following CO deposition at 40 K (36 ML at 0.6 ML/min) after processing samples at 409 – 414 K for 1h. Band at 2090 cm^{-1} is shifted to 2037 cm^{-1} when depositing isotopically labelled reagent gas, indicating CO/Au spectral feature corresponds to vibration of CO oscillator adsorbed to Au site. Spectra collected at 0.5 cm^{-1} resolution.

5.4.4 TEM imaging of AuNPs formed via thermal de-wetting of Au film

The TEM micrographs provided in *Figure 5.8* verify formation of AuNPs after heating at both the 420 – 448 K and 566 – 585 K temperature ranges. Images of the as-sputtered Au film over TiO₂ nanocrystals were collected prior to thermal processing, and did not contain evidence of Au NPs, characterized by confined regions of dark contrast in the images (Fig. 5.8a). After heating at 420 – 448 K, NPs appeared dispersed throughout the sample, illustrated in *Figure 5.8b*. The NPs remained present after heating at 566 – 585 K (Fig. 5.8c). The average particle size estimated of the supported gold after thermal processing was around 5 – 10 nm, with some particles appearing smaller in micrographs.

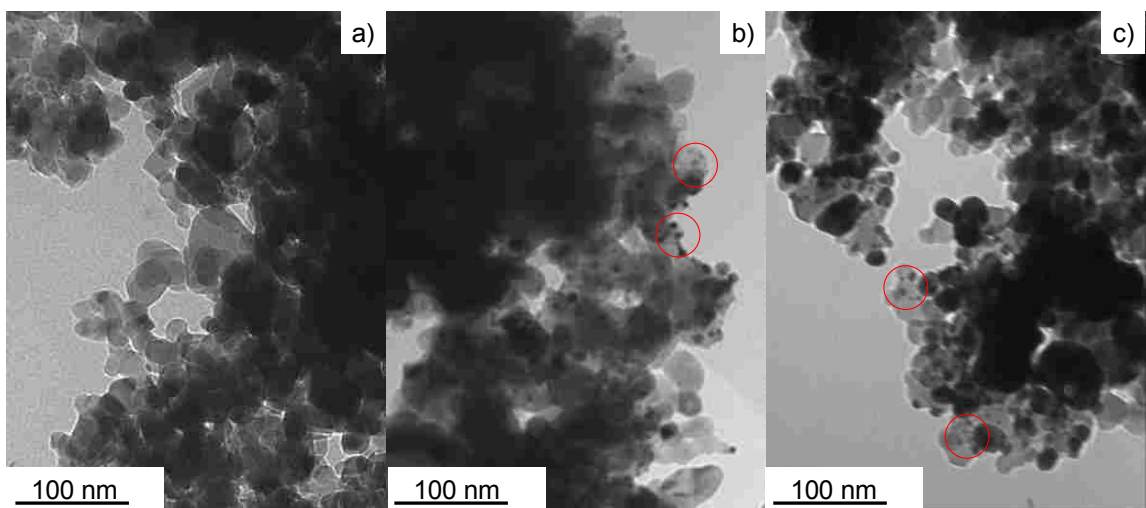


Figure 5.8. TEM images shown at 250,000x of Au/TiO₂ material a.) before thermal processing and after thermal processing at b.) 420 – 448 K and c.) 566 – 585 K.

5.4.5 Thermal behavior of CO/Au band: effect of support processing

To further explore the effect of support processing history on CO binding at AuNPs formed via thermal de-wetting, the FT-IR spectra were compared for CO deposited at 40 K over samples Au-UP, Au-LP, and Au-HP, all prepared by de-wetting

22.5nm Au film over the support at a temperature range of 420 to 453 K. These spectra, provided in *Figure 5.9a*, reveal differences in line-shape, position, and intensity of the CO/Au spectral feature for AuNPs formed over TiO₂ support which has been previously heated under vacuum and exposed to CO at low temperatures. For these samples, the broad feature at 2090 cm⁻¹ appeared to sharpen and contain a blue-shifted component at 2096 cm⁻¹. This shift is most notable for sample Au-HP, for which the band is also most intense.

Following CO deposition, the thermal behavior of both bands created after treating the Au/TiO₂ at 420 – 453 K was tested by warming the CO-covered surface from 40 to 150 K. At 120 K, the band at 2090 cm⁻¹ on sample Au-LP remained broad and shifted to around 2100 cm⁻¹, whereas the sharper 2096 cm⁻¹ feature on sample Au-HP blue-shifted to 2106 cm⁻¹ (*Fig. 5.9b*). Further heating to 150 K revealed that the Au feature was gone from the spectra of samples Au-UP and Au-LP, while it remained in sample Au-HP. The support band at 2180 cm⁻¹ was also notably more intense for Au-UP, and was retained to a higher desorption temperature, as clear from the spectra collected at 150 K (*Fig. 5.9c*).

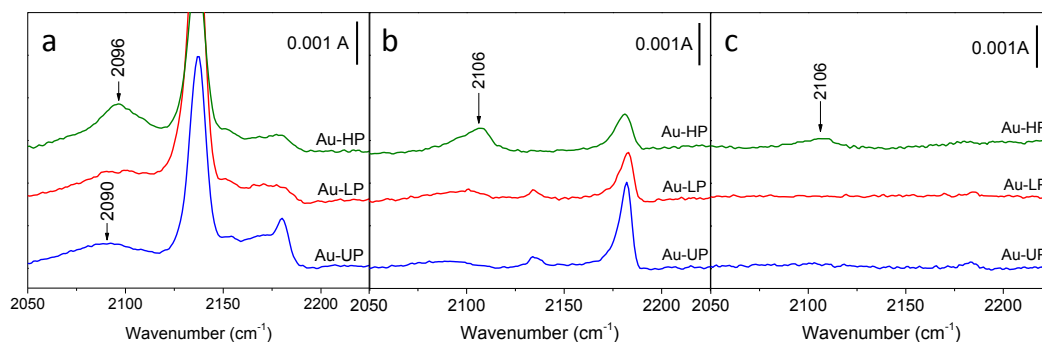


Figure 5.9. FT-IR spectra taken following CO deposition (0.1% in He at 1sccm for 60 min at 40 K) on AuNPs formed over TiO₂ support processed to various degrees, samples Au-UP (blue), Au-LP (red), and Au-HP (green). The AuNPs were prepared at a dewetting temperature of 420 K (Au-UP), 448 K (Au-LP), and 453 K (Au-HP). Spectra collected at a) 40 K and after warming CO-covered surface up to b) 120 K and c) 150 K.

In addition to probing the relative thermal stability of the bands, the evolution of bands during surface warming steps was also tracked to monitor population transfer between sites of varied enthalpy. The full progression of spectral bands for each of the three samples is provided in *Figure 5.11* of the Appendix, Section 5.7. Similar to analogous temperature studies on the bare TiO₂ support that were presented in Chapters 3 and 4, population transfer from the physisorbed sites to support sites is observed upon warming the surface from 40 to 60 K. Lorentzian fits were completed for each spectrum collected at 40 K, 60 K, 90 K, 120 K, and 150 K while warming the surface of all three samples after CO deposition, and for clarity, these fits are provided in the Appendix, Section 5.7. Fitting analysis was conducted by dividing the empirically fit bands into three separate types: CO physisorption bands, CO/Au bands, and CO/support bands. To summarize the findings of this analysis, plots of the temperature progression of the relative area sums for these separate types of bands for each of the samples are provided

in *Figure 5.10*. The trends in relative areas, where the ratio of the area sum for each group of bands to the total area of all bands, indicate that for sample Au-UP, the total intensity is greatest for the support bands after warming the sample to 60 K, and this remains the case until desorption of all CO above 150 K. The total intensity of CO bands is greatest for the Au sites in sample Au-LP at 60 K, and is slightly greater at higher temperatures, but nearly matched to that of the support bands. For sample Au-HP, however, the intensity of CO bound to Au sites was greater than that for CO bound to support sites after warming the surface to 60 K. This increased CO/Au to CO/support intensity ratio was maintained during the entire warming process up to 150 K. Another difference in the thermal progression of bands among the three samples was the presence of the physisorbed CO feature, which disappeared from the spectra above 60 K for Au/TiO₂ sample prepared over support subjected to the most amount of processing (Au-HP).

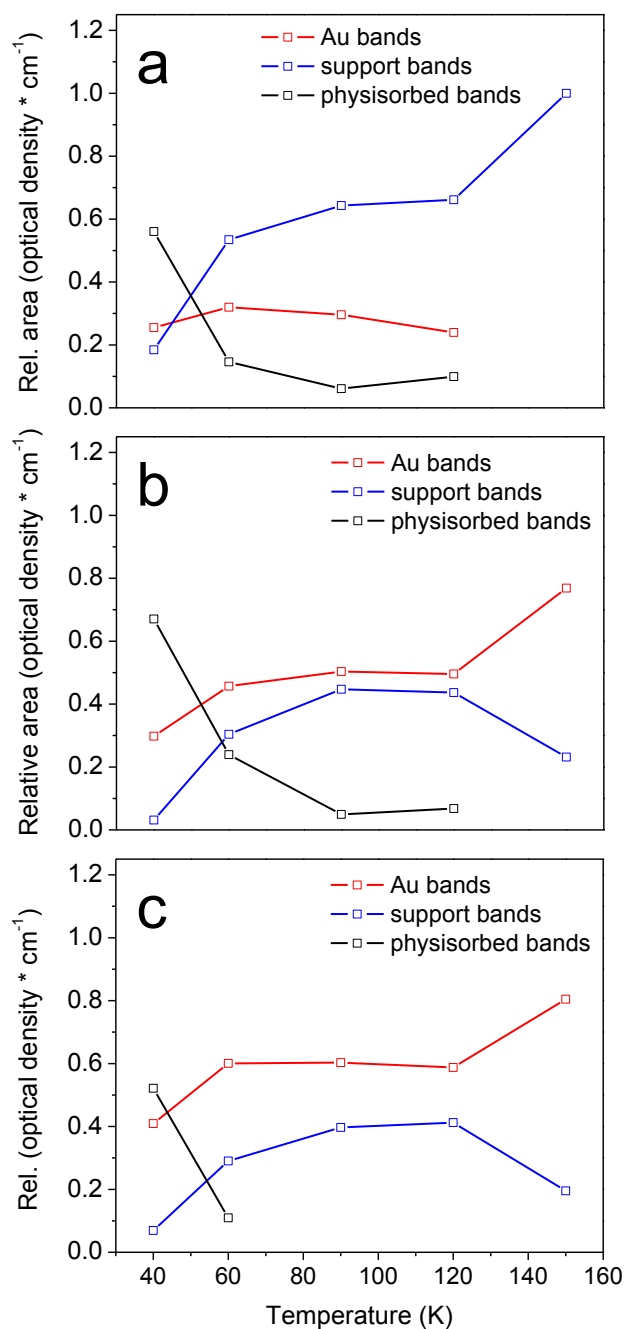


Figure 5.10. Absolute area sums of FT-IR spectra taken during surface warming steps following CO deposition (0.1% in He at 1sccm for 60 min at 40 K) on AuNPs formed over TiO₂ support processed to various degrees, samples a) Au-UP, b) Au-LP, and c) Au-HP. The AuNPs were prepared at a de-wetting temperature of 420 K (Au-UP), 448 K (Au-LP), and 453 K (Au-HP). The error bars in area appear smaller than data points on the figure.

5.5 Discussion

5.5.1 Sample preparation: Thermal de-wetting of gold film

Pretreatment of the Au/TiO₂ and TiO₂ samples discussed here at 373 – 585 K under vacuum frees CO-binding sites of surface-bound contaminants, as well as drives spontaneous reorganization of the as-sputtered Au film over the support to create a nanostructured surface for CO binding. De-wetting mechanisms have been previously investigated for Au films, and are a well-known phenomenon of metals over oxide surface.¹² The driving force for Au film de-wetting into NPs is a reduction in surface free energy, a property originating from the lack of atomic coordination at the surface of materials compared to the bulk material. For Au/TiO₂ surfaces, the greater surface free energy of Au compared to oxide surfaces prevents wetting of the interface at equilibrium.¹²⁻¹⁴ In this case, cohesion forces dominate over adhesion at the Au/TiO₂ interface, and Au surface energy is more effectively reduced by interactions with other Au atoms, leading to more spherical shaped particles dominating over flat films. It has been previously demonstrated that smaller sized NPs are produced at increased temperatures and decreased Au film thicknesses.^{12,15} Preparation of supported metallic nanoparticles NPs by thermal de-wetting of thin films has not been explored to our knowledge, and has some potentially advantageous aspects, as it avoids the need for precursor materials, reducing the risk of contamination from residual synthesis reactants, and is also a simple, reproducible method for nanostructuring surfaces.

Effects of de-wetting temperature on the AuNP surface morphology during preheating the Au/TiO₂ and TiO₂ samples under vacuum at 373 – 585 K were monitored

using TEM imaging to track the de-wetting and formation of Au NPs. Analysis of electron micrographs at particle edges, where single layers of support and Au can be visualized, reveals 5 – 10 nm Au NPs for Au/TiO₂ sample heated at 420 – 448 K (Fig. 5.8). The presence of AuNPs at the edge of the support particles is also an indication of strong wetting between the AuNP and the support; these images are similar to those obtained for Au/TiO₂ synthesized by DP and IMP methods.^{11,16-18} After increased heating at 566 – 585 K, images confirmed AuNPs of similar size were still present on the support.

5.5.2 FT-IR Spectroscopy: CO binding on Au/TiO₂ and TiO₂ at 40 K

In this work, the effect of sample preheat temperature on CO adsorption over both TiO₂ and AuNPs prepared from thermal de-wetting of Au film was measured under conditions of at low temperatures and high vacuum (40 K at pressures below 10⁻⁵ Torr). Vibrational bands due to binding at CO interactions at support sites for samples with and without AuNPs present on the surface revealed binding at four chemically unique sites on the TiO₂ support, indicated by shifted CO vibrational frequencies appearing at 2137 cm⁻¹, 2150 – 2154 cm⁻¹, 2167 – 2170 cm⁻¹, and 2180 cm⁻¹ (Fig. 5.3). The binding site population was largely dependent on the temperature of thermal processing prior to CO adsorption, similar to the work presented in Chapter 4. As noted in Chapter 3, the band at 2137 cm⁻¹ is generally attributed to weak CO binding on nonspecific surface sites¹⁹ and the broad feature at 2154 cm⁻¹ to CO bound to hydroxyl groups covering the TiO₂ surface sites, present after processing at the lower temperatures.¹⁹ The feature at 2167 cm⁻¹ has

been previously attributed to both cationic gold sites⁴ and cationic support sites,³ however our spectra reveal this peak is present for samples both with and without gold so we assign it to carbonyls formed at weakly acidic Ti⁴⁺ sites. The sharp vibrational band at 2180 cm⁻¹ observed in both support-only and metal-covered support samples, has also been previously established to CO bound to TiO₂ beta-acidic sites.¹⁹⁻²² One significant difference across the three Au/TiO₂ samples prepared with varied ratios of Au:TiO₂ was an increase in the physisorption band at 2137 cm⁻¹. This increase, most evident in the full scale spectra provided in *Figure 5.11*, may be due to an enhancement of this band due to the presence of AuNPs on the surface.

Comparison of FT-IR spectra for Au/TiO₂ and TiO₂ samples revealed CO binding on Au sites, detected by the spectral feature at 2090 – 2096 cm⁻¹ absent from TiO₂ spectra. The CO/Au signal was also found to be strongly dependent on the de-wetting temperature, with the greatest intensity after de-wetting the film at 420 – 453 K. Analysis of spectra collected early in the deposition (within 5 – 10 min) shows that there is still some binding at this site even after heating the sample at 566 – 585 K (Fig. 5.4). This result is expected as the TEM micrographs show the presence of AuNPs after heating the Au film in this temperature range (Fig 5.8). The scans collected at early deposition times also reveal that the Au sites saturate first, before binding begins at the support.

Close inspection of all scans collected over time during the deposition of CO over sample Au-HP shows that changes in the carbonate bands formed after heating at 453 K occur only after binding at the support begins once the Au sites have saturated. This

suggests these interactions are primarily occurring at the support site and these species do not interfere with binding at AuNPs, or there is at least no spectra indication of such interaction (Fig 5.6). Comparing the Au signal for Au-LP and Au-UP after heating to 566 – 585 K (Fig 5.3b and 5.3c) reveals that this signal persists longer at higher de-wetting temperatures as the ratio of Au:TiO₂ is increased. Based on these data alone, it appears that increasing the surface area for de-wetting the film might cause the film would de-wet down into the TiO₂ powder into regions which become inaccessible to CO binding at the surface. This would be the case if the amount of TiO₂ is increased while maintaining the same Au film thickness because these films are powdered and do not form smooth layers. However, comparison of the CO/Au band observed after heating sample Au-HP to a similar temperature range suggests that the increased processing of support prior to coating with Au leads to a stronger wetting of the AuNPs at the oxide surface (Fig. 5.5). A stronger particle-support interaction would be expected to make the gold less mobile, and less prone to migration as the de-wetting temperature is increased.

5.5.3 Effect of processing TiO₂ prior to Au film deposition on CO/Au signal

The CO/Au signal observed in FT-IR spectra was dependent on the processing history of the support prior to deposition of the Au film. The position and line-shape of the 2090 cm⁻¹ band observed for CO binding to AuNPs prepared over support that had not been processed under vacuum is different from the 2106 cm⁻¹ band observed for binding to AuNPs prepared over processed support samples. While Kung²³ has reported binding of CO to Au at the reduced frequency of 2090 cm⁻¹, other observations at 2087 –

2088 cm^{-1} have been primarily for CO bound to Au film completely wetted on a TiO_2 support,²⁴ and when using Lorentzian line-fitting for more intense bands around 2100 cm^{-1} that contained a low-frequency component.⁸ Sharpening and blue-shifting of the CO/Au feature from 2090 cm^{-1} to 2096 cm^{-1} at 40 K was observed for binding at AuNPs prepared over TiO_2 support that was heated in vacuum and exposed to CO for extended periods of time. In addition, warming the CO-covered surface to 120 K caused blue-shifting of both features, where the 2096 cm^{-1} band was further shifted to 2106 cm^{-1} in sample Au-HP (Fig. 5.9b). The position of the band at 2106 cm^{-1} is consistent with what has been reported previously for CO adsorbing to neutral AuNPs supported over nanocrystals at 120 K;⁶ CO/Au⁰ assignments in the range of 2098 – 2106 cm^{-1} have been reported several times in the literature for studies conducted at 90 – 300 K.^{4,6,8,20,25,26} Further warming to 150 K revealed that the sharper feature initially deposited at 2096 cm^{-1} remained in the spectra for sample Au-HP, while the broad feature on sample Au-UP was no longer present in the spectra at this warmer temperature. The sharpness of this feature and thermal stability of the band suggests a stronger chemisorption interaction of the CO at this site, likely due to a stronger wetting of AuNPs to the TiO_2 nanocrystals at the metal/oxide interface afforded by deposition of the Au film over a “cleaner” support surface. This relationship between the desorption temperature of chemically unique binding sites and chemical stability has been previously discussed for TiO_2 support samples in Chapters 3 and 4.

A more complete analysis of the thermal progression of bands during surface warming steps from 40 to 150 K of CO adsorbed Au/ TiO_2 samples demonstrated that, in

addition to thermal stability, the ratio of intensity of CO bands at Au sites to support sites also increased in these samples where the TiO₂ was processed prior to Au film deposition. This trend is most prominent for sample Au-HP (Fig. 5.10). These data also suggest a stronger wetting of the AuNPs to the support and an increased availability of Au binding sites for CO when the de-wetting process is performed on support samples which are previously processed at high temperatures under vacuum. The effect of this processing, including heating *in vacuo* and CO exposure, is thought to reduce the surface of the TiO₂. This effect was studied and described in greater detail in Chapter 4.

Additionally, the population of CO binding at chemisorbed support sites at 40 K for Au/TiO₂ samples after thermal processing in the intermediate temperature range of 420 – 453 K was similar to those findings for the bare TiO₂ support for similar dosing rate and total CO exposure. Analysis of the dependence of the CO binding site population observed at 40 K and upon warming up to increased temperatures on the CO dosing rate and total exposure was presented in Chapter 4 for the system of bare TiO₂ in absence of AuNPs. The results of these investigations demonstrated that, for a dosing rate of 0.6 ML/min, chemisorption at 40 K over support sites was not observed for samples thermally processed at 420 – 453 K when the total exposure was kept at or below 60 ML CO (the maximum exposure measured for this dosing rate). These studies on the bare support revealed that transfer of population from the physisorbed site to chemisorbed sites at support was observed upon warming the sample at or above 60 K. Similar trends were observed for warming the Au/TiO₂ over the same temperature range.

5.6 Conclusion

Nanostructured Au/TiO₂ was successfully prepared by spontaneous thermal de-wetting of Au film over TiO₂ NPs. Comparison of TiO₂ and Au/TiO₂ samples provided the identification of newly assigned CO binding site over AuNPs which ranged from 2090 – 2096 cm⁻¹ at 40 K. Temperature-dependent studies on de-wetting of the Au film over nanoparticulate TiO₂ under vacuum reveal that an optimum temperature of 420 – 453 K provides the strongest signal for CO binding at AuNP sites when CO is deposited at 40 K over the de-wet film. The appearance of AuNPs in TEM micrographs indicate that AuNP structure is retained when preheating at 566 – 585 K, and analysis of multiple samples showed that a higher Au:TiO₂ ratio is required to observe CO/Au binding after higher de-wetting temperatures. In addition, repeated heating of the TiO₂ support in vacuum and exposure to CO prior to addition of the Au film was shown to produce a sharper spectral signal for CO binding at AuNPs which appeared blue-shifted in the spectra, and persisted longer when the surface was warmed from the deposition temperature of 40 to 150 K. Thermal de-wetting was shown to be a reproducible and simple method for preparation of Au/TiO₂ material.

5.7 Appendix

The FT-IR spectra collected during surface warming steps from 40 to 150 K following CO deposition over samples Au-UP, Au-LP, and Au-HP are provided in *Figure 5.11*. For each spectrum, a Lorentzian fit was completed to determine the total intensity in the bands attributed to CO physisorption, binding at Au sites, and support sites. The fits completed for each individual spectrum broken down into these three different groups of bands are provided in *Figures 5.12 – 5.16* and tabulated in Tables 5.2 – 5.4 for sample Au-UP, *Figures 5.17 – 5.21* and tabulated in Tables 5.5 – 5.7 for sample Au-LP, and *Figures 5.22 – 5.26* and tabulated in Tables 5.8 – 5.10 for sample Au-LP. Details on the Lorentzian fitting methods can be found in Chapter 3.

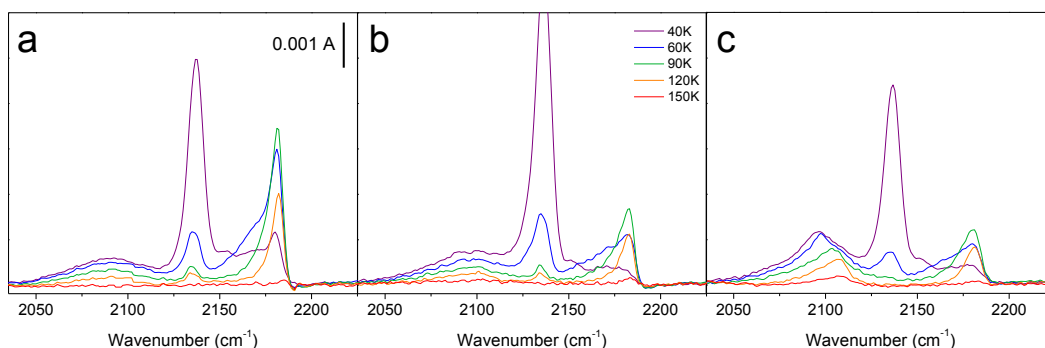


Figure 5.11. FT-IR spectra taken during surface warming steps following CO deposition (0.1% in He at 1sccm for 60 min at 40 K) on AuNPs formed over TiO₂ support processed to various degrees, samples a) Au-UP, b) Au-LP, and c) Au-HP. The AuNPs were prepared at a de-wetting temperature of 420 K (Au-UP), 448 K (Au-LP), and 453 K (Au-HP). Spectra collected at deposition temperature of 40 K and at each temperature shown while warming CO-covered surface up to 150 K. All panels display same vertical scale.

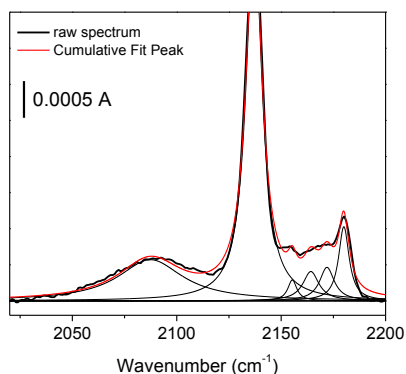


Figure 5.12. Lorentzian fitting analysis of FT-IR spectra taken of sample Au-UP at 40 K (Fit by 6 bands; 3 varying parameters).

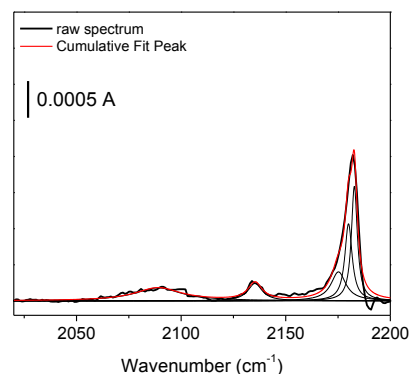


Figure 5.15. Lorentzian fitting analysis of FT-IR spectra taken of sample Au-UP at 120 K (Fit by 5 bands; 3 varying parameters).

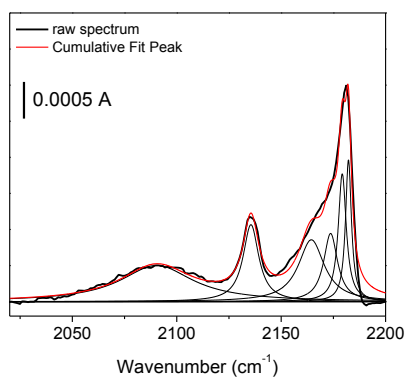


Figure 5.13. Lorentzian fitting analysis of FT-IR spectra taken of sample Au-UP at 60 K (Fit by 6 bands; 3 varying parameters).

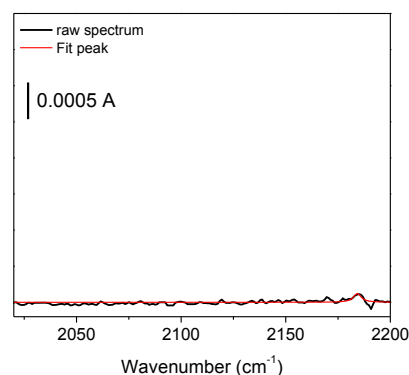


Figure 5.16. Lorentzian fitting analysis of FT-IR spectra taken of sample Au-UP at 150 K (Fit by 1 band; 3 varying parameters).

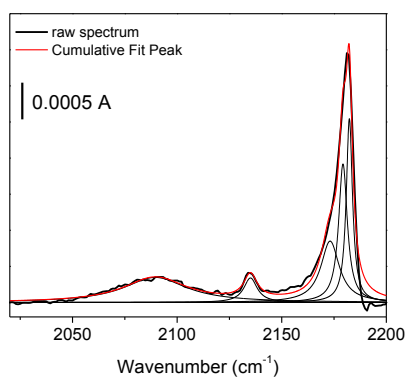


Figure 5.14. Lorentzian fitting analysis of FT-IR spectra taken of sample Au-UP at 90 K (Fit by 5 bands; 3 varying parameters).

Table 5.2. Lorentzian fit values showing temperature dependence of physisorbed CO band during surface warming of sample Au-UP from 40 to 150 K

temp	peak center	width	area
K	cm ⁻¹	cm ⁻¹	OD * cm ⁻¹
40	2137.0	9.21	0.074
60	2135.5	9.05	0.015
90	2135.1	7.74	0.004
120	2135.3	8.22	0.003
150			

Table 5.3. Lorentzian fit values showing temperature dependence of TiO₂ support CO bands during surface warming of sample Au-UP from 40 to 150 K

temp	peak center	width	area												
K	cm ⁻¹	cm ⁻¹	OD * cm ⁻¹	cm ⁻¹	cm ⁻¹	OD * cm ⁻¹	cm ⁻¹	cm ⁻¹	OD * cm ⁻¹	cm ⁻¹	cm ⁻¹	OD * cm ⁻¹	cm ⁻¹	cm ⁻¹	OD * cm ⁻¹
40	2155.3	5.22	0.002	2164.2	9.27	0.006	2171.9	8.50	0.006	2180.0	6.10	0.010			
60				2164.4	15.02	0.020	2173.7	8.05	0.012	2179.2	4.63	0.013	2182.2	3.38	0.010
90							2173.1	10.65	0.014	2179.3	5.00	0.015	2182.3	3.56	0.014
120							2175.2	8.52	0.005	2180.0	4.21	0.007	2182.8	3.41	0.008
150													2184.2	4.60	0.001

Table 5.4. Lorentzian fit values showing temperature dependence of CO/Au band during surface warming of sample Au-UP from 40 to 150 K

temp	peak center	width	area
K	cm ⁻¹	cm ⁻¹	OD * cm ⁻¹
40	2087.4	37.55	0.034
60	2090.4	42.10	0.033
90	2089.5	36.76	0.020
120	2089.0	26.82	0.008
150			

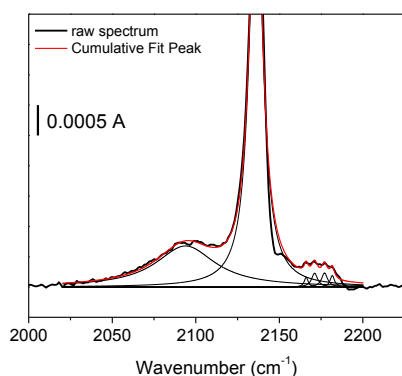


Figure 5.17. Lorentzian fitting analysis of FT-IR spectra taken of sample Au-LP at 40 K (Fit by 6 bands; 3 varying parameters).

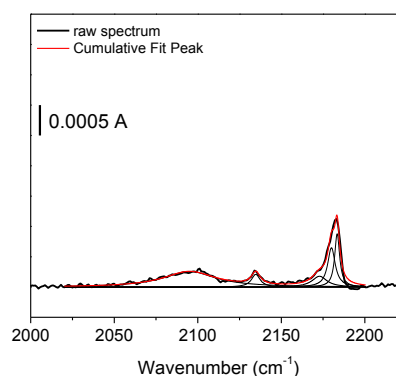


Figure 5.20. Lorentzian fitting analysis of FT-IR spectra taken of sample Au-LP at 120 K (Fit by 5 bands; 3 varying parameters).

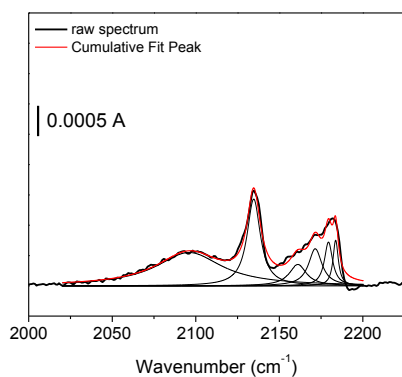


Figure 5.18. Lorentzian fitting analysis of FT-IR spectra taken of sample Au-LP at 60 K (Fit by 6 bands; 3 varying parameters).

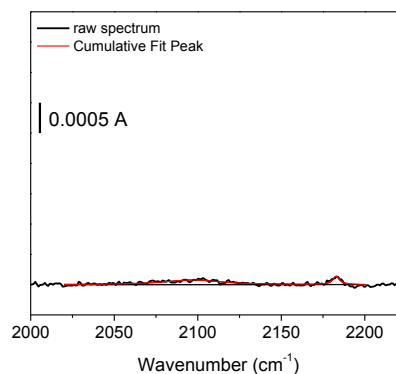


Figure 5.21. Lorentzian fitting analysis of FT-IR spectra taken of sample Au-LP at 150 K (Fit by 2 bands; 3 varying parameters).

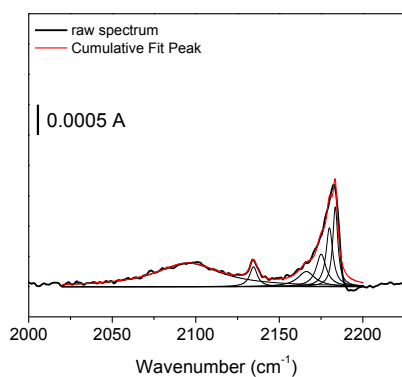


Figure 5.19. Lorentzian fitting analysis of FT-IR spectra taken of sample Au-LP at 90 K (Fit by 6 bands; 3 varying parameters).

Table 5.5. Lorentzian fit values showing temperature dependence of physisorbed CO band during surface warming of sample Au-LP from 40 to 150 K

temp	peak center	width	area
K	cm ⁻¹	cm ⁻¹	OD * cm ⁻¹
40	2136.0	9.37	0.103
60	2134.7	9.60	0.022
90	2134.6	5.52	0.003
120	2134.7	6.39	0.002
150			

Table 5.6. Lorentzian fit values showing temperature dependence of TiO₂ support CO bands during surface warming of sample Au-LP from 40 to 150 K

temp	peak center	width	area									
K	cm ⁻¹	cm ⁻¹	OD * cm ⁻¹	cm ⁻¹	cm ⁻¹	OD * cm ⁻¹	cm ⁻¹	cm ⁻¹	OD * cm ⁻¹	cm ⁻¹	cm ⁻¹	OD * cm ⁻¹
40	2166.1	2.83	0.001	2171.1	4.36	0.002	2177.1	4.32	0.002	2181.7	3.17	0.001
60	2161.1	12.40	0.007	2171.5	9.70	0.009	2179.4	5.92	0.007	2183.7	3.80	0.004
90	2166.2	12.44	0.005	2175.1	7.16	0.006	2180.0	4.84	0.007	2183.5	3.60	0.007
120				2172.8	10.75	0.003	2180.0	5.44	0.006	2183.4	3.57	0.005
150										2182.8	5.02	0.001

Table 5.7. Lorentzian fit values showing temperature dependence of CO/Au band during surface warming of sample Au-LP from 40 to 150 K

temp	peak center	width	area
K	cm ⁻¹	cm ⁻¹	OD * cm ⁻¹
40	2093.9	43.15	0.046
60	2096.0	47.69	0.041
90	2095.3	47.56	0.029
120	2095.0	37.86	0.015
150	2096.8	42.12	0.005

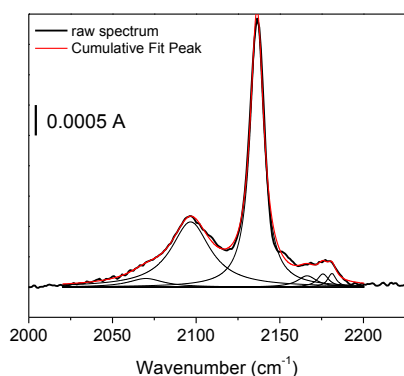


Figure 5.22. Lorentzian fitting analysis of FT-IR spectra taken of sample Au-HP at 40 K (Fit by 6 bands; 3 varying parameters).

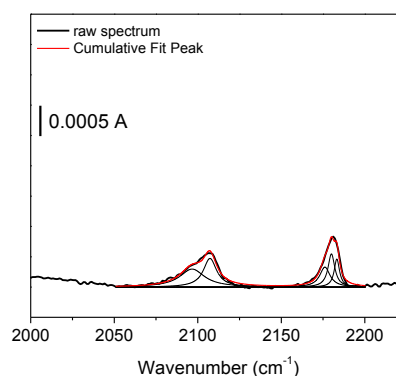


Figure 5.25. Lorentzian fitting analysis of FT-IR spectra taken of sample Au-HP at 120 K (Fit by 5 bands; 3 varying parameters).

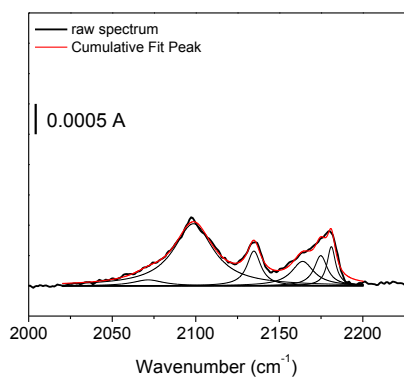


Figure 5.23. Lorentzian fitting analysis of FT-IR spectra taken of sample Au-HP at 60 K (Fit by 6 bands; 3 varying parameters).

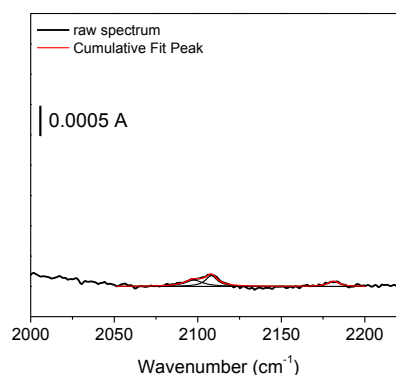


Figure 5.26. Lorentzian fitting analysis of FT-IR spectra taken of sample Au-HP at 150 K (Fit by 3 bands; 3 varying parameters).

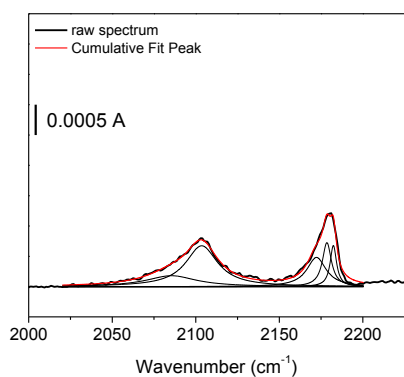


Figure 5.24. Lorentzian fitting analysis of FT-IR spectra taken of sample Au-HP at 90 K (Fit by 5 bands; 3 varying parameters).

Table 5.8. Lorentzian fit values showing temperature dependence of physisorbed CO band during surface warming of sample Au-HP from 40 to 150 K

temp	peak center	width	area
K	cm ⁻¹	cm ⁻¹	OD * cm ⁻¹
40	2136.4	9.76	0.068
60	2134.8	10.00	0.009
90			
120			
150			

Table 5.9. Lorentzian fit values showing temperature dependence of TiO₂ support CO bands during surface warming of sample Au-HP from 40 to 150 K

temp	peak center	width	area	peak center	width	area	peak center	width	area
K	cm ⁻¹	cm ⁻¹	OD * cm ⁻¹	cm ⁻¹	cm ⁻¹	OD * cm ⁻¹	cm ⁻¹	cm ⁻¹	OD * cm ⁻¹
40	2166.3	13.89	0.004	2175.8	8.30	0.003	2181.1	6.14	0.002
60	2164.0	16.08	0.010	2174.8	9.52	0.007	2181.2	6.13	0.006
90	2172.2	13.94	0.011	2178.5	6.50	0.007	2182.3	4.63	0.005
120	2176.1	7.45	0.004	2180.0	4.90	0.004	2183.2	3.86	0.003
150							2181.3	8.27	0.001

Table 5.10. Lorentzian fit values showing temperature dependence of CO/Au band during surface warming of sample Au-HP from 40 to 150 K

temp	peak center	width	area	peak center	width	area
K	cm ⁻¹	cm ⁻¹	OD * cm ⁻¹	cm ⁻¹	cm ⁻¹	OD * cm ⁻¹
40	2070.0	25.19	0.006	2096.67	28.26	0.048
60	2071.5	21.91	0.003	2098.62	28.62	0.046
90	2085.4	36.42	0.010	2103.55	23.12	0.024
120	2096.6	17.97	0.008	2107.31	9.56	0.007
150	2097.7	13.10	0.002	2108.14	8.60	0.002

5.8 References

- 1 Bond, G. C.; Thompson, D. T., **33**, 41-50 (2000).
- 2 Kung, M. C.; Davis, R. J.; Kung, H. H., *J. Phys. Chem. C* **111**, 11767-11775 (2007).
- 3 Green, I. X.; Tang, W.; Neurock, M.; Yates, J. T., Jr., *Science* **333**, 736-739 (2011).
- 4 Venkov, T.; Fajerweg, K.; Delannoy, L.; Klimev, H.; Hadjiivanov, K.; Louis, C., *Appl. Catal., A* **301**, 106-114 (2006).
- 5 Boccuzzi, F.; Chiorino, A.; Manzoli, M., *Surf. Sci.* **502**, 513-518 (2002).
- 6 Green, I. X.; Tang, W.; McEntee, M.; Neurock, M.; Yates, J. T., Jr., *J. Am. Chem. Soc.* **134**, 12717-12723 (2012).
- 7 Dekkers, M.; Lippits, M.; Nieuwenhuys, B., *Catal. Lett.* **56**, 195-197 (1998).
- 8 Manzoli, M.; Chiorino, A.; Boccuzzi, F. *Surf. Sci.* **532**, 377-382 (2003).
- 9 Klimev, H.; Fajerweg, K.; Chakarova, K.; Delannoy, L.; Louis, C.; Hadjiivanov, K., *J. Mater. Sci.* **42**, 3299-3306 (2007).
- 10 Meyer, R.; Lemire, C.; Shaikhutdinov, S. K.; Freund, H. J., *Gold Bull.* **37**, 72-124 (2004).
- 11 Haruta, M., *Cattech* **6**, 102-115 (2002).
- 12 Bowker, M.; Broughton, M.; Carley, A.; Davies, P.; Morgan, D.; Crouch, J.; Lalev, G.; Dimov, S.; Pham, D., *Langmuir* **26**, 16261-16266 (2010).
- 13 Shaffir, E.; Riess, I.; Kaplan, W. D., *Acta Mater.* **57**, 248-256 (2008).
- 14 Zhao, X.; Lee, U.; Lee, K., *Thin Solid Films* **519**, 706-713 (2010).
- 15 He, J.; Lu, J.; Dai, N.; Zhu, D., *J. Mater. Sci.* **47**, 668-676 (2012).
- 16 Panayotov, D. A.; Burrows, S. P.; Yates, J. T., Jr., *J. Phys. Chem. C* **115**, 22400-22408 (2011).
- 17 Zanella, R.; Giorgio, S.; Henry, C. R.; Louis, C., *J. Phys. Chem. B* **106**, 7634-7642 (2002).
- 18 Schumacher, B.; Plzak, V.; Kinne, M.; Behm, R. J., *Catal. Lett.* **89**, 109-114 (2003).
- 19 Hadjiivanov, K.; Lamotte, J.; Lavalley, J., *Langmuir* **13**, 3374-3381 (1997).
- 20 Bollinger, M. A.; Vannice, M. A., *Appl. Catal., B* **8**, 417-443 (1996).
- 21 Yates, D. J. C., *J. Phys. Chem.* **65**, 746-753 (1961).
- 22 Morterra, C., *J. Chem. Soc., Faraday Trans.* **84**, 1617-1637 (1988).
- 23 Henao, J. D.; Caputo, T.; Yang, J. H.; Kung, M. C.; Kung, H. H., *J. Phys. Chem. B* **110**, 8689-8700 (2006).
- 24 Chen, M. S.; Goodman, D. W., *Science* **306**, 252-255 (2004).
- 25 Boccuzzi, F.; Chiorino, A.; Manzoli, M.; Lu, P.; Akita, T.; Ichikawa, S.; Haruta, M., *J. Catal.* **202**, 256-267 (2001).
- 26 Boccuzzi, F.; Chiorino, A., *J. Phys. Chem. B* **104**, 5414-5416 (2000).

Chapter 6

Exploration of the CO adsorption over Au/TiO₂ and TiO₂ at steady-state pressure from 105 to 150 K

6.1 Abstract

Adsorption of CO over the surface of nanoparticulate TiO₂ (Degussa P25) and Au/TiO₂ formed via thermal de-wetting of an Au film over TiO₂ was investigated under steady-state pressure conditions (1 Torr CO) at 105 K using FT-IR spectroscopy. The thermal behavior of CO bound under steady-state pressure conditions was studied over the temperature range of 105 to 150 K by monitoring the thermal evolution of vibrational bands. For CO adsorption over the bare TiO₂ support, binding at physisorption sites as well as chemisorption sites were observed in the presence of 1 Torr CO at 2137 cm⁻¹ and 2180 cm⁻¹, respectively. The band at 2180 cm⁻¹ persisted evacuation after cooling the sample to 90 K, while the 2137 cm⁻¹ did not, confirming the assignments of these bands to chemisorption and physisorption, respectively. Absorption of CO over Au/TiO₂ at 105 K under steady-state pressure (1 Torr CO) produced similar bands vibrational bands as those found on the support, as well as a vibration at 2090 cm⁻¹ due to CO chemisorption at the AuNPs. This band persisted during evacuation of the gas phase at 90 K. After evacuation at 90 K, warming both samples up to 150 K resulted in decreased absorption intensity of the 2180 cm⁻¹ and 2090 cm⁻¹ as the sample temperature was increased, similar to the results obtained for previous adsorption studies under vacuum conditions (<10⁻⁵ Torr).

The effect of steady-state CO exposure at 105 K on the intensity of the CO/Au spectroscopic feature observed over Au/TiO₂ that had previously demonstrated a loss of signal during CO adsorption under vacuum was also explored. These investigations were a follow up to a series of gas adsorption studies on CO adsorption under vacuum conditions ($<10^{-5}$ Torr) at 40 K, in which the feature was observed to diminish with repeated experimental use. Exposure of the Au/TiO₂ sample to steady-state CO pressure of 1 Torr at 105 to 150 K was found to recover intensity of the 2090 cm⁻¹ vibrational band in the spectrum, suggesting that steady-state pressure conditions affect the surface chemistry responsible for this binding site.

6.2 Introduction

The investigations of CO adsorption of Au/TiO₂ and TiO₂ under at low temperature under vacuum conditions (10^{-3} to 10^{-8} Torr at 40 K) presented in Chapters 3 – 5 have characterized the population of binding sites which are thermodynamically stable in absence of steady-state CO pressure in the gas phase. As described in Chapter 1, CO adsorption experiments conducted by previous investigators on these surfaces have been primarily under conditions of static, equilibrium pressure at temperatures at or above 77 K.¹⁻¹⁷ One important aspect of these previous studies is to understand the effect of water in the binding site chemistry, as it should be non-negligible under conditions of equilibrium pressure. Water has been shown previously to be required for high catalytic activity.¹⁸ The presence of water, and more importantly, surface hydroxyl coverage, over TiO₂ and Au/TiO₂ is important to understand for the study of whether the Bond-

Thompson model is correct, as it proposes surface hydroxyl species to be catalytically relevant to the active site.¹⁹

The work presented in this chapter explores CO binding over TiO₂ and Au/TiO₂ under steady-state pressure conditions at 105 K. The gas phase in these experiments is still under dynamic flow (10 sccm), however the pressure above the surface during adsorption is maintained at a steady-state (1 Torr CO). Although the system here isn't a strictly a closed system, as it allows for the exchange of gas phase species outside of the vacuum chamber, the interpretation of the results is expected to be the same here as for that in previous investigations under static, equilibrium pressure. Foundation for this expectation is that equilibrium between adsorbed species and gas phase species should also be reached in our flow experiments, since the gas phase is maintained at a steady-state concentration which is in constant contact with the surface.

Exploration of CO adsorption over both TiO₂ and Au/TiO₂ under these steady-state conditions is anticipated to elucidate the effect of maintaining contact between the surface and equilibrium CO pressure on the CO binding site profile. This work also helps to corroborate the results of CO binding under vacuum conditions with the studies conducted by previous investigators. Additional studies are presented in this chapter in order to understand the evolution of CO binding sites on AuNPs during repeated experimental use in gas adsorption studies under vacuum. It was found that the signal for CO binding at Au sites was often diminished if the sample was used for extended periods of time (several months). The alteration of binding site chemistry with increased CO exposure was presented in Chapter 4 for bare TiO₂ samples. Exposure to CO at the

elevated pressures in the experiments presented here (1 Torr) may also produce changes to CO binding sites at AuNPs. A series of FT-IR spectra are presented for binding under steady-state conditions (1 Torr CO) at temperature ranging from 105 to 150 K, as well as subsequent evacuation to low pressures (10^{-8} Torr) over this same temperature range.

6.3 Experimental methods

A description of the instrument setup, sample preparation, and experiment parameters are provided in Chapter 2. As a brief overview, steady-state pressure experiments were conducted by maintaining a constant flow of CO over the sample (10 sccm) and simultaneously maintaining a total pressure of 10 Torr in the chamber using a back pressure regulator. The partial pressure of CO under these conditions was 1 Torr. For the experiment on TiO₂, the surface was exposed to steady-state pressure for 71 min prior to collection of the presented spectra, while spectra collection began at 43 min for the experiment on the Au/TiO₂ sample. The experiments were conducted at 90 K instead of 40 K for several reasons. The results of these experiments should be comparable to those conducted by previous investigators, and allow for connection between results obtained during adsorption under vacuum conditions to those at equilibrium pressure. In addition, the population of CO binding sites on the surface is more complex at 90 K. The ability to compare spectra obtained in this experiment to those under vacuum would provide valuable insight into the relative enthalpy of adsorption sites based on comparison of the behavior of CO in the presence of the steady-state pressure and under vacuum.

For the steady-state pressure studies, two powder TiO₂ samples were prepared using a 1:10 acetone:water solution, and one was coated with 22.5 nm Au film. Both samples were heated prior to the CO adsorption experiments, in which the measured temperature was 458 K for preheating the Au/TiO₂ sample, and 422 K for preheating the TiO₂ sample. The preparation of AuNPs via thermal de-wetting of Au film is developed in Chapter 5. Steady-state experiments were conducted on the TiO₂ and Au/TiO₂ samples after extensive use of the samples in vacuum studies. The effect steady-state conditions on the binding site profile over the Au/TiO₂ sample was measured following repeated use of the sample in CO gas adsorption experiments where the sample was processed in the temperature range of 453 – 458 K over a duration of 13 days of the sample held under vacuum.

All spectra were collected under steady-state pressure conditions were collected at a resolution of 6 cm⁻¹ to prevent gas phase lines from appearing spectrum, which are diminished at this resolution due to broadening, as their intensities are low. The spectra were averaged over 200 scans. All other spectra presented for the Au/TiO₂ gas adsorption experiments conducted under vacuum prior to steady-state exposure were collected at a resolution of 2 cm⁻¹, averaged over 500 – 1000 scans.

6.4 Results

6.4.1 CO adsorption at steady-state pressure

The steady-state adsorption of 1 Torr CO was measured over the bare TiO₂ support at 105 to 150 K, followed by cooling the sample to 90 K and evacuating the gas

phase. The TiO_2 sample was then warmed from 90 to 150 K in order to observe thermal dependence on the progression of vibrational bands. FT-IR spectra collected of CO adsorbed over TiO_2 under 1 Torr CO is presented in *Figure 6.1a* in the temperature range of 105 to 150 K. Exposure to CO at 105 K (after 71 min) produced bands around 2137 and 2180 cm^{-1} , corresponding to physisorbed CO and CO chemisorbed at Ti^{4+} centers, respectively. These bands remained in the spectrum upon warming to 150 K under steady-state conditions. The physisorbed band broadened and red-shifted with increasing temperature. After evacuation and cooling the sample to 90 K, the physisorbed band was removed from the spectrum. Warming the surface from 90 to 150 K caused a decrease in the intensity of the 2180 cm^{-1} band.

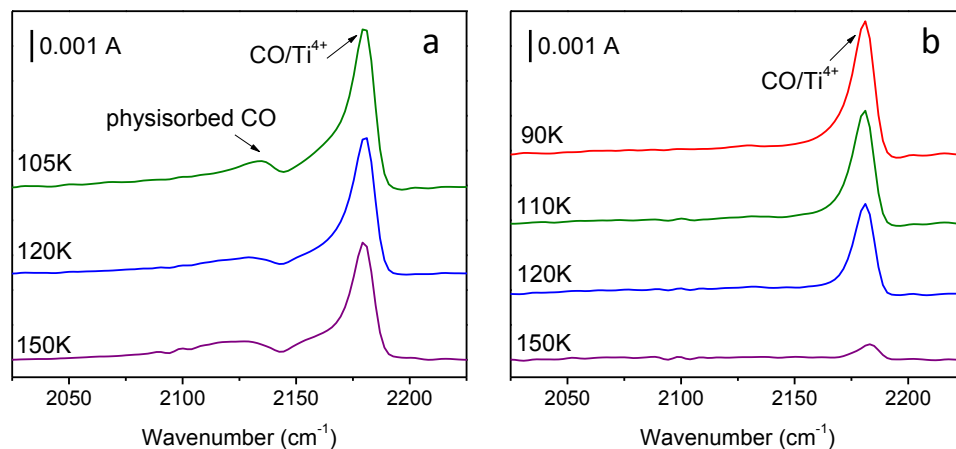


Figure 6.1. FT-IR spectra of CO adsorbed on TiO_2 a) under 1 Torr CO steady-state pressure conditions at 105 – 150 K and b) after evacuation to 10^{-8} Torr at 90 – 150 K.

After analysis of CO adsorption under 1 Torr steady-state pressure of CO over bare TiO_2 , an analogous experiment was repeated to measure CO adsorption over Au/TiO_2 under the same conditions. These results are provided in *Figure 6.2*.

Adsorption of CO at 105 K produced bands at both 2137 cm^{-1} and 2180 cm^{-1} , similar to adsorption over the bare TiO_2 support. A vibrational band at 2090 cm^{-1} was also observed for CO binding at AuNPs. All three bands remained present in the spectra upon increasing the sample temperature from 105 to 150 K under 1 Torr steady-state pressure CO. The physisorbed band red-shifted and broadened at 150 K, and had a similar thermal response to the observation upon warming the TiO_2 surface. Evacuation and cooling the Au/ TiO_2 down to 90 K resulted in loss of the physisorbed band, while the CO/Au and CO/ Ti^{4+} chemisorbed CO features persisted during evacuation. Warming from 90 to 150 K caused a decrease in the intensity of both bands.

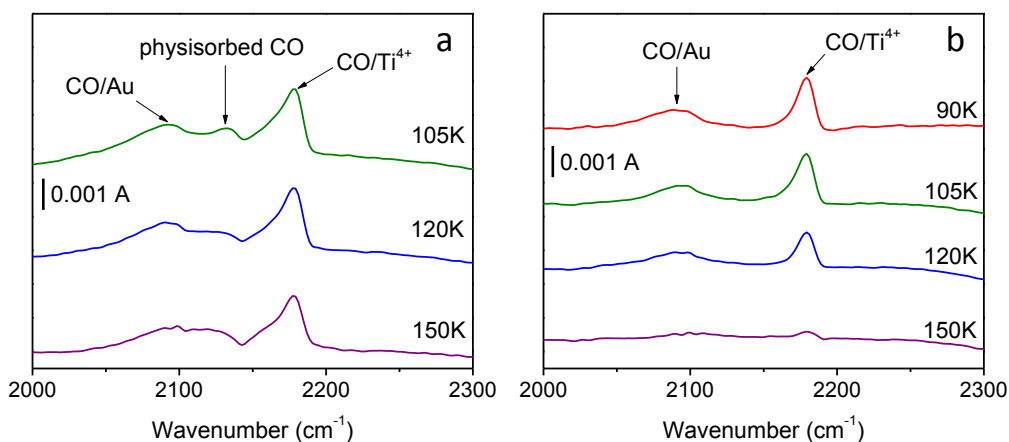


Figure 6.2. FT-IR spectra of CO adsorbed on Au/ TiO_2 a) under 1 Torr CO steady-state pressure conditions at 105 – 150 K and b) after evacuation to 10^{-8} Torr at 90 – 150 K.

6.4.2 Regeneration of bands under steady-state pressure

As mentioned briefly in the introduction, the signal for CO binding to Au sites, which has been characterized in the region of $2090 - 2106\text{ cm}^{-1}$ for the samples used in this work, has been found to diminish with repeated use in adsorption experiments. The

largest signal is observed immediately after de-wetting the film at 420 to 450 K. The Au/TiO₂ sample used to measure adsorption of CO under steady-state pressure conditions in the previous section was also used repeatedly in several experiments in which CO adsorption was measured under vacuum ($<10^{-5}$ Torr). The signal for CO/Au diminished in this sample over a period of 6 days while the sample was held under vacuum, following initial de-wetting of the Au film. The effect of exposure to 1 Torr steady-state pressure CO was assessed for this sample by comparing evolution of the CO/Au signal over time to the signal after exposure to steady-state pressure. The FT-IR spectra are provided in *Figure 6.3a* which show the progression of CO bands after adsorption at 40 K under vacuum conditions ($<10^{-5}$ Torr) after 1, 4, and 6 days. Day 1 represents the day on which the Au film was heated for the first time and the AuNPs were created via thermal de-wetting. Subsequent days count the number the sample was left in the vacuum chamber. These spectra demonstrate that the most intense and sharp vibrational band for CO/Au is observed for day 1, and after day 6 the band has significantly diminished. Heating the sample to 120 K probes the thermal stability of the band, which is shown in *Figure 6.3b*. Here, the spectrum collected on day 1 clearly contains the sharp CO/Au feature, which has blue-shifted to 2106 cm⁻¹ (Chapter 5). The vibrational signature for CO binding to Au sites is no longer present in the spectrum collected after warming the sample to 120 K during the experiment performed on day 6 of sample use.

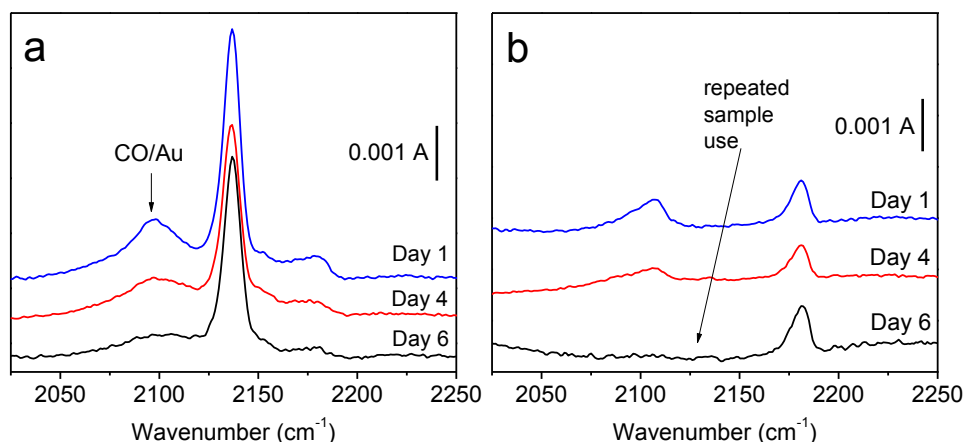


Figure 6.3. FT-IR spectra demonstrating effect of repeated sample use. Spectra collected at 40 K of CO adsorbed over Au/TiO₂ on day 1 (blue spectrum), day 4 (red spectrum), and day 6 (black spectrum) following CO deposition under vacuum (10^{-5} Torr). Spectra were collected at a) 40 K and b) 120 K after warming up CO-covered surface.

Adsorption of CO under vacuum conditions was measured on the Au/TiO₂ several additional times without return of the CO/Au signal. After thirteen days under vacuum, the steady-state pressure experiments discussed in Section 6.4.1 were performed on the sample. FT-IR spectra collected at 90 K before and after the evacuation of the steady-state CO pressure, provided in *Figure 6.2a* and *6.2b*, respectively, show a relatively intense CO/Au vibrational band. The sample was also heated to 120 K following evacuation of the steady-state pressure during this experiment. A comparison of the spectra at 120 K on day 6 to day 13 should indicate whether the band intensity has in fact been recovered, as these spectra were both collected at the same temperature and pressure (10^{-8} Torr). The FT-IR spectra provided in *Figure 6.4* compares the CO/Au signal observed at 120 K following the evacuation (day 13) to the signal that was observed upon warming the surface to 120 K on day 6 after the adsorption experiment conducted under

vacuum conditions. Here, it is clear that the CO/Au signal has returned in the spectrum following the exposure to 1 Torr CO steady-state pressure.

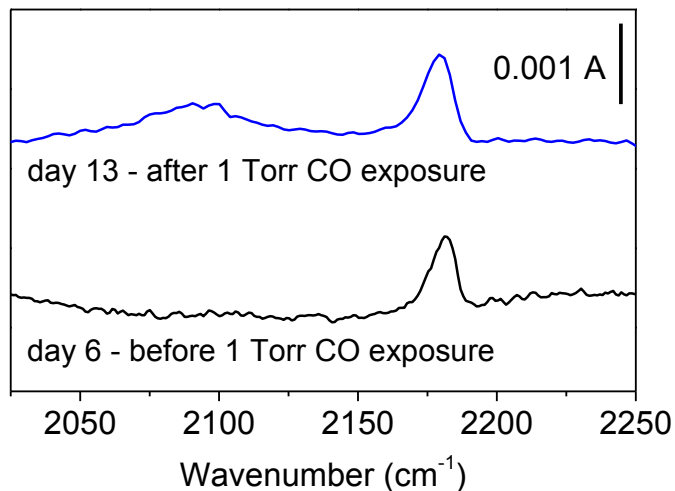


Figure 6.4. FT-IR spectra of CO adsorbed on Au/TiO₂ collected at 120 K on Day 6 (black spectrum; after 40 K CO exposure at 10⁻⁵ Torr, prior to exposure to steady-state CO pressure) and Day 13 (blue spectrum; following evacuation after exposure to CO at 1 Torr steady-state pressure at 105 – 150 K).

Additional spectra are provided in *Figures 6.5 – 6.7* in the Appendix, Section 6.7, showing changes carbonate and OH-stretching region to attempt to elucidate the effect of exposure to steady-state pressure on the surface. In *Figure 6.5*, difference spectra showing the changes to the sample from day to day, where all spectra are collected at 4 K after thermal processing and prior to deposition, and are referenced to the spectrum collected at 4 K after processing on the first day. These spectra show a depletion of the band around 1600 cm⁻¹, attributed to the water bending mode, and indicates that less water was present on the surface on later days (days 4, 5, and 6) compared to day 1. Also evident is a growing depletion of a broad spectral band centered around 1670 cm⁻¹ with each day. This is the region of the spectrum where bridged carbonate species appear, as

described in greater detail in Chapter 1.²⁰ The evolution of bands in this figure shows that the surface is not the same on each day, even though similar temperatures were reached during thermal processing each day (453 – 456 K). This loss of surface water is evident in spectra collected at 40 K after deposition of CO at the same temperature. Difference spectra referenced to 40 K prior to deposition are provided *Figure 6.6*, where the CO region shows the depletion of the CO/Au band over the first 5 days (Fig. 6.6a). The OH-stretching region shows the most perturbation to these bands occurs during the first day, and these changes are diminished to a greater extent with increased sample use (Fig. 6.6b). A final series of difference spectra are provided in *Figure 6.7* which show the changes before and after deposition, where the surface temperature was 90 K. Deposition for days 1 and 5 occurred under vacuum conditions at 40 K, and day 13 corresponds to the steady-state pressure experiment described above. The main significant feature among these spectra is the increased growth the vibrational feature around 1600 cm^{-1} , suggesting the adsorption of water has occurred during the steady-state exposure of CO.

6.5 Discussion

As described in the introduction, the majority of experiments conducted by previous investigators have been under conditions of equilibrium pressure without continuous pumping under vacuum. To make a more direct comparison between our results and those obtained by others, we measured the adsorption of CO at 105 K under steady-state CO pressure (1 Torr). Investigation of CO adsorption under these conditions resulted in observation of the vibrational band at 2180 cm^{-1} typically observed

for CO binding over nanoparticulate TiO₂ for both samples. This band is attributed to CO bound to Ti⁴⁺ centers in the support, as presented in greater detail in Chapter 3. The persistence of this band following evacuation corroborates with the assignment of this band as CO chemisorption at the support,^{1,4,10} and also with previous investigations comparing FT-IR spectra of CO over TiO₂ at equilibrium pressure and following evacuation.³

Stabilization of CO binding at weakly-interacting, physisorbed sites in the presence of the CO steady-state pressure is observed for both TiO₂ and Au/TiO₂ samples, where the vibrational band at 2137 cm⁻¹ is present under steady-state pressure conditions (Fig. 6.1a and 6.2a, respectively). Evacuation of the gas phase CO and returning the system to vacuum conditions, where the gas phase is continuously pumped away, removes this band from the spectra in both samples. This is consistent with previously reported behavior for this band measured at an equilibrium pressure of 1 Torr CO at 100 K by Hadjivanov, where vanishing of the band due to physisorbed CO was observed following evacuation.³ In this previous study, similar behavior was also observed for the vibrational band at 2155 cm⁻¹ which is attributed to CO hydrogen bonded to hydroxyl groups on the surface. The absence of that band in this study is likely due to the thermal pretreatment of these samples prior to deposition. The progression of the CO binding site population over the support as the thermal processing temperature is increased was presented in Chapter 4, where CO hydrogen bonding to OH centers was most prominent for the unheated sample. It was found that thermal processing diminishes the relative intensity of this band, even after treatment at the intermediate temperature of 375 – 460

K, for samples used in our study, while similar heating did not remove these features from the spectra collected by Hadjivanov.¹¹ A significant difference between the samples used by the previous investigator and those employed in the work here is the use of self-supported pellets, which may require a more rigorous thermal processing step than that required for the thin powder films heated under high vacuum (10^{-8} Torr).

The presence of water in these experiments by previous investigators is thought to have a significant role in the observed binding site population, and is also important to the CO oxidation mechanism as proposed by Bond-Thompson.¹⁹ Increased water levels would be expected for experiments conducted at equilibrium pressure as water is a prominent background contaminant which will exist at increased concentration at higher pressures. For the studies presented in this dissertation, however, the concentration of water is expected to be minimal. A quick calculation would predict that the reagent gas should only contain a concentration of ~0.001% water vapor, if it is assumed that all background pressure in the gas delivery system (10 milliTorr) is due to water. Another possible source of water could be due to the thermal processing of the sample prior to CO exposure, which is thought to free water from the surface. The nature of the cryostat instrument is that a significant portion of the surfaces remain cold during this heating step (<30 K), and likely trap water which is removed from the sample window during heating. It is possible that the increased number of gas collisions with the cold surfaces while due to increased pressure in the vacuum chamber while the system is under steady-state flow could have the effect of removing some water from the cold traps. Some evidence for this during the experiment is the condensation of water on the outside of the vacuum

chamber due to cooling of the surface, resulting from gas molecules providing thermal conduct between the cold surfaces and the outside walls of the vacuum shroud. It remains possible, then, that water could influence the results of the experiments presented here.

Adsorption of CO over the Au/TiO₂ sample at 105 – 150 K under steady-state pressure conditions also resulted in appearance of a vibrational band around 2090 cm⁻¹, due to CO binding at AuNPs. This band persisted after evacuation, similar to the 2180 cm⁻¹ band (Fig. 6.2). It appears from the regained intensity of the CO/Au band after Day 6 following exposure to 1 Torr CO (Fig. 6.3) that the binding site was regenerated during the steady-state experiment. The thermal behavior of this band demonstrates the regained population of this binding site. The band was not present after day 6, and had been repopulated after exposure to 1 Torr CO and subsequent evacuation on day 13. As mentioned earlier in the discussion, the presence of water under these steady-state conditions may influence the binding site chemistry of these experiments. Exposure of the Au/TiO₂ to these conditions may have resulted in repopulation of surface water groups which were depleted during repeated experimental processing (heating and CO exposure under vacuum). Some evidence for water adsorption at the surface was observed in the difference spectra showing changes to the surface before and after exposure to 1 Torr CO steady-state pressure at 105 K (Fig. 6.7). Here a clear increase in the water bending mode following CO adsorption under steady-state conditions is present in the spectrum, and at a larger intensity than that observed for deposition under vacuum conditions (10⁻⁵ Torr). Additional experiments which employ a water flow cell to allow

for deliberate introduction of water into the system are proposed as part of the future directions for this research in Chapter 8.

Another possible effect of water adsorption is the reversal of changes to the carbonate species which occur throughout repeated sample use. It is also known that carbonate species build up on the surface of these catalysts with extensive exposure to CO₂, and they have also been proposed to be involved in catalyst deactivation mechanisms. To check for buildup of carbonates in the Au/TiO₂ sample discussed here, the evolution of bands in this region during successive experiments was checked by calculating difference spectra referenced to surface on day 1 (Fig. 6.5). Here a progressive increase in some of the bands is observed as the amount of time the sample was left under vacuum was extended. Most intense is a band at 1515 cm⁻¹, which becomes increasingly present on day 6 in comparison to the intensity after days 4 and 5. Additional band intensity is also increased around 1450 cm⁻¹ over this same duration of days. In Chapter 1, Table 1.1 is provided which contains the complicated assignments of bands in this region. Although many of these assignments overlap and span several wavenumbers in range, the bands observed here do correspond to carbonate groups, possibly monodentate carbonates, and the increased intensity over time indicates a build-up may be occurring over the duration of repeated experimental use. An experimental explanation for this may also be explained in a similar way to that of the water adsorption in these experiments. The cold surfaces of the cryostat will also trap the carbonaceous species which are removed during thermal processing. It was observed that a small heat load is released upon shutting off the helium compressor at the end of the experimental

day, causing deposited gases to re-adsorb the sample window which may still be cold enough to condense them. This may be a contributing factor in the evolution of the sample surface chemistry with repetitive use.

The buildup of carbonate species on the sample after day 6 was also coincident with a decrease in the intensity of the CO/Au signal on this day (Fig. 6.6a). Small changes in the O-H stretching region were also noted in the difference spectra after deposition on day 1, which were barely detectable after day 4, and not at all on day 5 (Fig. 6.6b), and might also indicate a decreased water content present on the surface after extensive experimental use. It is also known that these stable carbonates break down to less stable bicarbonates upon exposure to water.²¹⁻²³ It is possible that the buildup of carbonates during successive experiments was reversed by the increased presence of water during exposure to steady-state pressure of CO.

6.6 Conclusion

The work presented here explores CO adsorption over TiO₂ and Au/TiO₂ under steady-state pressure conditions at 90 K and 1 Torr CO, and following subsequent evacuation of the gas phase. It was found that binding of CO at the 2180 cm⁻¹ and 2090 cm⁻¹ sites persisted after evacuation, in contrast to binding at the 2137 cm⁻¹, as this band was removed from the spectrum of both sample after returning the system to vacuum (<10⁻⁶ Torr). The lack of stability of CO bound in the site corresponding to the band at 2137 cm⁻¹ supports that this site is due to non-specific CO physisorption, while bands persisting under vacuum support their assignment to chemisorption. The regeneration of

the band at 2090 cm^{-1} following exposure to 1 Torr CO under steady-state pressure conditions was observed, and suggests that these conditions facilitate surface changes which favor binding of CO to AuNPs. Additional studies investigating O_2 adsorption over CO-covered Au/ TiO_2 and TiO_2 under vacuum conditions ($< 10^{-5}$ Torr) showed evidence for CO_2 production, although no transient species were observed under these conditions.

6.7 Appendix

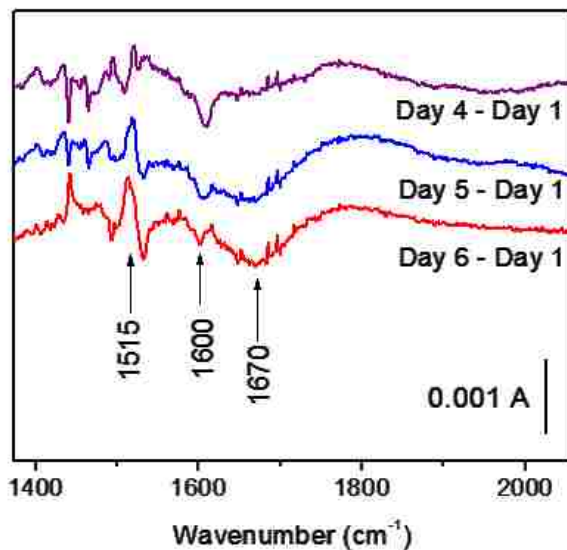


Figure 6.5. FT-IR difference spectra collected at 4 K after preheating Au/ TiO_2 . All spectra are referenced to spectrum collected at 4 K following thermal processing on day 1 to emphasize progressive changes to surface occurring over repeated experiments.

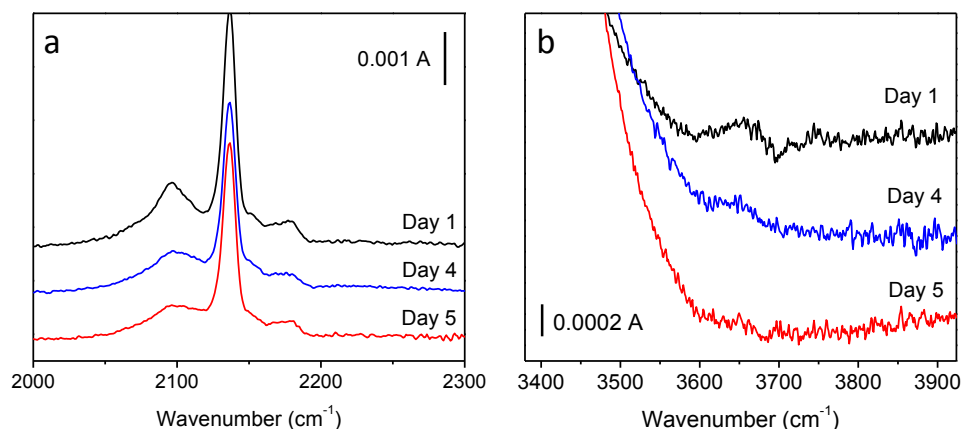


Figure 6.6. FT-IR difference spectra collected at 40 K after CO deposition over Au/TiO₂ on day 1 (black spectrum), day 4 (blue spectrum), and day 5 (red spectrum) showing a) CO stretching region changes and b) OH stretching region changes. All spectra are referenced to spectrum collected on the same experiment day at 40 K, prior to CO deposition.

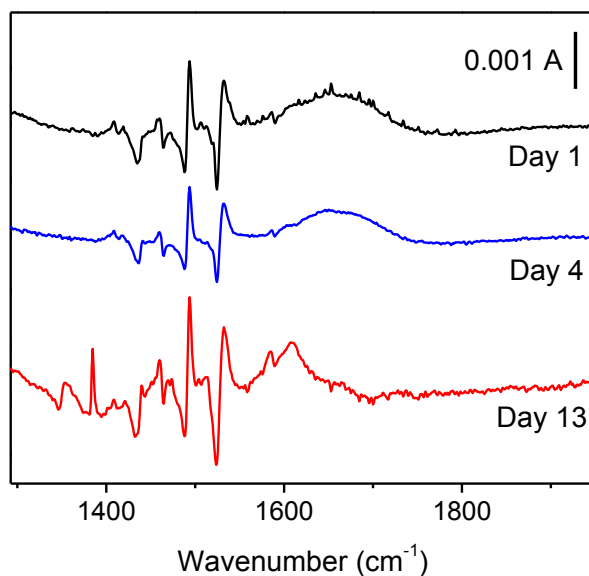


Figure 6.7. FT-IR difference spectra collected under vacuum (10^{-8} Torr) at 90 K after exposure of Au/TiO₂ to CO on day 1 (black spectrum; deposition at 40 K at 10^{-5} Torr), day 4 (blue spectrum; deposition at 40 K at 10^{-5} Torr), and day 13 (red spectrum; steady-state exposure of 1 Torr CO at 105 K). All spectra referenced to spectrum collected at 90 K on the same experiment day, prior to CO exposure.

6.8 References

- 1 Morterra, C., *J. Chem. Soc., Faraday Trans.* **84**, 1617-1637 (1988).
- 2 Garrone, E.; Bolis, V.; Fubini, B.; Morterra, C., *Langmuir* **5**, 892-899 (1989).
- 3 Hadjiivanov, K.; Lamotte, J.; Lavalley, J., *Langmuir* **13**, 3374-3381 (1997).
- 4 Yates, D. J. C., *J. Phys. Chem.* **65**, 746-753 (1961).
- 5 Martra, G., *Appl. Catal., A* **200**, 275-285 (2000).
- 6 Zaki, M. I.; Knozinger, H., *Mater. Chem. Phys.* **17**, 201-215 (1987).
- 7 Green, I. X.; Tang, W.; Neurock, M.; Yates, J. T., Jr., *Science* **333**, 736-739 (2011).
- 8 Dekkers, M.; Lippits, M.; Nieuwenhuys, B., *Catal. Lett.* **56**, 195-197 (1998).
- 9 Green, I. X.; Tang, W.; McEntee, M.; Neurock, M.; Yates, J. T., *J. Am. Chem. Soc.*, **134**, 12717-12723 (2012).
- 10 Bollinger, M. A.; Vannice, M. A., *Appl. Catal., B* **8**, 417-443 (1996).
- 11 Venkov, T.; Fajerweg, K.; Delannoy, L.; Klimev, H.; Hadjiivanov, K.; Louis, C., *Appl. Catal., A* **301**, 106-114 (2006).
- 12 Manzoli, M.; Chiorino, A.; Boccuzzi, F., *Surf. Sci.* **532**, 377-382 (2003).
- 13 Boccuzzi, F.; Chiorino, A.; Manzoli, M.; Lu, P.; Akita, T.; Ichikawa, S.; Haruta, M., *J. Catal.* **202**, 256-267 (2001).
- 14 Boccuzzi, F.; Chiorino, A., *J. Phys. Chem. B* **104**, 5414-5416 (2000).
- 15 Grunwaldt, J.; Baiker, A., *J. Phys. Chem. B* **103**, 1002-1012 (1999).
- 16 Henao, J. D.; Caputo, T.; Yang, J. H.; Kung, M. C.; Kung, H. H., *J. Phys. Chem. B* **110**, 8689-8700 (2006).
- 17 Kung, M. C.; Davis, R. J.; Kung, H. H., *J. Phys. Chem. C* **111**, 11767-11775 (2007).
- 18 Date, M.; Okumura, M.; Tsubota, S.; Haruta, M., *Angew. Chem. Int. Ed.* **43**, 2129-2132 (2004).
- 19 Bond, G. C.; Thompson, D. T., *Gold Bull.* **33**, 41-50 (2000).
- 20 Davydov, A. A.; Rochester, C. H. *Infrared Spectroscopy of Adsorbed Species on the Surface of Transition Metal Oxides*; (Wiley: Chichester; New York; Brisbane; Toronto; Singapore, 1990).
- 21 Heiz, U.; Landman, U., Eds.; *Nanocatalysis*; Avouris, P., Bhushan, B., Bimberg, D., von Klitzing, K., Sakaki, H. and Wiesendanger, R., Eds.; Nanoscience and Nanotechnology; (Springer-Verlag: Berlin, 2007).
- 22 Clark, J. C.; Dai, S.; Overbury, S. H., *Catal. Today* **126**, 135-142 (2007).
- 23 Tanaka, K.; White, J. M., *J. Phys. Chem.* **86**, 4708-4714 (1982).

Chapter 7

Adsorption of both CO and O₂ over TiO₂ and Au/TiO₂ under vacuum at 40 K

7.1 Abstract

Preliminary studies exploring adsorption of O₂ over CO-covered Au/TiO₂ and TiO₂ resulted in depletion of the vibrational bands due to physisorbed CO and CO bound to AuNPs (vibrational bands at 2137 cm⁻¹ and 2090 cm⁻¹, respectively). An increase in the chemisorbed CO/Ti⁴⁺ band at 2180 cm⁻¹ and the concomitant formation of small amounts of CO₂ in the spectra were also observed following O₂ deposition. Thermal progression of the bands upon warming the surface from 40 to 120 K revealed similar trends in the spectra for samples containing O₂ as in analogous previous investigations with CO only. The FT-IR spectra of changes to the carbonate species present on the surface TiO₂ indicated an overall growth of these bands following exposure to O₂, compared to complicated depletion of red-shifted bands and growth of blue-shifted bands observed during CO exposure.

7.2 Introduction

In addition to CO studies at higher temperature and steady state pressures, adsorption studies using both CO and O₂ under vacuum conditions were also explored. These preliminary experiments lay the foundation for the desired studies where binding of both CO and O₂ are measured in the presence of a cryogenic matrix, the subject matter of Chapter 8. These experiments provide a basis for moving forward with studies in the

presence of a cryogenic matrix, and comparison of these results to those found from IMSS studies should allow for an assessment of the stabilization afforded by the matrix environment. Previous investigations of O₂ and CO adsorption over TiO₂ under equilibrium pressure conditions at 120 K have been completed by Yates¹. These studies indicated that CO adsorption over O₂-saturated TiO₂ resulted in the displacement of O₂ from the surface. However, conduction of these experiments under static, equilibrium pressure would be expected to yield significantly different results than for adsorption under vacuum at 40 K. This is the subject of the Chapter 6, which discusses the differences in these two conditions in greater detail. In the studies presented here, the effect of O₂ adsorption over CO-covered surfaces of nanoparticulate TiO₂ and Au/TiO₂ is investigated using FT-IR to determine if bands due to CO-O₂ complexes would be observed at 40 K under vacuum ($<10^{-5}$ Torr). Following deposition of both CO and O₂, surface warming up to 120 K was completed in order to determine differences in the thermal behavior of the CO bands due to the presence of O₂. Additional experiments in which these two gases were adsorbed in a layered deposition were also completed to study the differences in effect of CO and O₂ adsorption to the carbonate species present on the TiO₂ support. A series of FT-IR spectra are presented here to detail the results of CO and O₂ interactions over both nanoparticulate TiO₂ and Au/TiO₂ at temperatures of 40 – 120 K under vacuum.

7.3 Experimental methods

A description of the instrument setup, sample preparation, and experiment parameters are provided in Chapter 2. For the studies presented in this chapter, two powder TiO₂ samples were prepared using a 1:10 acetone:water slurry. One sample was used for layered adsorption experiments, where deposition was done in layers of CO/O₂/CO. This sample was thermally processed at 550 K prior to the experiments, where the actual temperature at the sample reached 422 – 428 K. For the layered experiment, the oxygen was isotopically labelled (¹⁸O₂). An additional experiment in which unlabeled ¹⁶O₂ was also done on this same sample for comparison, and these results are presented in the Appendix, Section 7.7 in *Figure 7.7*.

The second TiO₂ sample was prepared as a split sample to be used for investigations of adsorption of both CO and O₂ over both TiO₂ and Au/TiO₂. A single sample which was prepared first with bare TiO₂ powder over the entire CaF₂ window, and half of the support coated in a 40 nm Au film which was subsequently de-wet at 391 K. Details on sample masking to coat the window in this way, and the translation of the cryostat sample holder through different positions of the IR beam are provided in Chapter 2. For this particular sample, the Au film was sputtered over the support after 5 months of containing the support sample in a dry environment in a desiccator. The usual time in between preparation of the support powder sample and coating with Au is only 1 – 7 days. Explanation of AuNPs preparation via thermal de-wetting of Au film is provided in Chapter 4. All spectra were collected at a resolution of 2 cm⁻¹, averaged over 500 – 1000 scans.

7.4 Results

7.4.1 Adsorption studies over TiO_2 with both CO and O_2

In preparation for matrix isolation studies of CO and O_2 interaction and binding at the surface of Au/ TiO_2 , investigations were initiated to first study these interactions over the bare support under vacuum conditions ($<10^{-5}$ Torr). For this experiment, adsorption of both gases was measured during a layered deposition over the surface to monitor changes specific to either CO or O_2 . The deposition layering first involved adsorption of CO (720 ML CO at 12 ML/min), followed by O_2 (36 ML $^{18}\text{O}_2$ at 0.6 ML/min), and then back to CO (720 ML CO at 12 ML/min) again. This layered deposition will be referred to using the following notation throughout this chapter: CO/ O_2 /CO.

FT-IR difference spectra collected before and after each layer are provided in *Figure 7.1a* and *7.1b* to emphasize changes to the carbonate and CO region of the spectrum, respectively, occurring with each gas. Bands in the carbonate region responded to CO adsorption during the first layer in a similar way to that previously observed. The effect of CO exposure on this region of the spectrum was discussed previously in Chapters 4–6. For this particular TiO_2 sample, a clear depletion is observed for bands in the range of $1400 - 1500 \text{ cm}^{-1}$, while two of the most intense bands to the blue of this region ($1500 - 1550 \text{ cm}^{-1}$) increase after CO exposure. The CO region confirms CO interaction at the support, as vibrational bands due to CO physisorption and chemisorption at the 2137 and 2180 cm^{-1} sites, respectively, were both observed (*Fig. 7.1b*).

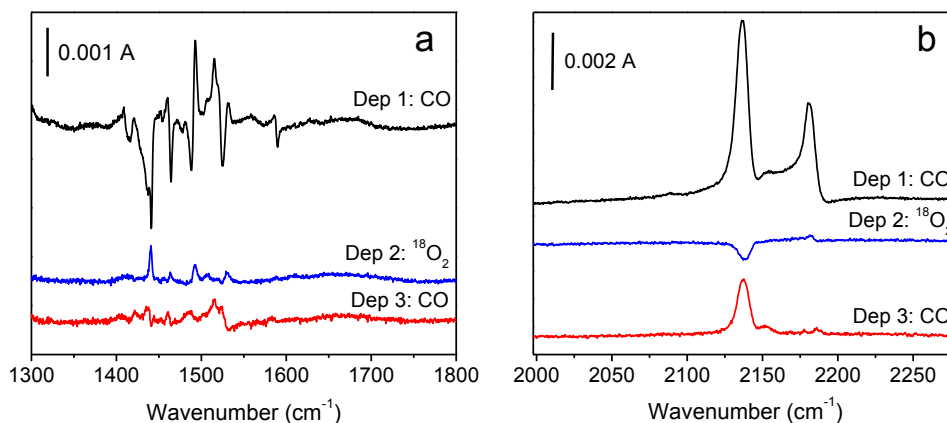


Figure 7.1. FT-IR difference spectra collected following layered deposition of CO (black spectrum; 720 ML CO at 12 ML/min) / O₂ (blue spectrum; 36 ML ¹⁸O₂ at 0.6 ML/min) / CO (red spectrum; 720 ML CO at 12 ML/min) showing a) carbonate region and b) CO region.

The subsequent adsorption of ¹⁸O₂ over the CO-covered surface resulted in very different changes to the vibrational signature of the carbonate and CO species than those observed following CO adsorption. Increased intensity was observed for several of the bands in the carbonate region which were depleted during CO deposition. While the magnitude of these changes is much smaller, the dosing rate and total exposure were also reduced during the adsorption of the ¹⁸O₂ (Fig. 7.1a). As a check to understand the potential differences in deposition of ¹⁸O₂ vs. ¹⁶O₂ over the TiO₂ support, FT-IR spectra were collected for a separate experiment in which only ¹⁶O₂ was deposited over the support (no layering with CO). These results are provided in the appendix for brevity, where slight shifts in the increased bands in the carbonate region were noted (Fig. 7.7). An expanded window of the changes occurring to the Ti-O region upon deposition of ¹⁶O₂ is also provided for this same experiment in the appendix. Similar absorbance decrease to that noticed for CO deposition at 40 K was observed in this region (Fig. 7.8).

In addition to these changes to the carbonate bands, the physisorbed CO vibrational band was depleted during the adsorption of the $^{18}\text{O}_2$ at 40 K, while a slight increase in the chemisorbed CO band at 2180 cm^{-1} was evident in the difference spectra for this adsorption step (Fig. 7.1b). Addition of a third adsorption layer of CO over-top of the CO and O_2 layer resulted in complicated changes to the carbonate region. Overall increase in the band intensity was observed, but the band changes did not correlate to those observed for either of the previous adsorption steps. Investigation of changes to the CO region indicated that CO adsorbed at physisorbed sites, as evident from the intense band at 2137 cm^{-1} , and also to some degree at the surface hydroxyl sites (2150 cm^{-1}) and support chemisorption sites at Ti^{4+} centers (2180 cm^{-1}) (see Chapter 3 for detailed assignments of these support bands).

To further understand these changes to the spectrum occurring during each step in the layered adsorption of $\text{CO}/^{18}\text{O}_2/\text{CO}$, the incremental changes occurring over time throughout the deposition process were analyzed. FT-IR difference spectra are provided in *Figure 7.2* for the first layer of CO, where the carbonate region is shown in *Figure 7.2a* and the CO region in *Figure 7.2b*. Each spectrum is referenced to the previous spectrum, with the exact timeframe during the deposition labelled on the figure.

Incremental changes during the deposition reveal that a significant amount of the changes to the carbonate species occur within the first 10 min of CO exposure (Fig. 7.2a). Similarly, most changes to CO support bands also occur in this timeframe (Fig. 7.2b). The intensity level is almost consistent for the next several increments, until the last spectrum which contains changes occurring during 40–50 min of deposition. Here, only

small hints are detected above the baseline for the carbonate region, and similarly the CO region only contains a relatively small growth of the physisorbed band. These spectra do show adsorption of CO at the 2150 cm^{-1} during the first 5 min of deposition which is present at a greater relative intensity than in the final adsorption spectrum after the full exposure time has passed. This detail is missed in the spectrum collected after deposition (Fig. 7.1b).

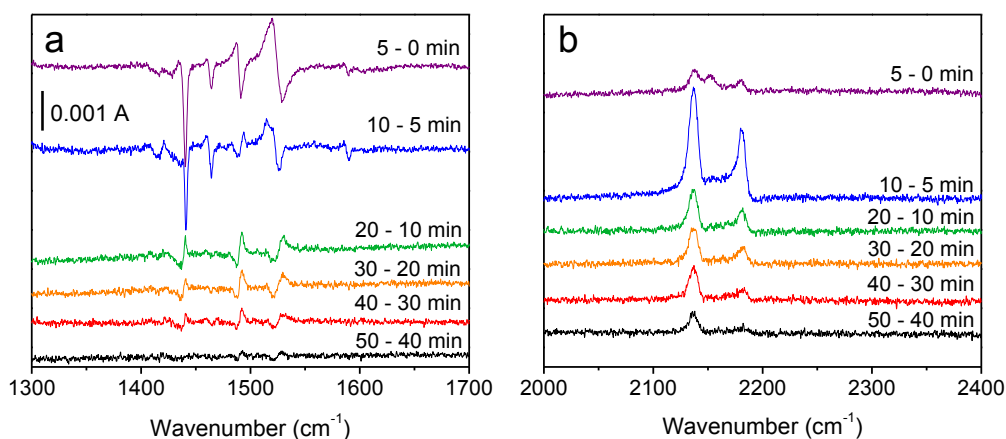


Figure 7.2. FT-IR difference spectra of incremental changes during adsorption over TiO_2 of the first layer of deposition (720 ML CO at 12 ML/min), showing a) carbonate region and b) CO region.

Analogous difference spectra were calculated for the adsorption of the second and third layers ($^{18}\text{O}_2$ and CO, respectively), and these spectra are provided in *Figures 7.3a* and *7.3b*. These spectra indicate that the changes to both the carbonate and CO region occur initially during the adsorption process for $^{18}\text{O}_2$ and CO layers. Changes to the physisorption band at 2137 cm^{-1} persist at a small intensity level throughout the deposition in the case of both layers. The first 5 min of deposition of CO during the third

layer also indicates adsorption at the 2150 cm^{-1} corresponding to CO hydrogen-bonded to Ti-OH centers, similar to in the first layer (Fig. 7.3b and 7.2b).

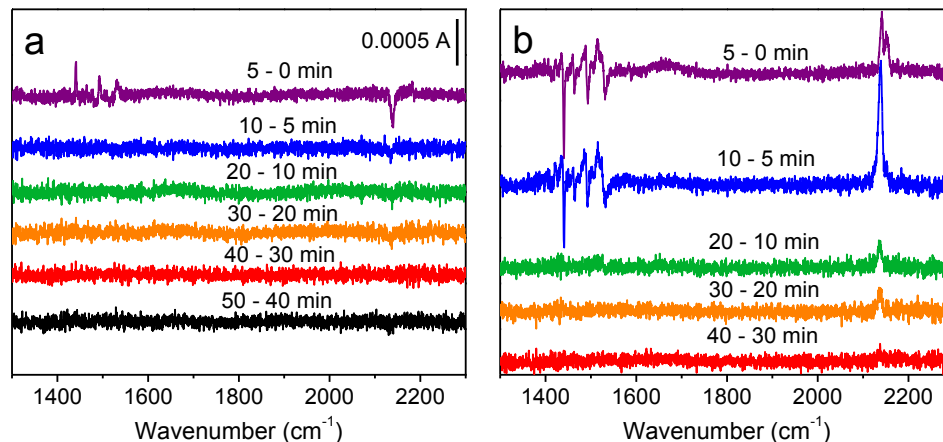


Figure 7.3. FT-IR difference spectra of incremental changes during adsorption over TiO_2 of a) the second layer of deposition (36 ML $^{18}\text{O}_2$ at 0.6 ML/min) and b) the third layer of deposition (720 ML CO at 12 ML/min).

7.4.2 Adsorption studies over Au/TiO_2 and TiO_2 with CO and O_2

In order to characterize the binding of CO in the presence of O_2 under vacuum conditions over both Au/TiO_2 and TiO_2 , adsorption of O_2 over CO-covered samples was investigated using FT-IR. For these studies, a single sample was prepared in which half of the CaF_2 window was coated in TiO_2 , and the other half was coated with Au/TiO_2 , as described in the Experimental section. A two-step layered deposition was then completed, where CO was deposited first over the sample (36 ML CO at 0.6 ML/min at 40 K), followed by deposition of O_2 (36 ML $^{16}\text{O}_2$ at 0.6 ML/min at 40 K). FT-IR spectra were monitored for both halves of the window during a single experiment. Difference spectra showing the changes to the CO region of the spectrum for both TiO_2 and Au/TiO_2 during each deposition step are provided in *Figure 7.4*. The reference spectrum for the

spectra showing the changes occurring during CO deposition, shown in *Figure 7.4a*, is the spectrum collected at 40 K prior to CO deposition, where the reference for changes occurring during O₂ deposition, shown in *Figure 7.4b*, is the spectrum collected at the end of CO deposition. Presentation of the data in this way emphasizes the changes to TiO₂ and Au/TiO₂ due to both CO and O₂ during the separate deposition steps.

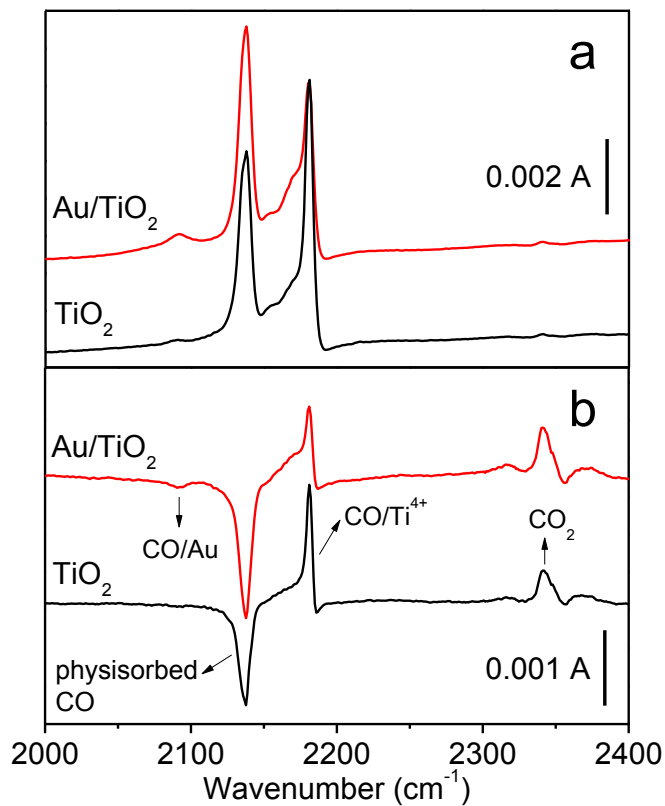


Figure 7.4. FT-IR difference spectra collected at 40 K of Au/TiO₂ (red spectrum) and TiO₂ (black spectrum) following a) CO deposition (36 ML CO at 0.6 ML/min at 40 K) and subsequent b) O₂ deposition (36 ML O₂ at 0.6 ML/min at 40 K). Spectra in panel b are referenced to spectra collected following CO deposition to emphasize O₂-dependent changes to CO vibrational bands.

Deposition of CO over Au/TiO₂ and TiO₂ at 40 K under vacuum conditions resulted in the appearance of CO bands typically observed following thermal processing

at 420 – 460 K. Both spectra in *Figure 7.4a* contain bands for physisorbed CO at 2137 cm^{-1} , and CO chemisorbed at the support at 2180 cm^{-1} . The spectrum for CO adsorbed over Au/TiO₂ contained the additional vibrational band around 2090 cm^{-1} due to CO adsorption at AuNPs. Comparison of the 2180 cm^{-1} band intensity on the part of the sample containing Au to the 2180 cm^{-1} band on the TiO₂-only half of the sample revealed that the signal of this site was diminished in comparison with the presence of AuNPs on the surface. Subsequent deposition of O₂ at 40 K over the CO-covered surface resulted in the depletion of the physisorption band at 2137 cm^{-1} and increase in the chemisorption band at 2180 cm^{-1} . In the sample containing AuNPs, depletion of the band at 2090 cm^{-1} was also observed. It is important to mention here the reduced magnitude of the changes observed during O₂ deposition in comparison to CO deposition (note the difference in vertical scale in *Figure 7.4a* and *7.4b*).

The thermal behavior of CO bands upon warming the surface from 40 to 120 K was also monitored spectroscopically in order to determine the effect of O₂ deposition over the CO. The FT-IR spectra collected while warming the TiO₂ surface are provided in *Figure 7.5*. The 2180 cm^{-1} remained in the spectrum up to 120 K, while the band at 2137 cm^{-1} lost most intensity upon warming from 40 to 60 K. At 90 K, the band was completely gone.

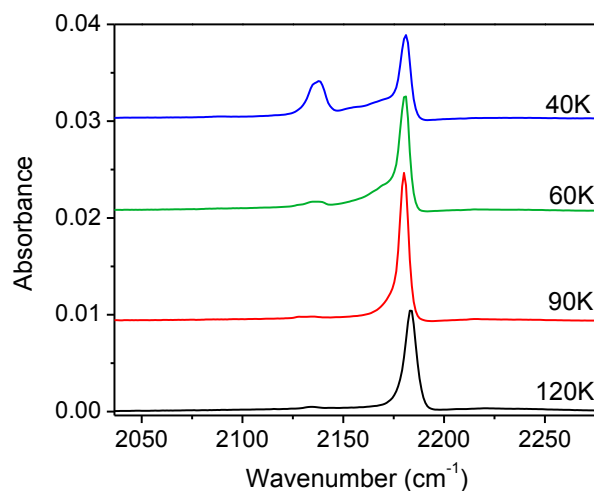


Figure 7.5. FT-IR difference spectra during surface warming steps of CO adsorbed over TiO₂ at 40 K (blue spectrum), 60 K (green spectrum), 90 K (red spectrum), and 120 K (black spectrum).

Analogous difference spectra collected while warming the Au/TiO₂ surface up from 40 K are provided in *Figure 7.6a*. The CO/Au feature appeared at relatively low intensity compared to the vibrational bands due to physisorbed CO and CO chemisorbed at Ti⁴⁺ center sites, and an expanded view of the region around 2090 – 2100 cm⁻¹ was provided in *Figure 7.6b*. The behavior of the support bands was overall the same as in the spectra of the bare TiO₂ support, however a persistence of the some of the intensity of band at 2137 cm⁻¹ at 120 K was observed for the Au/TiO₂ sample. The CO/Au band appeared at 2091 cm⁻¹ at 40 K, and was blue-shifted up to 2099 cm⁻¹ after warming the sample to 120 K.

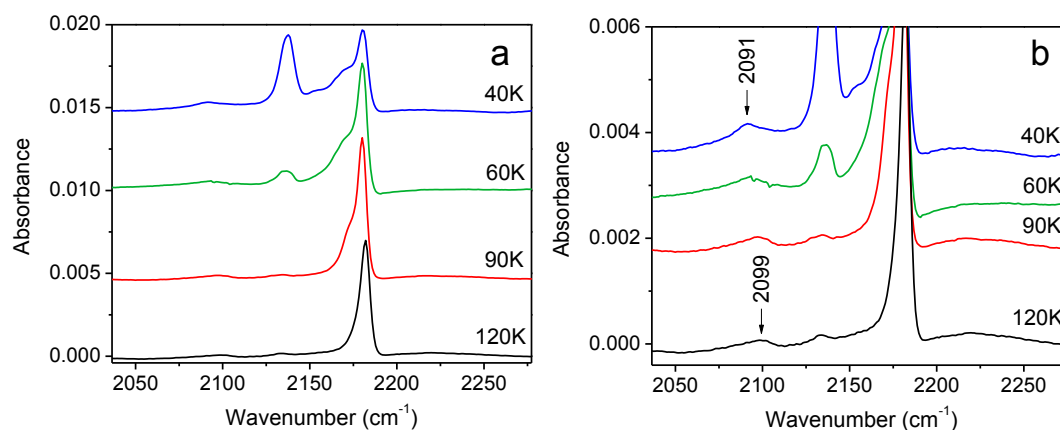


Figure 7.6. FT-IR difference spectra during surface warming steps of CO adsorbed over Au/TiO₂ at 40 K (blue spectrum), 60 K (green spectrum), 90 K (red spectrum), and 120 K (black spectrum), showing a) the full CO region and b) expanded view of the CO/Au region.

7.5 Discussion

Investigations of layered deposition of CO and O₂ over the bare TiO₂ support demonstrated that the changes observed in the carbonate region are dependent on the identity of the reagent gas. This result supports the findings that CO may be reacting with these species, as proposed in Chapter 4. This can be understood as the same effect would be expected for all gases if the vibrational bands of carbonate species were simply changing due to coverage of species at the surface which could be affecting the vibrational mode. If this were the case, this effect would be expected to be present with other gases as well, without distinct differences in position and intensity changes in the bands. The carbonate region indicated an overall increase in several of the bands with exposure to O₂ which had been previously depleted during CO deposition.

Adsorption of O₂ at 40 K over CO-covered Au/TiO₂ and TiO₂ resulted in the depletion of physisorbed CO, and increase in CO binding at the 2180 cm⁻¹ site due to

chemisorption (Fig. 7.4). For the sample containing AuNPs, depletion is also observed in the CO/Au signal around 2090 cm^{-1} . In addition to these changes in the CO region, the difference spectra revealed an increase in the band around 2340 cm^{-1} due to CO_2 at the surface. The CO_2 vibrational band is also slightly more intense for the Au/ TiO_2 sample. For catalyzed oxidation, the presence of AuNPs would be expected to result in the increased conversion of CO to CO_2 . As described in the experimental section, this experiment was conducted with both Au/ TiO_2 and TiO_2 present on different halves of the sample substrate. Any background CO_2 should be the same for both samples as the experiment was conducted on the same day. However, extensive isotopic studies in which $^{13}\text{C}^{18}\text{O}$ is deposited are required to verify the catalytic validity of this product in the spectrum, and these studies are proposed as part of the future work for this project in Chapter 9. What is most clear from these preliminary studies with CO and O_2 is that no transient species or new vibrational bands are observed from the interaction of both reagents at the surface. These results are important to consider before moving forward with IMSS studies, the subject of Chapter 8.

The thermal behavior of the CO bands following O_2 deposition was similar to the results previously observed for warming CO-covered surfaces where O_2 was not present. One interesting feature in the data was the persistence of intensity under the physisorbed feature at 120 K for the Au/ TiO_2 sample. This band may be enhanced by the presence of AuNPs on the surface. Enhancement of this band intensity was also observed in the data presented in Chapter 5 following deposition of CO over Au/ TiO_2 , in which the sample containing the largest Au: TiO_2 ratio was found to have the highest intensity in this band

at 40 K (Fig. 5.11). Additionally, warming the Au/TiO₂ sample up to 120 K caused a blue-shifted of the CO/Au feature to 2099 cm⁻¹. It is not entirely clear from these studies alone as to whether this effect is due to the presence of O₂ on the surface. A similar blue-shift was observed for Au/TiO₂ samples which were prepared by de-wetting Au film over TiO₂ which was previously processed in adsorption experiments (see Chapter 5 for a detailed presentation of these effects). While this sample was not processed in this way prior to coating the TiO₂ film with Au, the bare support sample was prepared 5 months in advance to coating the film. The support was placed in a desiccator during this time, so it is possible that significant drying of the sample occurred during this time which facilitated a stronger wetting at the support interface. (Typical times in between TiO₂ preparation and Au film deposition were 1–7 days). The solvent for this preparation is mostly water (1:10 water:acetone, see Chapter 2 for sample preparation details), so it is possible that not all of the water is removed while heating the oxide during sample preparation and that additional drying occurred in the desiccator.

7.6 Conclusion

The work presented here explores CO adsorption over TiO₂ and Au/TiO₂ under steady state pressure conditions at 90 K and 1 Torr CO, and following subsequent evacuation of the gas phase. It was found that binding of CO at the 2180 cm⁻¹ and 2090 cm⁻¹ sites persisted after evacuation, in contrast to binding at the 2137 cm⁻¹, as this band was removed from the spectrum of both sample after returning the system to vacuum (<10⁻⁶ Torr). The lack of stability of CO bound in the site corresponding to the band at

2137 cm^{-1} supports that this site is due to non-specific CO physisorption, while bands persisting under vacuum support their assignment to chemisorption. The regeneration of the band at 2090 cm^{-1} following exposure to 1 Torr CO under steady state pressure conditions was observed, and suggests that these conditions facilitate surface changes which favor binding of CO to AuNPs. Additional studies investigating O_2 adsorption over CO-covered Au/ TiO_2 and TiO_2 under vacuum conditions ($< 10^{-5}$ Torr) showed evidence for CO_2 production, although no transient species were observed under these conditions.

7.7 Appendix

FT-IR difference spectra collected after deposition of $^{18}\text{O}_2$ and $^{16}\text{O}_2$ (36 ML at 0.6 ML/min) over TiO_2 support at 40 K during separate experiments are provided in *Figure 7.7*. These spectra indicate slight shifts in the increased intensity noted in the carbonate region during exposure to O_2 . Changes to the Ti-O region during deposition of $^{16}\text{O}_2$ are provided in *Figure 7.8*, which appear similar to those during exposure of TiO_2 to CO (see Chapter 4 for presentation of these spectra).

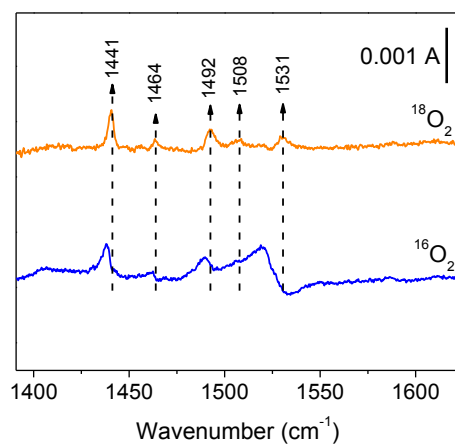


Figure 7.7. FT-IR difference spectra of TiO₂ following adsorption of ¹⁸O₂ (orange) and ¹⁶O₂ (blue) after exposure of 36 ML (0.6 ML/min).

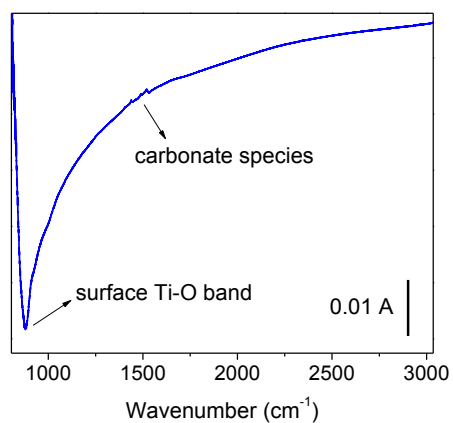


Figure 7.8. FT-IR difference spectra of TiO₂ following adsorption of ¹⁶O₂ (36 ML at 0.6 ML/min).

7.8 References

- 1 Green, I. X.; Yates, J. T., Jr., *J. Phys. Chem. C* **114**, 11924-11930 (2010).

Chapter 8

Interfacial Matrix Stabilization Spectroscopy (IMSS) studies of CO and O₂ interactions over nanoparticulate TiO₂ and Au/TiO₂: FT-IR investigation of matrix-controlled transport of reactant molecules to surfaces and complex stabilization at matrix/surface interfaces

8.1 Abstract

A new spectroscopic tool for analysis of species at surfaces is developed, Interfacial Matrix Stabilization Spectroscopy (IMSS), which employs energy-dissipating cryogenic matrix isolation techniques combined with FT-IR to enable stabilization and detection of pre-reactive complexes of CO and O₂ formed on titanium oxide-supported AuNPs. The temperature-mediated transport of CO isolated in an argon matrix at temperatures of 4 K and 20 K over the surface of nanoparticulate TiO₂ is investigated, where annealing the argon matrix at temperatures of 37 K is accomplished without matrix loss through the use of a krypton matrix over-layer. Interaction of the CO at the support surface was identified by observation of the vibrational band at 2180 cm⁻¹, characteristic of CO chemisorption at 5-coordinate Ti⁴⁺ sites. The benefit of matrix caging effects is investigated through stabilization of weakly-bound CO in hydrogen-bonded sites at the support by annealing an argon matrix over a CO-covered TiO₂ surface. Increase in the band around 2150 cm⁻¹, characteristic of this site, is observed after matrix annealing while the physisorption CO band at 2137 cm⁻¹ decreases, signifying population transfer of CO to this weakly interacting site. Finally, controlled interactions between CO and O₂

are verified during IMSS experiments where annealing of an O₂-doped argon matrix over CO-covered Au/TiO₂ produced a new vibrational band at 2112 cm⁻¹. This band is not observed in absence of the matrix, or before the annealing step, and is most prominent for samples which contain AuNPs and when the matrix contains O₂.

8.2 Introduction

As explained in great detail in Chapter 1, previous investigations of CO adsorption over TiO₂ have been conducted in absence of a cryogenic matrix. The work presented in Chapters 3–7 developed the understanding for the adsorption of CO and O₂ over TiO₂ and Au/TiO₂ under various deposition conditions, both *in vacuo* and under steady state pressure conditions, for the experimental system used in this work. These investigations serve as the foundational work for matrix studies at these nanoparticulate surfaces. Traditionally, matrix isolation has enabled the study of transient species such as radicals^{1,2} and weakly-bound complexes^{2,3} in the absence of nanoparticulate surfaces in close proximity. In this chapter, the interactions of CO and O₂ at the surface of Au/TiO₂ and pure TiO₂ samples were studied in the presence of a cryogenic argon matrix using a modified matrix isolation technique, IMSS. The novelty of IMSS is that the matrix is deposited over the surface, which creates an energy-dissipating environment at surface binding sites for CO and O₂ and is expected to stabilize complexes formed from interaction the adsorbed species in order to allow for spectroscopic characterization. The goal of these preliminary investigations is to demonstrate that species can be isolated from the surface upon deposition, and subsequently transported through the matrix to

binding sites at the surface through the process of matrix annealing. In these studies, several variations of matrix experiments were conducted which focus on the demonstration of three crucial components as a proof of concept of the IMSS technique: matrix-controlled transport of CO to catalyst, stabilization of weakly bound species at the matrix/surface interface, and stabilization of transient species formed from the interaction of reactant species at the surface during annealing.

In order to verify the transport of CO deposited in the matrix to the matrix/surface interface, IMSS experiments were designed which employed the use of an argon under-layer to serve as a protective barrier between the CO-doped matrix and the surface. The purpose of implementing the argon under-layer was to distinguish between two different possible mechanisms to explain CO-binding observed upon annealing: transport of CO through the matrix, and thermally activated chemisorption of CO in contact with the surface after deposition. Comparison of results from these experiments and similar IMSS studies in which an argon under-layer was not deposited is expected to separate between these two distinct processes as the argon under-layer requires the transport mechanism for the observation of CO chemisorption at the surface. The scheme in *Figure 8.1* was provided to more clearly illustrate the difference between these two mechanisms for CO binding at the surface. Here, in *Figure 8.1a*, the process labelled “1” illustrates the transport mechanism, where the process labelled “2” illustrates the thermal promotion of chemisorption. Protection of the surface sites from CO using the argon under-layer to avoid process “2” is illustrated in *Figure 8.1b*.

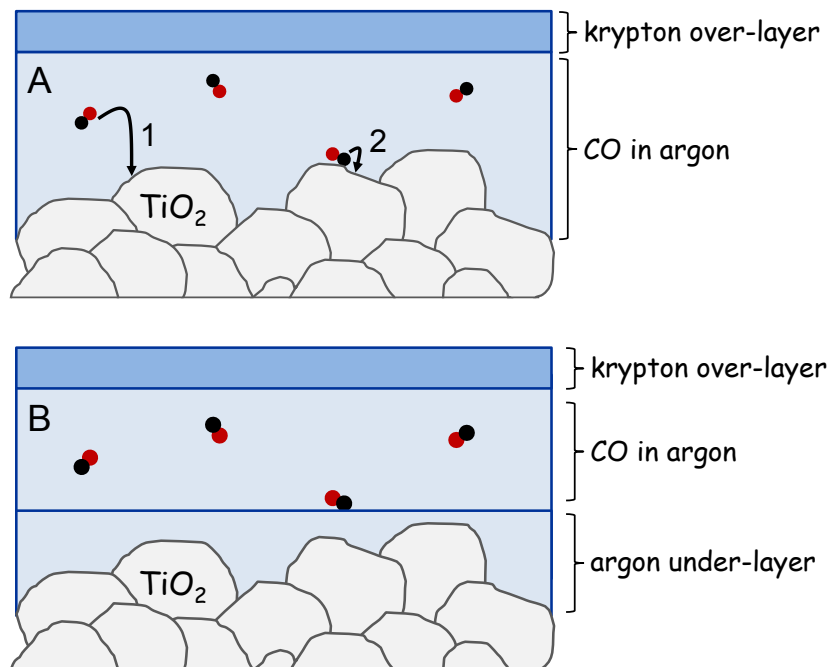


Figure 8.1. Schematic illustration of matrix isolation of CO above TiO₂ surface A) with and B) without the presence of un-doped argon under-layer protecting support sites.

Studies were also conducted which explore the effect of matrix deposition temperature on CO transport through the matrix. The transport mechanism is expected to be dependent on the quality of the matrix created during deposition, which is strongly correlated to deposition temperature. Matrices deposited at 20 K are partially annealed, and species in these matrices are better solvated than those deposited in the matrix at low temperatures. The Moore group has previously investigated⁴ these matrix transport mechanisms in other matrix studies. The importance of deposition temperature in the IMSS studies presented here was assessed through comparison of FT-IR spectra collected during deposition and annealing steps for matrices deposited at 4 K and 20 K using an argon under-layer.

The presence of the matrix over the nanoparticulate surface also serves to stabilize the species at weakly-bound sites due to the effect of matrix caging. This feature is a known property of matrices, where the species sit in sites in the empty lattice sites in the matrix where there are missing argon atoms.⁵ At the surface of the nanocatalyst, the surrounding argon creates a cage around the species at the weakly-bound sites which stabilizes the species at the surface. Annealing the matrix causes the argon to rearrange around the surface-bound species which is anticipated to facilitate enhanced solvation and stabilization of these complexes. In order to confirm this stabilization effect of the matrix, an IMSS experiment was designed in which CO was first covered over the surface of TiO₂ in absence of the matrix by depositing in helium carrier gas at 40 K. The surface was then cooled to 20 K and coated in an un-doped argon matrix. Spectral monitoring of the CO bands during annealing steps was used to assess population transfer and stabilization of weakly-bound surface species, such as CO hydrogen-bonded to surface hydroxyl groups on the oxide.

The transport of species through the matrix and subsequent stabilization of weakly-bound species at the surface were then used in combination to study the interaction of CO and O₂ at the surface of Au/TiO₂ in an effort to stabilize transient complexes at the surface. Here, an O₂-containing argon matrix was deposited over the surface of Au/TiO₂ which was previously covered in CO. Matrix annealing steps are expected to promote the transport of O₂ from the matrix to the matrix/surface interface, where the O₂ can interact with adsorbed CO. An illustration of these experimental steps designed to transport O₂ to the CO-bound surface sites during annealing step is provided

in *Figure 8.2*. This scheme shows the separation of both reactants and subsequent, thermally-driven interaction, in *Figures 8.2A* and *8.2B*, respectively. During deposition and annealing steps, the evolution of vibrational bands was tracked with FT-IR Spectroscopy to monitor species formed from interaction of CO and O₂ at the nanostructured Au/TiO₂ surface. A series of FT-IR spectra are presented here which detail the results of these IMSS studies, including control experiments in which either AuNPs or O₂ was not present in the system.

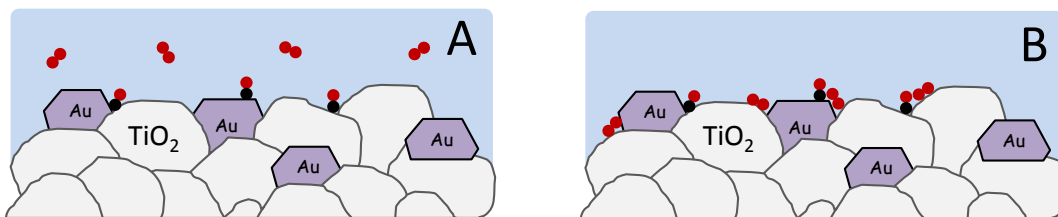


Figure 8.2. Schematic illustration of IMSS technique for O₂ in Argon matrix deposited over CO-covered Au/TiO₂ surface after A) deposition (isolation of CO and O₂ reactants) and B) annealing (transport of O₂ and stabilization at CO-covered catalytic interface).

8.3 Experimental methods

A description of the instrument setup, sample preparation, and experiment parameters are provided in Chapter 2. A brief description of the IMSS technique is provided here. The sample is initially heated *in vacuo* prior to gas deposition, similar to studies in absence of the matrix, in order to prepare the surface for CO binding. The basic structure of an IMSS experiment consists of cooling the sample to 4 K after thermal processing, and then warming the surface to the matrix deposition temperature (if above 4 K). The matrix is deposited, and then the surface is re-cooled to 4 K, the temperature at

which all spectra are collected to avoid temperature-induced changes in spectral features which do not correlate to matrix processing. After deposition, the matrix is slowly warmed up to the annealing temperature (5 K/min), where the temperature is held constant for 30 min. After 30 min of annealing, the sample is cooled back down to 4 K and a spectrum is collected. Depending on the experiment, this annealing process is repeated several times at various temperatures (actual annealing temperatures are indicated in relevant figure captions). As described in the introduction, several variations of IMSS experiments were conducted to explore various matrix processes at the surface. An experimental profile in which the temperature and various experimental steps is provided in *Figure 8.3* to illustrate the general steps performed during an IMSS experiment in which a matrix was deposited over a CO-covered surface (similar to that illustrated in the scheme in *Figure 8.2*).

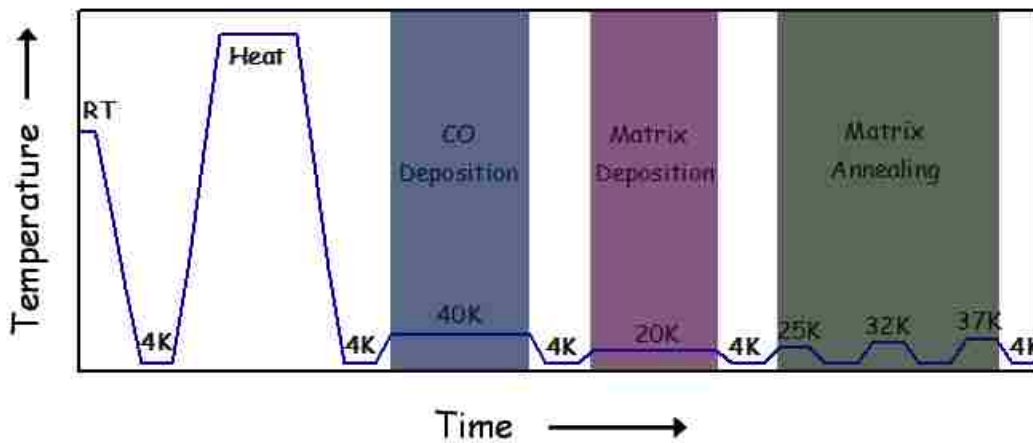


Figure 8.3. Experimental profile illustrating temperature progression throughout duration of experiment during gas deposition and annealing steps

For this specific study, adsorption experiments were conducted on two separate samples of TiO₂ powder prepared from a slurry of 1:10 acetone:water. One of the support samples was coated in 40 nm of Au film to prepare AuNPs via thermal de-wetting at 500 K for the studies on Au/TiO₂ (presented in Section 7.4.3 of this Chapter). Thermal de-wetting of the Au film is explained in great detail in Chapter 5. The Au/TiO₂ sample was thermally processed at 500 K *in vacuo* prior to the reagent gas during IMSS experiments with this sample (see Chapter 4 for a detailed study on the temperature effects of the thermal processing step). The actual temperature measured at the Pt sensor for these experiments was 374 – 375 K. The second sample used for these studies was bare TiO₂ which was thermally processed at a set-point of 500 – 550 K, and the measured temperature in these experiments was 404 – 435 K. Specific matrix gases employed are specified in detail below in context with the discussion of experiments and results. All spectra shown were collected at 4 K and are referenced to the 4 K spectrum collected after thermal pretreatment and prior to deposition, as described in Chapter 2. Spectra were collected at a resolution of 2 cm⁻¹ and averaged over 1000 scans, unless otherwise specified.

8.4 Results

8.4.1 Matrix-controlled transport of CO to catalyst

Development of IMSS as a spectroscopic tool for monitoring chemical reactions at surfaces requires that species can be transported from isolated positions in the matrix to binding sites at the surface in a controlled manner. In order to differentiate between the

desired process of species transport through the matrix from the mechanistically different process of the thermally promoted binding of species which lie at the bottom of the deposited matrix during the annealing step, comparisons were made between experiments where the matrix was prepared in two different ways. In a control experiment, an argon under-layer without CO dopant was deposited as a protective layer separating the support surface from the CO doped matrix. This layered deposition is notated as follows: Ar at 1 sccm for 20 min // 0.5% CO in Ar at 1 sccm for 1 h // Kr at 2 sccm for 30 min. The FT-IR spectra collected for these experiments are compared to experiments in which the CO-doped matrix was deposited directly onto the support surface (0.5% CO in Ar at 1 sccm for 1 h // Kr at 2 sccm for 30 min).

The results of these preliminary, proof-of-concept experiments demonstrating the controlled CO transport are provided in *Figure 8.4*. Each step in the experiment, FT-IR spectra collected at 4 K following deposition at 20 K, annealing at 30 K, and annealing at 35 K, are shown in individual panels, or *Figures 8.4a*, *8.4b*, and *8.4c*. The inset provided for each panel highlights the region of the spectrum at 2180 cm^{-1} where the characteristic vibrational band for CO bound to the support appears (see Chapter 3 for explanation of this assignment).

The spectra of CO isolated in a matrix above the support surface contains two main bands after deposition is complete which correspond to the perturbed vibrational frequency of CO in an argon matrix, and of CO/H₂O clusters isolated in argon⁶ (Fig. 8.4a). FT-IR spectra for matrices deposited without an argon under-layer lacks the band at 2180 cm^{-1} in the as-deposited matrix spectrum. After annealing the matrix at 32 K and

cooling back down to 4 K, the 2180 cm^{-1} band is observed in the spectrum for the matrix deposited without the argon under-layer, evident in the inset in *Figure 8.4b*. After annealing the matrix at the increased temperature of 35 K, the intensity of the 2180 cm^{-1} support band increased (Fig. 8.4 inset). Also evident in *Figure 8.4c* are the vibrational bands due to CO in Ar and CO/H₂O in Ar, indicating that the matrix is still present on the surface after annealing at 35 K.

For the matrix containing the argon under-layer, similar results were obtained upon deposition at 20 K. The band at 2180 cm^{-1} was not present in the spectrum (Fig. 8.4a). In contrast to the matrix experiment without the argon under-layer, however, annealing at 32 K did not promote binding of CO at the 2180 cm^{-1} site. With the under-layer present, the matrix had to be annealed at the higher temperature of 35 K before binding at the 2180 cm^{-1} site was observed. The need to anneal the matrix to higher temperatures with the argon under-layer present demonstrates the observed phenomenon is in fact due to transport of CO through the matrix to the surface.

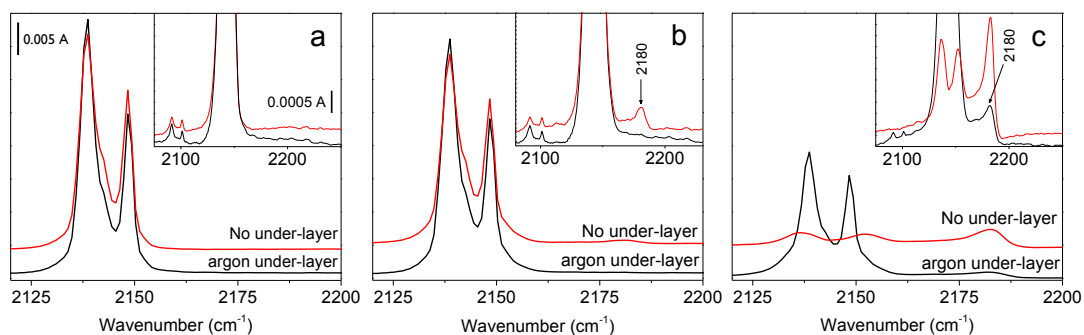


Figure 8.4. FT-IR difference spectra collected at 4 K during IMSS experiment with argon under-layer (Ar at 1 sccm for 20 min // 0.5% CO in Ar at 1 sccm for 1 h // Kr at 2 sccm for 30 min; black spectrum) and without argon under-layer (0.5% CO in Ar at 1 sccm for 1 h // Kr at 2 sccm for 30 min; red spectrum) after a) 20 K matrix deposition, b) annealing matrix at 32 K for 30 min, and c) annealing matrix at 37 K for 30 min. All panels and insets display the same vertical scale.

The effect of the matrix on the isolation of CO from the support binding sites is also useful in monitoring the changes in bands in the carbonate region of the spectrum. FT-IR spectra collected following deposition of the CO-containing argon matrix at 20 K with an argon under-layer (Ar at 1 sccm for 20 min // 0.5% CO in Ar at 1 sccm for 1 h // Kr at 2 sccm for 30 min) and subsequent annealing step are provided in the black and blue spectra in *Figure 8.5*, respectively, where the carbonate region of the spectrum is shown.

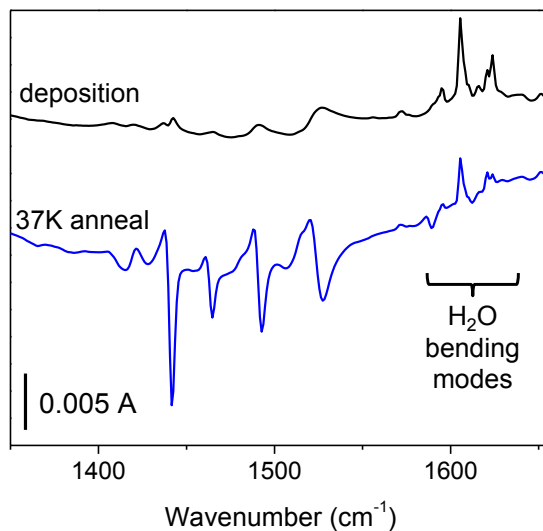


Figure 8.5. FT-IR difference spectra collected at 4 K during IMSS experiment after 20 K matrix deposition with argon under-layer (Ar at 1 sccm for 20 min // 0.5% CO in Ar at 1 sccm for 1 h // Kr at 2 sccm for 30 min; black spectrum) and annealing matrix at 37 K for 30 min (blue spectrum).

Upon deposition of the CO-doped argon matrix, the most intense vibrational bands in spectrum observed are those around 1600 cm^{-1} , which are due to bending modes of water clusters isolated in argon.⁷ Deposition of the matrix results in small increases in the baseline at positions where the sharp carbonate bands appear in the spectrum following thermal treatment of the sample at intermediate temperatures (see Chapter 4). After annealing the matrix at 37 K, there spectrum shows a strong depletion of these features. The depletion observed after matrix annealing is akin to that observed during adsorption of CO in absence of the matrix (see Chapter 4 and 5).

Additional experiments were also conducted to explore the effect of matrix deposition temperature on CO transport to matrix/surface interface. In two separate experiments, CO was deposited over TiO_2 support in an argon matrix over an argon

under-layer at both 4 K and at 20 K (Ar at 1 sccm for 20 min // 0.5% CO in Ar at 1 sccm for 1 h // Kr at 2 sccm for 30 min). FT-IR spectra collected at 4 K following deposition, annealing at 32 K, and annealing at 37 K, are shown in individual panels, or *Figures 8.6a*, *8.6b*, and *8.6c*, where at deposition at 4 K is shown in red and 20 K is shown in black. Again, an inset is provided for each panel to highlight the region of the spectrum at 2180 cm^{-1} .

For conditions where the matrix was deposited at both 4 K and 20 K, FT-IR spectra were collected after deposition and annealing steps to assess the effect of deposition temperature on CO transport through the matrix. Similar to the previous IMSS study on CO transport with and without the argon under-layer, the observation of a vibrational band at 2180 cm^{-1} signifies chemisorption of CO at the support sites. Appearance of this band upon annealing at a lower annealing temperature is indicative of the species being less solvated in the matrix. For conditions where the matrix was deposited at both 4 K and 20 K, FT-IR spectra collected following matrix deposition contained both the vibrational bands due to CO isolated in Ar and CO/H₂O isolated in Ar (Fig. 8.6a). For both deposition temperatures, the band at 2180 cm^{-1} in the as-deposited matrix spectrum was not present. After annealing the matrix at 30 K and cooling back down to 4 K, the 2180 cm^{-1} band was observed only in the spectrum for the matrix deposited at 4 K, evident in the inset in *Figure 8.6b*. Increasing the annealing temperature to 35 K resulted in a band at 2180 cm^{-1} in the spectrum collected for matrices deposited at both 4 K and 20 K (c.f. Fig. 8.6c). Also evident in *Figure 8.6c* are the vibrational bands due to CO in Ar and CO/H₂O in Ar in both spectra.

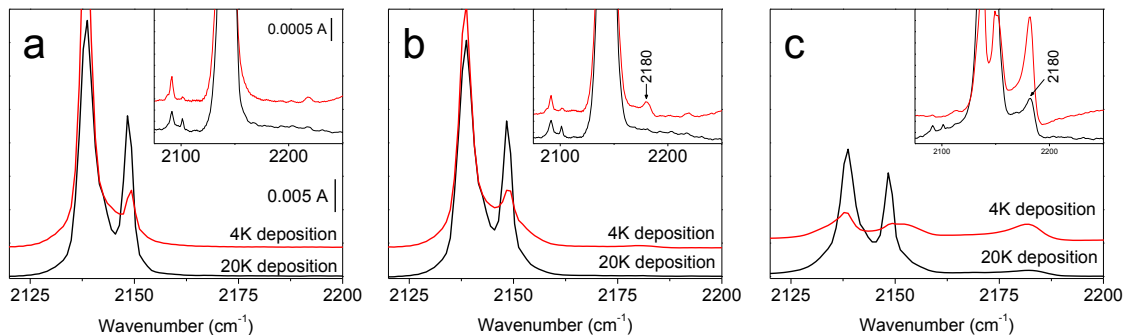


Figure 8.6. FT-IR collected at 4 K during IMSS experiment a) matrix deposition with argon under-layer (Ar at 1 sccm for 20 min // 0.5% CO in Ar at 1 sccm for 1 h // Kr at 2 sccm for 30 min) at 4 K (shown in red) and 20 K (shown in black), b) after annealing matrix at 32 K for 30 min, and c) after annealing matrix at 37 K for 30 min. All panels and insets display the same vertical scale.

8.4.2 Stabilization of weakly bound species

To demonstrate the ability of the matrix to stabilize weakly-bound species at the matrix/surface interface, a modified matrix experiment was performed over the surface of TiO_2 support. Here, CO was first deposited over the surface at 40 K in helium carrier gas in a similar way to the experiments presented in Chapters 3 and 4, followed by cooling the surface down to 20 K with subsequent deposition of an un-doped argon matrix with a krypton over-layer (0.1% CO in He at 1 sccm for 1 h at 40 K // Ar at 1 sccm for 1 h // Kr at 2 sccm for 30 min). FT-IR spectra collected at 4 K following deposition at 20 K (shown in black) and annealing at 30 K (shown in red) are provided in *Figure 8.7*. The spectrum collected following deposition of the matrix over the CO-covered support contains three main vibrational bands. The most pronounced is the band at 2137 cm^{-1} , due to physisorbed CO, and two smaller bands around 2150 cm^{-1} and 2180 cm^{-1} , due to

CO hydrogen bonded CO at Ti-OH sites and chemisorbed CO, respectively. After annealing the matrix at 30 K, the spectrum shows a decrease in the intensity of the 2137 cm^{-1} band. Additionally, the intensity of the bands at 2150 cm^{-1} and 2180 cm^{-1} increase in the spectrum, where the increase is most prominent for the 2150 cm^{-1} vibrational band. This enhancement of the vibrational band characteristic of CO hydrogen-bonded at Ti-OH centers is unique to the results for these IMSS experiments. Binding at this site is typically not observed at such large relative intensities following deposition of CO at 40 K under vacuum conditions ($<10^{-5}$ Torr). Results for experiments measuring CO adsorption over TiO_2 under vacuum were presented in great detail in Chapter 4. These results here demonstrate the caging effect of the matrix enabling observation of a species that would typically be pumped away.

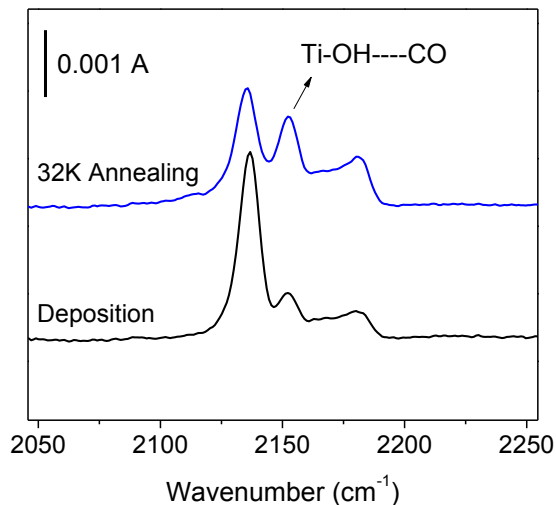


Figure 8.7. FT-IR difference spectra collected at 4 K following deposition (0.1% CO in He at 1 sccm for 1 h at 40 K // Ar at 1 sccm for 1 h // Kr at 2 sccm for 30 min; black spectrum) and annealing at 32 K for 30 min (blue spectrum).

8.4.3 Stabilization of transient species formed during annealing

In addition to experiments testing reactant transport and stabilization at the surface, a series of IMSS experiments was completed to evaluate the ability of the matrix to stabilize transient complexes formed from interactions between CO and O₂ at the surface/matrix interface on both TiO₂ and Au/TiO₂ samples. For this study, CO was first deposited in helium at 40 K over both TiO₂ and Au/TiO₂ surfaces. During two separate experiments, the TiO₂ and Au/TiO₂ samples were subsequently cooled to 20 K and an argon matrix containing O₂ was deposited over the CO-covered surface. Following matrix deposition, the matrix was annealed at 32 K. FT-IR spectra collected following the matrix deposition and annealing steps for experiments on both Au/TiO₂ and TiO₂ samples are provided in *Figure 8.8a* and *8.8b*, respectively. The inset in both panels shows an expanded view of the spectral region from 2100 to 2120 cm⁻¹ for the spectrum collected after annealing the matrix.

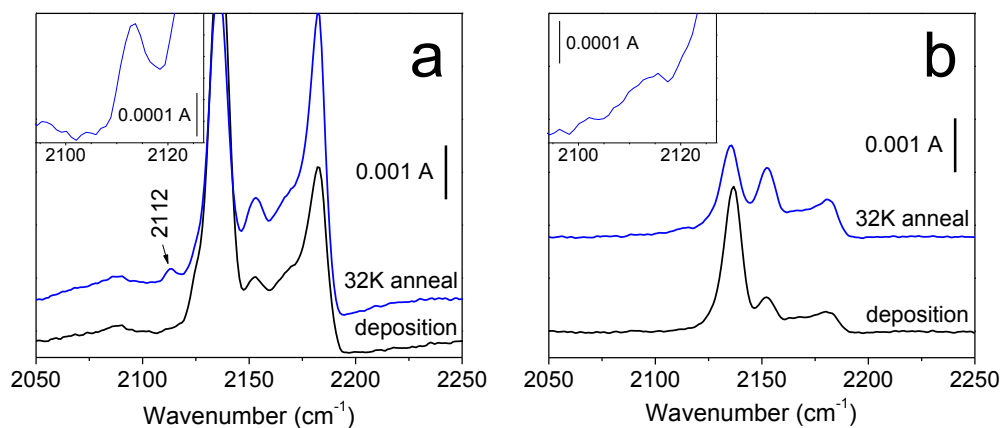


Figure 8.8. FT-IR spectra tracking CO bands after deposition (black), annealing to 32 K (blue) for argon matrices containing O₂ deposited over CO-saturated a) Au/TiO₂ and b) TiO₂.

Vibrational bands observed following the deposition of CO and the O₂-doped argon matrix over-layer produced bands in the CO-region that are typically observed for CO binding at the support and Au sites after heating the sample at 500 K (see Chapters 3 – 5), shown in the black spectrum of *Figure 8.8*. After annealing the matrix at 32 K over the Au/TiO₂ sample, the blue-colored spectra reveal a new vibrational band at 2112 cm⁻¹. This band is only present in the spectrum after annealing the matrix, and is clearly most prominent for samples which contain AuNPs, as is most emphasized in the inset of each panel in *Figure 8.8*. While a weak shoulder appears around 2112 cm⁻¹ following annealing the matrix over the TiO₂ sample, it is much less intense than the band observed for the Au/TiO₂ sample.

In order to verify whether the species with the vibrational signature at 2112 cm⁻¹ was created by the interaction of O₂ and CO at the matrix/surface interface, additional experiments were conducted in which the deposition steps were carried out in the same way, except the argon matrix did not contain an oxygen dopant. FT-IR spectra collected during the deposition and annealing steps over the both Au/TiO₂ and TiO₂ samples are provided in *Figures 8.9a* and *8.9b*, respectively. Again, an inset is provided in both panels to show an expanded view of the spectral region from 2100 to 2120 cm⁻¹ for the spectrum collected after annealing the matrix.

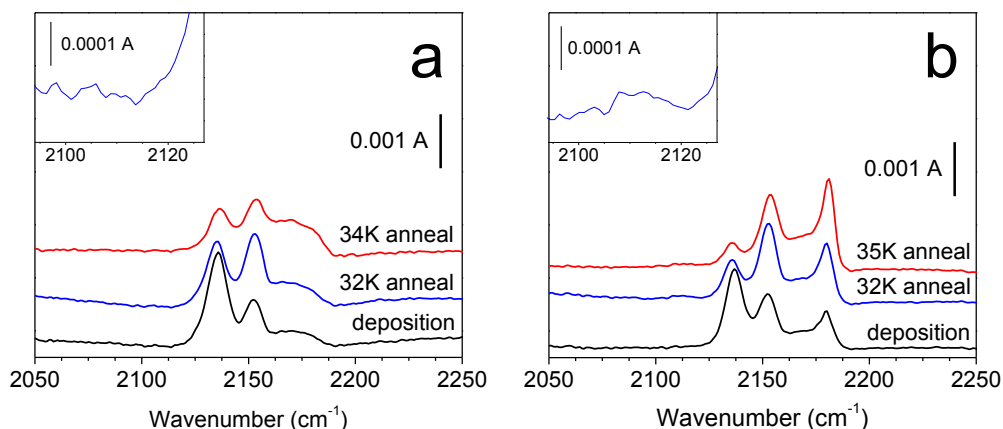


Figure 8.9. FT-IR spectra tracking CO bands after deposition (black), annealing to 32 K (blue), and annealing to warmer temperatures (red) for argon matrices without O₂ deposited over CO-saturated a) Au/TiO₂ and b) TiO₂.

Vibrational bands observed following the deposition of CO and the argon matrix over-layer without O₂ produced bands in the CO-region that are typically observed for CO binding at the support after thermal pretreatment of the sample at 500 K for both the Au/TiO₂ and TiO₂ samples, shown in the black spectrum of *Figure 8.9*. The band centered around 2090 cm⁻¹ was not observed in the Au/TiO₂ sample, likely due to degradation of Au sites observed during repeated use in experiments, a process which is explained in greater detail in Chapter 6. After annealing the matrix over the Au/TiO₂ sample at 32 K, and even at the warmer temperature of 34 K, the blue-colored spectra in *Figure 8.9a* did not show evidence of the vibrational band at 2112 cm⁻¹. A small feature is observed in the spectrum after annealing the matrix over the bare TiO₂ support (*Fig. 8.9b* inset), but only appears as a hint above the detection limit.

In order to confirm that the new vibrational band observed at 2112 cm⁻¹ observed upon matrix annealing was indeed the vibrational signature of a single CO vibrating on

the surface, and not a product of noise in the spectrum, isotopic studies were done by replacing ^{12}CO with ^{13}CO . The FT-IR spectra collected following the layered deposition (0.1% ^{13}CO in He at 1 sccm for 1 h at 40 K // 1% O_2 in Ar at 1 sccm for 1 h at 20 K // Kr at 1 sccm for 20 min at 20 K) over Au/TiO₂ after thermal processing at 500 K is provided in *Figure 8.10*, where the spectrum collected after deposition is shown in black. The translation of all CO bands including the band at 2112 cm⁻¹ is observed in the FT-IR spectra collected after annealing the matrix, and indicates that these bands are truly due to stabilized CO complexes at the catalyst surface.

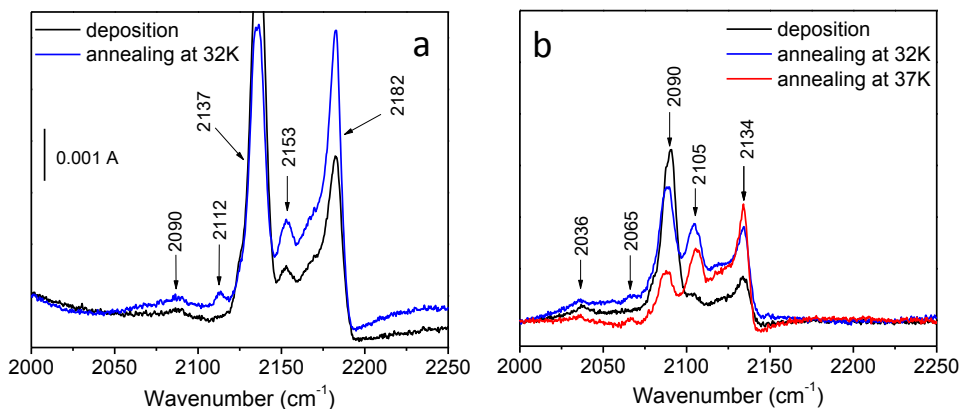


Figure 8.10. FT-IR spectra of Au/TiO₂ after deposition (0.1% CO in He at 1 sccm for 1 h at 40 K // 1% O₂ in Ar at 1 sccm for 1 h at 20 K // Kr at 1 sccm for 20 min at 20 K; black spectrum), annealing to 32 K for 30 min (blue spectrum), and annealing at 37 K for 30 min (red spectrum) using a) ^{12}CO and b) ^{13}CO . These spectra indicate the isotopic shift in band position of the 2112 cm⁻¹ feature to 2065 cm⁻¹ with substitution of ^{13}CO for the ^{12}CO in reagent gas. Both panels displayed at same vertical scale.

8.5 Discussion

8.5.1 Matrix-controlled transport of CO to catalyst

The first step in developing IMSS as a spectroscopic tool to monitor reactions between CO and O₂ at the surface of Au/TiO₂ was to show that species could be isolated above the surface of the matrix and transported down to the matrix/surface interface in a controlled way by adjusting the temperature of the matrix. The ability of IMSS to control the delivery of reactant molecules to the catalyst interface was demonstrated through deposition of CO isolated an argon matrix over bare TiO₂ support, followed by transport of the CO down to the support during an annealing step. The results from these experiments demonstrated that CO could be isolated from binding sites at the support, and that binding to the support could be promoted during the annealing step. This process is confirmed in the data by the lack of 2180 cm⁻¹ vibrational band in the spectra of the as-deposited matrix, and appearance of the band following annealing.

Parallel experiments which employed the use of a protective argon under-layer between the CO-doped argon layer and the surface verified that the vibrational band at 2180 cm⁻¹ was indeed the result of annealing-promoted transport of CO through the matrix, and not thermal promotion of chemisorption of the CO situated at the bottom of the deposited matrix. The IMSS results shown here have also served to elucidate the source of the depletion of carbonate bands during CO deposition previously observed during deposition of CO in absence of the matrix. Initial coating of the surface with argon and argon-isolated CO did not produce depletion of these bands (Fig. 8.4a). After annealing the matrix and promoting the transport of CO down to the support surface,

similar depletion in the carbonate region is observed to that when CO adsorption occurs in absence of the matrix (see Chapters 4 and 5 for these experiments). The IMSS technique helps to confirm that these changes are in fact due to CO interactions at the surface, as they don't occur when only argon is in contact with these surface species. These results also corroborate with those presented in Chapter 4, which demonstrate that CO chemisorption at the 2180 cm^{-1} site and weakly-acidic support sites is tied to reactions of surface species which exist on the oxide.

Investigation of differences in the transport of CO for deposition of the matrix at 4 K and 20 K revealed that CO was more readily transported through the matrix deposited at 4 K. This can be understood as it is known that matrices deposited at lower temperature are more polycrystalline than those deposited at higher temperature. Matrices deposited at 20 K are partially annealed, and species in these matrices are better solvated than those deposited in the matrix at low temperatures. The Moore group has previously investigated⁴ these matrix transport mechanisms in other studies.

8.5.2 Stabilization of weakly bound species

The results of argon matrix deposition and annealing over CO-covered support demonstrated population transfer of the physisorbed species, characterized by the band at 2137 cm^{-1} , to the bands at 2150 cm^{-1} and 2180 cm^{-1} . The increased population at 2150 cm^{-1} is not observed in absence of the matrix (see Chapter 4), demonstrating the effect of matrix caging on weakly bound species such as CO hydrogen-bonded to the Ti-OH groups at the support surface. The steps occurring during this experiment is illustrated in

Figure 7.8 to clarify the way in which the deposition was conducted to verify the effect of matrix caging on weakly-bound species at the support surface. Here, *Figure 7.8a* shows the surface following deposition of the CO in helium, prior to deposition of the matrix. The deposition of the argon matrix over-layer over the CO-covered surface is illustrated in *Figure 7.8b*.

8.5.3 Isolation of transient species formed during annealing

To complete the studies for the proof of concept experiments to demonstrate the IMSS spectroscopic technique, reactant transport and species stabilization were combined in the final studies which demonstrated the ability to thermally control the interaction of CO and O₂ at the nanostructured surface of Au/TiO₂. The results of these experiments demonstrated that by isolating the O₂ in the matrix above the surface after prior deposition of CO, annealing steps promoted the transport of O₂ down to the surface where it could interact with the CO-bound sites. The separation of the O₂ from the surface-bound CO is an important component of these matrix experiments. This allows for the controlled formation of complexes at the interface which can be monitored spectroscopically. This formation was verified spectroscopically by the appearance of the band at 2112 cm⁻¹ during the annealing step, afforded by transport of the O₂ through the matrix and the matrix caging effect on the species formed at the surface. In addition, the observation of the new vibrational band at 2112 cm⁻¹ that was previously unobserved for CO and O₂ experiments conducted in absence of the matrix demonstrated that the matrix could in fact isolate transient species at the surface. This experiment builds on

those of the two previous sections, where reactant transport and stabilization were initially verified experimentally.

The extensive control experiments in this investigation helped to determine the species involved in the binding site corresponding to the new vibrational band at 2112 cm^{-1} . Deposition of the O_2 -containing matrix over samples which did not contain AuNPs indicated that observation of an intense signal required the presence of AuNPs at the surface, suggesting that Au contributes to the chemistry of this binding site. Additional control experiments in which matrices without O_2 were deposited over Au/ TiO_2 and TiO_2 revealed that both CO and O_2 were required to be present in order to observe this band. The combined results of these experiments verify that this band requires CO, O_2 , the matrix, and probably AuNPs supported on the TiO_2 . Isotopic analysis of this band was used to confirm that this species is indeed due to oscillation of a CO molecule adsorbed to the surface. Calculation of the ratio of the vibration of the $^{12}\text{CO}/^{13}\text{CO}$ indicates that the shift of the 2112 cm^{-1} band is comparable to the other bands for CO adsorbed at support sites (Table 8.1).

Table 8.1. Isotopic shift of CO bands with substitution of ^{13}CO in IMSS experiments

assignment	^{12}CO	^{13}CO	isotope ratio
CO/Au	2090	2036	1.027
Transient CO species	2112	2065	1.023
physisorbed CO	2137	2090	1.023
CO H-bonded to Ti-OH	2153	2105	1.023
CO/ Ti^{4+}	2182	2134	1.023

Previous assignments for CO vibrations at or near 2112 cm^{-1} have been made by other groups for conditions where CO, O₂, and Au/TiO₂ have been present under equilibrium pressure conditions. Behm has noted a shift in the band typically observed at 2105 cm^{-1} for pure CO on Au/TiO₂ to $2110\text{-}2112$ for a mix of CO and O₂ on Au/TiO₂. In this study conducted under equilibrium pressures at room temperature, the band was observed to blue-shift with increasing gold coverage.⁸ It is possible that this band is a CO-O₂ complex formed at the perimeter of AuNPs and the TiO₂, given the requirement that all species be present in order to observe the band. While similar assignments have been made previously, the novelty of the IMSS technique is to allow for the controlled formation of these complexes to facilitate their characterization using spectroscopy. Additionally, IMSS enables the ability to isolate these complexes from other species on the surface so they can be more carefully studied.

8.6 Conclusion

This work demonstrates the validity of IMSS as a powerful tool for the study of species formed the interactions of gaseous reactants at nanoparticulate surfaces. The FT-IR spectra presented here demonstrate the transport of CO through an argon matrix deposited over the TiO₂ in a controlled manner using temperature during matrix annealing steps. Chemisorption was detected at support sites by the characteristic vibrational band at 2180 cm^{-1} only after annealing the matrix, and where higher annealing temperatures were required if a protecting argon under-layer was present which affords additional isolation of CO from support sites at the surface. Similar annealing steps of

argon matrices deposited over the CO bound at the surface were found to stabilize weakly-bound hydrogen-bonded species at the matrix/oxide interface. Here, population transfer was observed upon annealing from the physisorbed CO well to the potential wells corresponding to CO hydrogen-bonded at hydroxylated support sites, where an increase in the band at 2150 cm^{-1} was observed. The observation of a new vibrational band at 2112 cm^{-1} during matrix annealing steps where both CO and O₂ were present at the surface confirmed the ability of IMSS to isolate short-lived, transient species and enable their spectroscopic characterization. This band appeared at the greatest intensity for samples which exhibited CO/Au features in the spectra, and when O₂ was present in the argon matrix.

8.7 References

- 1 Jacox, M. E., *Chem. Soc. Rev.* **31**, 108-115 (2002).
- 2 Andrews, L., *Annu. Rev. Phys. Chem.* **22**, 109-132 (1971).
- 3 Ault, B., *Rev. Chem. Intermed.* **9**, 233-269 (1988).
- 4 Ludwig, R. M.; Moore, D. T., *J. Chem. Phys.* **139**, 244202-244209 (2013).
- 5 Dunkin, I. R. *Matrix Isolation Techniques: A Practical Approach*; (Oxford University Press: Oxford; New York, 1998).
- 6 Abe, H.; Yamada, K. M. T., *J. Chem. Phys.*, **114**, 6134-6141 (2001).
- 7 Michaut, X.; Vasserot, A. M.; Abouaf-Marguin, L., *Low Temp. Phys.* **29**, 852-857 (2003).
- 8 Diemant, T.; Zhao, Z.; Rauscher, H.; Bansmann, J.; Behm, R. J., *Surf. Sci.* **601**, 3801-3804 (2007).

Chapter 9

Conclusions and future continuation of this work

9.1 Conclusions

We developed a new spectroscopic tool, IMSS, for the study of heterogeneous catalysts involving gas phase reactants forming products over solid nanostructured surfaces in the energy-dissipating environment of cryogenic matrices. This technique enabled the spectroscopic observation of transient species formed over the surface that were not previously observed in our system in absence of the matrix. To begin development of this technique, this work started out with the development of sample preparation methods for Au/TiO₂ material. These materials were prepared via thermal de-wetting of an Au film sputtered over powder nanocrystalline TiO₂ (Degussa P25) *in vacuo*. Creation of supported NPs in this way was verified using TEM imaging. As part of the sample preparation, processing steps prior to gas adsorption were also developed as a way to clean surface sites and make them available for binding of reactants once the sample was installed in the vacuum system.

In preparation of IMSS studies of CO and O₂ adsorption over Au/TiO₂, adsorption of CO in absence of O₂ was characterized over the surface of both bare TiO₂ and Au/TiO₂. Adsorption of CO at 40 K under vacuum conditions was used to characterize the binding site profile at low temperature, and subsequent surface warming steps from 40 to 150 K was used to monitor the thermal behavior of each band. The evolution of these bands in the spectra was analyzed using the Redhead equation¹ to estimate barriers

between minima based on temperature thresholds for disappearance of associated bands. These studies also included the exploration of CO exposure and dosing rates, as well as comparison of the binding site population under vacuum conditions ($<10^{-5}$ Torr) to binding under conditions of steady state CO pressure. Adsorption experiments in vacuum conditions as compared to direct adsorption conditions under equilibrium CO pressure reveal which binding sites exist as metastable species, only present in dynamic equilibrium with the gas phase. The ability of exposure to increased CO pressure of 1 Torr under equilibrium binding conditions to regenerate the AuNP binding sites for CO reveals that these conditions may serve to restructure the surface, and that the presence of hydroxyl groups and water on the surface may be crucial to the catalytic activity observed by others. Adsorption of CO and O₂ was also probed under vacuum conditions to emphasize the stabilizing effect of the matrix during IMSS studies. These results demonstrated that no transient bands were observed from interaction of CO and O₂ at the surface under vacuum conditions, in absence of the matrix.

The observation of a new vibrational band at 2112 cm⁻¹ for CO and O₂ interactions in IMSS studies which was not present under direct adsorption conditions reveals the ability of the technique to enable the controlled delivery of reactants to the surface, as well as the careful, controlled study of isolated, short-lived transient species. This band was most prominent for samples containing AuNPs, and when O₂ was present in the matrix. These results demonstrate IMSS as a powerful tool for the study of surface species previously unobservable using today's current spectroscopic tools.

9.2 Future work

This section outlines suggestions for continuation of this. Much of the work presented here was developmental and part of an effort to establish the proof-of-concept for a new spectroscopic technique. A significant amount of effort was placed on design of experimental apparatus for gas adsorption measurements, and the assessment of FT-IR signal interpretation. These studies have provided a foundation for future experiments on catalytic systems, mainly CO oxidation over Au/TiO₂ nanocatalysts.

9.2.1 Isotope studies to demonstrate catalytic conversion of CO to CO₂

Future experiments on this system could focus on isotopic studies of CO and O₂ adsorption over Au/TiO₂ surfaces to verify catalytic conversion of the reactants to products in gas adsorption experiments. These experiments could be conducted under all three adsorption conditions explored in this dissertation: under vacuum, under steady state pressure conditions, and in the presence of a cryogenic matrix. Use of ¹³C¹⁸O would rule out possibility of background contamination in the CO₂ product, as this is the only case in which the expected product would be ¹⁶O¹³C¹⁸O. Another way to verify the catalytic activity of the Au/TiO₂ material prepared in this study is to generate a large amount of material and measure CO₂ conversion in the fixed-bed reactor described in Chapter 2. The small amounts used in the studies (<1 mg) here were not sufficient to show evidence for catalysis. A larger amount could be prepared by coating a large glass slide with material and de-wetting the sample using a vacuum oven. Using the fixed-bed

reactor to compare these samples with equal amounts of commercially available catalysts for CO conversion to CO₂ would confirm the catalytic validity.

9.2.2 Experimental design modifications

In addition to isotopic studies, several experimental design modifications would enable a more detailed study of the CO oxidation mechanism. The first is installation of a water flow cell in the deposition line, which would permit introduction of water vapor (including isotopically labelled water) into the system in a controlled way. Introducing water vapor would allow evaluation of the importance of water on the catalytic conversion of CO and O₂ to CO₂. The role of water is discussed in Chapters 1 and 7.

Another design modification proposed for this work is the use of a copper Integrating Sphere (IS) as a sample holder. The signal level in many of these experiments is low due to a short path length through the sample. The thin coating of TiO₂ powder on the samples used in these studies is beneficial for experimental control of the surface properties, especially during thermal processing and maintaining vacuum without extensive outgassing from the sample, however it does not generate a large signal compared to self-supported pellets. In addition the absorbance baseline reveals significant losses of light due to scattering at the surface and does not contribute to absorbance. This occurs due to the powder form of the sample, and corrugated surface which diffuses the incoming light. The IS reflective geometry creates multiple passes through the matrix, increasing the transmission absorption signal, and captures diffuse

and specular reflection components which recover signal lost to scattering. A design for implementation of the IS into the current system is illustrated in *Figure 9.1*. For this design, the CaF₂ sample mount would be removed from the sample stage of the cryostat and replaced with the copper IS. The thin powder films could then be coated directly onto the inside of the sphere, which should be made in two halves that can be fit together. Gas deposition lines would be required to deliver both reagent gases to the inside of the sphere.

One caveat of IS signal detection is, contrary to transmission spectroscopy, the signal is detected at an angle of 90 degrees from the incoming beam. The spectrometer will need to be modified, so that the mirror currently directing the beam (M3) through the sample 180 degrees from the detector would be removed to permit passage of the beam outside of the spectrometer box. Two mirrors (labelled M1 and M2) would be mounted outside the spectrometer box to direct the beam back into the IS at an angle 90 degrees from the currently positioned detector. Here M1 is a flat mirror, which simply changes the beam path, and M2 is a parabolic mirror, which will focus the beam into a light port on the IS. Detection at 90 degrees can also be accomplished by moving the detector to outside the spectrometer box to the current position of M2 in *Figure 9.1*; some trial and error is anticipated with these configurations.

The difference in detection angle also presents some additional complications to the data analysis. The collection of a correct reference spectrum will be essential, which may be challenging to obtain a spectrum which can be used for cases with the matrix present on the inside of the sphere, during IMSS experiments. Some experiments may be

required in which the sample was cooled and reference spectra were collected for undoped matrices at various cold temperatures. Additionally, the diffuse reflectance data would need to be processed using the Kubelka–Munk algorithm, further complicating the analysis.² The data obtained from these experiments would contain three distinct signal types (transmission, specular reflectance and diffuse reflectance). While analysis of these signals has been accomplished for experiments in the near-IR and UV-vis regions, the increased scattering efficiency at those shorter wavelengths may mean that the diffuse reflectance would dominate in a way that cannot be assumed in the mid-IR. Some work has been done using integrating spheres to detect species in matrices and over thin films using infrared light;³⁻⁶ the investigator proceeding with this research should use these studies as resources.

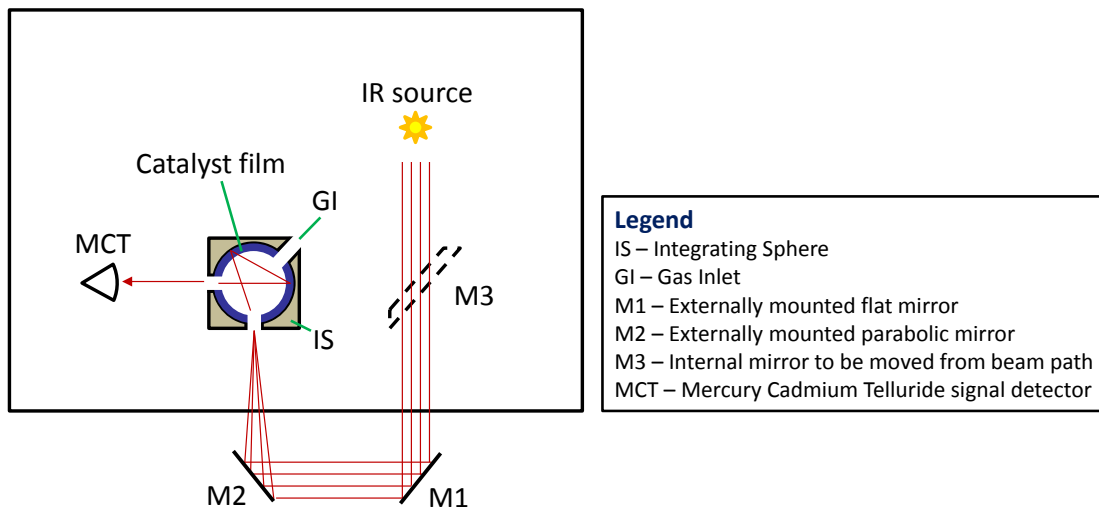


Figure 9.1. Top view of FT-IR spectrometer, illustrating modifications to incorporate the use of a copper integrating sphere as a sample substrate to be installed on the sample stage of the cryostat.

9.2.3 Expansion of sample characterization

Beyond isotopic studies and the suggested design modifications, additional exploration of the Au/TiO₂ system can be completed by using additional characterization techniques in these experiments. The use of x-ray photoelectron spectroscopy (XPS) and TEM to monitor the sample over the course of the de-wetting process, before and after CO exposure during repeated adsorption experiments, and before and after IMSS studies could help to elucidate changes to the surface oxidation state, as well as the AuNP size evolution. Implementation of a way to transport the sample from the vacuum chamber to the XPS instrument would make these studies most fruitful. This is typically accomplished using a vacuum suitcase, or small vacuum transport system to prevent exposure to atmosphere which may influence the measurement of changes due to the experiment.^{7,8}

Several experiments would be helpful in further understanding the changes to surface binding site chemistry that occurs during thermal processing steps and during the adsorption experiments both under vacuum and in the presence of the matrix. In particular, experiments could focus on more thoroughly understanding the effect of processing the TiO₂ under vacuum and with CO exposure on the wetting of AuNPs to the support during sample preparation. Monitoring the oxidation state of surface sites on the TiO₂ with XPS while heating the surface under vacuum, and comparing the results to XPS monitoring of a similar sample during exposure to CO for extended amounts of time should indicate whether the same chemistry can be achieved using these two different processes. The effect of moisture should also be explored in these studies, by cycling

between “wet” and “dry” states with frequent XPS monitoring. This could be accomplished with implementation of the water cell described above in the proposed experimental modifications, and use of a vacuum suitcase to transport the sample back and forth from the vacuum chamber. Additionally, the effect of water on the oxidation state should also be explored for samples containing AuNPs in a similar way, which may help to sort out the loss of signal apparent after repeated exposure to CO and heat under vacuum, and may help to elucidate the results suggesting that replenishing water of these surfaces seems to restore the CO/Au band in the spectrum.

Another focus of these experiments could be to further investigate the changes to the surface occurring during CO exposure, and investigate the effect on the oxidation state of the surface species. Thus, IMSS studies could be done in which elevated concentrations of CO were delivered to the surface under the matrix. It is possible that the caging effect of the matrix might enhance reaction of CO over the oxide surface. Monitoring this process with XPS before and after experiments would help to elucidate the changes in oxidation state, and correlate the resulting changes in the spectrum which would aid in characterization of CO adsorbed to species in various states. As described in Chapter 1, the vibrational signature for CO adsorbed to at cationic and anionic centers will vary and enable them to be distinguished.

9.3 Experimental plan for moving forward with this research

To begin the continuation of this research with the ideas presented in this chapter, one should first begin by working towards generation of large amounts of Au/TiO₂

catalyst material via thermal de-wetting. This is a good starting point because it would allow for many of these analyses to be carried out simultaneously and also because experimental design modifications will take additional time due to the necessary involvement of drafting designs for parts, machining of those parts, and finally the assembly of them. This material could be used in XPS studies to determine the oxidation state of the material after preparation and after use in adsorption experiments, and also for the isotopic studies to assess catalytic activity. Preparation of this material may also present a more ideal way to accomplish sample preparation. The Au/TiO₂ material could be sprayed out of solvent in a similar way to the preparation of powdered TiO₂ samples, and this approach may aid in getting a more uniform sample.

The next step should be to design and implement the use of the water flow cell. This part of the experiment is crucial in assessing the importance of the hydroxyl groups, which are proposed by Bond-Thompson⁹ to be present at the catalytically active centers at the Au/TiO₂ interface. This design modification should also be the simplest of those proposed above. The next step should be implementation of a way to vacuum containment system for the sample which would allow the sample to be transported to the XPS in order to monitor the evolution of the oxidation state throughout the course of adsorption experiments. This modification may be challenging, but would offer the most insight into the binding site chemistry. It is necessary to isolate the sample from the atmosphere so that a true analysis of the surface chemistry changes due to exposure of the sample to reagents in the experiment can be obtained. The addition of a vacuum

compartment for sample transport would also enable the experiments described in Section 9.2.3 to be completed.

Finally, in tandem to these efforts, work should begin on completion of the design modifications for the copper integrating sphere. After completion of the sphere design and installation, a thorough investigation of the signal should begin with collection of a reference spectrum, prior to any experiments with an actual sample. Even with the sample cooled to 40 K, CO deposited on the bare sphere should produce a signal around 2137 cm^{-1} due to physisorption. Once an interpretable signal is obtained, research should move forward with gas adsorption experiments on actual catalyst material. This experimental plan would serve as a good starting point for investigators pursuing work on elucidating the mechanism of CO oxidation over nanoparticulate Au/TiO₂.

9.4 References

- 1 Redhead, P. A., *Vacuum* **12**, 203-211 (1962).
- 2 Molenaar, R.; Bosch, J. J. t.; Zijp, J. R., *Appl. Opt.* **38**, 2068-2077 (1999).
- 3 Hanssen, L. M.; Snail, K. A., *Integrating Spheres for Mid- and Near-Infrared Reflection Spectroscopy*; Chalmers, J. M., Griffiths, P. R., Eds.; In Handbook of Vibrational Spectroscopy; (Wiley: West Sussex, 2002) Vol. 2, pp 1175-1192.
- 4 Ogawara, Y.; Bruneau, A.; Kimura, T., *Anal. Chem.* **66**, 4354-4358 (1994).
- 5 Berger, E.; Griffith, D. W. T.; Schuster, G.; Wilson, S. R., *Appl. Spectrosc.* **43**, 320-324 (1989).
- 6 Berger, E.; Griffith, D. W. T.; Schuster, G.; Wilson, S. R., *Mikrochim. Acta* **2**, 239-241 (1988).
- 7 Pomeroy, J.; Grube, H.; Perrella, A.; Sosolik, C.; Gillaspay, J., *Nucl. Instrum. Meth. B*, **256**, 319-323 (2007).
- 8 Pacchioni, G.; Valeri, S. *Oxide Ultrathin Films: Science and Technology*; (Wiley: 2012).
- 9 Bond, G. C.; Thompson, D. T., *Gold Bull.* **33**, 41-50 (2000).

Curriculum Vitae

Nina Jarrah
ninajarrah@gmail.com

PHYSICAL CHEMIST

More than 8 years analytical laboratory experience; expertise in cryogenic FT-IR spectroscopy, vacuum science, carbon capture, gas separation, and heterogeneous catalysis

National conference presenter (ACS, APS); successful writer of proposals & peer-reviewed manuscripts

Developed patent of new technology for gas separation

KEY SKILLS AND EXPERIENCE

- FT-IR; GC; GC/MS; TEM; VASE; SEM
- electrochemistry (CV, GCD)
- gas mix preparation
- API emulsion formulation
- GMP operations; FDA guidelines; USP protocol
- aseptic technique
- organic extraction
- particle size / surface area analysis
- Labview, Origin LabTalk, Visual basic
- PowerPoint, Excel, Word, OriginLab, SolidWorks

EDUCATION

PhD Student, Physical Chemistry, Lehigh University, Bethlehem, PA 2009 – 2014
Graduate Research Advisor: Dr. David Moore

Bachelor's degree, Chemistry, University of Colorado, Boulder, CO 2006

RESEARCH PROJECTS (ACADEMIC)

FT-IR and Interfacial Matrix Stabilization Spectroscopy studies of CO and O₂ adsorption over Au/TiO₂ nanoparticles 2012 – Present

- developed new FT-IR-based cryogenic spectroscopy technique to study gas/surface interactions
- prepared nanostructured gold-oxide catalysts
- characterized catalysts using various surface analysis techniques (FT-IR, TEM, VASE, SEM)

RESEARCH PROJECTS (ACADEMIC) - Continued

- Supercapacitive Swing Adsorption for carbon capture applications 2009 – 2013
- prepared nanoporous carbon samples / characterized electrochemical properties (CV, GCD)
 - assessed energy efficiency of implementing new technology
 - developed and patented new technology for gas separation while meeting strict grant deadlines
- Time Resolved Studies of Ultrafast Non-Adiabatic Electronic Dynamics 2006
- studied solution-phase dynamics of light harvesting species using femtosecond-pulsed FT-IR
 - set up experiments for nonlinear optic systems and time-resolved fluorescence spectroscopy

RESEARCH PROJECTS (INDUSTRIAL)

- Research and development of Taxol chemotherapy drug formulation for FDA application 2007
- developed scale-up of a chemotherapy drug formulation for FDA application
 - formulated API emulsion using a microfluidizer
 - characterized drug product using light scattering analysis to detect particle size
 - trained on aseptic technique; completed sterile intravenous drug fill for a toxicological study
 - followed USP protocol, operated under GMP-regulated conditions, and completed technical writing of production batch records

ADDITIONAL INDUSTRIAL EXPERIENCE

- Organic Chemist at Benchmark Analytical Laboratories, Inc. 2008 – 2009
- organic extraction following EPA methods
 - environmental trace analysis testing utilizing GC and GC/MS

U.S. PATENT

- App. No. 14/112,666 “Supercapacitive Swing Adsorption” filed 2/3/14

MEMBERSHIPS

- American Chemical Society 2011
Sigma Xi, The Scientific Research Society 2012
American Physical Society 2013

PUBLICATIONS

(“co-first author”) Kokoszka, B.; **Jarrah, N. K.**; Liu, C.; Moore, D. T.; Landskron, K., Supercapacitive Swing Adsorption of Carbon Dioxide. *Angew. Chem. Int. Ed.* **53**, 3698-3701 (2014).

Jarrah, N. K.; Klimas, R. D.; Moore, D. T. “Elucidating the binding of CO to TiO₂ using cryogenic FT-IR spectroscopy: surface diffusion and desorption between 40–150 K”, *J. Phys. Chem. C*, submitted 7/10/14.

Jarrah, N. K.; Moore, D. T. “FT-IR studies of sample pre-treatment temperature on CO adsorption at 40 K over nanostructured Au/TiO₂ generated via thermal de-wetting of gold film”, *J. Phys. Chem. C*, manuscript in preparation.

Jarrah, N. K.; Moore, D. T. “The effect of thermal pre-treatment, dosing rate, and exposure on CO adsorption over TiO₂ determined from cryogenic FT-IR spectroscopy: population of sites of weaker Lewis acidity”, manuscript in preparation.

Jarrah, N. K.; Moore, D. T. “Interfacial Matrix Stabilization Spectroscopy (IMSS) studies of CO and O₂ interactions over nanoparticulate TiO₂ and Au/TiO₂: FT-IR investigation of matrix-controlled transport of reactant molecules to surfaces and complex stabilization at matrix/surface interfaces”, manuscript in preparation.

ORAL PRESENTATIONS

Jarrah, N. K.; Moore, D. T. “ Interfacial Matrix Stabilization Spectroscopy (IMSS) studies of temperature and pressure effects on CO and O₂ adsorbed over nanostructured Au/TiO₂ formed by thermal de-wetting of Au film over TiO₂ NPs”, ACS National Meeting, Indianapolis, IN, 2013

Jarrah, N. K.; Moore, D. T. “FT-IR studies of CO Adsorption on Au/TiO₂ at 40 K”, APS National Meeting, Baltimore, MD, 2013